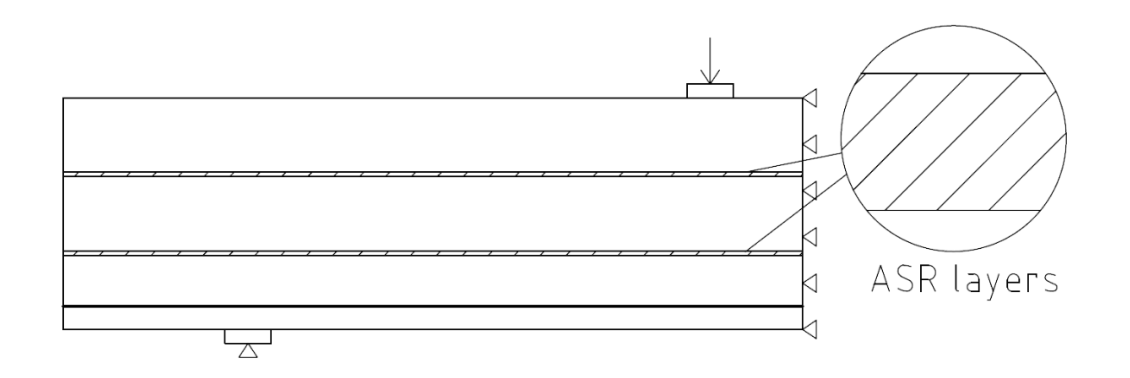
# Influence of ASR Degradation on Structural Behavior of Concrete Structures

Nan Lin





# Influence of ASR Degradation on Structural Behavior of Concrete Structures

By

#### Nan Lin

in partial fulfilment of the requirements for the degree of

#### **Master of Science**

in Structural Engineering, Concrete Structures

at Delft University of Technology

Thesis committee: Prof.dr.ir. D.A. Hordijk

Dr.ir. C.B.M. Blom

Dr.ir. M. Lukovic

Dr. R. Esposito



An electronic version of this thesis is available at <a href="http://repository.tudelft.nl/">http://repository.tudelft.nl/</a>.



# **Abstract**

A lot of concrete structures suffering from ASR show a decrease in material properties. However, it is not clear what might be the influence of ASR on structural behavior. Influence of restraint is often ignored in material property measurement, while reinforcement is present as a restraint of ASR expansion in most structures. This results in so called chemical prestress effect, which should not be neglected. In the presented study, the result indicates that neglecting the chemical prestress would miss the failure mechanism transition and lead to a lower beam stiffness. Therefore, a new way to model ASR-affected structures is proposed, called the ASR-layered model. The numerical analysis is done with ATENA. Depending on the reinforcement arrangement and amount, with longitudinal reinforcement acting as a restraint, expansion to the greatest extend occurs in the direction of least confinement and the cracks become parallel to reinforcement. Considering the potential to connect with each other and form long horizontal cracks, the ASR cracking in restrained structures are modelled as horizontal layers with reduced material properties. The property reduction is concentrated in ASR layers only, this local reduction is more realistic than the traditional method done by (Ferche, Sheikh, & Vecchio, 2017) in which a global reduction on material properties is applied. For chemical prestress, it is difficult to separate the influence of prestress in experiments, so experimental result is always affected both by the reduction of properties and prestress and probably some other phenomena that exist. The chemical prestress effect is modelled here in the way of physical prestress, but the expansion of ASR gel in chemical prestress would possibly influence the bond strength between concrete and reinforcement, so bond model is also considered.

Some conclusions can be drawn on this study. The material reduction caused by ASR would only result in a decrease of load capacity. While in combination with prestress, the load capacity of ASR affected beam may be increased to be even higher than the unaffected beam. The application of prestress could also lead to the possible change of failure mechanism from shear to bending failure, which is also observed in experiments. Including the bond-slip effect in prestressed ASR-layered model provides a better fitting with experimental results, but the influence of ASR on bond strength remains unclear. With parameter study, no obvious influence on ASR-affected structures could be linked to a/d ratio and reinforcement ratio. 1 or 2 ASR layers will only influence slightly on the ultimate load. The limitations of this model exist, the expansion caused by ASR is not directly modelled. Information on ASR layer property is quite limited, it would be difficult to measure the cracking part of ASR affected structures alone. In addition, the chemical prestress and possible cracking depend on the amount of ASR expansion as well as the reinforcement arrangement and amount, but they are not considered to correlate with each other in this model.

Keywords: ASR, Finite Element Method, Structural Behavior, Failure Mode

# Acknowledgements

Looking back on this thesis period, it was a challenging but also enjoyable journey, I am grateful to many who gave me help and support.

First of all, I would like to thank my supervisors Dr. Kees Blom and Dr. Mladena Lukovic for their guidance throughout this time. They worked in different styles, but I learnt much from both. Dr. Kees Blom taught me to think in an engineer way and from a higher level. Dr Mladena Lukovic was always earnest and patient, she gave me a lot of useful advice and encouragement whenever I was lost.

I was grateful to Professor Dick Hordijk, for offering me this opportunity to work on this fantastic project. Also, I want to express my gratitude to Dr. Rita Esposito, for her great work on ASR, which provided me a lot of useful information in this research field, and all the discussion time with me.

In addition, I want to thank all my friends, I could always get encouragement from them. Especially, I was thankful to my friend as well as housemate Xin Chen, for exchanging all the helpful opinions and spending the leisure time with me.

Moreover, appreciation goes to Denis Ho Wan-see, Anthony Wong Yiu-ming and Ellen Joyce Loo. Not only being my favorite singers, but also keeping on fighting for democracy, striving equal rights for the LGBTQ community, and caring for the minority and vulnerable groups in society. Thank you for being the light in the darkness.

A special thanks goes to Ru Zhou, for all the accompany with tears and joy. It is enjoyable to share my life with you, and you gave me the courage to face every obstacle. Love you to the moon and back.

Last but not least, I would like to express my greatest gratitude to my family, for their unconditional and consistent love. Thanks for giving me the deepest love and the most freedom.

Nan Lin Rotterdam, the Netherlands January, 2019

# Contents

1	Intro	oduction	5
	1.1	Background	5
	1.2	Problem statement	5
	1.3	Objectives	5
	1.4	Basic assumptions	5
	1.5	Main principles	6
	1.6	Strategy	8
	1.7	Thesis outline	8
2	Lite	rature review	9
	2.1	Influence of ASR on concrete degradation	9
	2.2	Influence of restraints on ASR cracking and expansion	10
	2.3	Influence of ASR on structural behavior for structures	13
	2.3.	Structures without stirrups	13
	2.3.	2 Structures with stirrups	14
	2.4	FEM models on ASR affected structures	16
3	Mod	lel introduction	19
	3.1	Introduction	19
	3.1.	Boundary conditions	19
	3.1.	2 Load	19
	3.1.	3 ASR layer modelling	20
	3.1.	Model parameters defined in ATENA	21
	3.2	ASR-layered model	25
4	Exp	eriments simulation	27
	4.1 S2-C &	The static and fatigue strength of reinforced concrete beams affected by alkali-silica reactors S2-A	
	4.1.		
	4.1.	•	
	4.1.		
	4.1.		35
	4.2	Structural consequences of ASR: an example on shear capacity-HS1-South	
	4.2.		
	4.2.	2 Modelling	56

	4.2.3	Results	57
	4.2.4	Optimization	59
	4.3	Limitations of the model	62
5	Analy	ysis on basic models	65
	5.1	Introduction	65
	5.1.1	Geometrical and cross-sectional properties	65
	5.1.2	Material type	66
	5.1.3	Boundary conditions	66
	5.2	ATENA analysis of a/d=2 models	67
	5.2.1	Introduction	67
	5.2.2	Shear capacity and failure mode	69
	5.2.3	Discussion	72
	5.3	ATENA analysis of different a/d ratio models	73
	5.3.1	Introduction	73
	5.3.2	Moment & shear capacity of original models	75
	5.3.3	Moment & shear capacity of models with ASR layers	76
	5.3.4	Failure mode	78
	5.4	ATENA analysis of models with prestressing	80
	5.4.1	Introduction	80
	5.4.2	Force-displacement curve and failure mode	80
	5.4.3	Discussion	81
	5.5	ATENA analysis of models with prestressing and bond	82
	5.5.1	Introduction	82
	5.5.2	Force-displacement curve and failure mode	82
	5.5.3	Discussion	84
	5.6	Conclusions	84
5	Sumr	nary	85
7	Conc	lusions and recommendations	87
	7.1	Conclusions	87
	7.2	Recommendations	89
4	ppendix.		91
	Append	ix 1 Calculation on ATENA models a/d=2	91
	Appe	ndix 1.1 Force-displacement response	91

Appendix 1.2 Crack pattern	94
Appendix 1.3 Principal strain	98
Appendix 2 Calculation on ATENA models with various a/d ratios	102
Appendix 2.1 Force-displacement response	102
Appendix 2.2 Crack pattern	109
Appendix 2.3 Principal strain	113
Appendix 3 Calculation of bending & shear capacity of original models	117
Appendix 4 Calculation on ATENA models with prestressing	119
Appendix 4.1 Force-displacement response	119
Appendix 4.2 Crack pattern	122
Appendix 4.3 Principal strain	125
Appendix 5 Calculation on ATENA models with prestressing and bond model	128
Appendix 5.1 Force-displacement response	128
Appendix 5.2 Crack pattern	131
Appendix 5.3 Principal strain	134
Appendix 6 Element size study for beam S2-C	137
Appendix 7 Limit check of steel strain in S2-C	139
Appendix 8 Discussion on fixed shear retention factor	141
Appendix 8.1 Introduction	141
Appendix 8.2 Failure mechanism	141
Appendix 8.3 Discussion	142
Bibliography	143

#### 1 Introduction

#### 1.1 Background

ASR is a chemical reaction in concrete structures over time in the presence of water when silica from reactive aggregate is reacting with alkalis from cement forming alkali-silica gel. The expansion of formed alkali-silica gel builds up an internal pressure and causes cracks in the aggregates and cement paste. Mechanical properties of the concrete affected by alkali-silica reaction are degrading.

Current guidelines recommend replacing structures suffering from ASR, which is a conservative solution. Some research is available on the influence of ASR on concrete compressive and tensile strength and the Young's modulus. Lack of knowledge exists how ASR influences structural behavior. It is known that structures might last very long even though they are affected by ASR.

For practical use, a good understanding how ASR influences structural behavior will be quite useful.

#### 1.2 Problem statement

An elevated light rail track in Rotterdam consisting of prefabricated girders supported on post-tensioned pier caps and piers indicates to suffer from ASR. And it requires a way to well indicate the effects of ASR degradation on the failure mechanisms and the ULS verification. This study is going to evaluate the structural behavior and failure mechanisms of the ASR affected structures. By the end, a conclusion on structure safety will be drawn.



Figure 1 ASR induced surface cracking in a prestressed pier cap; mapped cracking visible from the bottom side of pier cap no. 29 (left) and 31 (right)

## 1.3 Objectives

The first objective is to numerically analyze the ASR affected structures in comparison with available experimental results to indicate the effects on failure mechanisms and the ULS.

The second objective is to numerically analyze a series of ASR affected structural element to understand the influence of different parameters on failure mechanisms and load capacity.

### 1.4 Basic assumptions

To start from the very simple case, the light rail track is comparable to a basic beam. Slab is not applicable here as the light rail track bears the load by itself.

For the basic model, a four-point bending beam is adopted in this study. It is a commonly used test which is capable of analyzing both bending and shear behavior. A three-point bending beam is also an option and these two methods are quite similar. The advantage of four-point bending method is that it allows for uniform distribution between the two loading points, while the maximum stress in the three-point bending method is located under the loading point. In reality, the three-point bending beam is more sensitive as the existence of imperfections and notches in structure. With the non-homogenous material due to ASR influence, four-point bending is more reliable and thus adopted here.

ASR will cause swelling and cracks in structure, which means this part suffering from ASR is likely to be weaker and more vulnerable to loading. Interface is not used here as the swelling part has its thickness instead of an ideally thin layer with zero thickness. Therefore, the effect of ASR is modelled using layers with small elements which represent cracked layers in concrete. And these cracked layers have reduced material properties caused by ASR, which is also verified by many tests.

In this study, the beam is modelled idealistic in ATENA as no imperfections or notches are present. Therefore, the displacement, strain, stress, etc. are symmetric in ATENA. It is possible to use symmetry to ease the models and save computing time.

#### 1.5 Main principles

In plain concrete, free expansion is induced by ASR. While in reinforced structures, expansion in horizontal direction is restrained by main reinforcement. In such conditions, the cracks are oriented more parallel to the restrained direction, the cracking part with reduced material properties are modelled by introducing the ASR layers. Reinforcement is stressed in tension and concrete is stressed in compression parallel to the reinforcement, this is the so-called chemical prestress effect, prestress is applied here to model this effect.

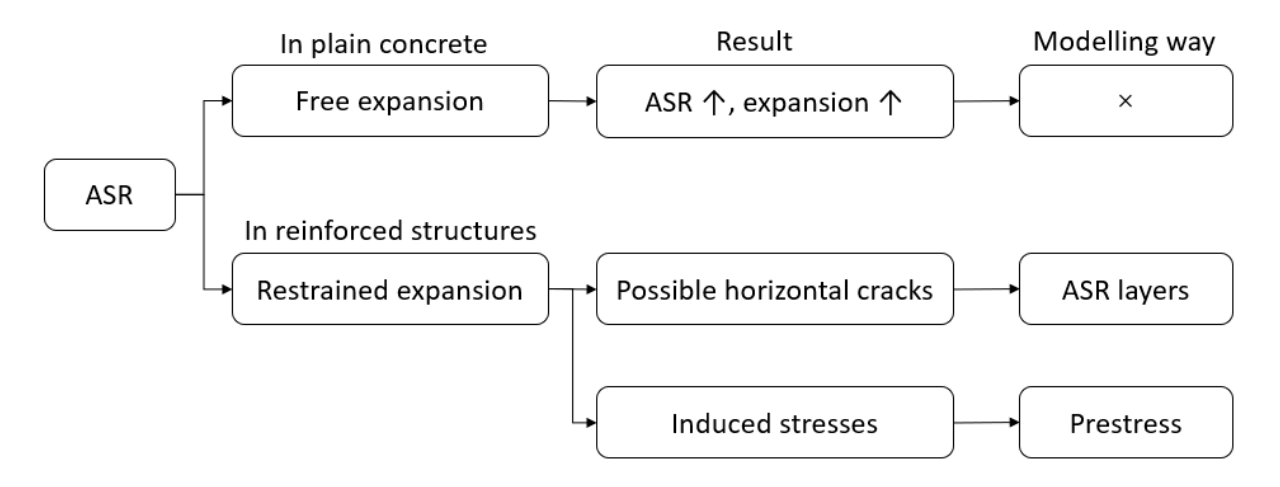


Figure 2 Main principles of modelling

The sketches of the main principles on material and structure are shown in Figure 3 and Figure 4.

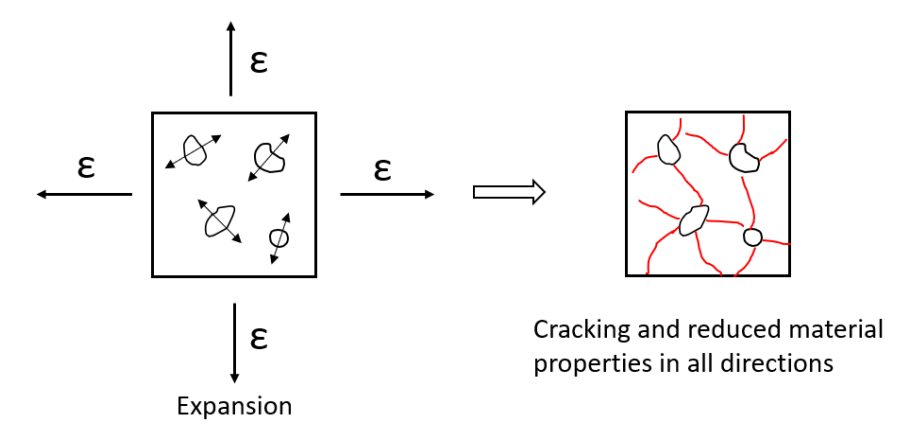


Figure 3 Material

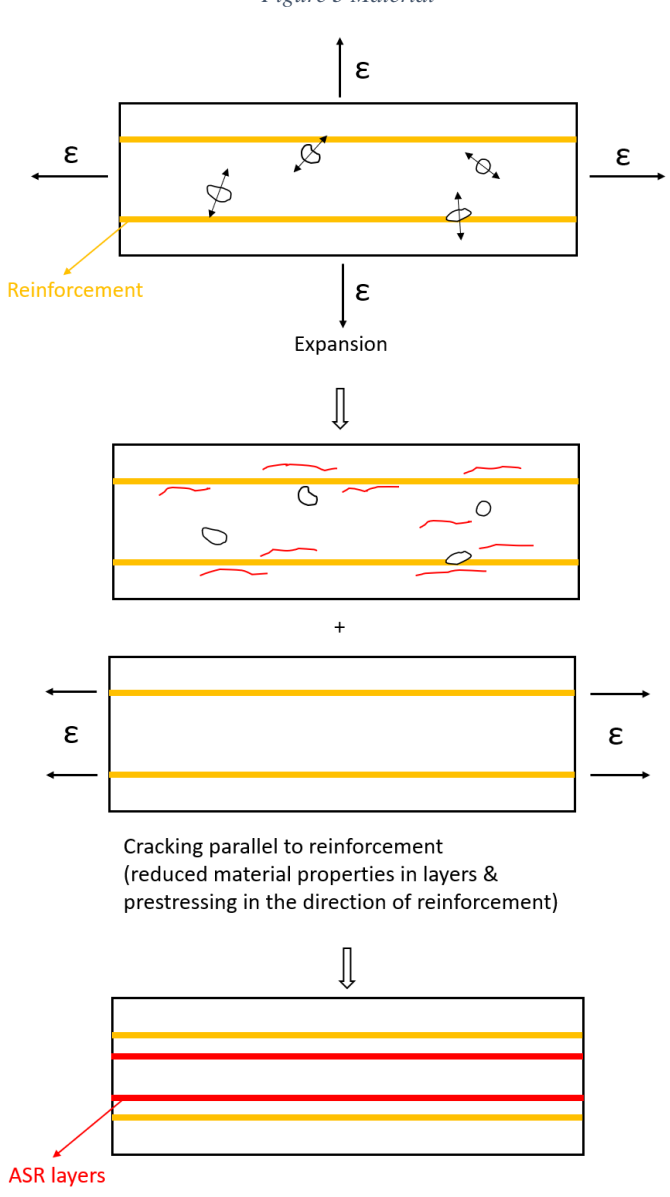


Figure 4 Structure

#### 1.6 Strategy

First step of this research is the numerical analysis on experimental results. The ASR effect is taken into account by creating layers, representing concrete with cracked layers, where the layers have decreased material properties. These material properties might vary between full concrete parameters to e.g. sliding parameters as ultimate boundaries. An optimization is also performed to get a better fitting.

Then, numerical analysis is done on a basic FEM model of a series of simple structures in ATENA such as a bending beam. The results are compared with analytical solutions. From the results, influencing parameters are extracted for the structural behavior of concrete suffering from ASR.

#### 1.7 Thesis outline

Chapter 1 gives a brief introduction to the problem and the strategy used in this research.

Chapter 2 provides a review on previous research work related in the influence of ASR in concrete structures.

Chapter 3 is an introduction to the adapted FEM properties and the newly proposed ASR-layered model.

In Chapter 4, a comparison between experimental results and ATENA results are made. With a deeper investigation in the parameters, hypotheses can be drawn for the structural behavior of ASR models.

In Chapter 5, a series of basic beams are modelled, a description of these beams and the material properties are given. Then ATENA analysis and analytical calculation are performed to draw the hypotheses.

Chapter 6 is a summary of this thesis work, and chapter 7 draws the conclusions and gives some recommendations for future research.

Some calculations are included in appendix part.

#### 2 Literature review

#### 2.1 Influence of ASR on concrete degradation

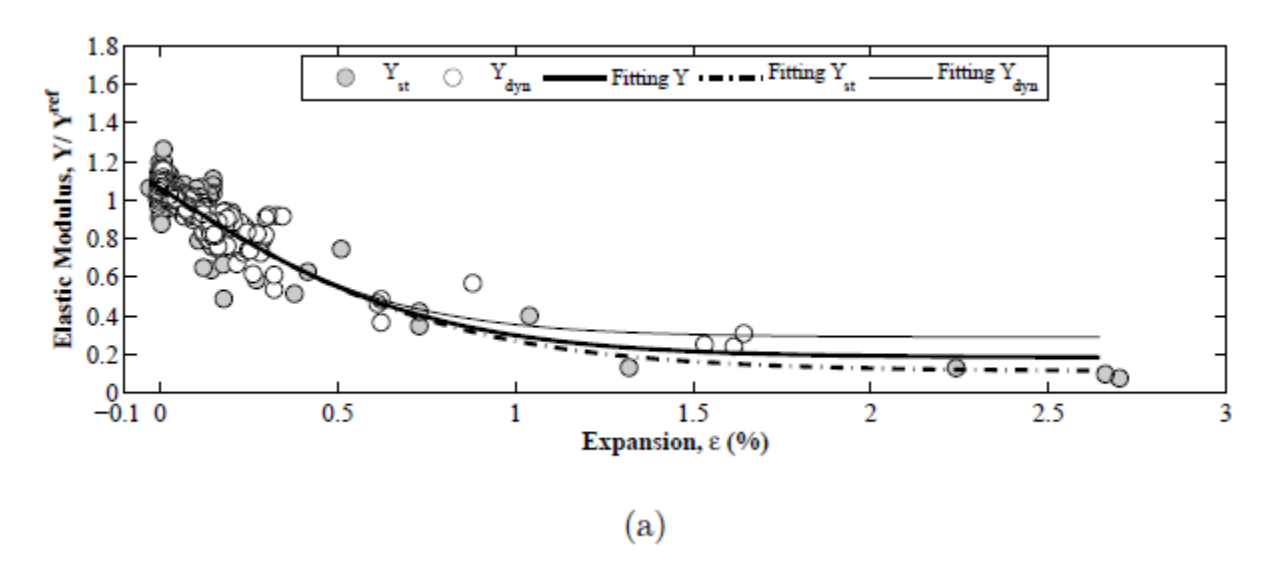
ASR can result in internal microcracking, expansion and external macrocracking of concrete. The microcracking causes a deterioration of concrete properties which is related to the amount of expansion. The expansion causes a prestressing of the reinforcement in structures affected by ASR (Jones & Clark, 1996). The micro-cracks within a mass of unrestrained concrete are orientated randomly. The combination of the variability of expansion and greater expansion of the interior concrete results in tensile strain at the surface, which can develop into macro-cracking (ISE, 1992).

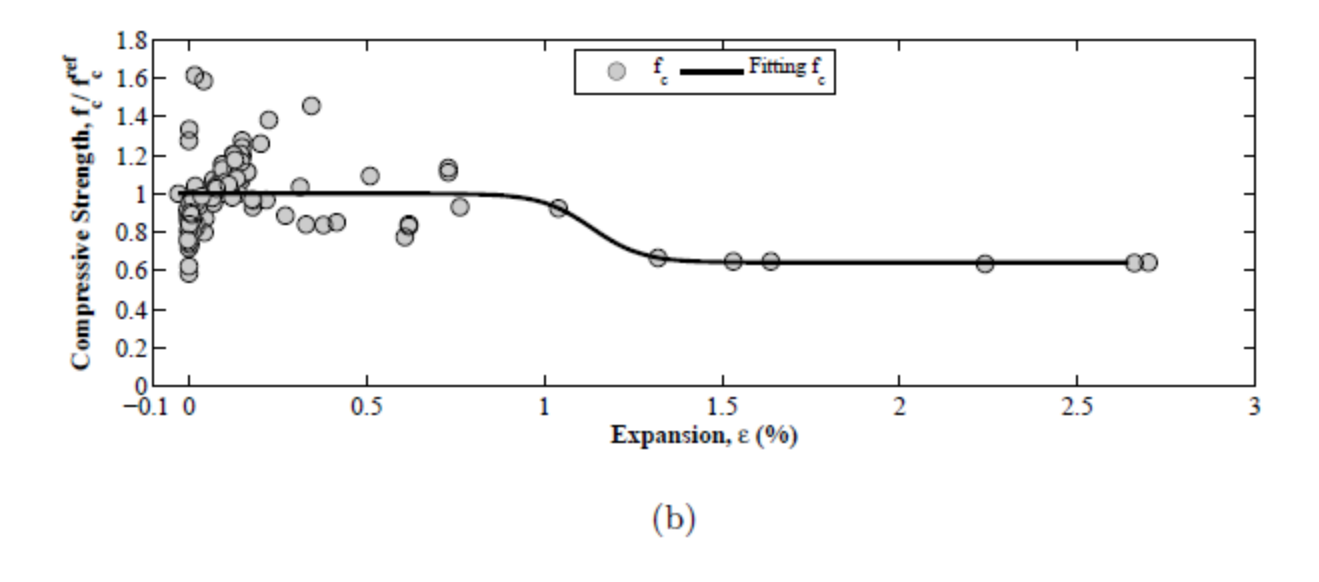
An estimation of the lower bounds to the residual mechanical properties of unrestrained concrete for various ASR free-expansions is proposed by (ISE, 1992), the values are listed in Table 1. Young's modulus and tensile strength decreases rapidly with the increasing expansion, and compressive strength decreases with a slower rate.

Table 1 Lower bounds to the residual mechanical properties as percentages of values for unaffected concrete at 28-day (ISE, 1992)

Property		Lov	wer bou	nds	
Expansion (%)	0.05	0.10	0.25	0.50	1.00
Cubic compressive strength	1.00	0.85	0.80	0.75	0.70
Cylindrical compressive strength	0.95	0.80	0.60	0.60	-
Splitting tensile strength	0.85	0.75	0.55	0.40	-
Elastic modulus	1.00	0.70	0.50	0.35	0.30

From (Esposito, 2016), the relations between degradation of material properties and ASR expansion rate are illustrated. Young's modulus and tensile strength are affected by ASR expansion greatly, while reduction on compressive strength could be ignored when expansion is not larger than 1%. Reduced value of Young's modulus could be as low as 20% of the sound value not affected by ASR. And the minimum value of tensile strength could be about 60% of the sound value.





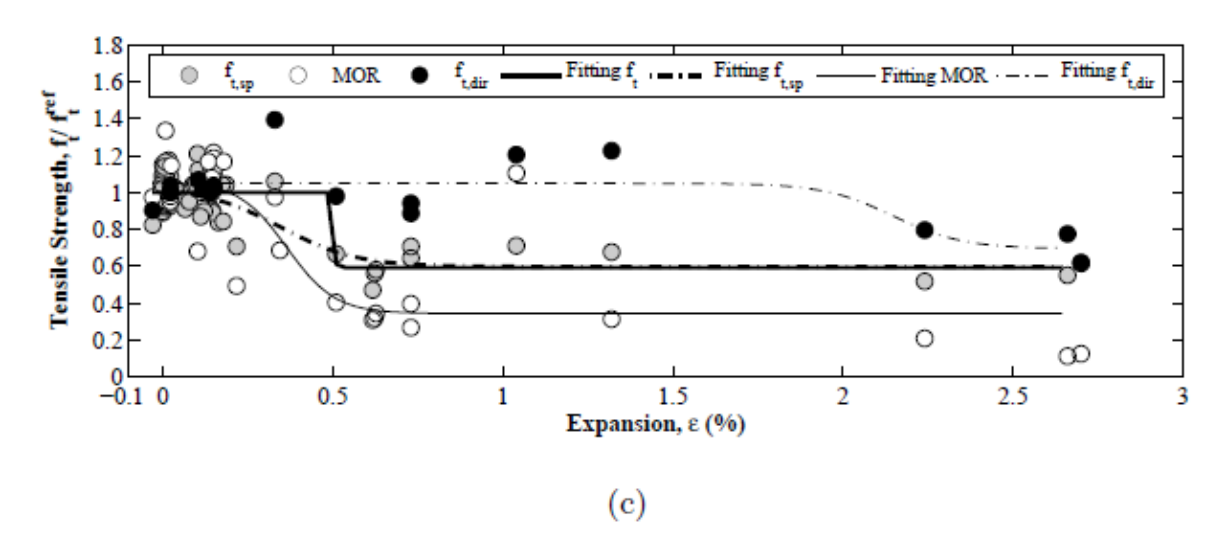


Figure 5 Fitting adopting the S-shaped curve (a) Elastic modulus; (b) Compression strength; (c) Tensile strength. (Esposito, 2016)

# 2.2 Influence of restraints on ASR cracking and expansion

From (ISE, 1992), If concrete is restrained by surrounding non-reactive concrete, applied stress or reinforcement, the expansion is inhibited in the direction of restraint, and the dominant cracks form parallel to this direction.

The restraining influence of reinforcement is illustrated in Figure 6.

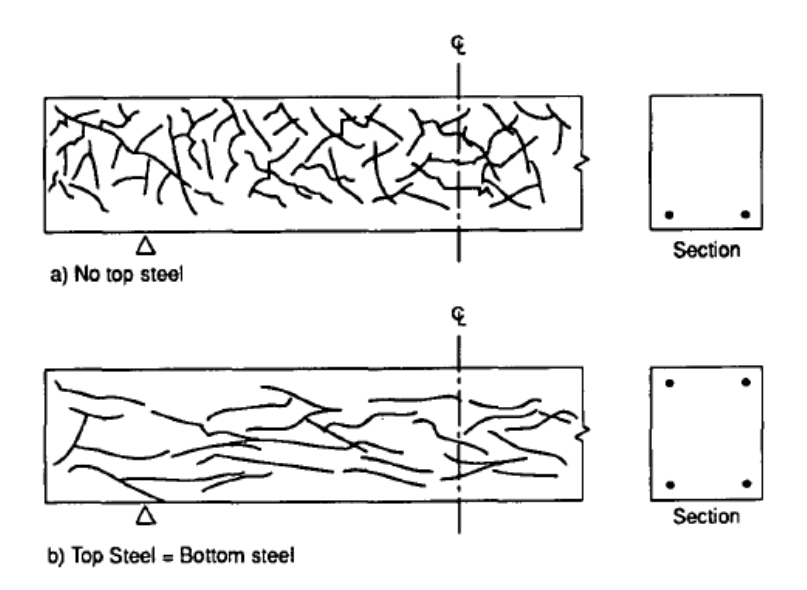


Figure 6 Influence of reinforcement on ASR cracking (ISE, 1992)

From (Fan & Hanson, 1998), relatively large concrete prisms made with reactive aggregate were tested. These concrete prisms have a dimension of 225 x 225 x 400 mm, similar results were also reported here.

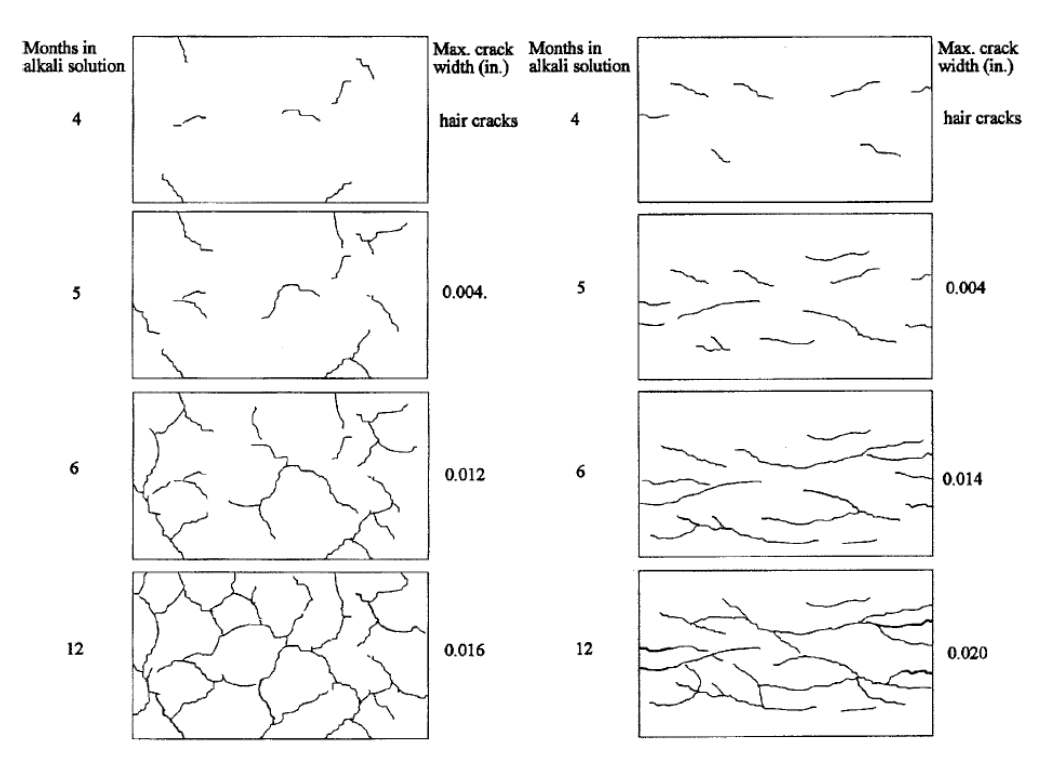


Figure 7 Typical cracking of 225 x 225 x 400 mm plain reactive prisms (left) and reinforced reactive prisms (right) (Fan & Hanson, 1998)

The effects of reinforcement restraint in terms of expansion and induced stresses are:

- 1) The net expansion is reduced from the unrestrained value.
- 2) The reinforcement is stressed in tension.

3) The concrete is stressed in compression parallel to the reinforcement.

From the available test data, even a small amount of reinforcement significantly restrains expansion, though the scatter is wide.

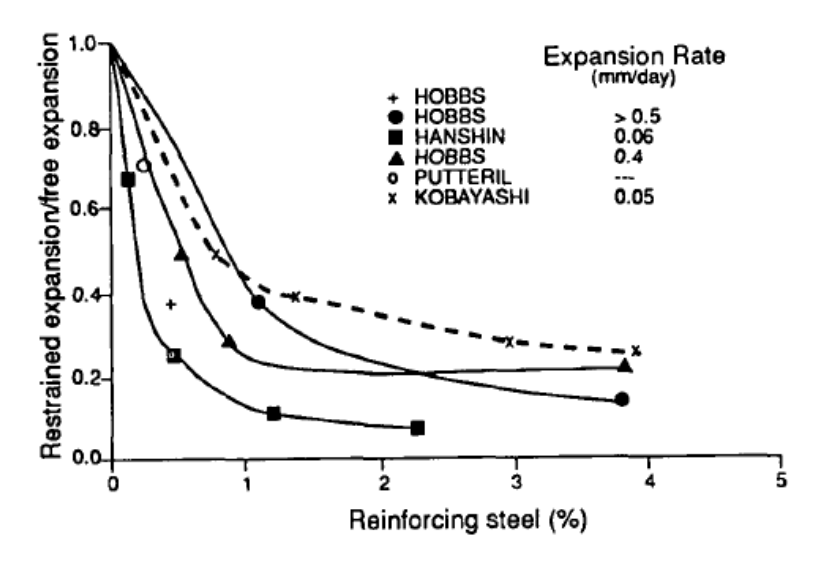


Figure 8 Restrained expansion (ISE, 1992)

From the available test data (Cope, 1993) (Chana & Korobokis, 1991) (Ng, 1991) (Clayton, Currie, & Moss, 1990), the induced compressive stress tends to a limiting value of not greater than about 4 MPa. In practical terms this implies that reinforcement yield could occur. Figure 9 (Chen, 2018) collects data from the above mentioned literature.

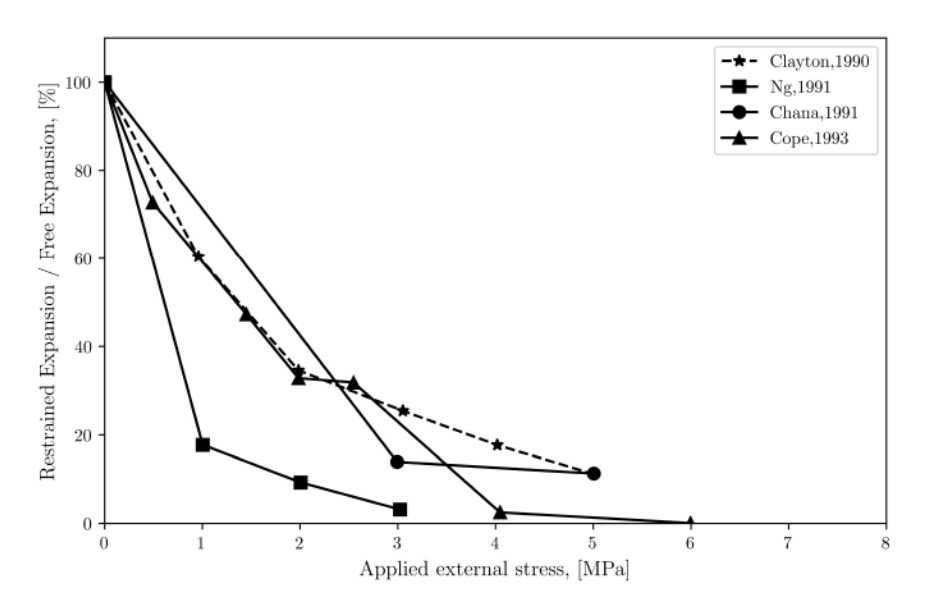


Figure 9 Relation of applied stress and expansion (Chen, 2018)

#### 2.3 Influence of ASR on structural behavior for structures

The presence of ASR might give some influence on the structural behavior. With obvious material property reduction caused by ASR, the ultimate load reduction may not be that much. In some ASR structures, shear capacity was even observed to have an increase. Also, the failure mode was observed a change from shear to bending failure in some cases. In this part, several typical cases collected from literature are illustrated.

#### 2.3.1 Structures without stirrups

1) Load capacity increases, remain shear failure:

(Ahmed, Burley, & Rigden, 1998) studied the influence on structural capacity due to ASR. In both reactive and control mixtures, a series of beams without or with links, and poor or good anchorage of longitudinal reinforcement were casted. ASR increases the shear capacity of reinforced concrete beams with or without shear links. The authors explained that the beneficial effect of hydration of the cement is greater than the detrimental effect of cracks due to ASR. Good anchorage also reduced the expansion and increased the ultimate shear strength of the ASR concrete beams. Beam without links all failed in shear.

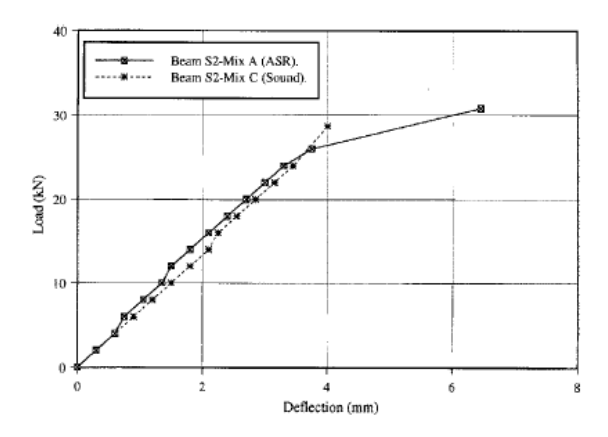


Figure 10 Deflection of Beam S2 (without links and good anchorage) against load (Ahmed, Burley, & Rigden, 1998)

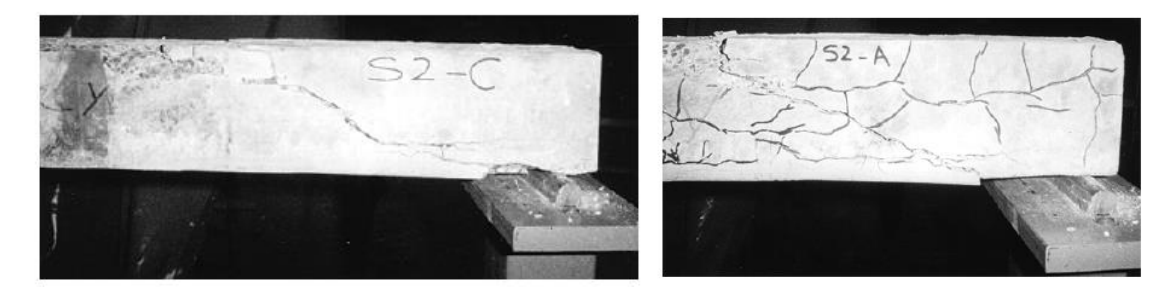


Figure 11 Failure mode for Beam S2-C (left, shear) and S2-A (right, shear) (Ahmed, Burley, & Rigden, 1998)

#### 2) Load capacity decreases, remain shear failure:

(den Uijl J., 2000) tested the beams sawn from the most affected area of an ASR-affected slab viaduct. Before test, some beams were strengthened by steel strips to avoid early yielding of steel, numbered as HS-beams. Though the unaffected material properties were not available, they compared the test results

with estimated shear strength according to (Rafla, 1971). The average capacity in case of shear failure was 75% of the value when no ASR damage had occurred. Due to the reduction of tensile strength caused by ASR, the failure mode is of the shear tension type, while without ASR damage flexural shear would have been expected.

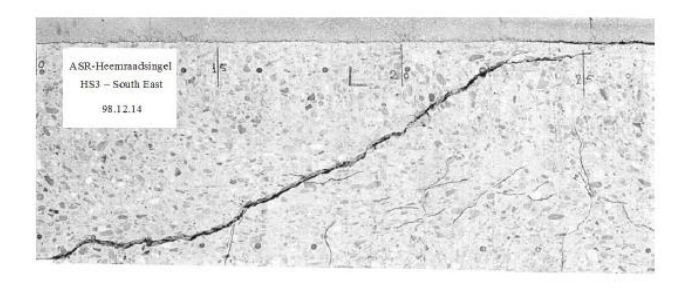


Figure 12 Beam end HS3-South after shear failure (ASR affected beam) (den Uijl J., 2000)

#### 3) Almost no change in load capacity, remain bending failure:

(Fan & Hanson, 1998) set up a four-point bending test for beams with various reinforcement ratio. Two concretes were produced, one with the reactive aggregate and the other with the nonreactive aggregate. The ASR expansion and cracking did not reduce the flexural loading capacity of the concrete beams, despite the substantial reduction in material properties. In other words, ASR had a much more detrimental effect on the mechanical properties of concrete cylinders than on the structural behavior of reinforced concrete beams.

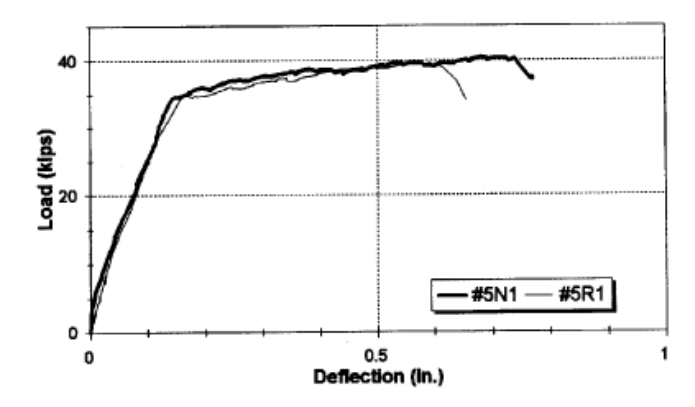


Figure 13 Deflection at center vs load for beam #5N1 (unaffected) and #5R1 (affected) (Fan & Hanson, 1998)

#### 2.3.2 Structures with stirrups

For structures with stirrups, the structure is also restrained in vertical direction. The shear resistance of the beam is increased by stirrups. In addition, the effect of ASR on tensile strength loss is partly compensated by the compressive stress induced by stirrups.

#### 1) Load capacity increases, change from shear to bending failure:

As stated in 2.3, (Ahmed, Burley, & Rigden, 1998) tested the beams both with and without shear links. The provision of shear links increased the shear resistance of both the ASR beams and control. This increases in shear strength for the ASR beams with links is due to the fact that the loss in tensile strength of the concrete caused by ASR is compensated by the compressive stress induced as the ASR expansion

is restrained by the links. Though beams without shear links remained shear failure, in the case of the ASR beams, the existence of shear links increased shear resistance to a sufficient extent to change the failure mode from a shear failure to bending failure. This failure mode change is due to the increased shear resistance caused by the prestressing stress resulting from the existence of ASR in the concrete.

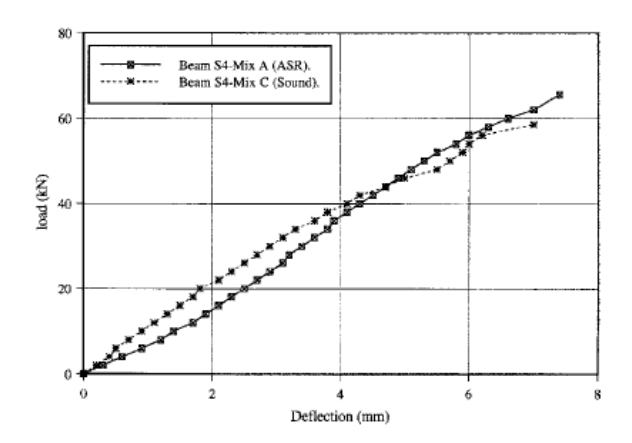


Figure 14 Deflection of Beam S4 (with links and good anchorage) against the load (Ahmed, Burley, & Rigden, 1998)

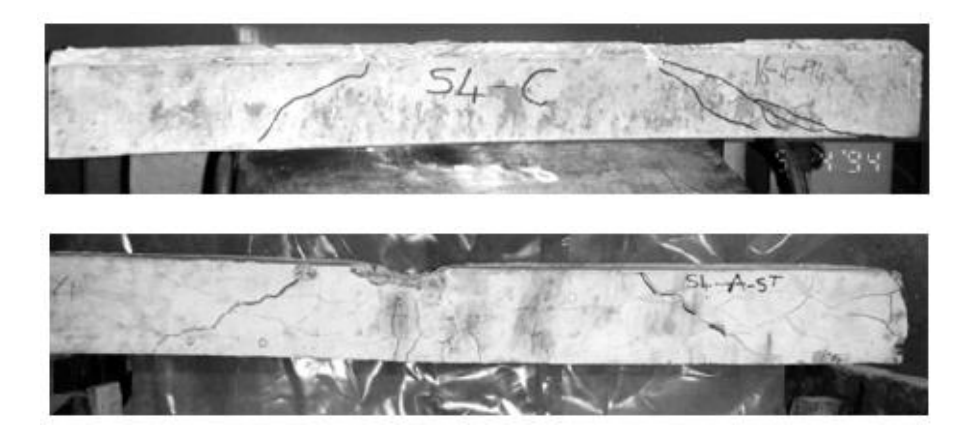


Figure 15 Failure mode for Beam S4-C (top, shear) and S4-A (bottom, bending) (Ahmed, Burley, & Rigden, 1998)

#### 2) Little reduction in load capacity, remain bending failure:

(Kobayashi, Inoue, Yamasaki, & Nakano, 1988) studied strength and deformation of prestressed beams with stirrups affected by ASR. Three kinds of concrete mixes with non-reactive (mix I), all reactive (mix II), half non-reactive and half reactive aggregate (mix III) were tested. These beams have an a/d ratio of 2.5 and 4.0 respectively. And two levels of prestress corresponding to approximately 4.90 MPa and 9.80 MPa respectively, were introduced by tensioning the prestressing bars. Using symmetrical four-point bending test, they found out all beams failed finally in flexural irrespective of a/d ratios of 2.5 and 4.0. the ultimate strength reduction of ASR beams is about 10% compared with that of normal beams.

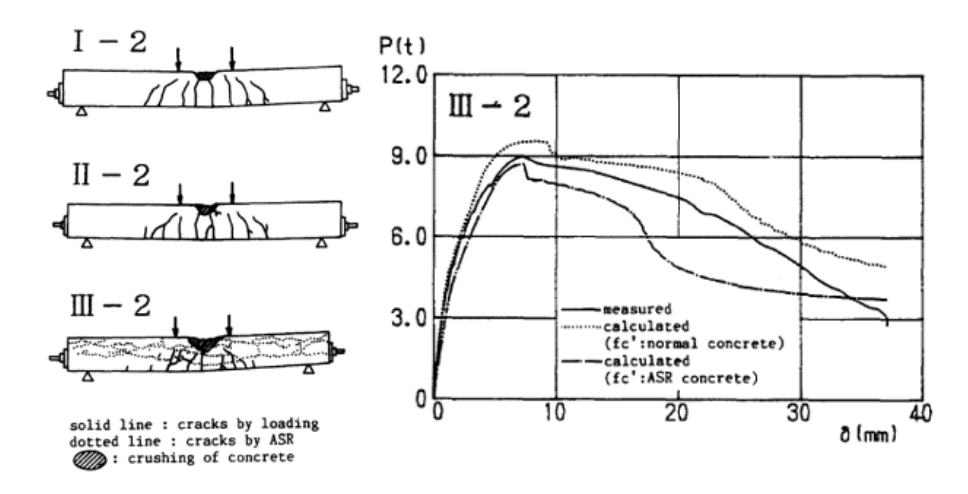


Figure 16 Bending failure occurred in all three mixes (Kobayashi, Inoue, Yamasaki, & Nakano, 1988)

#### 3) Little reduction in load capacity, change from shear to bending failure:

(Inoue, Fujii, Kobayashi, & Nakano, 1989) tested beams with different amount of reinforcement ratio of 0.77%, 1.2%, 1.74% respectively. All the beams have the same web reinforcement ratio of 0.3%. The reduction in yield strength and ultimate strength of ASR-affected beams was about 10% of the unaffected beams. And they found a special case when comparing the failure mode. For the case with 1.74% reinforcement ratio, the ASR affected beam failed in flexural with enough ductility while the unaffected one failed in shear and in a brittle manner.

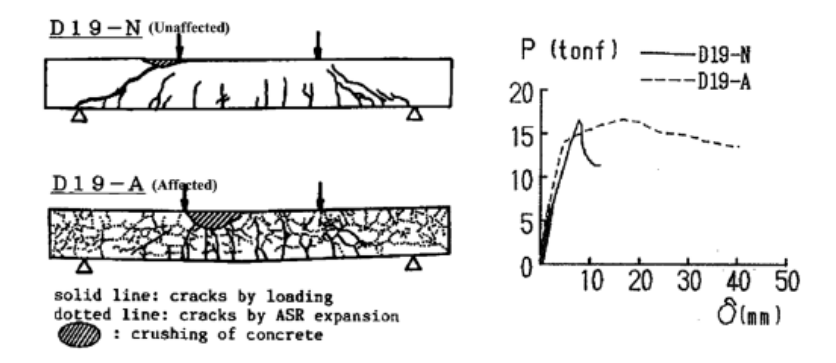


Figure 17 Failure mode changed from shear in unaffected beam to bending in affected beam (Inoue, Fujii, Kobayashi, & Nakano, 1989)

#### 2.4 FEM models on ASR affected structures

In previous research, some finite element models were proposed for ASR affected structures. Focusing on the global behavior of a structure affected by ASR, some macro-models are collected here.

A macroscopic AAR model developed within the framework of a smeared fixed crack finite element approach is presented by (Farage, Alves, & Fairbairn, 2004). The model is based on the following assumptions: uncoupling between stress and AAR gel formation; anisotropic behavior represented by means of a smeared crack approach. As a simplification, free expansion was considered as isotropic. Reaction kinetics is given as input data representing the gel expansion evolution in relation to time. This model was able to simulate laboratory tests performed at LCPC-France concerning reactive concrete

samples under constant uniaxial loading. However, the representation of free expansion could be improved, it is overestimated herein due to the consideration of isotropic behavior in the absence of external stresses or restrains. Further studies concerning the coupling between stresses and AAR should be developed to extend the model application to structures under more sophisticated loading and boundary conditions.

A smeared rotating crack model is proposed by (Ferche, Sheikh, & Vecchio, 2017). The Modified Compression Field Theory (MCFT) and the Disturbed Stress Field Model (DSFM) form the theoretical basis for the model. ASR expansion is treated as an offset strain, evaluated in an iterative manner in the first load stage of the analysis. As to the degradation of mechanical properties, two options are available. One alternative consists of directly using the value of the tested material properties in the analysis. The other option evaluates the compressive and tensile strengths, and the modulus of elasticity, as a function of the free expansion based on the (ISE, 1992) prescriptions. The load-deformation response is simulated, the input values of concrete properties are determined as explained above. The ultimate loads were estimated reasonably well, but the computed responses overestimate the initial stiffness of the reactive beams. There are some limitations found in this model. Due to anisotropic expansion, reductions in concrete mechanical properties are non-uniform in principal directions, while it was not accounted for in this model. Bond degradation is expected to occur as a result of ASR, but this issue is not addressed. The confinement effect caused by transverse reinforcement in beams is also not included.

Table 2 ASR modelling from literature

Reference	Anisotropic behavior	Induced stresses due to restraint
(Farage, Alves, & Fairbairn, 2004)	No	No
(Ferche, Sheikh, & Vecchio, 2017)	No	No

#### 3 Model introduction

#### 3.1 Introduction

The present report deals with the modelling of a beam according to the Finite Element Method, using the software ATENA 2D v5.

The present beam is simply supported and loaded, between the supports, by two point-loads. The reason for choosing this four-point bending model is explained in previous introduction chapter.

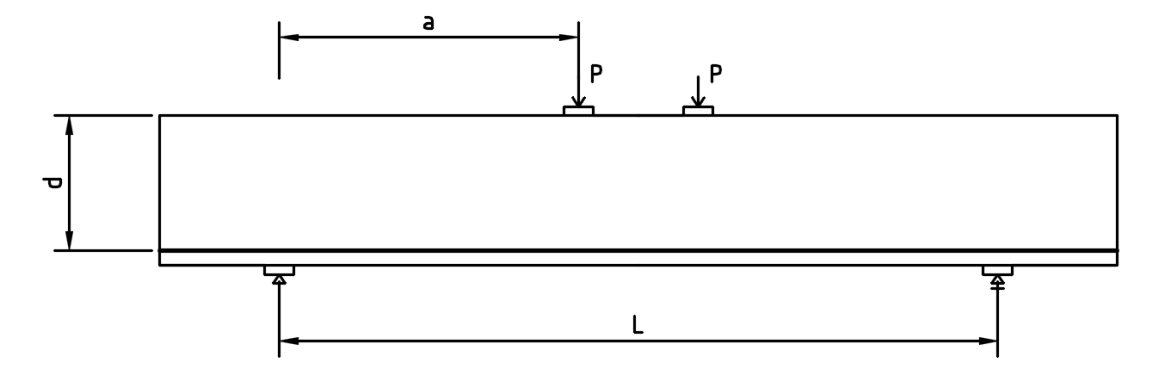


Figure 18 Basic model with reinforcement

#### 3.1.1 Boundary conditions

Due to the symmetry of both structure and load, it is possible to consider only half of the entire beam. In the analysis, just the left half is considered. In order to satisfy the symmetry, appropriate boundary conditions must be applied. The mid-vertical axis is constrained horizontally, and the left end support is modelled as a sliding support in order not to over constrain the structure with a hinge.

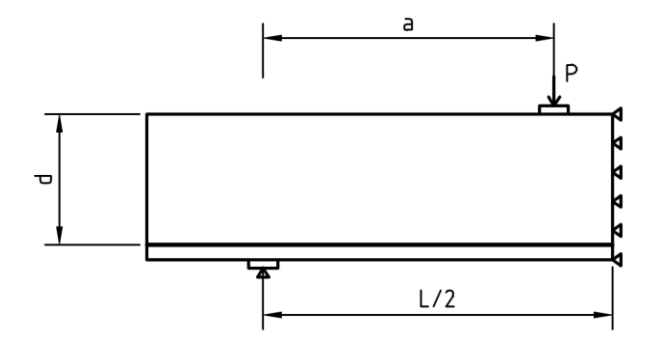


Figure 19 Boundary conditions for the left half with reinforcement

#### 3.1.2 Load

#### 3.1.2.1 Displacement control

In the displacement control analysis, the beam is loaded by two prescribed displacements each applied on the mid-point of the upper steel plate. To attach a displacement, it is necessary to attach a support in the direction of the load and then attach the prescribed displacement in the same direction. These displacements are no longer degrees of freedom. In this case, the reference load is directed downward.

#### 3.1.3 ASR layer modelling

It is important to model the reduced material properties of ASR layers properly to get a more precise structural behavior. From previous experiments, ASR has a great influence on Young's modulus, tensile strength and fracture energy.

A single concrete element under prescribed displacement is investigated here to get an impression of how reduction of material properties will affect its behavior.

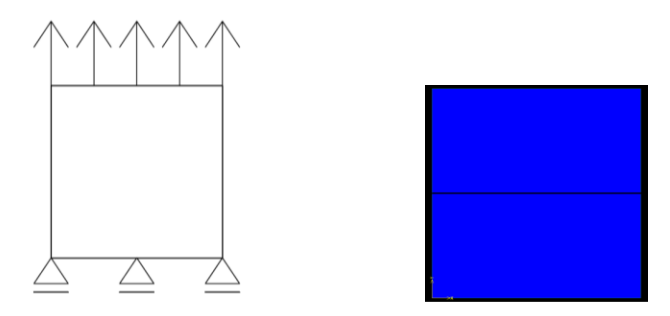


Figure 20 Structural schematic diagram (left) and damage image (right)

Tuote E Maure tun properties					
Number	Ec (MPa)	ft (MPa)	Gf (MN/m)		
1	30000	2.3	5.80E-05		
2	10000	2.3	5.80E-05		
3	10000	0.8	5.80E-05		
1	10000	0.8	1 00F 05		

Table 3 Material properties

Force displacement curves for the above four sets of concrete properties are shown in Figure 21. Reduction of Young's modulus will cause a less steep curve before the peak, which means the material is less stiff. Reduction of tensile strength gives a lower peak force; the load capacity of the material is reduced in this case. Fracture energy displays the area under the stress-strain curve, when fracture energy is reduced, a more concave softening part is displayed.

These curves clearly show the behavior of concrete with different properties. To model the ASR layers properly, it is safe to say that Young's modulus, tensile strength as well as fracture energy should be taken into consideration.

Experimental results show a scatter in material properties. From (ISE, 1992), splitting tensile strength and elastic modulus goes down to 0.4 and 0.35 of the sound values respectively at the expansion rate of 0.5%. From (Esposito, 2016), the lower bound of tensile strength affected by ASR is about 0.6, while Young's modulus can go to 0.2 of its initial value. Some experimental results also mentioned that the reduction on material properties of concrete due to ASR are much larger than the reduction in flexural or shear strength of the beams, so the variation between assumption value and the real value probably will not cause a large difference to the structural behavior. Without a specific case, an easy way in calculation to consider these parameters is to assume them reducing in the same proportion. Therefore, in the following analysis, these properties are assumed to reduce in the same proportion.

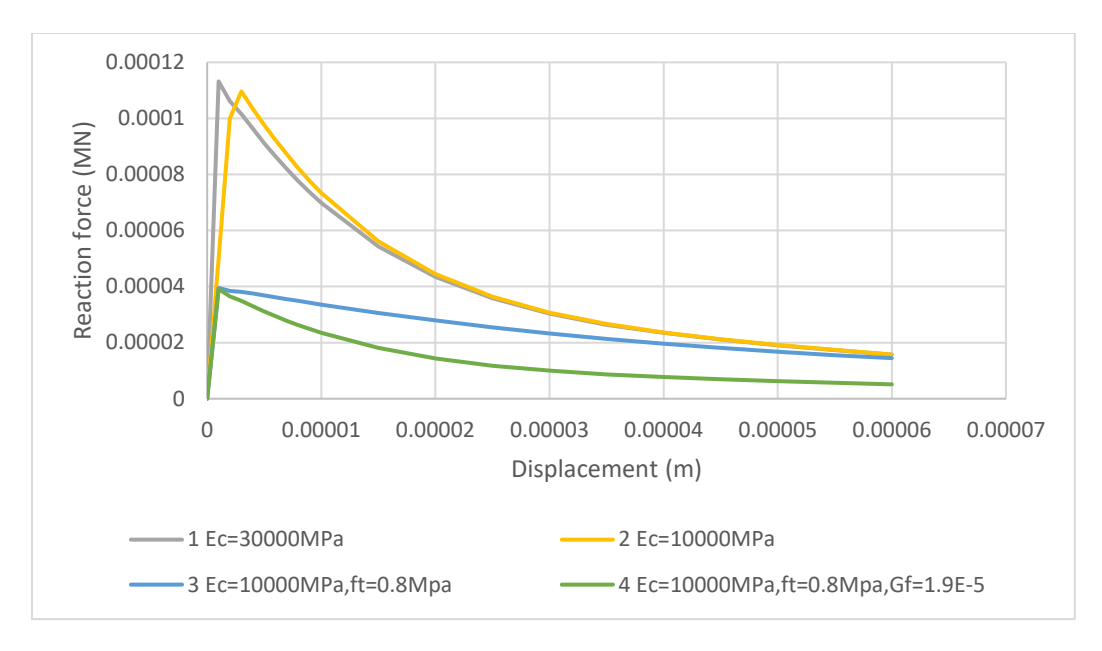


Figure 21 Force-displacement curves

#### 3.1.4 Model parameters defined in ATENA

#### 3.1.4.1 Concrete constitutive model

In this study, SBeta material model is used for concrete.

The material model SBETA describes the concrete behavior as following (Cervenka, Jendele, & Cervenka, 2016):

- 1) Nonlinear behavior in compression, including hardening and softening;
- 2) Fracture of concrete in tension based on the nonlinear fracture mechanics;
- 3) Biaxial strength failure criterion;
- 4) Reduction of compressive strength after cracking;
- 5) Tension stiffening effect;
- 6) Reduction of the shear stiffness after cracking (variable shear retention);
- 7) Two crack models: fixed crack direction and rotated crack direction;

Cubic strength of concrete is taken as an input. Fracture energy is calculated according to CEB-FIP Model Code 2010. Most of the other parameters are generated according to CEB-FIP Model Code 1990. To simplify the following calculation, Young's modulus for sound concrete is taken as 30000 MPa. An example of SBeta material is shown below in Table 4.

Table 4 SBeta material example(sound concrete)

#### Sbeta Basic fcu 30 MPa Elastic modulus E 30000 MPa Poisson's ratio 0.2 2.4 MPa **Tensile strength ft** Compressive strength fc -25.5 MPa

Tensile		
Type of tension softening	Exponential	
Fracture energy Gf	5.80E-05	MN/m
Crack model	Fixed	
Compressive		
Compressive strain at compressive strength in	-1.68E-03	
EPS_C		
Reduction of compressive strength due to cracks	0.8	
Type of compression softening	Crush band	
Critical compressive displacement wd	-5.00E-04	m
Shear		
Shear retention factor	Variable	
<b>Tension-compression interaction</b>	Linear	

Table 5 shows the material properties according to Model Code.

Table 5 Material parameters according to Model Code

Parameter	Formula
Cylinder strength (MPa)	$f_c^{'} = -0.85 f_{cu}^{'}$
Tensile strength (MPa)	$f_t' = 0.24 f_{cu}'^{2/3}$
Initial elastic modulus (MPa)	$E_c = (6000 - 15.5 f_{cu}) \sqrt{f_{cu}}$
Poisson's ratio	$\nu = 0.2$
Softening compression (mm)	$W_d = -0.0005$
Type of tension softening	Exponential
Reduction of compressive strength due to cracks	c=0.8
Shear retention factor	Variable
<b>Tension-compression function type</b>	Linear
Fracture energy (N/m)	$G_f = 73 \cdot f_{cm}^{0.18}$

The uniaxial stress-strain diagram for concrete is shown in Figure 22. In compression, the stress-strain curve goes linear in the beginning. Before reaching the maximum compressive strength, it increases gradually. After the maximum compressive strength, stress decreases linearly in the softening part. Concrete crush occurs at the ultimate strain  $\varepsilon_d$ . In tension, the stress-strain curve goes linearly until maximum tensile strength. Afterwards, the it decreases exponentially.

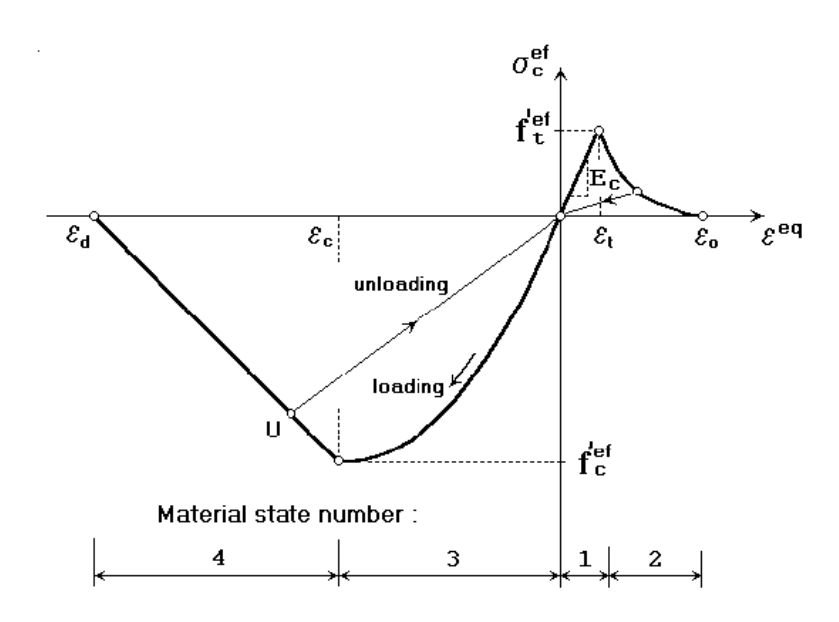


Figure 22 Uniaxial stress-strain law for concrete (Cervenka, Jendele, & Cervenka, 2016)

The biaxial stress failure criterion is used as shown in Figure 23. Cracking occurs when principal stress lies outside the failure surface of biaxial failure function. Crush occurs when all principal stresses are compressive and lie outside the failure surface.

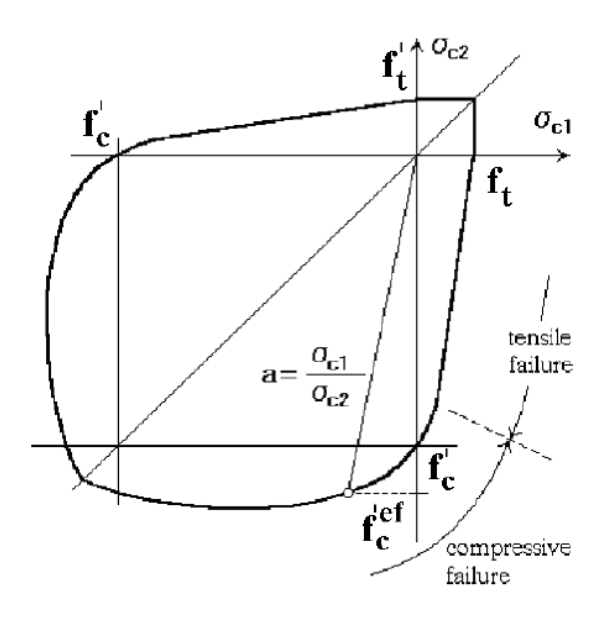


Figure 23 Biaxial failure function for concrete (Cervenka, Jendele, & Cervenka, 2016)

#### 3.1.4.2 ASR layer constitutive model

As stated above, ASR has an unignorable effect on Young's modulus, tensile strength and fracture energy, so these parameters are those need to be paid attention to. The basic material of ASR layers is also SBeta material, but with a proportional reduction of all these three parameters. Other parameters remain the same with sound concrete. An example of ASR layer model is presented in Table 6Error! Reference source not found., with 20000 MPa Young's modulus, 1.6 MPa tensile strength and 3.8E-5 MN/m fracture energy.

Table 6 SBeta material example(ASR layer)

#### Sbeta

Basic			
fcu	30	MPa	
Elastic modulus E	20000	MPa	
Poisson's ratio	0.2		
Tensile strength ft	1.6	MPa	
Compressive strength fc	-25.5	MPa	
Tensile			
Type of tension softening	Exponential		
Fracture energy Gf	3.80E-05	MN/m	
Crack model	Fixed		
Compressive			
Compressive strain at compressive strength in	-1.68E-03		
EPS_C			
Reduction of compressive strength due to cracks	0.8		
Type of compression softening	Crush band		
Critical compressive displacement wd	-5.00E-04	m	
Shear			
Shear retention factor	Variable		
<b>Tension-compression interaction</b>	Linear		

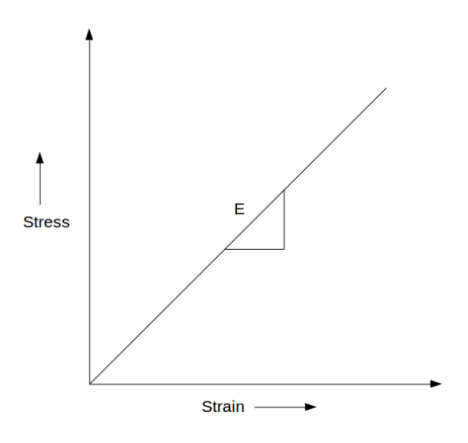
#### 3.1.4.3 Steel plate constitutive model

Steel plates are used for supports and loading points to avoid singularities in models. Each steel plate has the same width as concrete beam, with a thickness of 30 mm. Steel plate model is taken to be perfectly elastic.

Table 7 Steel plate properties

#### Plane stress elastic isotropic

Elastic modulus E	200000	MPa
Poisson's ratio	0.3	



 $Figure\ 24\ Constitutive\ model\ for\ steel\ plate$ 

#### 3.1.4.4 Reinforcement constitutive model

A bilinear model is taken here, with an elastic to perfectly plastic stress-strain relation.

Table 8 Reinforcement properties

#### Reinforcement

Туре	Bilinear	
Elastic modulus E	200000	MPa
Yielding strength	435	MPa

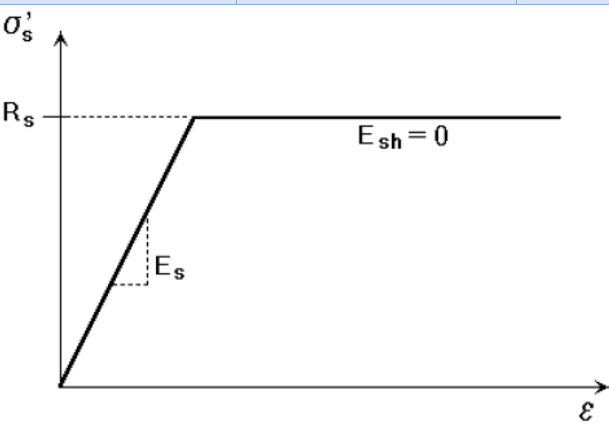
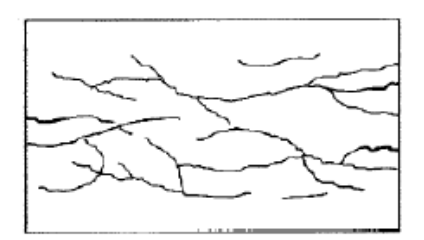
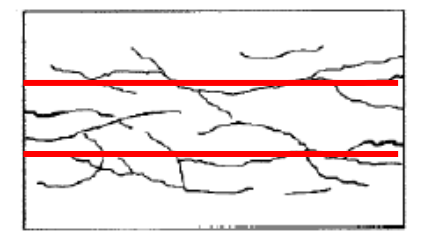


Figure 25 Bilinear stress-strain law for reinforcement (Cervenka, Jendele, & Cervenka, 2016)

#### 3.2 ASR-layered model

In the traditional model from (Ferche, Sheikh, & Vecchio, 2017), a global reduction on material properties is applied to the whole structure. The anisotropic material properties due to ASR could not be presented, this aspect was not accounted for in many other analyses. Restrained expansion and the resulting cracking formation are not considered either. In addition, the induced chemical prestress is totally ignored. Without considering the possible beneficial influence of ASR cracks and chemical prestress, the increase of load capacity and change of failure mechanism could not be observed with this traditional model.





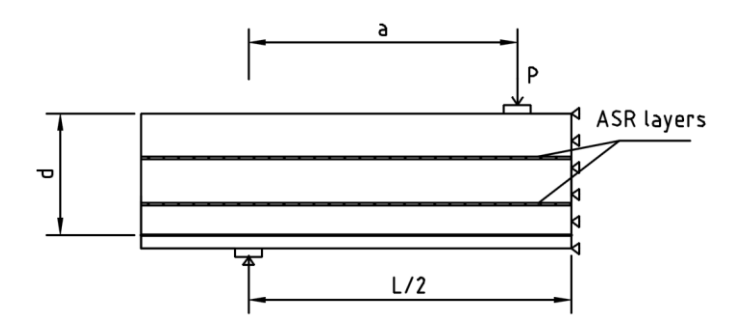


Figure 26 Restrained ASR affected structure (top left), model replacing ASR cracks with horizontal layers (top right),

ASR-layered model (bottom)

With the presence of longitudinal reinforcement, the restrained expansion is reduced from the free expansion value. Instead of occurrence of map cracking in case of no restraint, the restrained cracks are mostly oriented parallel to the reinforcement. The reinforcement is stressed in tension and the concrete is stressed in compression, this is the chemical prestress effect induced by ASR.

These restrained ASR cracks on surface tend to form potential long cracks along the horizontal direction. Taking this local property reduction into account, the ASR cracks could be modelled by introducing layers in the structure. These ASR layers are modelled in small elements representing cracked parts in concrete. The reason for not using an interface is due to the ASR expansion, these layers are swelling part in reality, but not ideally thin layers without thickness. With only material property reduction in the ASR layers, the local property reduction as real structure is applied. The horizontal layers parallel to reinforcement indicate the restrained crack formation.

In this thesis, the ASR-layered model is proposed. The ASR affected structure is modelled by applying the horizontal ASR layers in the sound model. The property reduction caused by ASR is assumed to concentrate in these layers, while the other part of the structure remains unaffected sound property. As for chemical prestress, an initial steel strain is added to reinforcement as a simulation of this effect. In the following experiment simulation (Ahmed, Burley, & Rigden, 1998), the researchers measured the steel strain before loading, so the applied prestressing level could be obtained from this clue. Without a convenient way to apply ASR expansion, therefore, the expansion caused by ASR is not included in this model, only material reduction and chemical prestressing are considered. The degree of expansion is linked to the hogging deflection of the structure, the neglection of expansion might give an influence on load capacity or failure mechanism.

Table 9 Comparison between traditional model and ASR-layered model

Sheikh, & Vecchio, 2017)  ASR-layered model		
Material reduction	Global	Local
Crack orientation due to restraint	×	V
Chemical prestressing	×	V
Expansion	×	X

# 4 Experiments simulation

In this chapter, several experiments from literature are modelled. Whether this model is capable of modelling the structural behavior of ASR affected structure is investigated.

# 4.1 The static and fatigue strength of reinforced concrete beams affected by alkali-silica reaction-S2-C & S2-A

# 4.1.1 Experiment

This experiment was done by Tarig Ahmed, Eldon Burley, and Stephen Rigden, the paper was published in ACI Materials Journal in 1998 (Ahmed, Burley, & Rigden, 1998). Both sound and ASR-affected concrete beams are tested.

The experimental program used eight rectangular beams cast from one reactive mix (Mix A) and eight cast from a control mix (Mix C). Mix A was the Building Research Establishment mix for investigation into ASR which contains Thames Valley Sand as a reactive aggregate, whereas in Mix C the Thames Valley Sand is partially replaced by 2 mm crushed limestone (dust). The proportion of reactive silica in the combined sand-limestone aggregate was the "Pessimum" proportion so that the reaction was maximized.

All sixteen beams were cast in timber molds. One batch of concrete was required for four beams, and the beams were vibrated externally using a table vibrator. After troweling the concrete surfaces smooth, the beams were covered with polyethylene sheet and left in the laboratory for 24 hours before demolding. After demolding, they were placed in a cold-water tank to cure at 20 C and 100 percent RH for 28 days after which the specimens were placed in a hot water tank at 40 C to accelerate the reaction for 5 months.

Mix type	Cement (OPC)	Water	10 mm lime- stone aggregate	20 mm lime- stone aggregate	Reactive aggregate (Thames valley sand)	2 mm (dust) limestone non- reactive aggregate
Mix A (ASR)	1.00	0.50	1.06	2.14	1.39	_
Mix C (sound)	1.00	0.50	1.06	2.14	_	1.39

Table 10 Details of the ASR mix (Mix A) and the control mix (Mix C) (Ahmed, Burley, & Rigden, 1998)

In the study below, beams S2-C and S2-A are modelled. As a reference for reinforcement bond study, S1-A is also presented. The only difference between S1-A (poor) and S2-A (good) is the anchorage. Force control of 2 kN per step is used in the experiment.

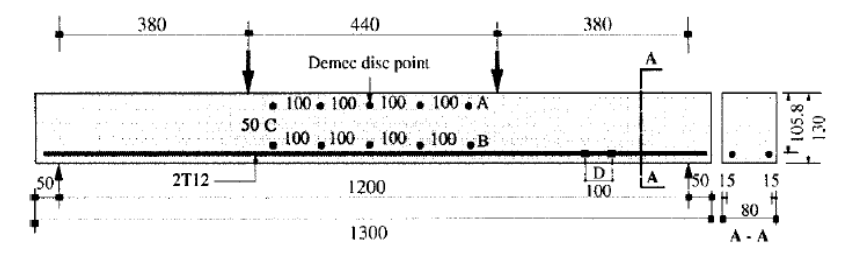


Figure 27 Beam S1, without links and poor anchorage, mm (Ahmed, Burley, & Rigden, 1998)

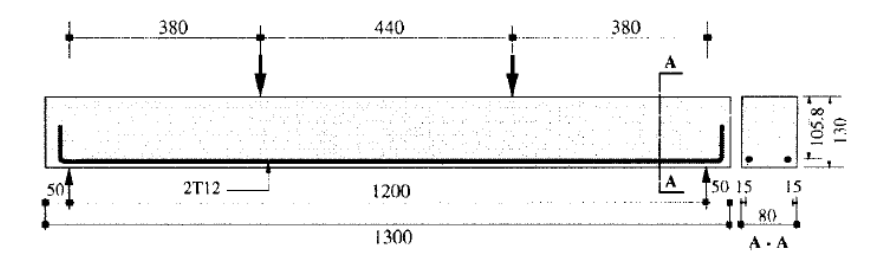


Figure 28 Beam S2, without links and good anchorage, mm (Ahmed, Burley, & Rigden, 1998)

The surface cracking of beam S2-A before test is shown in Figure 29.

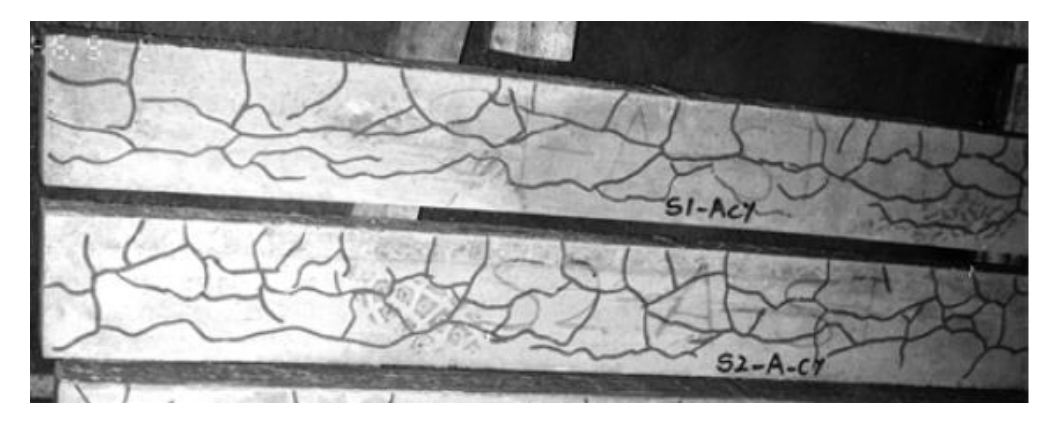


Figure 29 Typical ASR surface cracking for reactive Beam S1-A (top) & S2-A (bottom) (Ahmed, Burley, & Rigden, 1998)

### 4.1.1.1 Geometrical properties

In Table 11 the geometrical properties of the beam are reported.

Dimension	Value	Unit
Height	130	mm
Length	1300	mm
Span	1200	mm
Width	80	mm
Reinforcement height	25	mm

Table 11 Beam S2 dimensions

### 4.1.1.2 Material properties

Mechanical properties of Mix A and Mix C are listed in Table 12. They were measured both in 28 days and in the testing day.

The main difference between sound and ASR mixes are modulus of rupture and water absorption. Modulus of rupture, also known as bending strength, is defined as the stress in a material just before it yields in a flexural test. However, there is no constant factor to convert measured bending strength into direct tensile strength of concrete. The relation of the two values also depends on the fracture energy of the material from Wittmann's research. Therefore, in the following part, the difference of modulus of rupture between the sound and ASR-affected beams were not considered.

Table 12 Mechanical properties of the ASR mix (Mix A) and the control mix (Mix C) (Ahmed, Burley, & Rigden, 1998)

Mix type	Time, days	Compression strength, N/mm²	Indirect tensile strength, N/mm <sup>2</sup>	Modulus of rupture, N/mm <sup>2</sup>	Modulus of elasticity, kN/mm <sup>2</sup>	Water absorp- tion, g
A (ASR)	28	43.50	4.02	6.89	38.60	23.73
A (ASR)	Testing day	55.00	3.90	1.81	27.11	65.67
C (sound)	28	45.30	3.62	5.26	31.38	8.90
C (sound)	Testing day	61.60	4.11	6.37	33.95	7.93

There are also two 12 mm-diameter high-tensile bars in the tension zone. No shear reinforcement exists in these beams.

Table 13 Reinforcement properties

### Reinforcement

Elastic modulus	200000	N/mm²
Yield Strength	460	N/mm²
Reinforcement ratio	2.17%	/

### 4.1.1.3 Experimental force-displacement curve

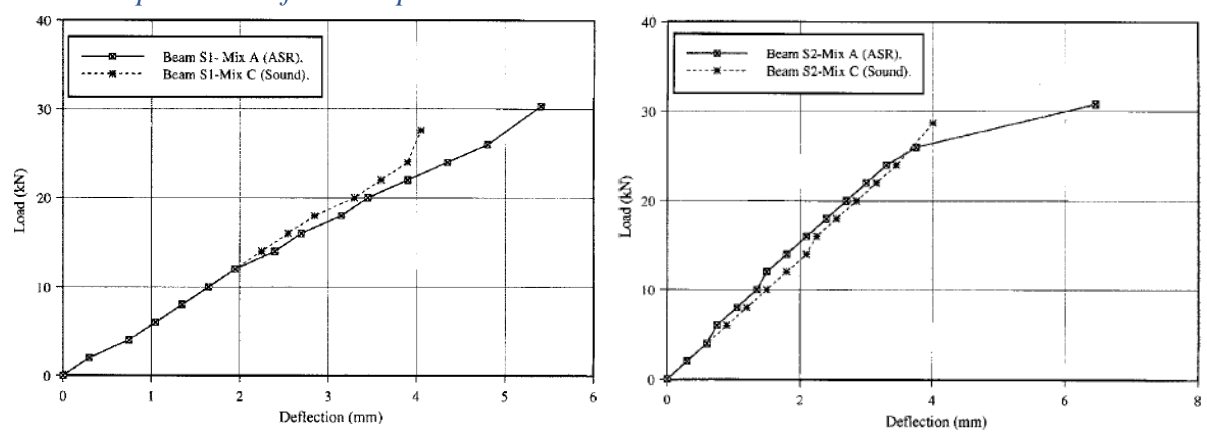


Figure 30 Beam S1-A (left) & S2-A (right) load-deflection diagram from experiment results (Ahmed, Burley, & Rigden, 1998)

Central deflection and ultimate load were measured for the beams. Load-deflection curves were presented above in Figure 30.

Alkali-silica reaction increases the shear capacity of reinforced concrete beams. The authors give an explanation that the beneficial effect of hydration of the cement is greater than the detrimental effect of cracks due to ASR.

The deflection of S2-A was similar to that of S2-C just prior to cracking, whereas at failure, the deflection of S2-A was higher than that of S2-C. The increasing deflection rate just prior to failure for ASR-affected beam suggests that the steel was beginning to yield and the beam, therefore, had reached its maximum load capacity.

One thing worth mentioning is the ASR-affected beam shows a more ductile behavior, more flexural cracks were observed than in unaffected beam. This is also found by (Inoue, Fujii, Kobayashi, & Nakano, 1989), for the case of reinforcement ratio 1.74%, the ASR affected beam failed in flexural with enough ductility while the unaffected one failed in shear and in a brittle manner. The crack pattern and load-deflection curve of this case is shown in Figure 31.

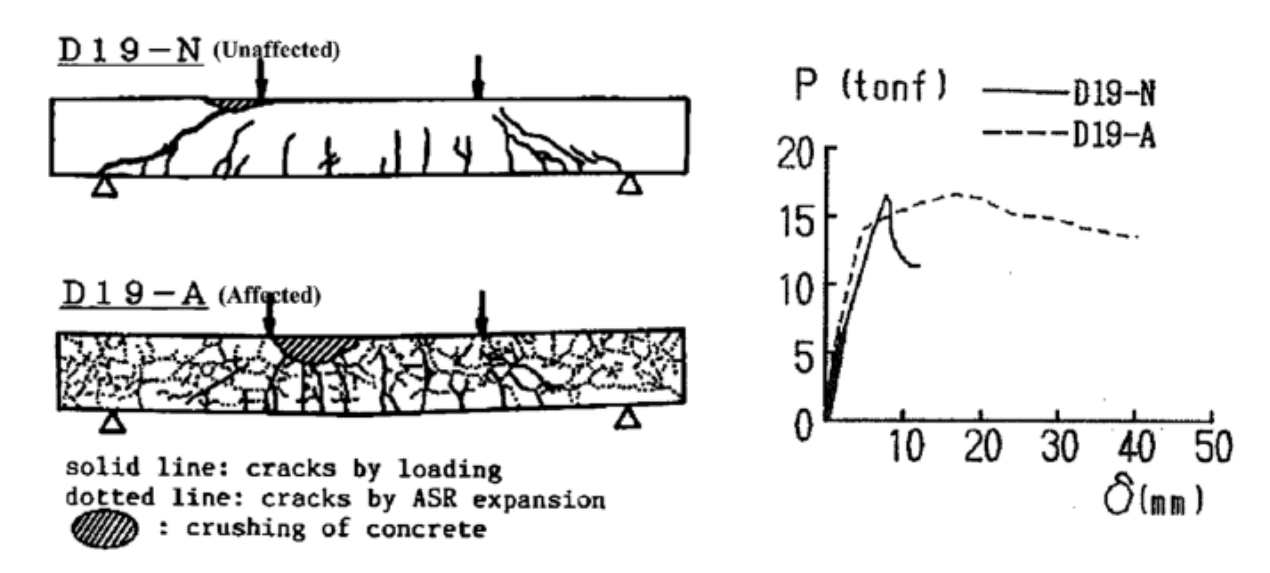


Figure 31 Unaffected beam failed in shear while affected beam failed in bending (Inoue, Fujii, Kobayashi, & Nakano, 1989)

### 4.1.1.4 Experimental failure mode

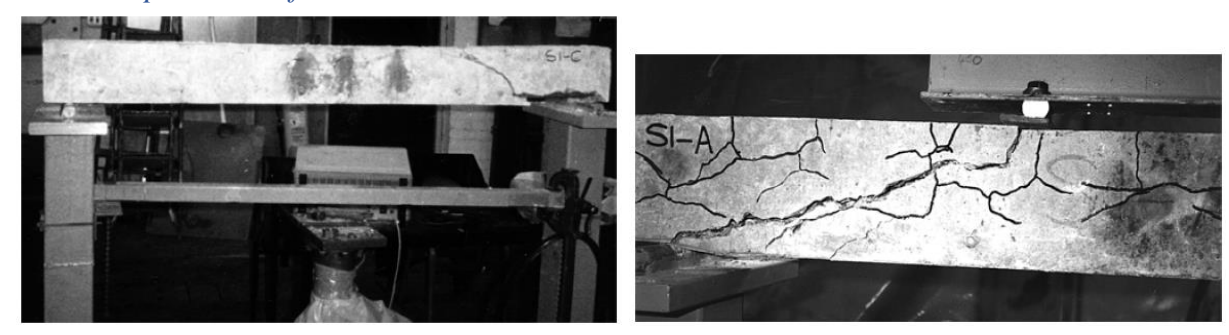


Figure 32 Failure mode S1-C (left) and S1-A (right) (Ahmed, Burley, & Rigden, 1998)

For Beam S1-A the failure occurred violently along the line of the reinforcement, and it appeared to be a bond failure caused by the poor anchorage. S1-C showed a similar failure mode to S1-A, but more flexural cracks were observed in the ASR-affected beam.

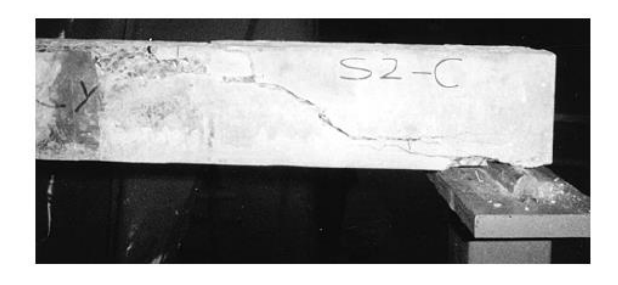




Figure 33 Failure mode S2-C (left) and S2-A (right) (Ahmed, Burley, & Rigden, 1998)

Under static load, a typical shear failure is observed at both beams. In S2-A, the failure cracks pass along an ASR crack for more than half of their lengths. The first shear crack was observed in S2-A and S2-C beams at 70 percent and 60 percent of their ultimate load. More flexural cracks occurred in ASR-affected beam as well.

### 4.1.2 Modelling

### 4.1.2.1 Introduction

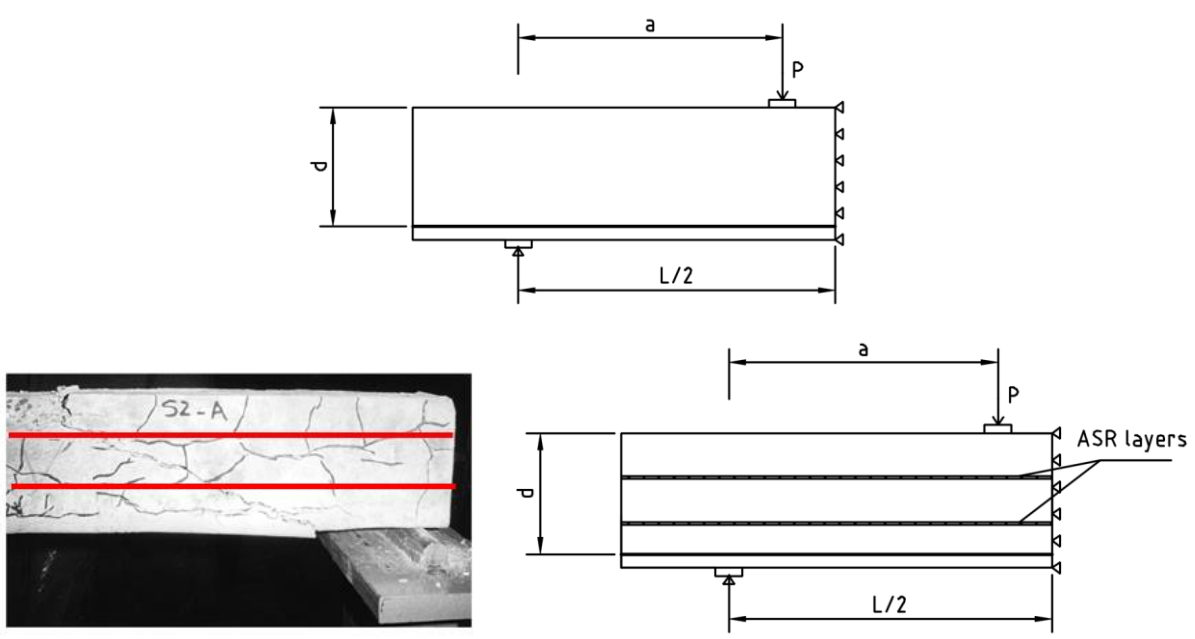


Figure 34 Structural schemes for S2-C (top) and S2-A (bottom right)

To save calculation time, symmetry is used in this case. Above in Figure 34 the structural scheme for beams S2-C (sound beam) and S2-A (ASR-affected beam) are given. From the experimental crack pattern, the ASR cracks in beam S2-A can be roughly assumed as two ASR crack layers. In ATENA analysis, displacement control is used to get a more realistic result.

The material types for concrete and steel are the same as those in previous study, "SBeta Material" for concrete and plane stress elastic isotropic for steel plate. For this specific case, material properties are shown in Table 14.

Table 14 Material properties from experiment

Property	Value	Unit				
Sbeta material (sound concrete)						
Compressive strength	61.6	N/mm²				
Elastic modulus	33950	N/mm²				
Tensile strength	4.11	N/mm²				
Poisson's ratio	0.2*	/				
Fracture energy	150*	N/m				
Plane stress elastic is	sotropic (steel p	late)				
Elastic modulus	200000	N/mm²				
Poisson's ratio	0.3	/				
Reinfor	cement					
Elastic modulus	200000	N/mm²				
Yield Strength	460	N/mm²				
*: Calculated based on Model Code 2010						

A mesh size dependency study could be found in Appendix 6.

Table 15 Mesh size and mesh type

Mesh size	0.005m
Mesh type	Quadrilateral

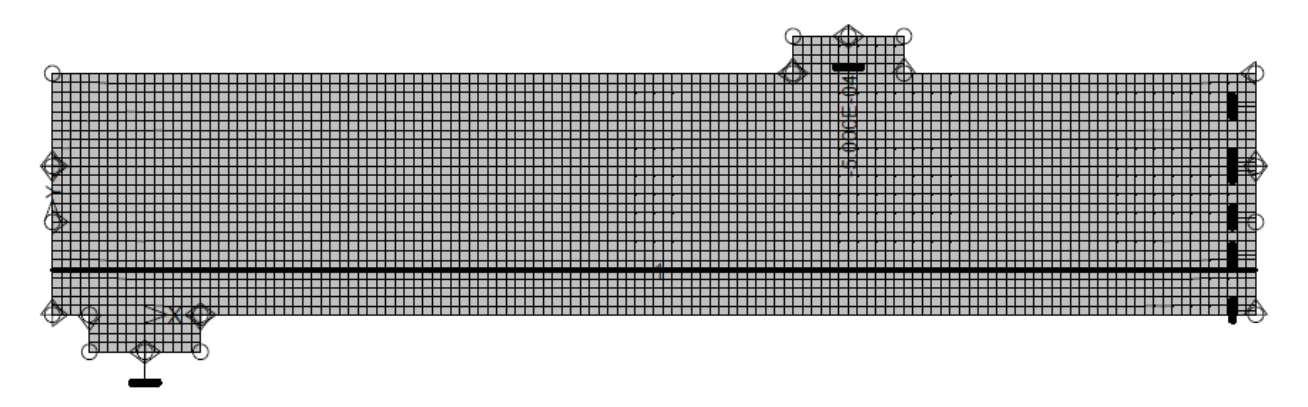


Figure 35 Mesh, load and boundary conditions

# 4.1.2.2 ASR layer modelling

Two layers of 0.005m located in the center of beam is taken as the ASR part. The location of ASR layers and the reduced properties are listed in Table 16 and Table 17.

Table 16 ASR layer locations

ASR layers	Height (mm)	
Layer 1	40-45	
Layer 2	85-90	

Table 17 Sound and ASR-affected properties

	Reduction rate	Ec (MPa)	ft (MPa)	Gf (MN/m)
Sound	1	33950	4.11	1.50E-04
ASR-1	0.9	30555	3.70	1.35E-04
ASR-2	0.75	25463	3.08	1.13E-04
ASR-3	0.5	16975	2.06	7.50E-05

### 4.1.3 Results

### 4.1.3.1 Force-displacement curve

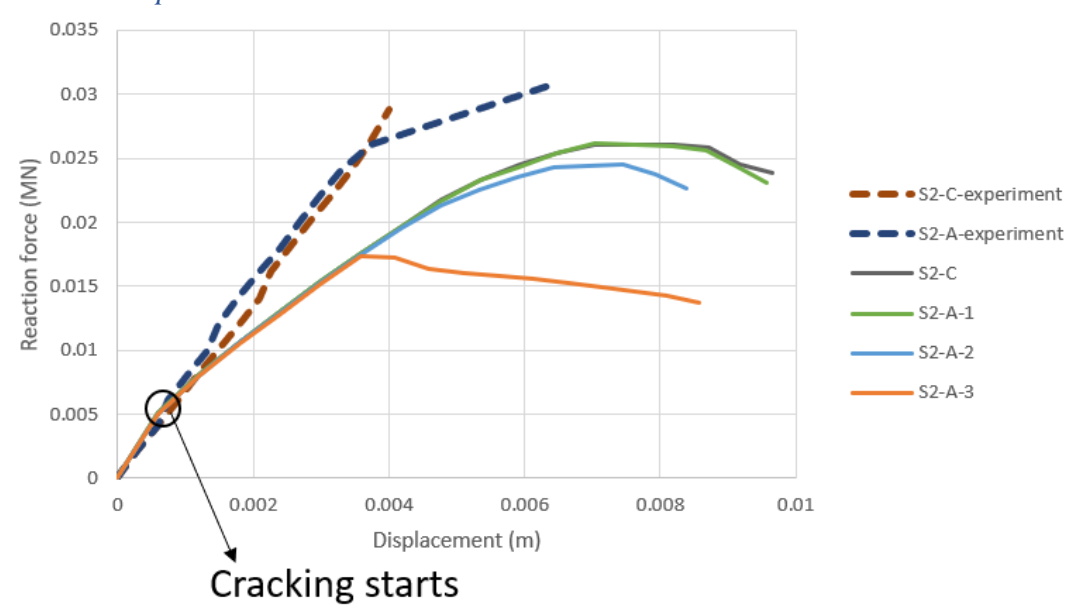
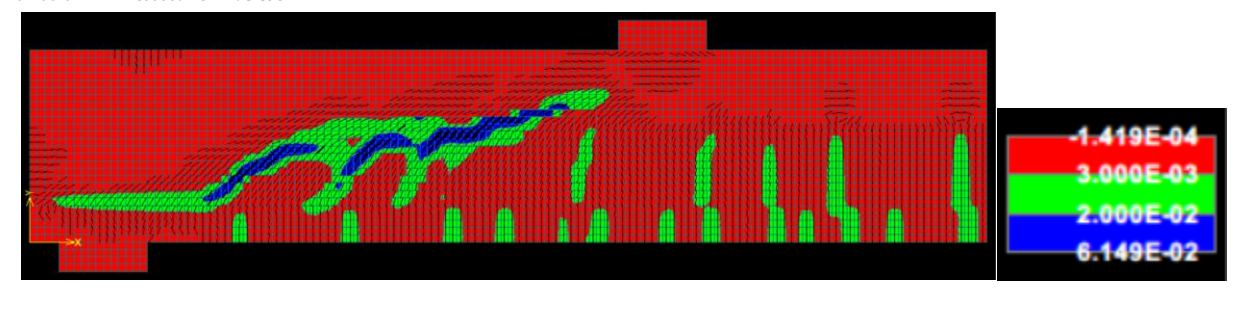


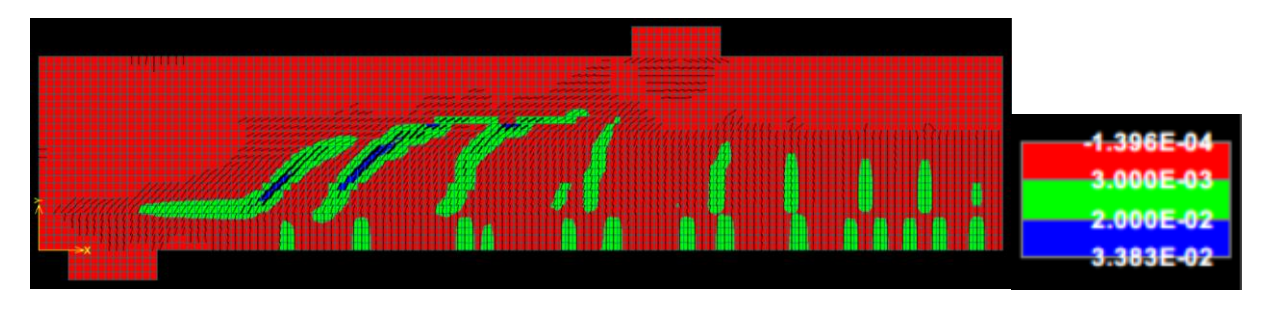
Figure 36 Force-displacement diagram for experimental results and ATENA results in various ASR reduction rates

In experiment results, the curves for sound beam and ASR-affected beam show similar trend in the beginning, which also holds for ATENA results. ATENA results of ultimate load for S2-A-1 and S2-A-2 is slightly smaller than S2-C, which is reverse from experiment. For S2-A-3, the reduction is even larger with the increase of ASR layer property decrease. In this case, material property reduction in ASR layers is 0.9, 0.75 and 0.5 time of the sound properties, in previous analysis it is proved that a small reduction in ASR layers will probably not have a great influence on the ultimate load.

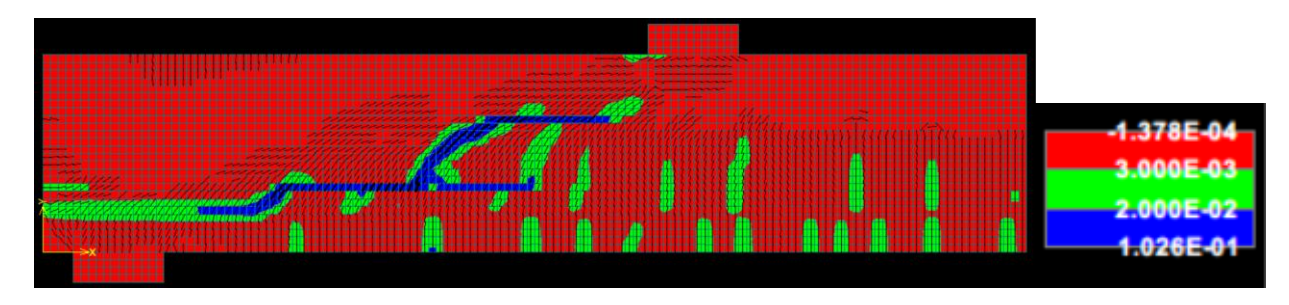
### 4.1.3.2 Failure mode



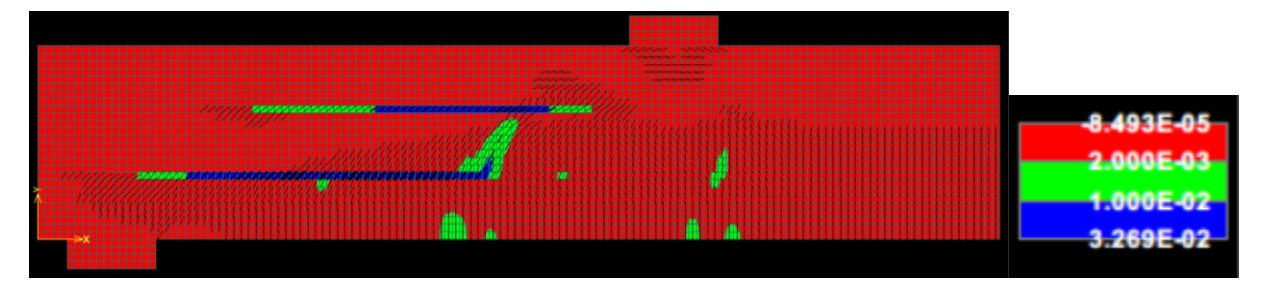
S2-C (shear)



S2-A-1 (shear)



S2-A-2 (ASR-affected shear)



S2-A-3 (ASR layers)

Figure 37 Crack patterns and principal strain patterns from ATENA

All beams fail in shear except S2-A-3, in which ASR layer failure is observed. In other beams, flexural cracks occur in the bottom before the large shear crack is formed. The shear crack in S2-A goes in a more horizontal direction than S2-C, especially when ASR properties are low. When ASR layer properties drop to 0.5 time of the sound property, cracks are concentrated in ASR layers and the diagonal shear crack disappears.

### 4.1.3.3 Discussion

Comparing to experiment results, it is worth noticing that:

1) Beam stiffness is underestimated in ATENA. Decrease of beam stiffness in ATENA analysis is caused by crack formation. However, the expansion of ASR gel already fills in the cracks. The cracks filled with gel are stronger than mechanical cracks filled with air. There might be no or closed cracks in ASR-affected structures. This might compensate for the beam stiffness after occurrence of cracks. This possibility was also stated by (Ahmed, Burley, & Rigden, 1998), the alkali-silica gel may act as a strong filler which increases the shear capacity of the cracks.

- 2) Increase of ultimate load is not observed. In other words, beneficial effects due to chemical prestress and ASR layers are not taken account of.
- 3) This model has the possibility to predict its failure mode when ASR property reduction is not too severe. In this case, the property reduction between sound beam and ASR-affected beam is small (Young's modulus reduction from 33950 MPa to 27110 MPa). However, if ASR layer properties are reduced severely, ASR layer failure might dominate.

### 4.1.4 Optimization

# 4.1.4.1 Parameter study

#### 4.1.4.1.1 Introduction

In this part, various parameters are analyzed to check the influence, including rotated crack model, fracture energy, shear retention factor. The parameters related to concrete are analyzed only on the ASR layers. It is useful to investigate what influence these parameters might cause to the ultimate load and failure mode.

S2-A-2 from previous analysis is taken as a reference. As prestressed model has already changed the failure mode to bending, it is better not to include prestress in this part to clearly see the influence of other parameters. In this parameter study, every time only the parameter to be studied is changed comparing to the reference.

Table 18 Parameter study comparison with reference

	Reference	Parameter study
Crack model	Fixed	Rotated
Fracture energy (MN/m)	1.50E-04	1.50E-05
Shear retention factor	Various	0, 0.1, 1

Fixed crack model is in which the stress-strain relationships are evaluated in a fixed coordinate system which is fixed upon cracking. In a rotated crack model, stress-strain relationships are evaluated in the principal directions of the strain vector.

Fracture energy is the energy required to open unit area of crack surface in concrete.

Shear retention factor refers to the amount of shear transfer across a crack. A shear retention factor of 0 refers to no aggregate interlock, whereas 1 represents full aggregate interlock. Shear retention factor  $\beta$  reduces the shear elastic modulus G to  $\beta G$  upon cracking. The shear stress strain relation with variable and fixed shear retention factor is shown in Figure 38.

$$\tau = \beta G \gamma$$

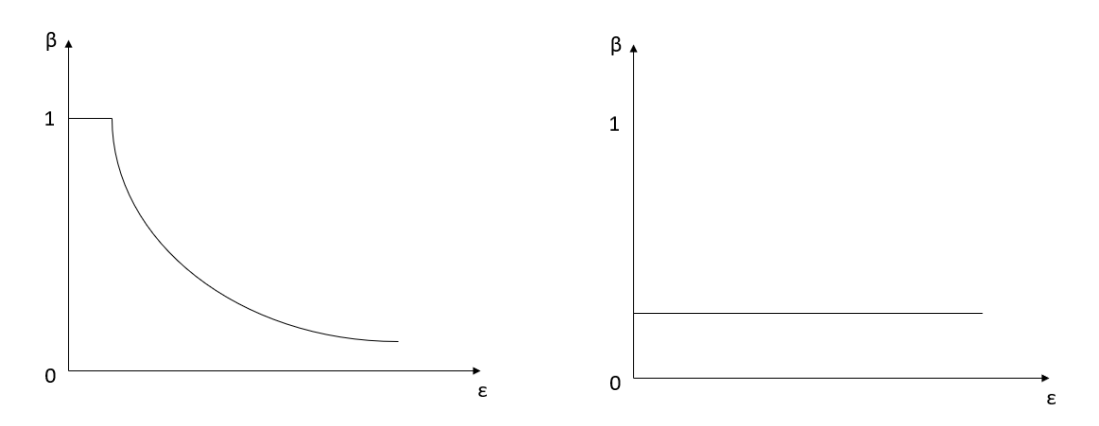
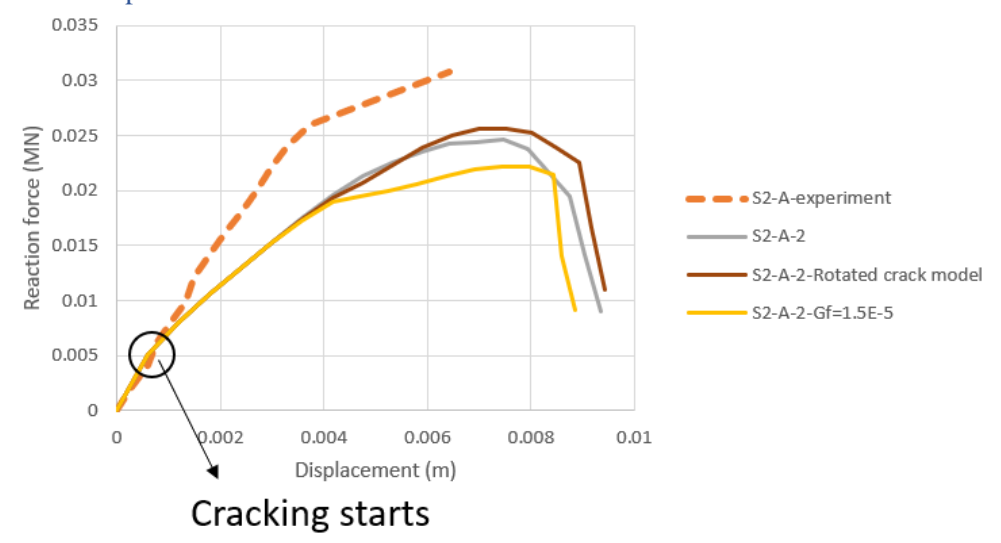


Figure 38 Various (left) and constant (right) shear retention factor description

### 4.1.4.1.2 Force-displacement curve & failure mode



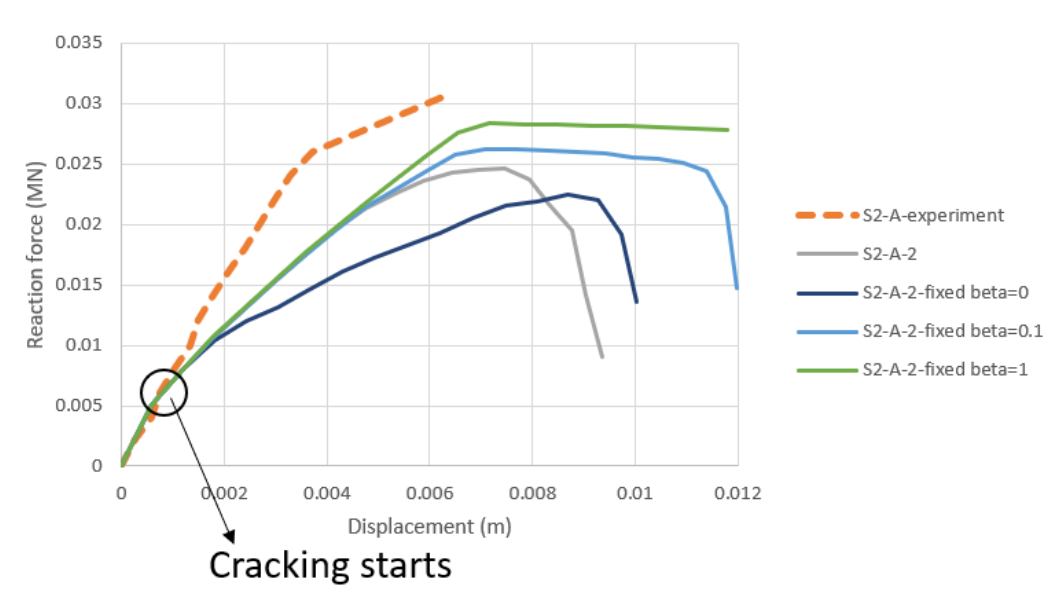
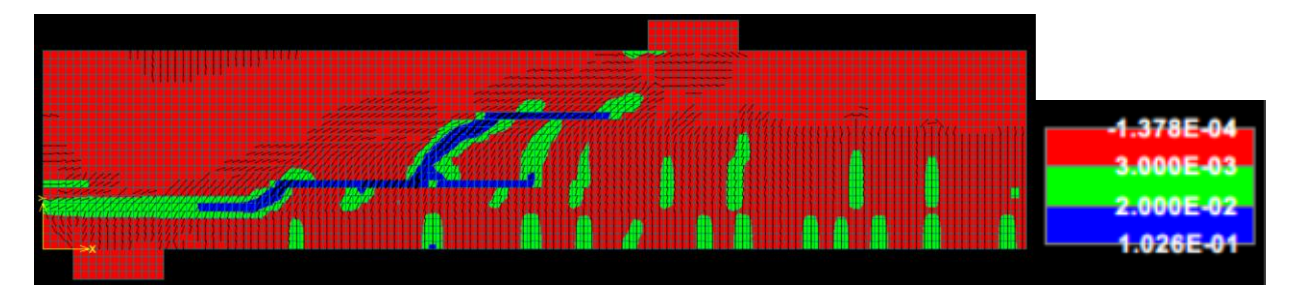
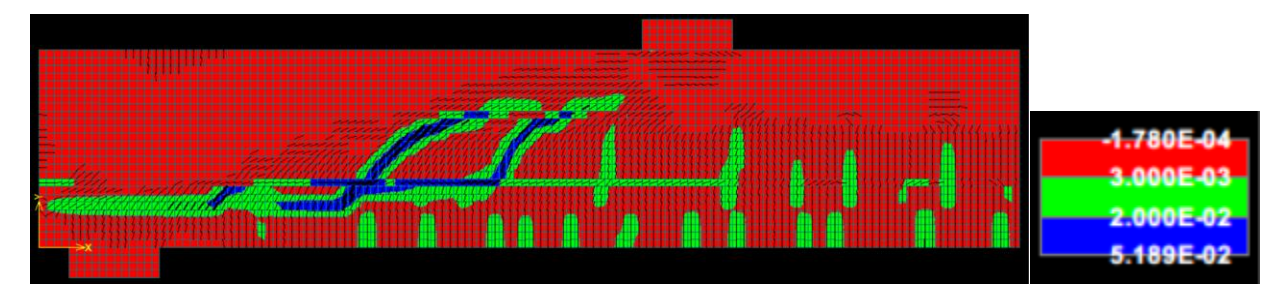


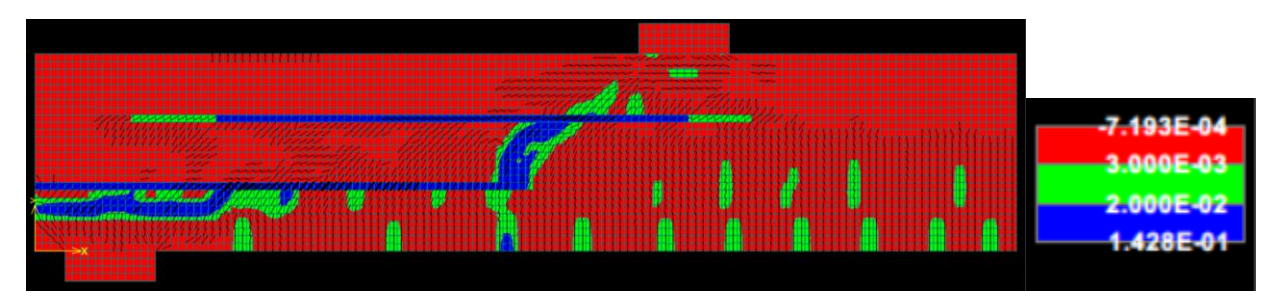
Figure 39 Force-displacement diagram for beams in parameter study (top: fixed and rotated crack model, fracture energy; bottom: various shear retention factor vs fixed shear retention factor)



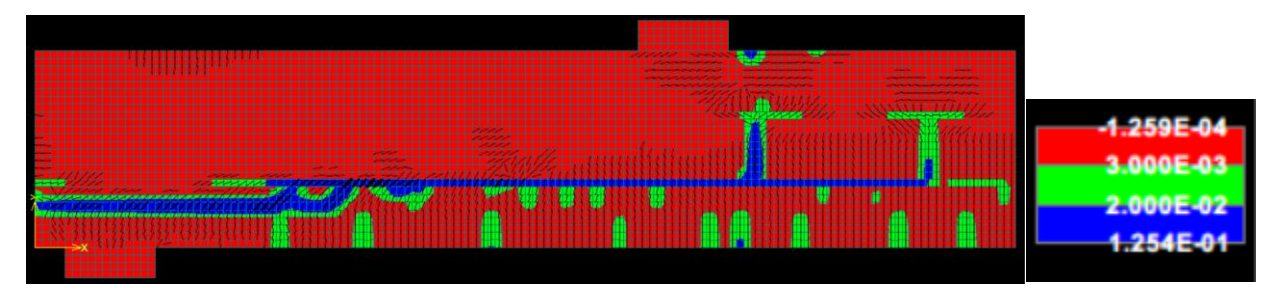
Reference: S2-A-2 (shear)



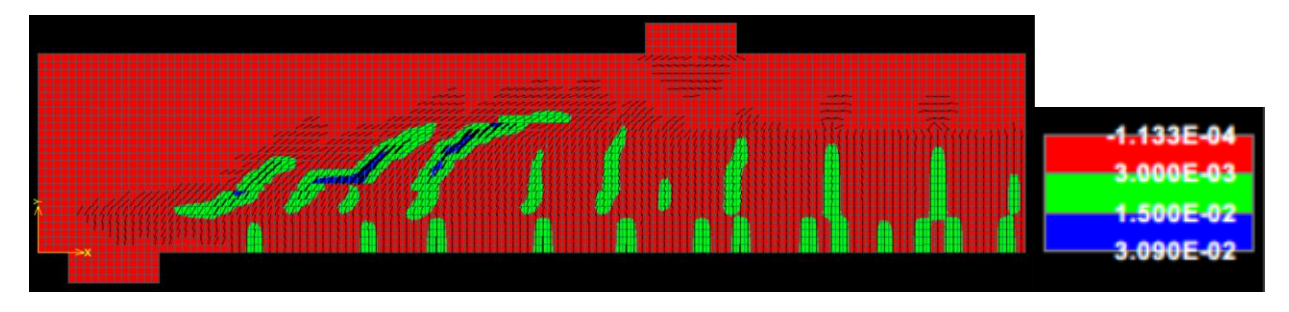
Rotated model (shear)

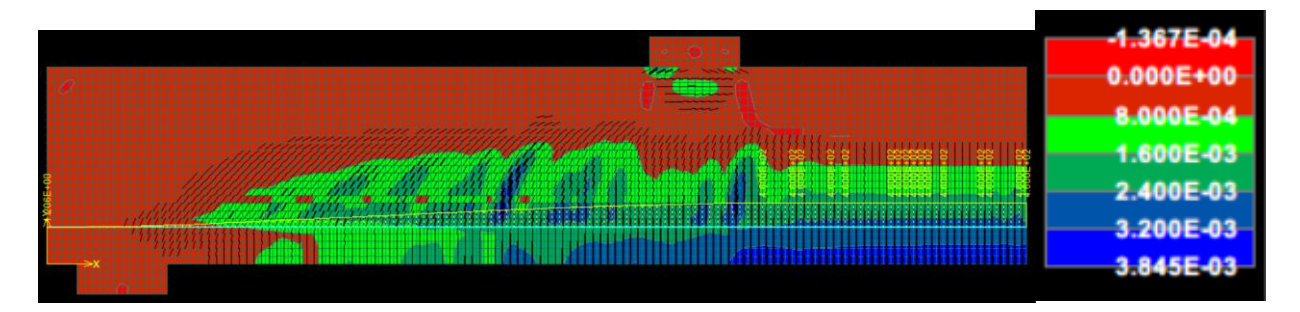


Gf=1.5E-5 MN/m (ASR layer)



Fixed shear retention factor = 0 (ASR layer)





Fixed shear retention factor = 1 (bending, yielding of reinforcement)

Figure 40 Crack patterns and principal strain patterns for beams in parameter study

As can be seen from the force-displacement curves, ultimate load varies, but the beam stiffness is seldom affected by these parameters.

The rotated crack model in ASR layers gives a slightly higher ultimate load than fixed crack model. In fixed crack model, the crack orientation will not change once it occurs. Elastic modulus will keep reducing after cracking. While in rotated crack model, crack direction is always coaxial with the principal strain. This means the ASR layers keep changing the principal strain direction, elastic modulus used to calculate the stress may not necessarily decrease. The increase observed in ultimate load could be explained by this.

As reduction of fracture energy goes into 0.1 time of the reference, ultimate load shows an obvious decrease as well. Cracks are more concentrated in the ASR layers.

In the case shear retention factor equals to 0, the initial stiffness is the same with other beams. The reduction of stiffness after several steps is due to the appearance of a large crack in the upper part of beam. The stress transfer ability in ASR layers are weak due to the very low shear retention factor, thus the reinforcement cannot cooperate with the upper part. If we only look to this part, which has no reinforcement in it, brittle failure occurs here, and the total beam stiffness is also reduced.

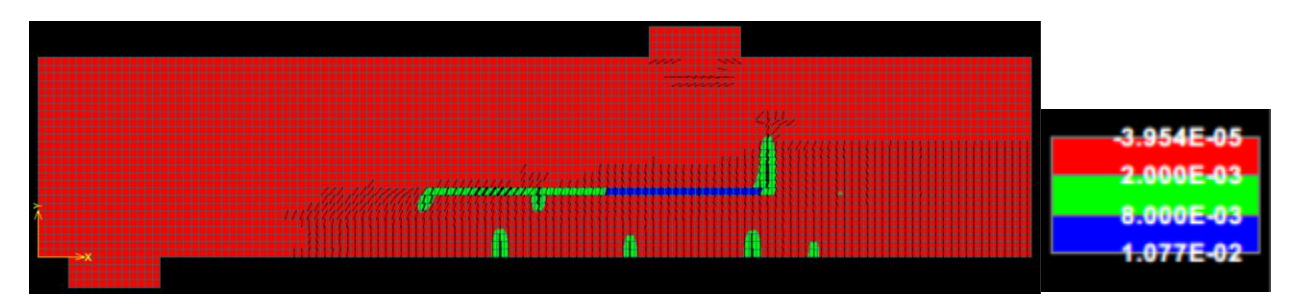


Figure 41 Crack pattern and principal strain pattern for beam with fixed shear retention factor = 0 (step 4)

Change of shear retention factor from 0 to 0.1 to 1 gives an interesting trend, the ultimate load increases, while the failure mode changes from ASR layers to shear failure to bending failure. The behavior of aggregate interlock could be a reason of it. As shear retention factor increases, the stress which concrete can take also increases, comparatively steel becomes the weak part. That's why yielding of steel is observed when shear retention factor equals to 1.

#### 4.1.4.1.3 Discussion

Under comparison, some points are worth mentioning,

- 1) Fixed crack model is a safe way to use. It has the possibility of incorporating shear effects from aggregate interlock models. While rotated crack model accommodates a unique shear term that enforces coaxiality between principal stress and strain, which introduces simplicity, but it inherently abandons the possibility of incorporating different crack shear models (Rots & Blaauwendraad, 1989).
- 2) Decrease of fracture energy results in a weaker part of ASR layers, as well as more concentrated cracks in ASR layers. Ultimate load reduction could be expected.
- 3) An increase of shear retention factor from 0.1 to 1 in ASR layers results in a change of failure mode from shear to bending failure. As shear retention factor refers to the amount of shear transfer across a crack, a higher shear retention factor represents a higher level of aggregate interlock. Considering the expansion of ASR gel fills the cracks, it could be seen as a kind of aggregate interlock. That might explain when comparing a sound beam and ASR-affected beam, a change from shear to bending failure is observed in some cases.
- 4) Only the pretension level and shear retention factor might influence the steepness of the load-deflection diagram, in other words, the beam stiffness.

### 4.1.4.2 Chemical prestress simulation using pretension

#### 4.1.4.2.1 Introduction

From the previous analysis, beam stiffness is underestimated in the nonlinear part, to include the effect of chemical prestress is a possible way to improve. In this part, a simulation of chemical prestress using the measured data from experiment is done.

Chemical prestress is introduced in a reinforced concrete member by expansive concrete overcoming the restraint by steel. In ASR-affected structures, ASR expansion restrained by steel could result in such kind of prestress.

In my study, although expansion is not directly modelled in ATENA, the effect of expansion is applied by adding an initial strain to reinforcement. Pre-tensioning is applied to the normal reinforcement to model the effect of chemical prestressing. Apart from pre-tensioning, all other inputs are kept the same with previous analysis.

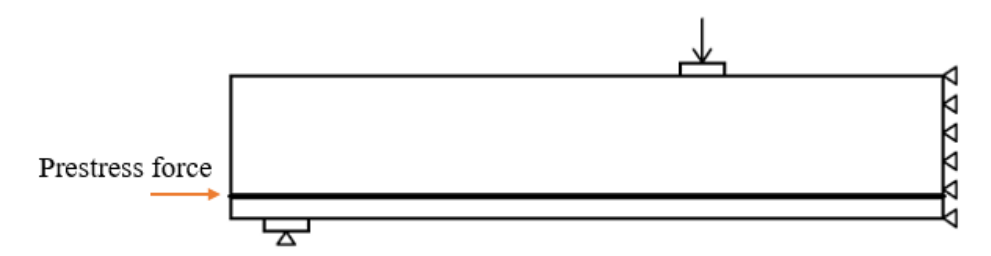


Figure 42 Pretensioned model

In experiment, steel strain is also measured. At the time of testing, steel strains of S2-A and S2-C are  $1511 \cdot 10^{-6}$  and  $119 \cdot 10^{-6}$  respectively. A limit check of the steel strain in S2-C according to RILEM recommendation is done in <u>Appendix 7</u>. The measured small steel strain in sound beam possibly comes from the ongoing hydration of concrete during its 20 weeks curing time. A much larger steel strain in

ASR-affected beam is observed, this can be explained by the chemical prestress induced by the restrained ASR expansion. The effect of chemical prestress can be roughly estimated as the difference between S2-A and S2-C, which is  $1392 \cdot 10^{-6}$ .

The initial steel stress in S2-A due to chemical stress can be calculated as

$$\sigma_s = \varepsilon_s \cdot E_s = 1392 \cdot 10^{-6} \cdot 2 \cdot 10^5 = 280 \text{MPa}.$$

Prestress force applied at reinforcement is

$$F_p = \sigma_s \cdot A_s = 280 \cdot 2 \cdot \frac{1}{4} \pi \cdot 12^2 = 63kN$$
.

As stated in previous chapter, different ASR reduction rates are marked with ASR-1, ASR-2, ASR-3. The beams in this analysis are marked with -pretension to make a difference with previous models without applying prestress.

	Reduction rate	Ec (MPa)	ft (MPa)	Gf (MN/m)
Sound	1	33950	4.11	1.50E-04
ASR-1	0.9	30555	3.70	1.35E-04
ASR-2	0.75	25463	3.08	1.13E-04
ASR-3	0.5	16975	2.06	7.50E-05

Table 19 Sound and ASR affected material properties

#### 4.1.4.2.2 Expansion and hogging

The expansion of unaffected beam S2-C was ignorable after 20 weeks in hot water. While for affected beam S2-A, restrained expansion is observed with the presence of reinforcement. Expansion of beam S2-A is shown in Figure 43. In vertical direction, the expansion was not restrained by reinforcement, so the largest expansion of 0.53% was found. In horizontal direction, the reinforcement restrained the expansion, this effect was stronger in the tensile part (bottom: 0.16%) comparing to the compressive part (top: 0.23%). The expansion resulted in a hogging (upward deflection) of 7 mm. S2-A failed at a deflection of 6 mm, which means at this point, hogging still existed in this beam.

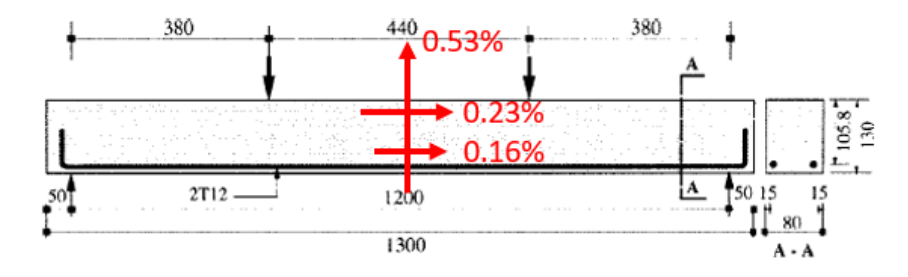


Figure 43 Expansion of beam S2-A measured from test

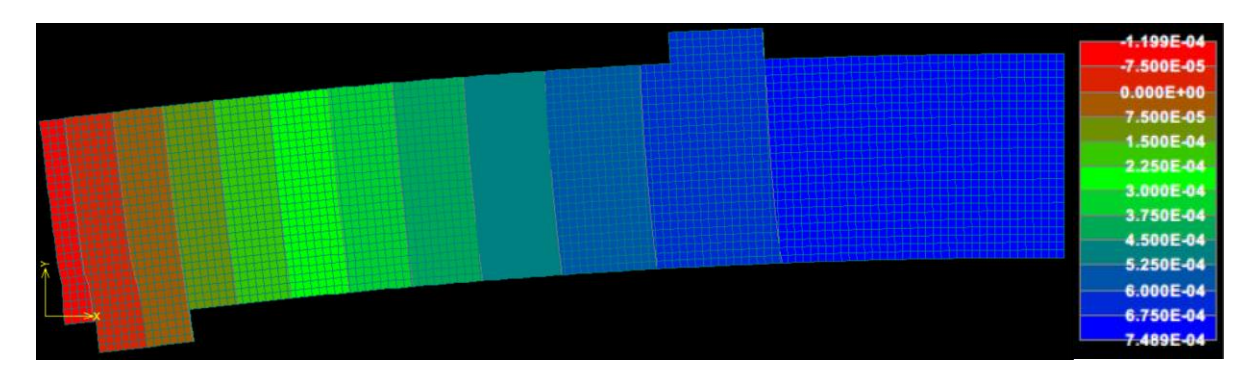


Figure 44 Hogging after applying prestressing

In numerical model, a hogging is also found here. The upward deflection of 0.75 mm is much smaller than measured value 7 mm. (Ahmed, Burley, & Rigden, 1998) found the hogging was largely proportional to the amount of expansion of the beam. Expansion was not directly modelled in this study; therefore, it might lead to this underestimation of hogging.

### 4.1.4.2.3 Force-displacement curve

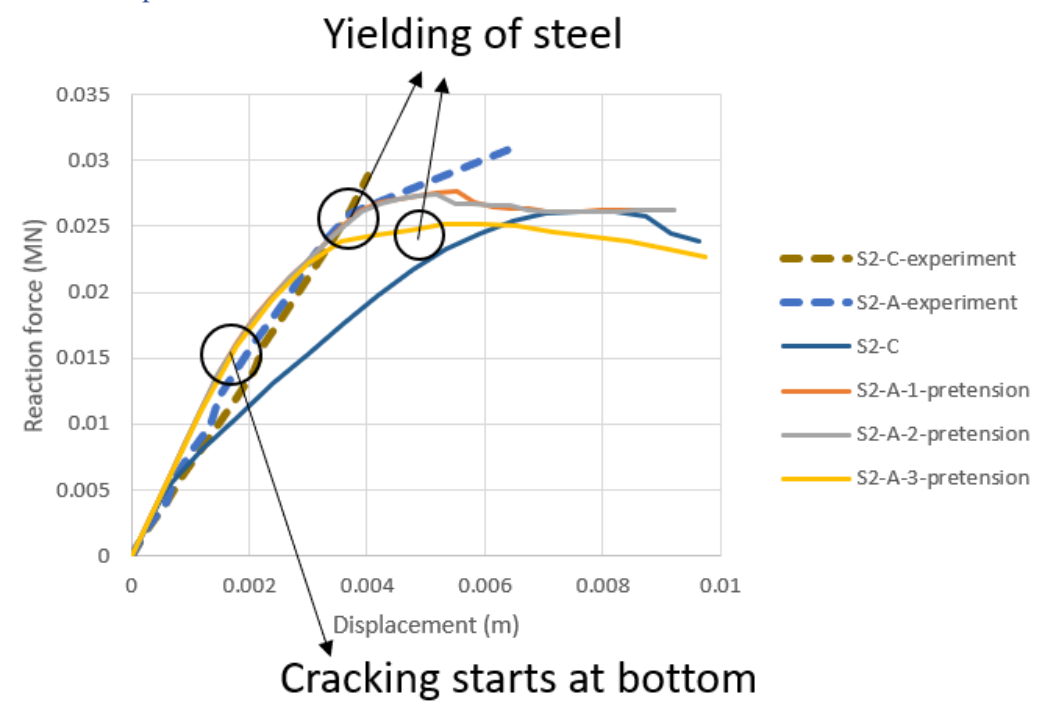


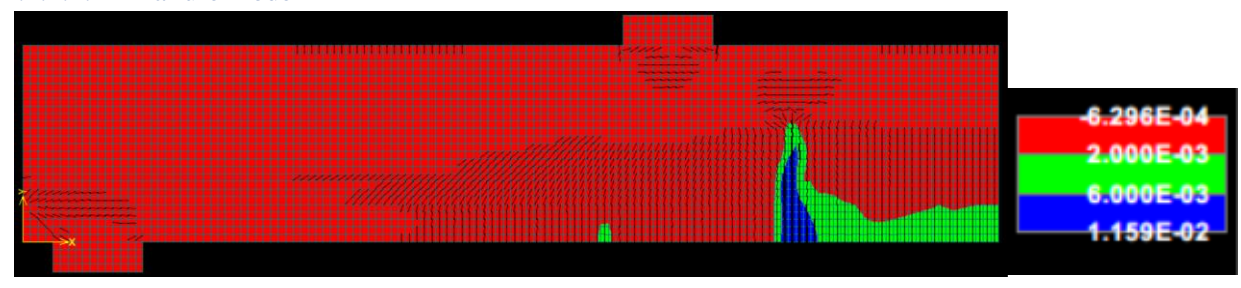
Figure 45 Force-displacement diagram for experimental results and ATENA results with and without pretension

The reduction in ASR layer properties increases from ASR-1 to ASR-3. According to the force-displacement curve, some changes can be noticed,

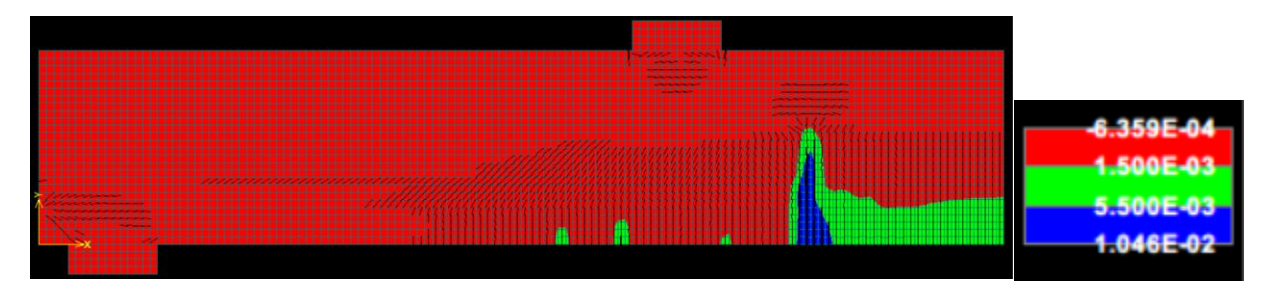
- 1) The stiffness of beam after cracking is increased due to prestressing, it is a good fit comparing with the experimental results. Yielding point of steel is brought forward comparing to models without prestressing.
- 2) A slightly larger ultimate load in two prestressed ASR-affected models than sound model S2-C could be observed. Prestressing gives an advantageous effect to ultimate load.

3) Though a large ASR layer property reduction may cause a huge decrease in ultimate load, this effect is compensated when prestressing is applied.

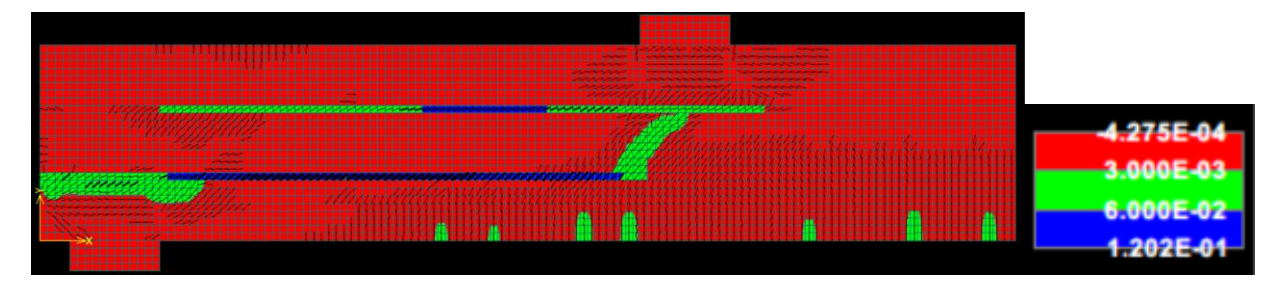
### 4.1.4.2.4 Failure mode



S2-A-1-pretensioned (bending)



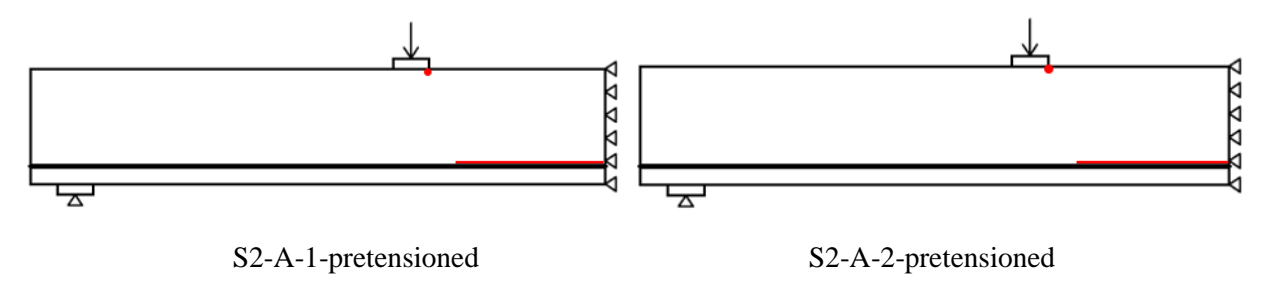
S2-A-2-pretensioned (bending)

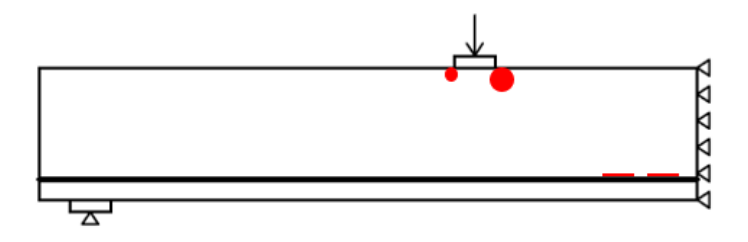


S2-A-3-pretensioned (ASR layers)

Figure 46 Crack patterns and principal strain patterns for beams with pretension

Concrete crush and steel yielding occur in all three beams. Under pretension, failure mode of S2-A-1 and S2-A-2 change from shear to bending, while S2-A-3 fail in ASR layers. The application of prestress result in the earlier failure of beams. The reason behind is, prestress already gives steel an initial strain, so in prestressed models steel will reach the yielding point earlier.





### S2-A-3-pretensioned

Figure 47 Concrete crush and steel yielding of pretensioned beams

#### 4.1.4.2.5 Discussion

Comparing the un-tensioned and pretensioned results, some conclusions can be drawn,

- Chemical prestress cannot just be simply modelled by physical prestress as the failure mode cannot be accurately predicted. Though they both result in the initial tensile strain in steel and compressive strain in concrete, ASR expansion is not modelled, and it will lead to an underestimation of the upward deflection.
- 2) With the measured steel strain, beam stiffness could be better predicted by prestressed model.
- 3) Ultimate load under prestress does not vary a lot under different ASR property reduction rates. A possible increase in ultimate load could be seen in ASR-affected model comparing to unaffected one.
- 4) The bond between reinforcement and concrete could be further studied to investigate whether it affects the change of failure mode.

### 4.1.4.3 A close look at pretension

### 4.1.4.3.1 Introduction

From the previous analysis, the prestress level calculated from measured steel strain could increase beam stiffness, but it also changes the failure mode. The actual chemical prestress might be lower than the applied physical prestress.

In the analysis without pretension, S2-A-2 could give a comparatively good result both in ultimate load and failure mode. So, we take S2-A-2 as a reference.

The yielding strain of reinforcement can be easily calculated as

$$\varepsilon_{v} = \sigma_{v} / E_{s} = 460 / 200000 = 0.23\%$$

According to the experiment, the measured steel strain due to chemical prestress is about 0.14%. As we apply this effect directly using physical prestress, it seems to be too much as it already changes the failure mode of the beam while it should not. Therefore, a series of physical prestressed beams at different levels are analyzed. If we can find a similar result, then physical prestress might be able to simulate chemical prestress in some aspects.

In some experiments where a change of failure mode is observed, chemical prestress and presence of ASR cracks are the two possible reasons. Therefore, a sound beam with prestress is also modelled here to help figure out where the possible change of failure mode comes from.

Table 20 Beams with various pretension levels

	Initial steel strain	Pretension stress (MPa)	Prestress force (MN)
	1.5E-04	30	6.8E-03
	7.5E-04	150	3.4E-02
S2-A-2	1.0E-03	200	4.5E-02
	1.3E-03	250	5.7E-02
	1.4E-03	280	6.3E-02
S2-C	1.5E-04	30	6.8E-03
	7.5E-04	150	3.4E-02

# 4.1.4.3.2 Force-displacement curve & failure mode

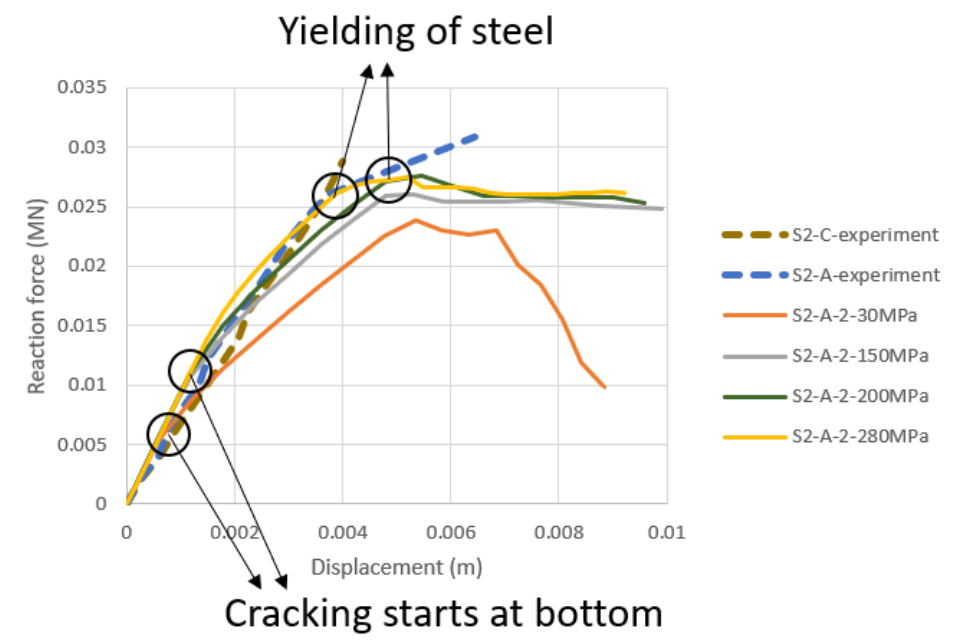
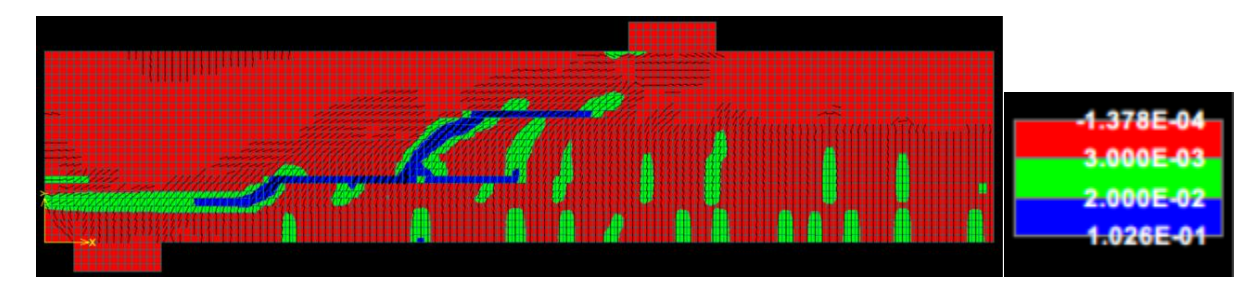
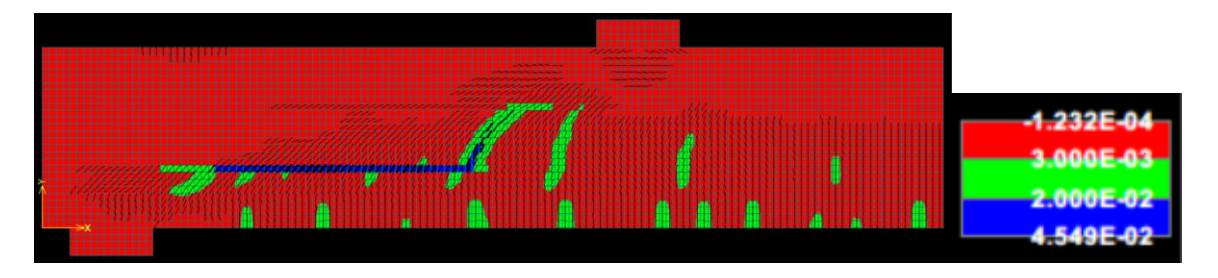


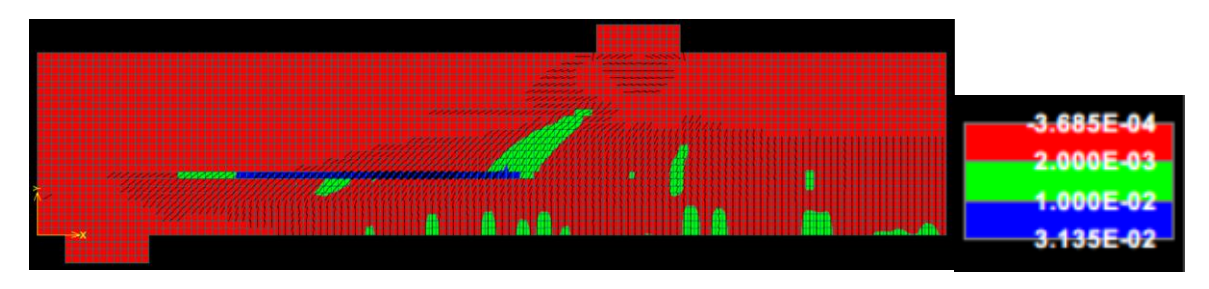
Figure 48 Force-displacement diagram for experimental results and ATENA results with different pretension levels



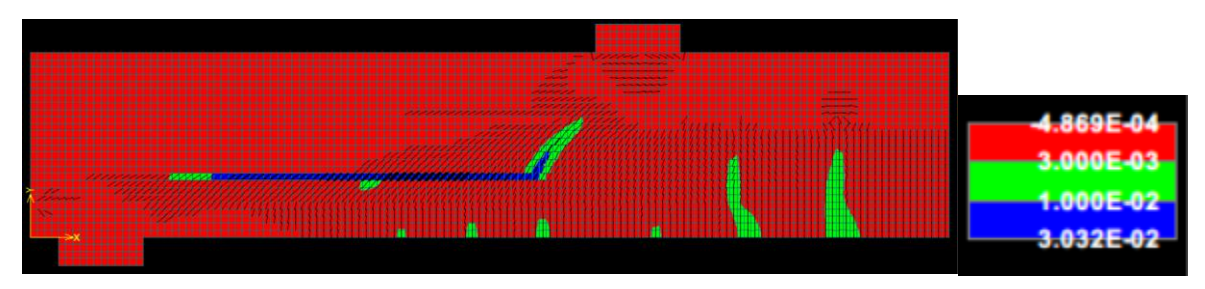
Reference: S2-A-2 (ASR-affected shear)



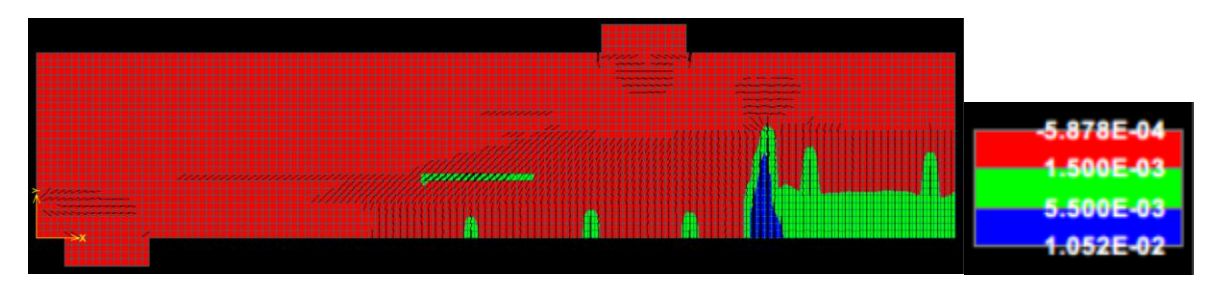
S2-A-2-30MPa (ASR layer)



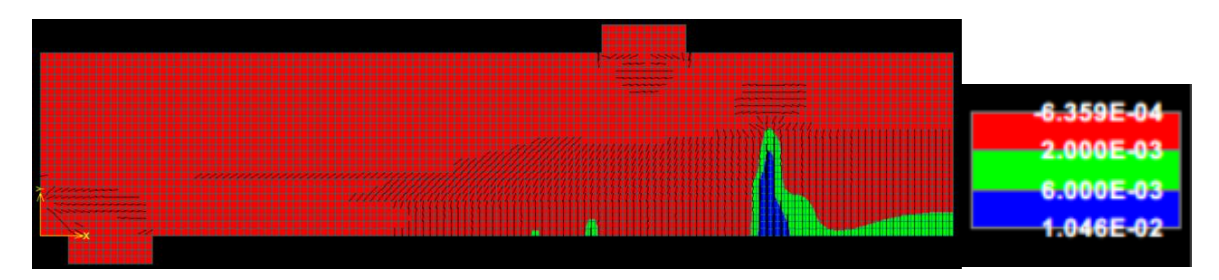
S2-A-2-150MPa (ASR layer)



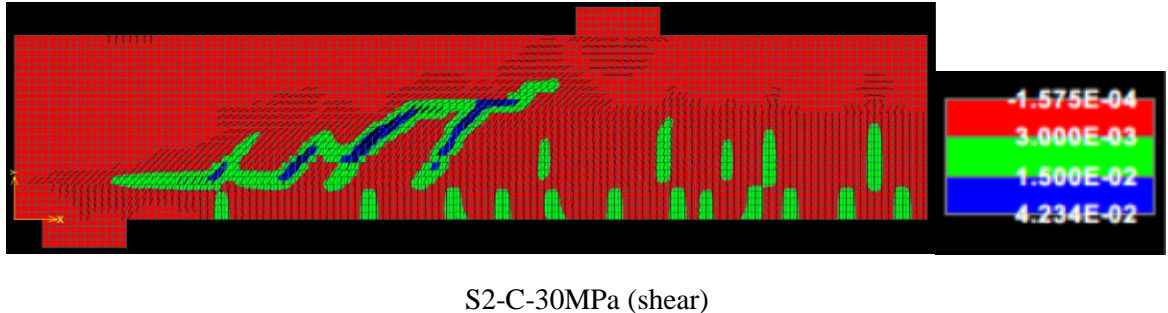
S2-A-2-200MPa (ASR layer, steel starts yielding)

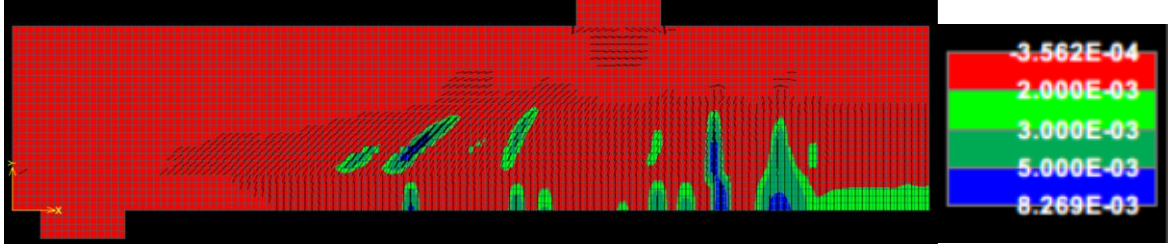


S2-A-2-250MPa (transition from ASR layer to bending failure)



S2-A-2-280MPa (bending, steel yielding and concrete crush)





S2-C-150MPa (bending, steel yielding and concrete crush)

Figure 49 Crack patterns and principal strain patterns for pretensioned beams

Due to the many curves obtained, only force-displacement curves at some representative prestressing levels are shown in Figure 48. Increased level of pretension will provide an earlier yielding of steel, a smaller deflection of beam can be observed. This can be explained that when the steel is pretensioned, it is closer to its yielding point, therefore the beam stiffness is steeper compared to the un-tensioned beam. It is also reasonable that the area of yielding part of reinforcement shows an increase when the pretension level increases. The yielding part of beam with 280 MPa prestressing is marked in red in Figure 51.

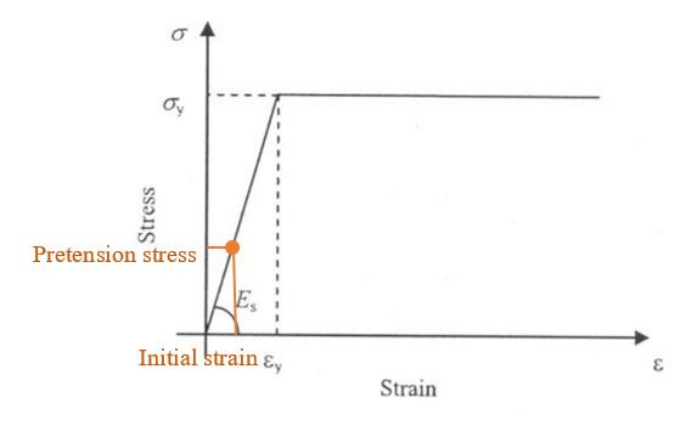


Figure 50 Stress-strain steel

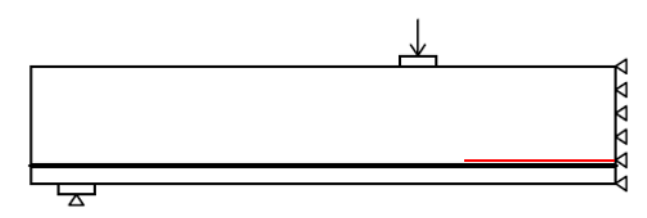


Figure 51 Yielding of steel in beam S2-A-2-280MPa (marked in red)

The increasing level of pretension has the potential to change shear failure into bending failure, with a transition part of ASR layer failure. With half of its prestressing value at 150 MPa, the steel is quite close to yielding at peak value. Though the ultimate load does not change a lot, a slightly increase is observed with an increase in prestress level before the failure mechanism changes to bending. Comparing the prestressing value of 200 MPa and 250 MPa, it is a process where a transition from ASR layer failure to bending failure occurs. With 200 MPa prestressing, the steel starts to yield, but the yielding part only happens at the large flexural cracks, the beam remains ASR layer failure. While 250 MPa prestressing is applied, the yielding part of steel is large enough to change the failure mechanism to bending failure. The failure mechanisms of the two beams could be seen in Figure 52.

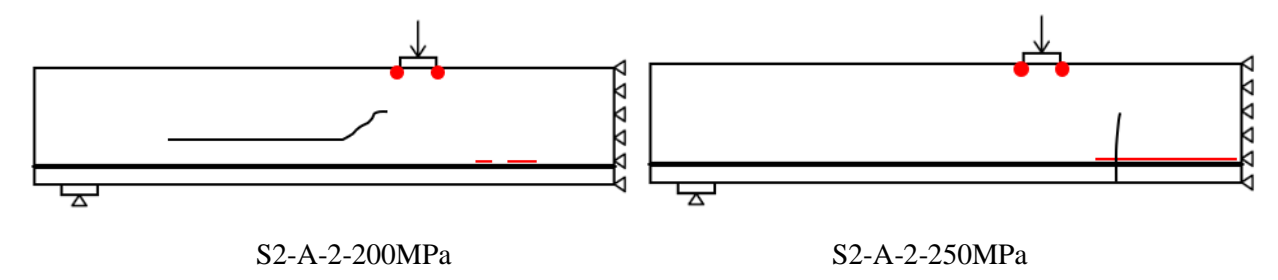


Figure 52 Failure mechanisms of beam S2-A-2-200MPa and S2-A-2-250MPa

Comparing both ASR-affected and sound beams in the prestress level of 150 MPa, an earlier transition to bending failure occurs in the sound beam. The ASR-affected beam failed in ASR layers, while bending failure occurred in the sound beam. Concrete crush is marked in red area and steel yielding marked in red line. At the location of large flexural cracks, steel starts to yield. It is the critical situation when concrete failure and steel yielding happens almost at the same time. In ASR-affected beam, due to the reduction of concrete properties in ASR layers, shear cracks are concentrated in this area, reinforcement has not reached its yielding point.

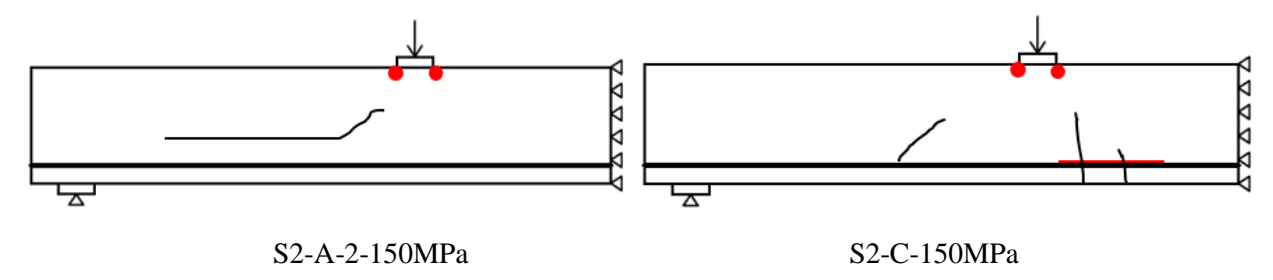


Figure 53 Failure mechanisms of beam S2-A-2-150MPa and S2-C-150MPa

### 4.1.4.3.3 Discussion

Though the shear failure in ASR-affected beam as experiment is not predicted well in ATENA, we can draw some conclusions through the analysis above,

- An increasing level of prestress gives a possibility to change the failure mode from shear to ASR layer failure to bending. It is caused by an earlier yielding of reinforcement and earlier concrete crush.
- 2) Comparing affected and unaffected models in a same prestress level, the failure mode transition from shear to bending is not caused by ASR cracks themselves. However, the appearance of ASR

cracks is always linked to ASR gel expansion, chemical prestress due to this expansion has the potential to change the failure mode.

### 4.1.4.4 Reinforcement bond analysis

#### 4.1.4.4.1 Introduction

In previous pretensioned model analysis, a good match with experimental force-displacement curve is already seen, but the failure mode does not fit experimental result. When good anchorage becomes poor, the failure mode changes from shear to bond failure. Considering this observation from experiments, it is worthwhile to put some efforts on the bond between concrete and steel.

Concrete is commonly reinforced with steel or prestressed by cables or steel bars, and for a composite material such as reinforced concrete to be effective, there must be adequate bond between the concrete and the steel. The bond resists the longitudinal forces that develop between concrete and reinforcement. Bond may be considered to be due to a combination of three factors: the chemical adhesion between the two materials, the friction due to the natural roughness of the bars, and the mechanical anchorage of the closely spaced deformations on the bar surfaces. The bond strength is affected by different variables such as concrete strength, concrete cover, bar size, anchorage length, transverse steel, and temperature (Ahmed, Burley, & Rigden, 1999).

Two possible bond models could be used,

- 1) ASR layer as a bond. The reduction in ASR layer properties could be treated as a kind of poor bond when it is close to the reinforcement. In the following analysis, the lower ASR layer from Figure 34 is located just above the reinforcement.
- 2) Traditional bond-slip model. This model defines the bond strength depending on the current slip between reinforcement and surrounding concrete. ATENA contains three bond-slip models, in the following analysis, the model based on CEB-FIP Model Code 1990 is used. (Cervenka, Jendele, & Cervenka, 2016)

A structural scheme is provided as Figure 54.

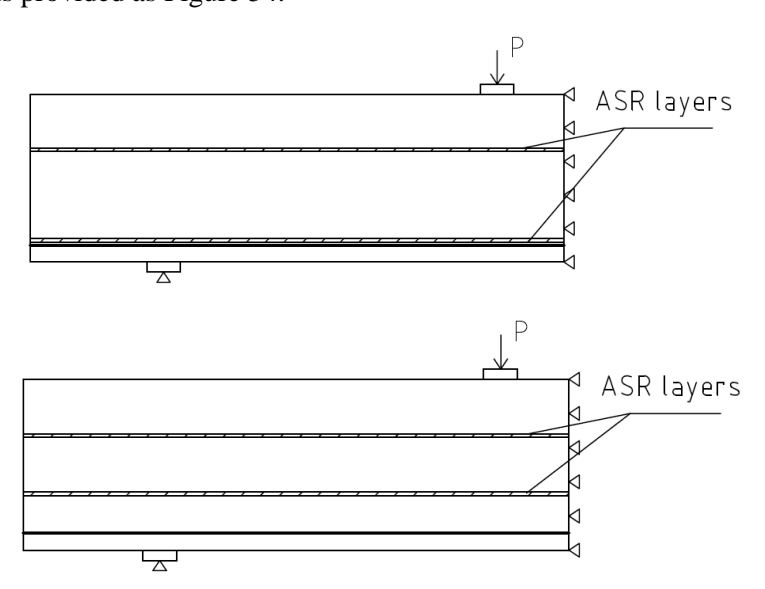


Figure 54 Structural scheme for bond models 1) ASR layer bond model (top) 2) bond-slip model (bottom)

In this part, S2-A-2-pretensioned beam is used as a reference, with a material property reduction rate 0.75 in ASR layers, and prestress level 280 MPa measured according to experimental value.

In ASR layer bond model, the only difference with reference model is the location of the lower ASR layer is closer to the reinforcement.

In traditional bond-slip model according to model code, the relation between bond strength  $\tau_b$  and slip s is defined as in Figure 55.

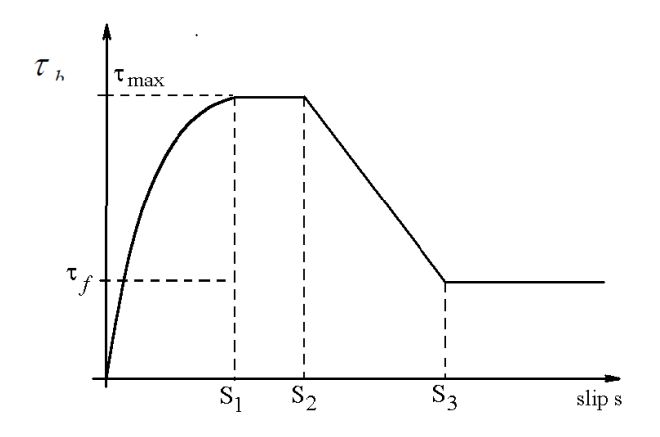


Figure 55 Bond-slip law by CEB-FIP Model Code 1990 (Cervenka, Jendele, & Cervenka, 2016)

The equations between bond strength and slip are:

$$\begin{split} \tau_b &= \tau_{\max} \left(\frac{s}{s_1}\right)^{\alpha}, 0 \leq s \leq s_1 \\ \tau_b &= \tau_{\max}, s_1 < s \leq s_2 \\ \tau_b &= \tau_{\max} - (\tau_{\max} - \tau_f) \left(\frac{s - s_2}{s_3 - s_2}\right), s_2 < s \leq s_3 \\ \tau_b &= \tau_f, s_3 < s_2 \end{split}$$

Table 21 Parameters for defining the mean bond strength-slip relationship for ribbed bars (Cervenka, Jendele, & Cervenka, 2016)

	2	3	4	5
Value	Unconfined concrete*		Confined concrete**	
	Bond conditions		Bond c	onditions
	Good	All other cases	Good	All other cases
S <sub>1</sub>	0.6 mm	0.6 mm	1.0 mm	
$S_2$	0.6 mm	0.6 mm	3.0 mm	
$S_3$	1.0 mm 2.5 mm		clear rib spacing	
α	0.4	1		).4
$\tau_{\rm max}$	$2.0\sqrt{f_{_c}}$	$1.0\sqrt{f_{_c}}$	$2.5\sqrt{f_{_{c}}}$	$1.25\sqrt{f_{_{c}}}$
$\tau_f$	$0.15   au_{ ext{max}}$		0.40	$ au_{ ext{max}}$

The bond law definition in ATENA is bond slip - bond strength, not bond slip - bond stress. In other words, no elastic bond slip is being considered explicitly in the ATENA bond model, the slip is zero until the bond strength is reached. This also means the bond function should not start with zero strength for zero slip (0, 0), which can make the system ill-conditioned. The manual suggests replacing the 0 with at least about 10% of the maximum bond strength for zero slip. (Pryl & Cervenka, 2017)

In this case, confined concrete is chosen, both good and poor bond conditions are modelled. The values used in the bond-slip model can be seen in Table 22. The bond-slip model with a good bond is approximately twice the strength of poor bond when they are at the same bond slip.

Table 22 Parameters for bond-slip model

Slip (mm)	Bond strength (MPa)		
	Good bond	Poor bond	
0.0	4.18	2.09	
0.3	5.49	2.75	
0.5	7.93	3.97	
1.0	10.46	5.23	
3.0	10.46	5.23	
15.0	4.18	2.09	
1000.0	4.18	2.09	

As the above analysis are all based on variable shear retention factor, to investigate the influence of the fixed one, a discussion on models with fixed shear retention factor can be found in Appendix 8.

# 4.1.4.4.2 Force-displacement curve & failure mode

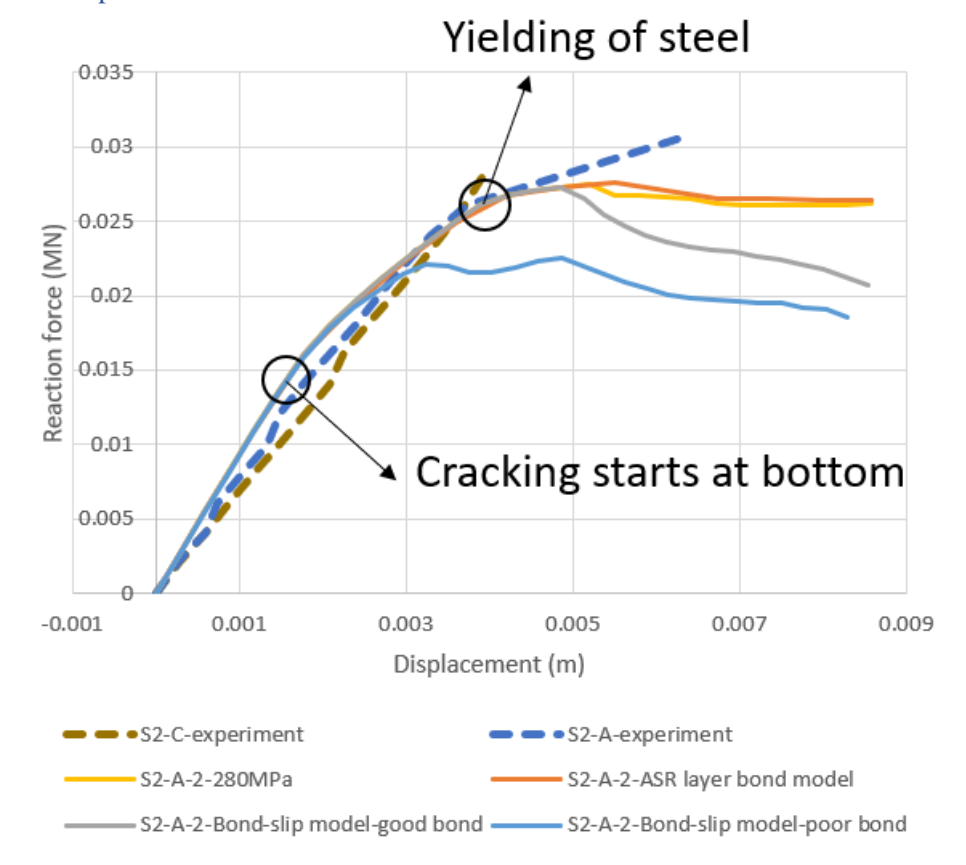
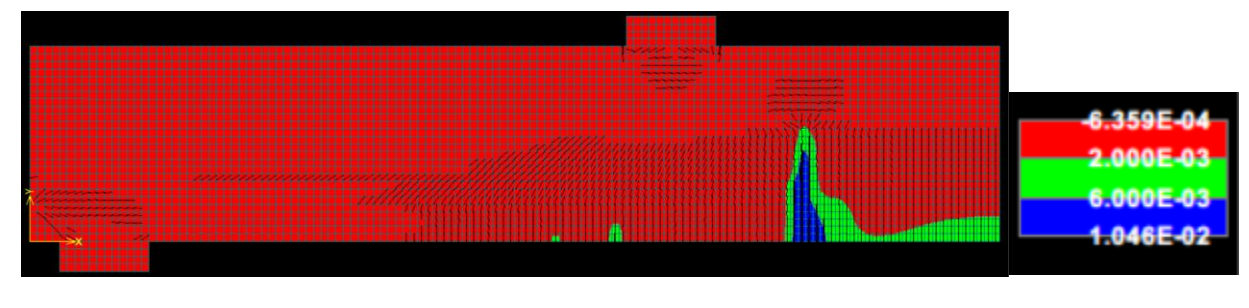
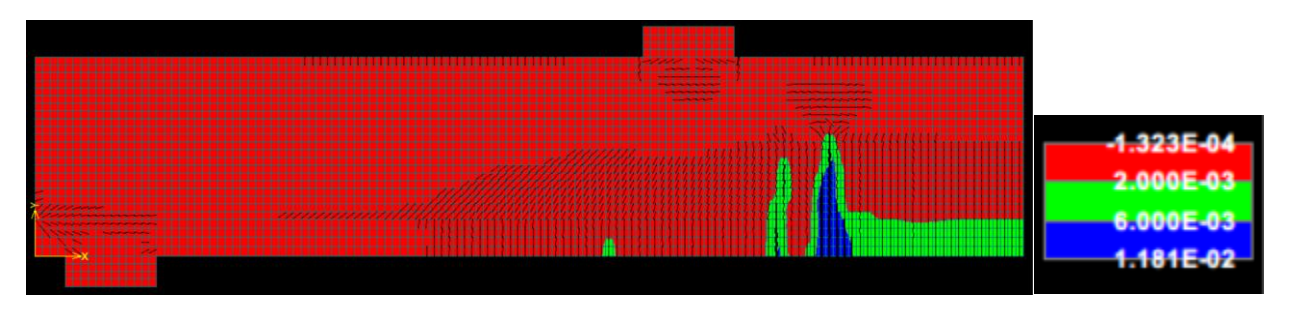


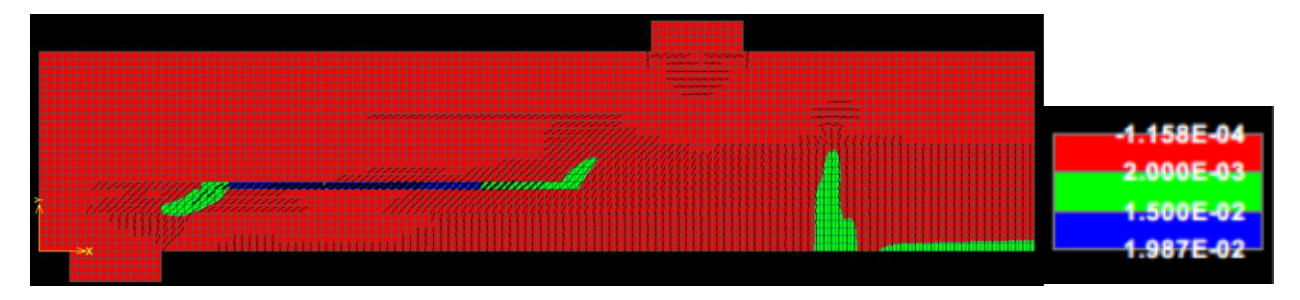
Figure 56 Load-displacement diagram for bond model analysis



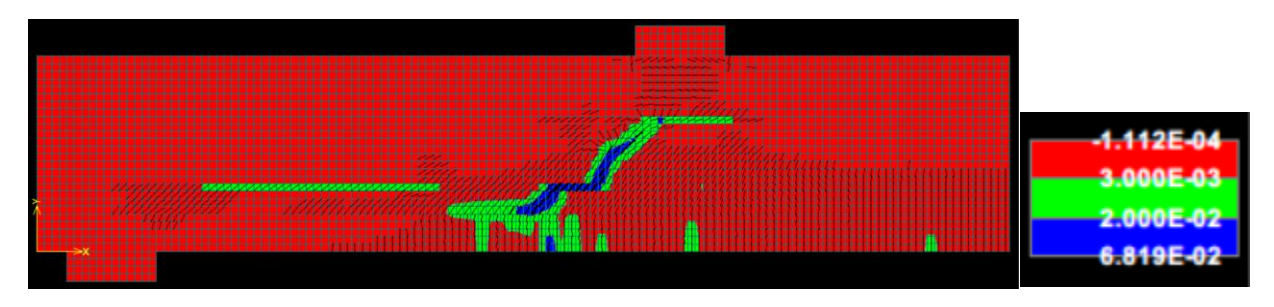
Reference: S2-A-2-280MPa (bending)



ASR layer bond model (bending, steel yielding)



Bond-slip model-good bond (ASR layer)



Bond-slip model-poor bond (shear)

Comparing the reference beam S2-A-2-280MPa with ASR layer bond model, they both fail in bending and the ultimate load shows almost no difference. The location of ASR layers does not have an obvious influence on this bending failure model.

Comparing the reference beam (perfect bond) with the traditional bond-slip models with good and poor bond, the influence is distinct. Good bond model fails in ASR layer, while poor bond model fails in shear. Reinforcement yielding occurs at both perfect bond model and good bond model, while the poor bond model already fails in shear before reaching the yielding point of steel. The ultimate load in good bond model is similar with the perfect bond model, while in poor bond model, a 20% decrease is observed. The bond-slip model could have an influence on ultimate load.

#### 4.1.4.4.3 Discussion

Some conclusions can be drawn from the above bond model analysis.

- The influence of ASR layer location, or the distance to reinforcement, is limited in the prestressed model. This result is based on the assumption that ASR layer is in perfect bond with reinforcement.
- 2) The traditional bond model is a good direction to go further. Using the bond-slip model in prestressed model could predict the failure mode and beam stiffness. But the results also depend on the bond strength.
  - (Ahmed, Burley, & Rigden, 1999) studied the influence of ASR on the bond strength of reinforced beams. A series of beams with different lap lengths at the center of the uniform bending zone were used, together with two datum beams casted with continuous bottom reinforcement. The load-deflection response is shown in Figure 57. The experimental results found that ASR reduced the ultimate load of the beam, and reinforcement lap length is a fundamental factor affecting bond strength. The authors explained the lower values of the

experimental bond strength is likely to be due to the interlocking between concrete and reinforcement being affected by the ASR.

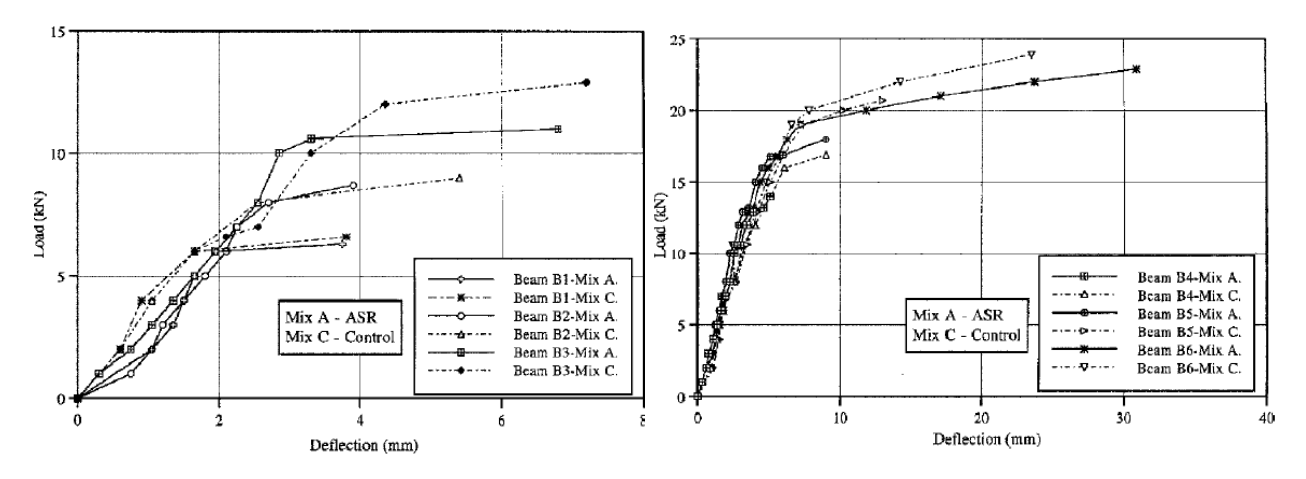


Figure 57 Deflection of Beam B1 to B3 (left, lap lengths: 5d, 8d and 12d) against load and Beam B4 to B6 (right, lap lengths: 20d, 32d and datum) (Ahmed, Burley, & Rigden, 1999)

# 4.2 Structural consequences of ASR: an example on shear capacity-HS1-South

### 4.2.1 Experiment

This experiment was done by Joop A. den Uijl, Niek Kaptijn and Joost C. Walraven, the report was published in April 2000 (den Uijl J. , 2000). ASR-affected concrete beams were sawn from the most affected area of the 35-year-old viaducts. Only these ASR-affected beams were tested, there was no sound concrete beam in this experiment.

Two series of beams were tested. ZB beams were sawn from the northern span of a three-span continuous slab bridge. And HS beams came out the southern span of a similar viaduct. The ZB-beams failed in bending, their load capacity was limited by the yielding of reinforcement. With even a lower reinforcement ratio, the HS-beams were strengthened by means of steel strips glued to the bottom side over the entire beam length to increase their bending resistance.

In the study below, beam HS1-South is modelled in a three-point-bending test. The load was stepwise applied with two hand-operated jacks in about 2 hours.

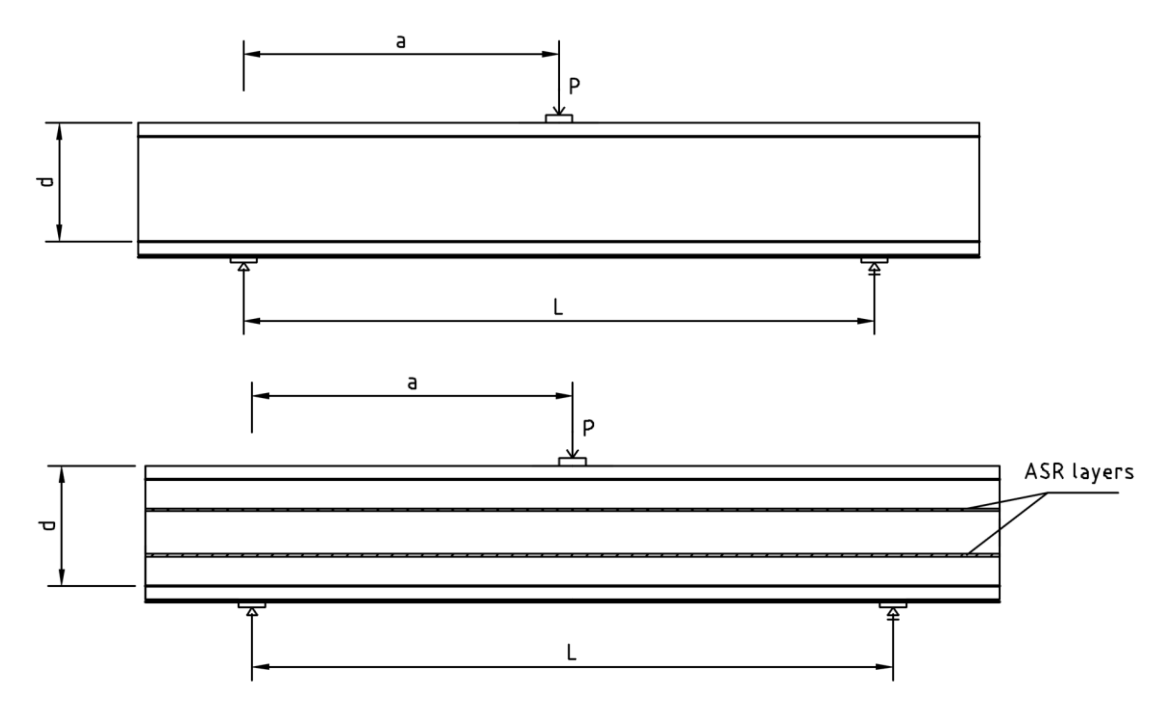


Figure 58 Beam HS1-South without (top) and with ASR layers (bottom)

Above in Figure 58 is the structural scheme for beam HS-1-South. It is a beam under three-point bending test. Beam height varies in longitudinal direction, to simplify the model, average height is used here.

### 4.2.1.1 Geometrical properties

In Table 23 the geometrical properties of the beam are reported.

Table 23 Dimensions for beam HS1-South

Dimension	Value	Unit
Height	670	mm

Length	7500	mm
Span	6000	mm
Width	480	mm
Reinforcement height	30 & 640	mm
Steel strips height	0	mm

### 4.2.1.2 Material properties

The material types for concrete and steel are the same as those in previous study, "SBeta Material" for concrete and plane stress elastic isotropic for steel plate. For this specific case, material properties are shown in Table 24. Sound concrete properties are estimated.

Table 24 Material properties for beam HS1-South

Property	Value	Unit			
Sbeta r	Sbeta material (sound concrete)				
Compressive strength 55 N/mm <sup>2</sup>					
Elastic modulus	40800	N/mm²			
Tensile strength	3.4	N/mm²			
Poisson's ratio	0.2	/			
Plane stres	s elastic isotropic (st	eel plate)			
Elastic modulus	200000	N/mm²			
Poisson's ratio	0.3	/			
Reinforcement					
Elastic modulus	200000	N/mm²			

In this beam, two types of reinforcement are applied. Reinforcement bars at both top and bottom of the beam, and additional steel strips glued to the bottom side to avoid bending failure. The amount and yield strength of reinforcement is shown in Table 25.

Table 25 Reinforcement details for beam HS1-South

	Area (mm2)	Reinforcement ratio	Yield strength (MPa)
Top reinforcement	201	0.06%	220
<b>Bottom reinforcement</b>	1909	0.54%	220
Steel strips	4738	1.34%	410

# 4.2.1.3 Experimental force-displacement curve

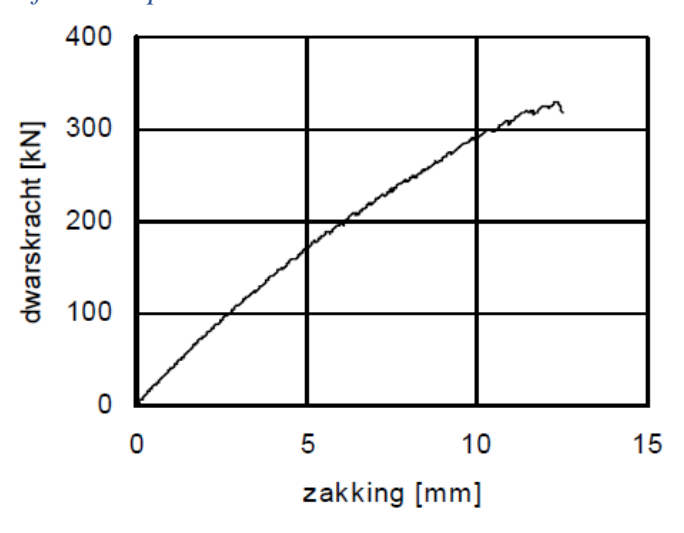


Figure 59 Load-deflection diagram from experiment (den Uijl J. , 2000)

# 4.2.1.4 Experimental failure mode

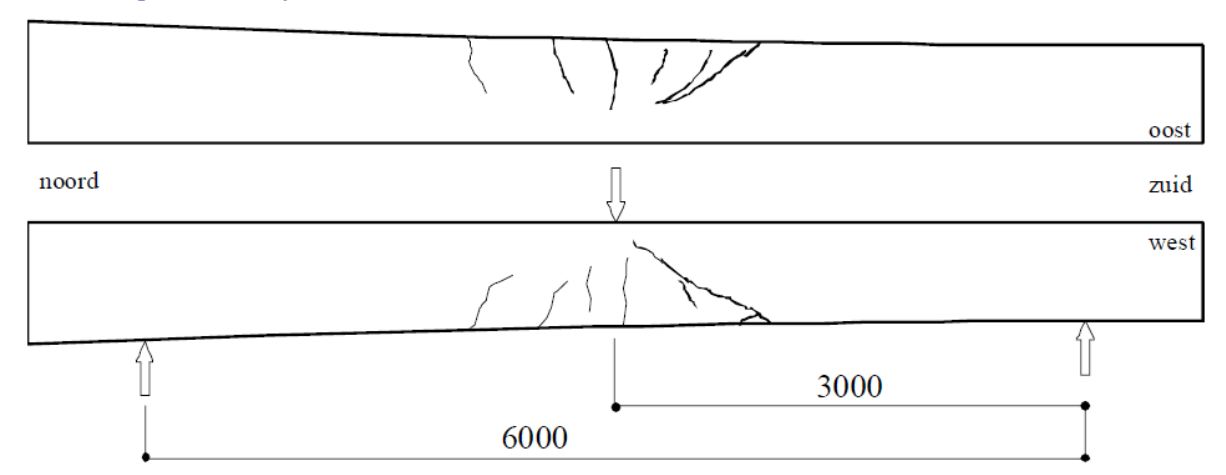


Figure 60 Beam HS1-South failure mode (den Uijl J. , 2000)

Beam HS1-South failed in shear and no yielding of reinforcement occurred.

# 4.2.2 Modelling

# 4.2.2.1 Element size

With an element size of 0.025 m, the model is already in a very fine mesh.

Table 26 Mesh size and mesh type

Mesh size	0.025m
Mesh type	Quadrilateral

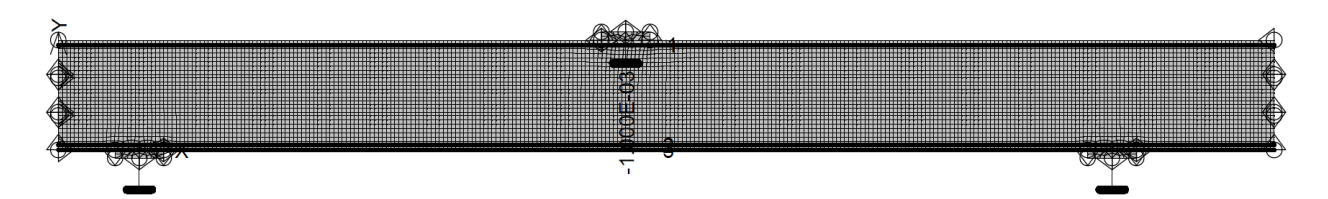


Figure 61 Mesh, load and boundary conditions

# 4.2.2.2 ASR layer modelling

Two thin layers evenly dividing the beam height are taken as the ASR cracking part. The ASR properties are unknown, so a series of various ASR properties are analyzed to simulate the experiment.

Table 27 Beam HS1-South ASR layer locations

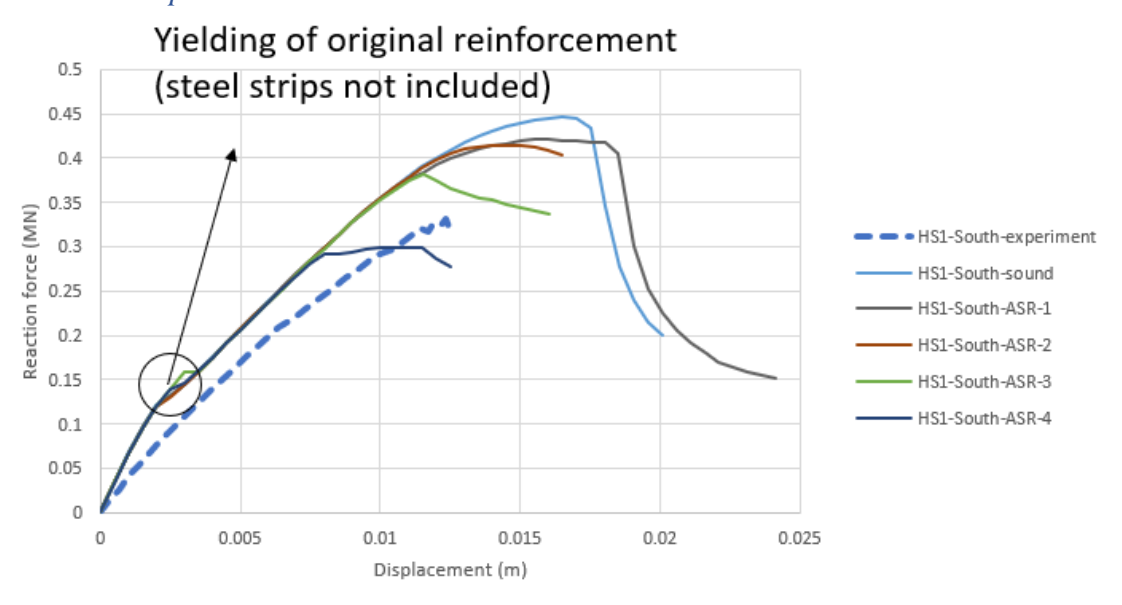
ASR layers	Height (mm)
Layer 1	210-230
Layer 2	440-460

Table 28 Beam HS1-South material properties

	Ec (MPa)	ft (MPa)	Gf (MN/m)
Sound	40800	3.40	1.00E-04
ASR-1	30000	2.55	7.50E-05
ASR-2	25000	2.13	6.25E-05
ASR-3	20000	1.70	5.00E-05
ASR-4	15000	1.28	3.75E-05

# 4.2.3 Results

# 4.2.3.1 Force-displacement curve



Figure~62~Load-displacement~diagram~for~beam~HS1-South~from~experiment~and~ATENA~results~in~different~ASR~reduction~rates

The curve HS-1-South-experiment shows the result from experiment while other curves show a simulation of sound beam and two-layer ASR affected beams with different ASR rate.

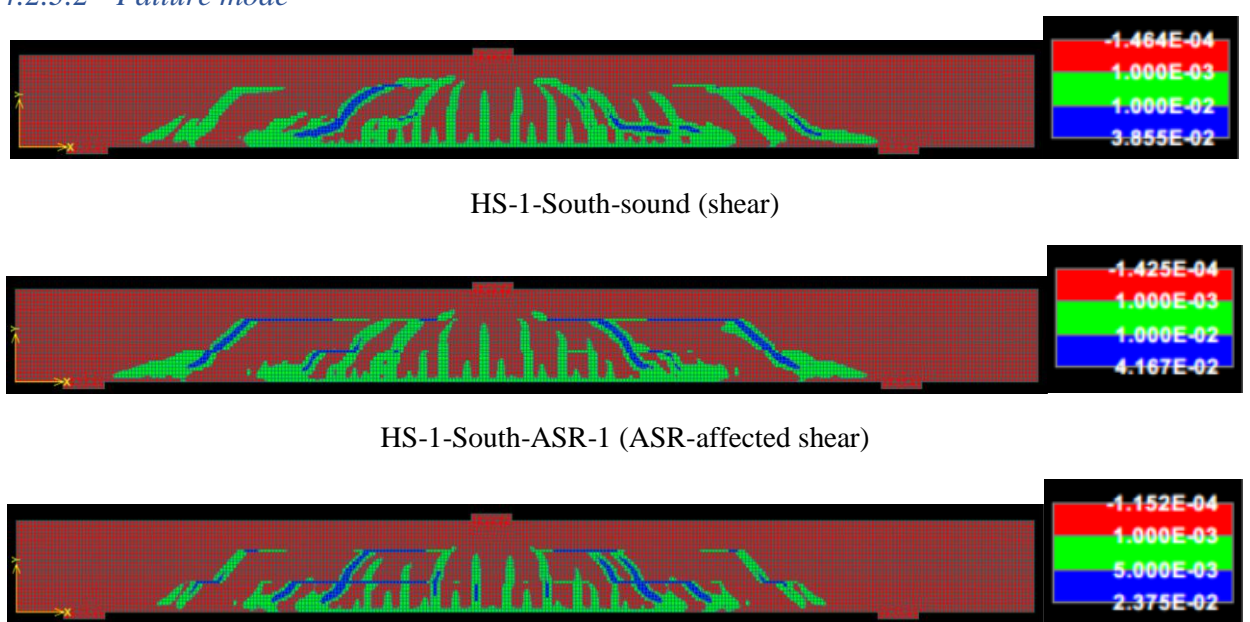
Comparing the experiment and ATENA results, the ultimate load of estimated sound beam is larger than all ASR-affected beams. With the increase of ASR property reduction, ultimate load for the beam also becomes smaller. While the ultimate load of ASR-affected beam from experiment result is 74% of sound beam from ATENA result, similar to the value of simulated ASR-affected beam with around 0.5 ASR reduction rate.

The ATENA ASR models are stiffer than experiment before cracks happen, and they show a similar slope after cracking. The ultimate loads of ASR-affected models depend on the layer properties. The experimental result shows a similar curve with beam ASR-3, and its peak value is 87% of this model. ATENA overestimates the result slightly in both stiffness and its peak load.

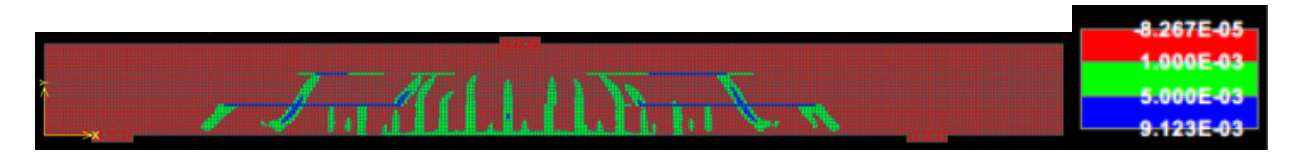
Possible reasons for overestimating ultimate load might be:

- 1) Material properties of sound concrete are estimated higher than reality. This can explain the higher initial stiffness of the beam before cracking happens.
- 2) Maximum stress in three-point test occurs at the point of loading. In experimental test, imperfections will influence the strength. While in numerical analysis, the imperfections are not considered.
- 3) The steel strips glued at the bottom is modelled as embedded reinforcement, the perfect connection between steel and concrete in ATENA is different from real test. In experiment, bond effects could be taken into consideration for these glued steel strips.

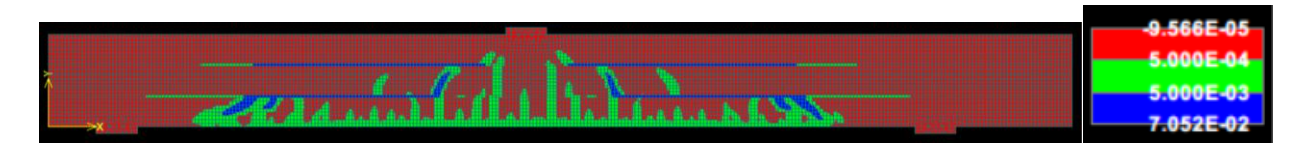
### 4.2.3.2 Failure mode



HS-1-South-ASR-2 (ASR-affected shear)



HS-1-South-ASR-3 (ASR layer)



HS-1-South-ASR-4 (ASR layer)

Figure 63 Crack patterns and principal strain patterns for HSI-South beams with different ASR reduction rates

Above in Figure 63 shows the principal strain pattern at peak load of sound beam and ASR beams. Sound beam fails in shear, the failure mode is the same as experiment and no yielding of reinforcement is observed. Existence of ASR layers allow the large shear crack to develop horizontally along the weak part. Increasing the reduction of ASR properties, more cracks are concentrated in the ASR layers. The failure mode changes from shear to ASR-affected shear failure, in the end, to ASR layer failure. The beams with obvious shear cracks have very close ultimate load to the sound model, while in beams fail in ASR layers, an obvious reduction in ultimate load is observed.

# 4.2.4 Optimization

#### 4.2.4.1 Introduction

From the previous chapter, some optimizations could be applied in this case. Taking beam HS1-South-ASR-3 and HS1-South-ASR-4 as a reference, the possible optimizations are listed in Table 29.

The prestress is added to both the top and bottom reinforcement as they experienced the whole process of ASR. The strengthened steel strips glued at the bottom side were not prestressed, because they are added after the ASR process only to increase the bending resistance. Measurement of residual longitudinal steel strains in the HS-beams showed that the prestress in the concrete varied between -0.1 and -0.6 MPa with an average of -0.3 MPa. This average prestress value is used in this study. With simple calculation, the prestress in steel is 1.5 MPa. The prestressing force added to top and bottom reinforcement is 0.27 kN and 2.6 kN respectively.

For the bond-slip model, considering poor bond gives a better prediction on the failure mechanism, and we do not have much information about the bond currently. Therefore, a poor bond is also applied in this case, including the top and bottom reinforcement, and the glued steel strips.

Table 29 Reference model vs optimized model

	Reference model (HS1-South-ASR-3/4)	Optimized model (HS1-South-ASR-3/4-Opt)
Prestressing	/	1.5 MPa
Bond-slip	Perfect bond	Poor bond

# 4.2.4.2 Force-displacement curve and failure mode

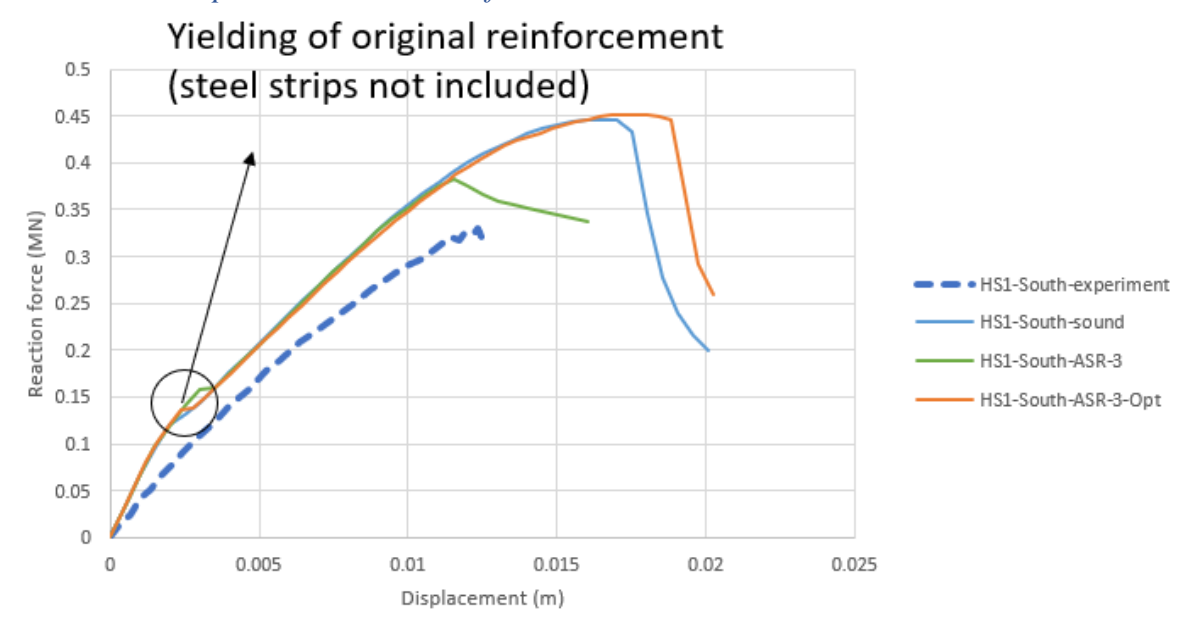
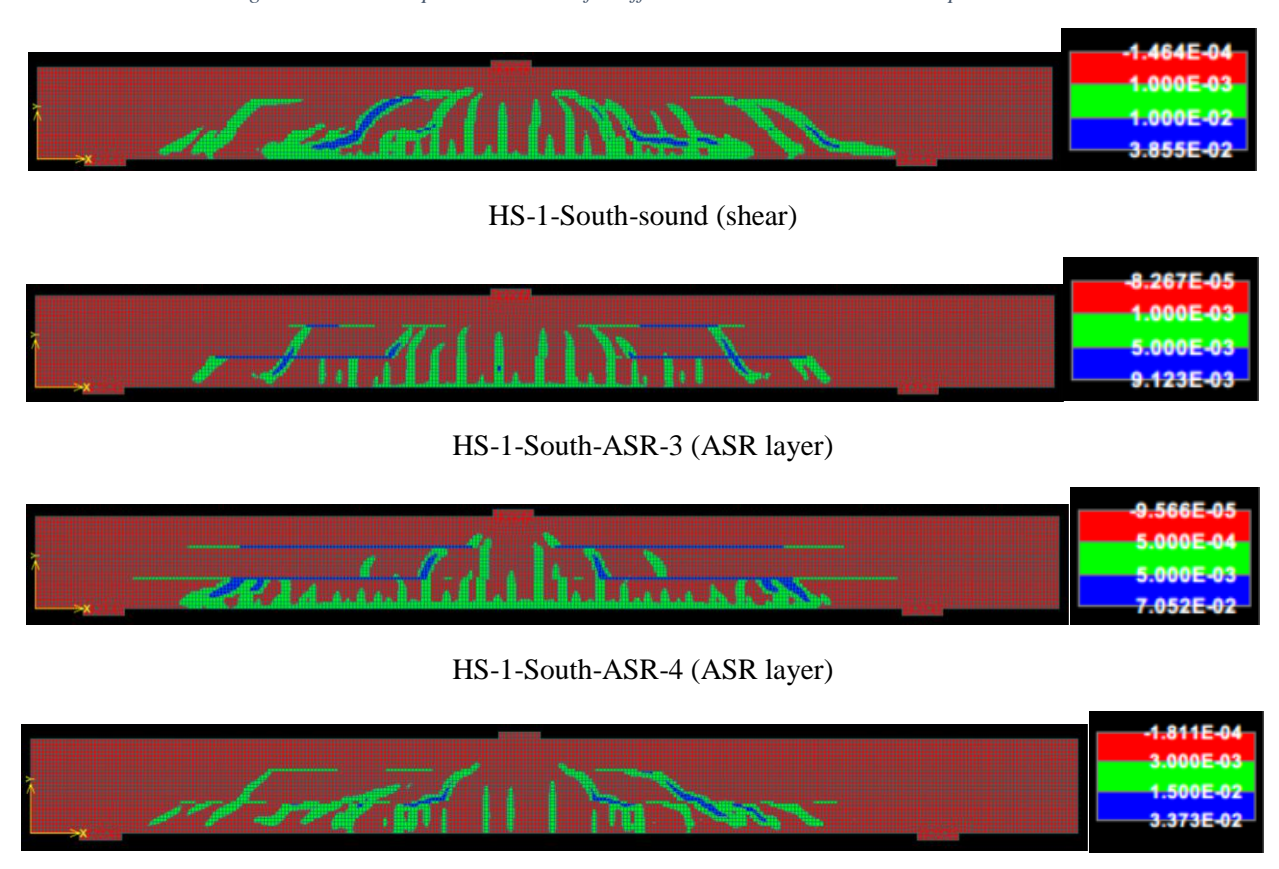
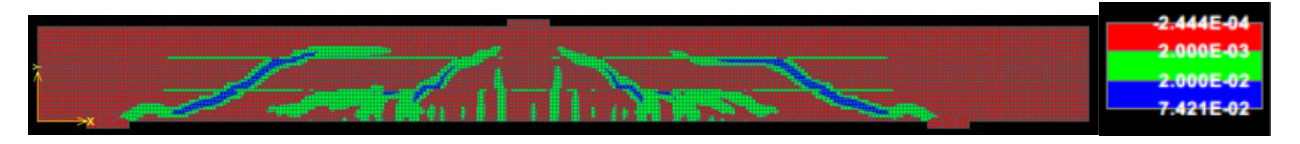


Figure 64 Force-displacement curve for affected beams with and without optimization



HS1-South-ASR-3-Opt (shear)



### HS1-South-ASR-4-Opt (shear)

Figure 65 Principal strain pattern for reference and optimized beams

Table 30 Beam HS1-South material properties

	Ec (MPa)	ft (MPa)	Gf (MN/m)
Sound	40800	3.40	1.00E-04
ASR-3	20000	1.70	5.00E-05
ASR-4	15000	1.28	3.75E-05

As a recap, the HS1-South-ASR-3 and HS1-South-ASR-4 refer to the beams with two different ASR reduction rates. The beams numbered with -Opt represent those in which prestressing as well as bond-slip model are also applied.

Looking at the optimized model with the chemical prestressing and bond-slip, some differences could be seen comparing to basic models.

Load capacity has shown an obvious increase, the beneficial effect due to prestressing overwhelmed detrimental effect caused by ASR property reduction. The ultimate load is even slightly larger than the calculated sound beam. The beam stiffness is not affected apparently, it is due to the low prestressing level.

Regarding to the failure mechanism, shear failure could be observed in optimized models, while ASR layer fails early in un-prestressed models. The material property reduction in ASR layers is compensated by the prestressing. Due to the poor bond between concrete and reinforcement, the increase of deformation capacity in other parts of the beam prevents the ASR layer slipping. That is the reason why shear failure is observed here.

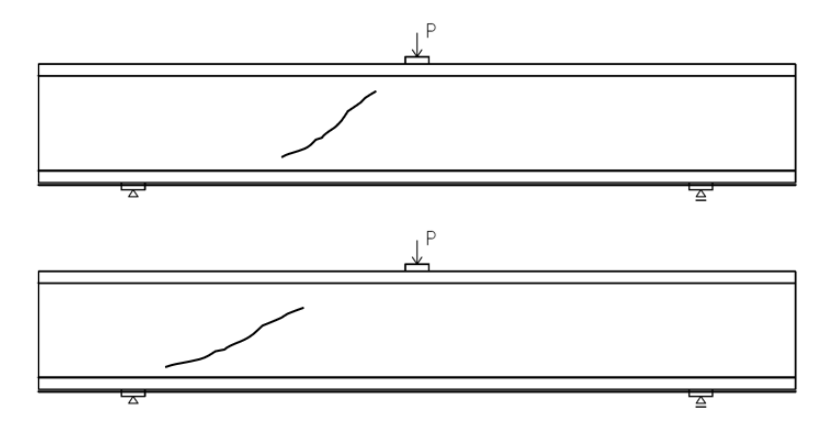


Figure 66 Crack inclination of HS1-South-sound (top) and HS1-South-ASR-4-Opt (bottom)

One thing worth mentioning is the shear crack inclination. With prestressing, the shear crack orientation is more horizontal comparing to the sound beam. (den Uijl J., 2000) also studied the influence of

prestress. If reinforcement is present in the main direction, this swelling is prevented, whereby the steel is under tension and the concrete is subjected to pressure. A consequence of this is that the occurrence of cracks is suppressed, so that the decrease of the tensile strength is less. Moreover, the generated pressure stresses can contribute to the shear stresses. The influence of a longitudinal compressive stress  $\sigma_x$  on the shear resistance in case of diagonal tension failure follows from Mohr's circle, see Figure 67. The magnitude of the ultimate shear stress  $\tau_{xy}$  and the crack inclination  $\varphi$  is given by:

$$\sigma_{xy} = \sqrt{f_{ct}^2 - f_{ct} \cdot \sigma_x}$$

$$\varphi = \arctan \frac{\tau_{xy} / f_{ct}}{1 - \sigma_x / f_{ct}}$$
Shear stress

$$\sigma_{xy} = \sqrt{f_{ct}^2 - f_{ct} \cdot \sigma_x}$$
Shear stress

$$\sigma_{xy} = \sqrt{f_{ct}^2 - f_{ct} \cdot \sigma_x}$$

Figure 67 Mohr's circle for stresses at the level of the neutral line (den Uijl J., 2000)

#### 4.2.4.3 Discussion

In this case, the ASR layered model with prestressing and bond-slip could also give a relatively good simulation as the experiment. Some conclusions could be drawn here,

Direction center

for planes

- 1) Only an increase in ultimate load comparing to the sound model is seen in the optimized models. There is a possibility that the bond model may be even poorer than the bond-slip model used here, which adopts the poor bond-slip model from CEB-FIP Model Code 1990. (Ahmed, Burley, & Rigden, 1999) suggested that the interlocking between concrete and reinforcement affected by ASR could result in a lower value of bond strength. More investigation could be done in this part.
- As to the failure mechanism, this model could predict it much better than the basic model without
  prestressing or bond-slip. The effect of crack inclination due to prestress could also be reflected
  in the result.

### 4.3 Limitations of the model

Based on the above analysis, there are still some limitations in this model.

1) Expansion due to ASR is not included, this might lead to a smaller hogging comparing to real structures. Whether it will influence the load capacity or failure mechanism is not clear.

- 2) Lack of information on ASR layer property. In this study, the properties are chosen based on the available data on unrestrained ASR-affected concrete. However, the material properties of the ASR layers, which represent only the ASR cracks and their surrounding part, are difficult to measure in laboratory.
- 3) The relationships between property reduction, chemical prestress and expansion are not considered so far. In fact, these parameters would correlate with each other instead of being separate. A more sever ASR level leads to more free expansion. The amount of ASR expansion, the reinforcement arrangement and amount lead to different amounts of chemical prestress and possible cracking, which result in lower properties in certain areas. In this analysis, the property reduction is assumed to occur only in ASR layers. This could be further studied.

## 5 Analysis on basic models

## 5.1 Introduction

The aim of this chapter is to evaluate the results of the numerical finite element analysis and compare them with the analytical beam analysis.

The present beam is simply supported and loaded, between the supports, by two point-loads.

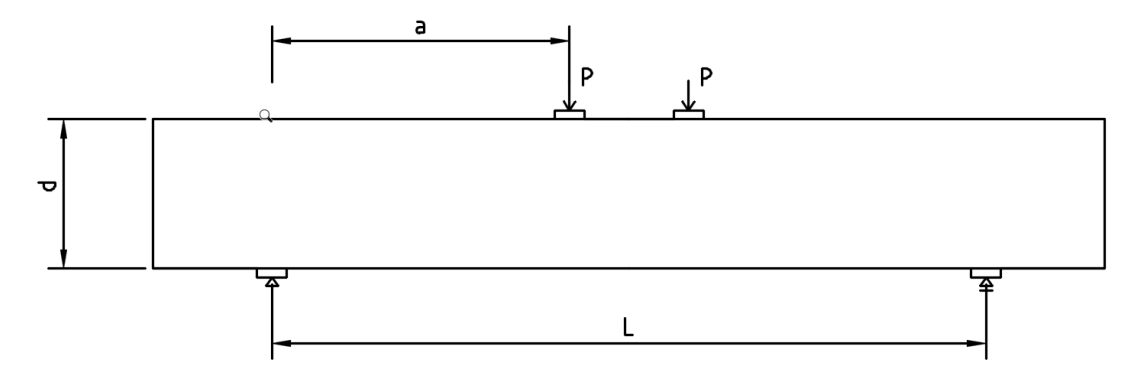


Figure 68 Basic model without reinforcement

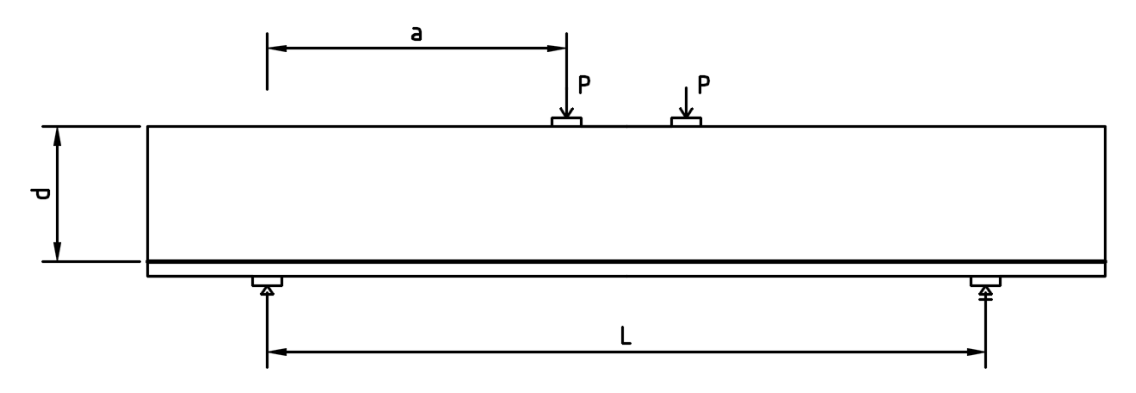


Figure 69 Basic model with reinforcement

## 5.1.1 Geometrical and cross-sectional properties

In Table 31 the geometrical and cross-sectional properties of the present beam are reported.

**Dimension** Value Unit Height 500 mm Length 3200 mm Span 2400 mm Width 500 mmReinforcement height 50 mm

Table 31 Geometrical properties

## 5.1.2 Material type

The beam is made of a linear elastic isotropic material, belonging to the class "SBeta Material", defined by the compressive strength of 30 MPa. The shear modulus can be obtained by the formula

$$G = \frac{E}{2(1+\nu)}$$
. For the steel plate at the loading points and the supports, plane stress elastic isotropic is

used. The stiffness of the plates is nearly 10 times higher than that of concrete, so it can guarantee rotation and avoid penetration.

Considering orthotropic material cannot be directly defined in ATENA 2D, for the ASR affected part, isotropic concrete with reduced properties is used.

The parameters of the materials are shown in Table 32.

**Property** Value Unit Sbeta material (concrete) Compressive strength 30  $N/mm^2$ **Elastic modulus** 30000  $N/mm^2$ Poisson's rate 0.2 Plane stress elastic isotropic (steel plate) **Elastic modulus** 200000 N/mm<sup>2</sup> Poisson's rate 0.3 Reinforcement 200000  $N/mm^2$ Elastic modulus **Yield Strength** 435  $N/mm^2$ 

Table 32 Material properties

## 5.1.3 Boundary conditions

As explained before, symmetry could be used in this case. The mid-vertical axis is constrained horizontally, and the left end support is modelled as a sliding support in order not to over constrain the structure with a hinge. The end supports are 100 x 30 mm steel plates and their centers are at a distance of 400 mm from the edges.

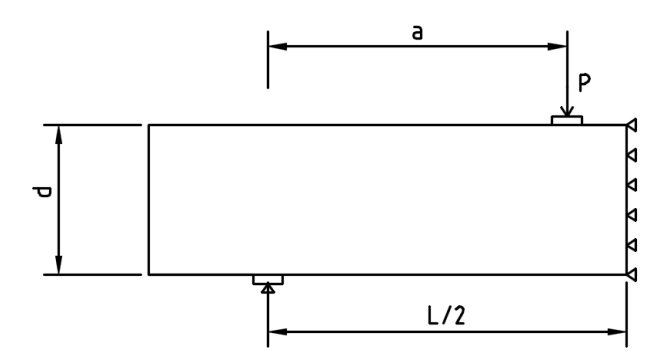


Figure 70 Boundary conditions for the left half without reinforcement

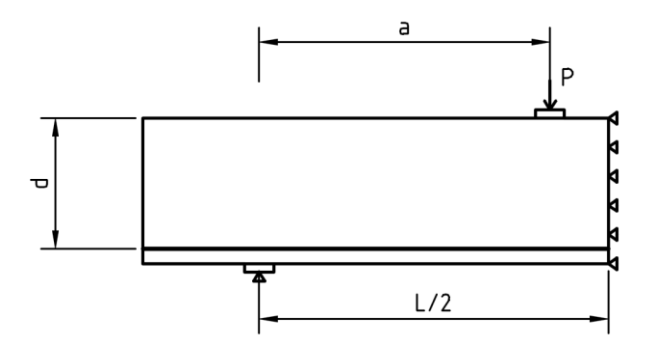


Figure 71 Boundary conditions for the left half with reinforcement

## 5.2 ATENA analysis of a/d=2 models

#### 5.2.1 Introduction

In case of reinforcement beams without shear reinforcement, according to Kani's Valley theory (Kani, 1966) (Adam, Reissen, & Hegger, 2017), the failure mechanism of beams is influenced by the a/d, which is shear span to effective depth ratio. In Figure 72, the x axis shows a/d, while y axis shows ultimate strength at failure/flexural strength. For beams with a lower a/d, the arch effect dominates, shear-compression failure tends to occur. While for the beams with a relatively higher a/d, beam effect is dominant, the governing mechanism is usually a diagonal-tension failure. Afterwards, bending failure occurs and no diagonal failure can be expected.

The influence of the percentage of main reinforcement p on shear strength was considerable. The minimum value of bending moment at failure for beams of identical cross section was obtained in the vicinity of a shear arm ratio, a/d, of 2.5. However, flexural load capacity varied considerably with percent of main reinforcement.

There exists a clearly defined region bounded by limiting values of p and a/d inside which diagonal failure is imminient and outside which full flexural strength is attained.

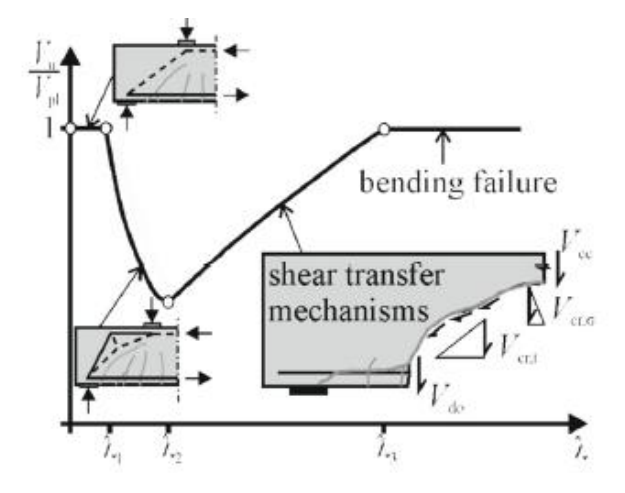


Figure 72 Kani's Valley relation (Adam, Reissen, & Hegger, 2017)

In this study, to study the possible failure mechanism change from shear to bending failure, several sets of beams with different a/d laying on the region of diagonal failure will be analyzed.

First, beams with a/d=2 are listed here.

A discussion about number of ASR layers, ASR-affected part with reduced properties, reinforcement ratio is done in the following sections.

The models with 1 and 2 horizontal ASR layers are analyzed. It is an assumption model based on theories. Due to the presence of reinforcement, the macro cracks tend to be parallel to the direction of restraints (ISE, 1992). The number of ASR layers is investigated to find out its influence, so we start from the very basic models, 1 and 2 ASR layers respectively.

The reduced properties in ASR layers are discussed in the introduction part <u>3.1.5</u>. Young's modulus, tensile strength and fracture energy are reduced in the same proportion in the ease of calculation.

The reinforcement ratio ranges from unreinforced (0%) to maximum allowed reinforcement ratio according to Eurocode (2%) as they could be seen as the two boundary values in most cases.

For sound concrete, Young's modulus is set as 30000 MPa.

The beams are numbered as following:

#### 5.2.1.1 a/d=2

Table 33 Properties of modelled beams

Beam no.	Number of ASR layers	Ec,red (MPa)	ft (MPa)	Gf (MN/m)	Reinforcement ratio
2A0	/	/	2.30	5.8E-05	0
2A1.2	1	100	0.01	1.9E-07	0
2A1.3	1	1000	0.08	1.9E-06	0
2A1.4	1	10000	0.77	1.9E-05	0
2A1.5	1	20000	1.53	3.9E-05	0
2A2.2	2	100	0.01	1.9E-07	0
2A2.3	2	1000	0.08	1.9E-06	0
2A2.4	2	10000	0.77	1.9E-05	0
2A2.5	2	20000	1.53	3.9E-05	0
2B0	/	/	2.30	5.8E-05	2%
2B1.2	1	100	0.01	1.9E-07	2%
2B1.3	1	1000	0.08	1.9E-06	2%
2B1.4	1	10000	0.77	1.9E-05	2%
2B1.5	1	20000	1.53	3.9E-05	2%
2B2.2	2	100	0.01	1.9E-07	2%
2B2.3	2	1000	0.08	1.9E-06	2%
2B2.4	2	10000	0.77	1.9E-05	2%
2B2.5	2	20000	1.53	3.9E-05	2%

Mesh sizes are listed in Table 34, mesh type is quadrilateral, an example of mesh, load and boundary conditions is shown in Figure 73:

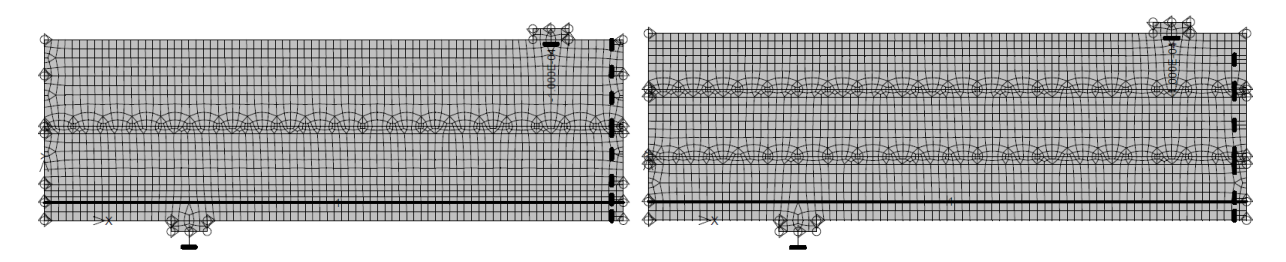


Figure 73 Mesh, load and boundary conditions (left: 1 ASR layer, right: 2 ASR layers)

Table 34 Mesh size

Material	Mesh size (mm)
Concrete	20
<b>Reduced concrete</b>	10
Steel plate	20

All the calculation results related to this part, including force-displacement response, crack pattern and principal strain pattern can be found in <u>Appendix 1</u>.

## 5.2.2 Shear capacity and failure mode

## 5.2.2.1 No reinforcement:

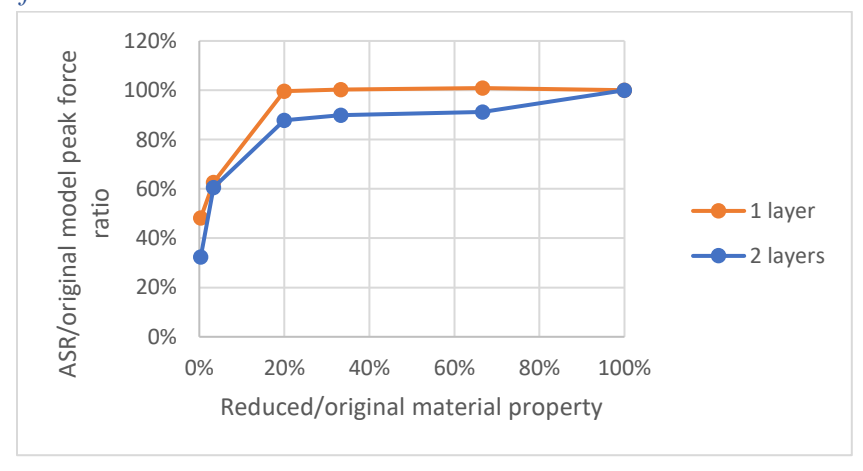


Figure 74 Ultimate load in relation with material reduction for beams with no reinforcement

Table 35 Ultimate load in relation with material reduction for beams with no reinforcement

	Ec,red (MPa)	Ec,red/Ec	Peak force (MN)	%
basic	30000	100%	7.70E-02	100%
1 layer	100	0%	3.72E-02	48%
	1000	3%	4.83E-02	63%
	6000	20%	7.67E-02	100%
	10000	33%	7.72E-02	100%
	20000	67%	7.77E-02	101%
2 layers	100	0%	2.50E-02	32%
	1000	3%	4.66E-02	61%

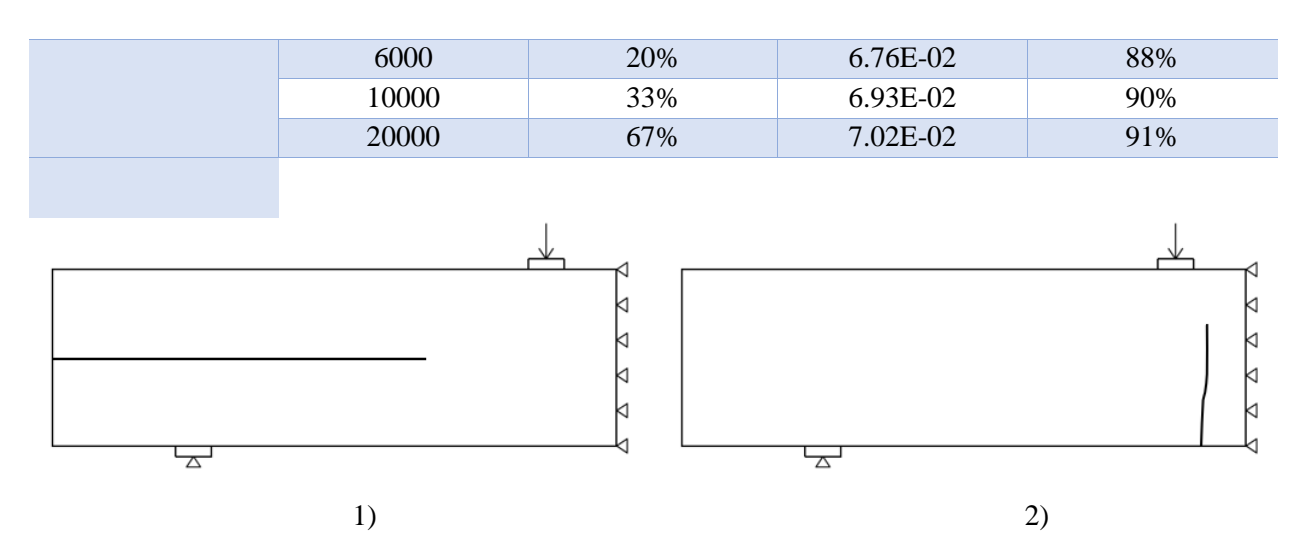


Figure 75 Failure mode in non-reinforced beams: 1) ASR layer failure (left) and 2) brittle failure (right)

From Table 35, Figure 74 and Figure 75 above, it is clear that the reduction on structural capacity is quite small when Ec,red is not less than 6000 MPa. For models with one ASR layer, almost no reduction is observed in the peak as long as Ec.red>6000 MPa. And for models with two ASR layers, the peak force can still reach 88% of the original one when Ec.red>6000 MPa.

In non-reinforced beams, two types of failure mode might occur,

- 1) Failure of ASR layers when ASR layers are weak.
- 2) Brittle failure at the bottom near the middle, this situation occurs when property reduction of ASR part is not too much. The force-displacement response is almost linear before reaching ultimate load, then instant decrease of structural capacity is observed, and wide cracks occur.

#### 5.2.2.2 2% reinforcement:

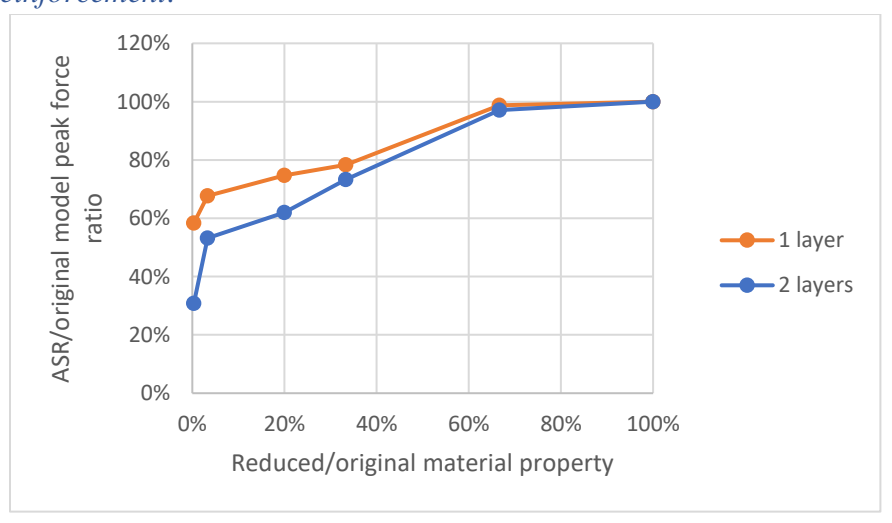


Figure 76 Ultimate load in relation with material reduction for beams with 2% reinforcement

Table 36 Ultimate load in relation with material reduction for beams with 2% reinforcement

	Ec,red (MPa)	Ec,red/Ec	Peak force (MN)	%
basic	30000	100%	3.36E-01	100%
1 layer	100	0%	1.96E-01	58%
	1000	3%	2.28E-01	68%
	6000	20%	2.51E-01	75%
	10000	33%	2.63E-01	78%
	20000	67%	3.32E-01	99%
2 layers	100	0%	1.04E-01	31%
	1000	3%	1.79E-01	53%
	6000	20%	2.08E-01	62%
	10000	33%	2.46E-01	73%
	20000	67%	3.26E-01	97%

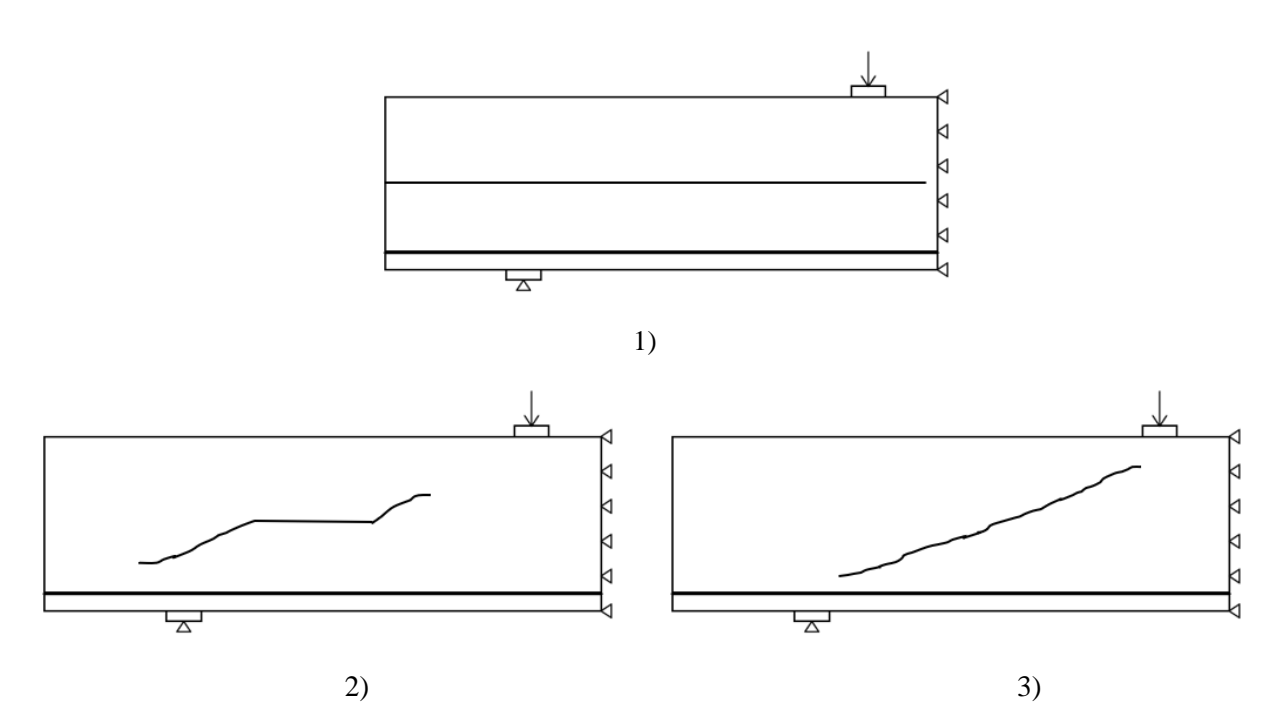


Figure 77 Failure mode of 2% reinforced beams: 1) ASR layer failure (top), 2) ASR-affected shear failure (bottom left) and 3) shear failure (bottom right)

From

Table 36, Figure 76 and Figure 77 above, the reduction on structural capacity is quite limited when Ec,red is not less than 20000 MPa. When material properties of ASR layers are further reduced, structural capacity decreases almost in a linear relation. Until Ec,red goes down to 1000 MPa, the structural capacity can still reach 70% and 50% respectively for 1 layer and 2 layers models.

Oppositely, when Ec.red is at a very low value, e.g., Ec.red<1000 MPa, the structural capacity will drop rapidly as Ec,red decreases. Great reduction of structural capacity is likely to happen with a tiny decrease

in material properties of ASR layers. As the structure tends to show a more brittle behavior, it is better to replace the whole structure when Ec,red is at this range.

Comparing the two series of models, the reduction of structural capacity tends to occur earlier in 2% reinforcement models (after 20000 MPa) than no reinforcement models (after 6000 MPa). A possible explanation is ASR layers might have different levels of effects on structural capacity on different failure mechanisms.

In reinforced beams, there are also three types of possible failure mode as previously discussed, respectively ASR layer failure, ASR-affected shear failure, and shear failure.

#### 5.2.3 Discussion

To summarize, the following conclusions can be drawn from the study above:

- 1) Models with 1 ASR layer and 2 ASR layers show similar trend in force-displacement diagrams. However, the models with 1 ASR layer mostly have a slightly higher peak reaction force than models with 2 ASR layers, though the difference is not too much.
- 2) For beams with ASR layers property reduction less than 1/3, the shear cracks tend to partly follow ASR cracks when they propagate to the level of ASR layers. This was also observed in some experiments. (Abe, Kikuta, Masuda, & Tomozawa, 1989) observed the horizontal slip failure which occurred connecting the horizontal cracks generated by ASR, see Figure 78.
- 3) Failure mechanisms might be affected due to the existence of ASR layers. Brittle failure and shear failure both have a possibility to switch to ASR layer failure if ASR layers are weak. Also see Figure 78 from (Abe, Kikuta, Masuda, & Tomozawa, 1989).

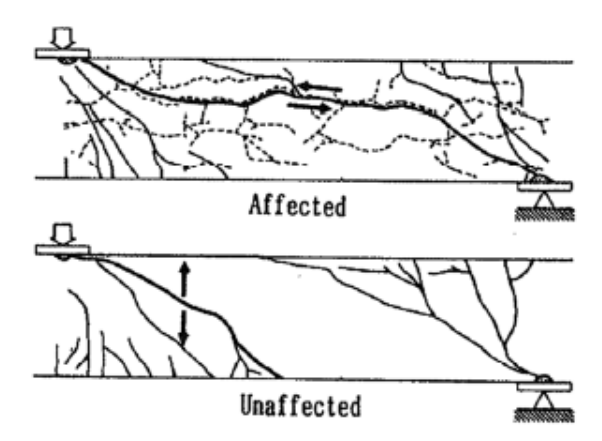


Figure 78 Failure mode changes from diagonal shear tension in unaffected beam to horizontal slip failure in affected beam (Abe, Kikuta, Masuda, & Tomozawa, 1989)

- 4) ASR layers might have different levels of effects on structural capacity on different failure mechanisms. Beams suffering brittle failure is less affected than shear failure.
- 5) For models with 1 or 2 ASR layers, when Ec,red>10000 MPa, the influence of the number of ASR layers is limited compared to other parameters. Therefore, in the following part, only 1-layer models are considered.
- 6) Models with Ec,red>6000 MPa and a more practical reinforcement range are worth further study. Therefore, a further study on these parameters is done in the following chapter.

## 5.3 ATENA analysis of different a/d ratio models

#### 5.3.1 Introduction

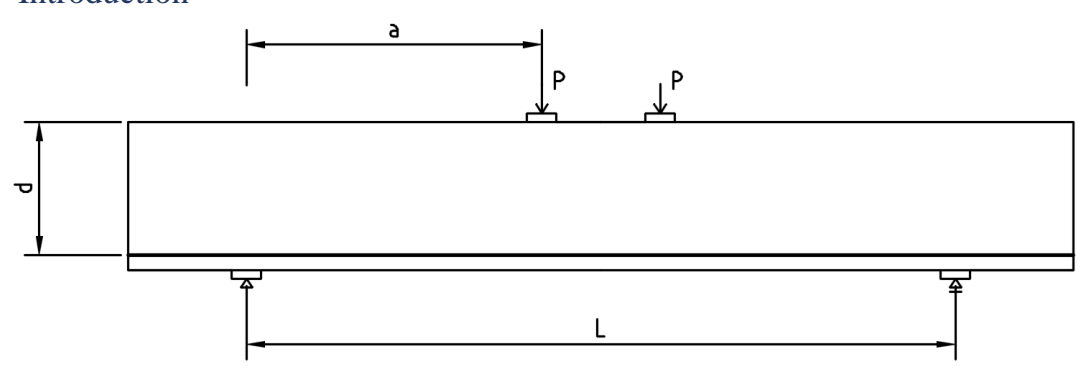


Figure 79 Basic beam with reinforcement

In addition to the previous chapter, several sets of models are analyzed here to get a better understanding of the parameters. These models all have the same height but various a/d ratios (=2, 3, 4). The geometry parameters of the models are shown in Table 37.

	a/d=2	a/d=3	a/d=4
Dimension	Value (mm)	Value (mm)	Value (mm)
Height	500	500	500
Shear span	1000	1500	2000
Length	3200	4200	5200
Span	<b>Span</b> 2400		4400
Width	-		500

Table 37 Beam dimensions for various a/d ratios

The additional models with a/d=2, 3, 4 are numbered as following in Table 38, Table 39 and Table 40. For models with 0.3% reinforcement ratio, one model with Ec,red=6000 MPa is also analyzed to check the effects of ASR layers on bending failures.

## 5.3.1.1 a/d=2

*Table 38 a/d=2 beam properties* 

Beam no.	Number of ASR layers	Ec,red (MPa)	Reinforcement ratio	Tensile strength ft	Fracture energy Gf (MN/m)
	-			(MPa)	
2B0	/	/	2%	2.30	5.80E-05
2B1.4	1	10000	2%	0.80	1.90E-05
2B1.5	1	20000	2%	1.60	3.80E-05
2C0	/	/	1%	2.30	5.80E-05
2C1.4	1	10000	1%	0.80	1.90E-05

2C1.5	1	20000	1%	1.60	3.80E-05
<b>2D0</b>	/	/	0.3%	2.30	5.80E-05
2D1.3.6	1	6000	0.3%	0.48	1.14E-05
2D1.4	1	10000	0.3%	0.80	1.90E-05
2D1.5	1	20000	0.3%	1.60	3.80E-05

## 5.3.1.2 a/d=3

Table 39 a/d=3 beam properties

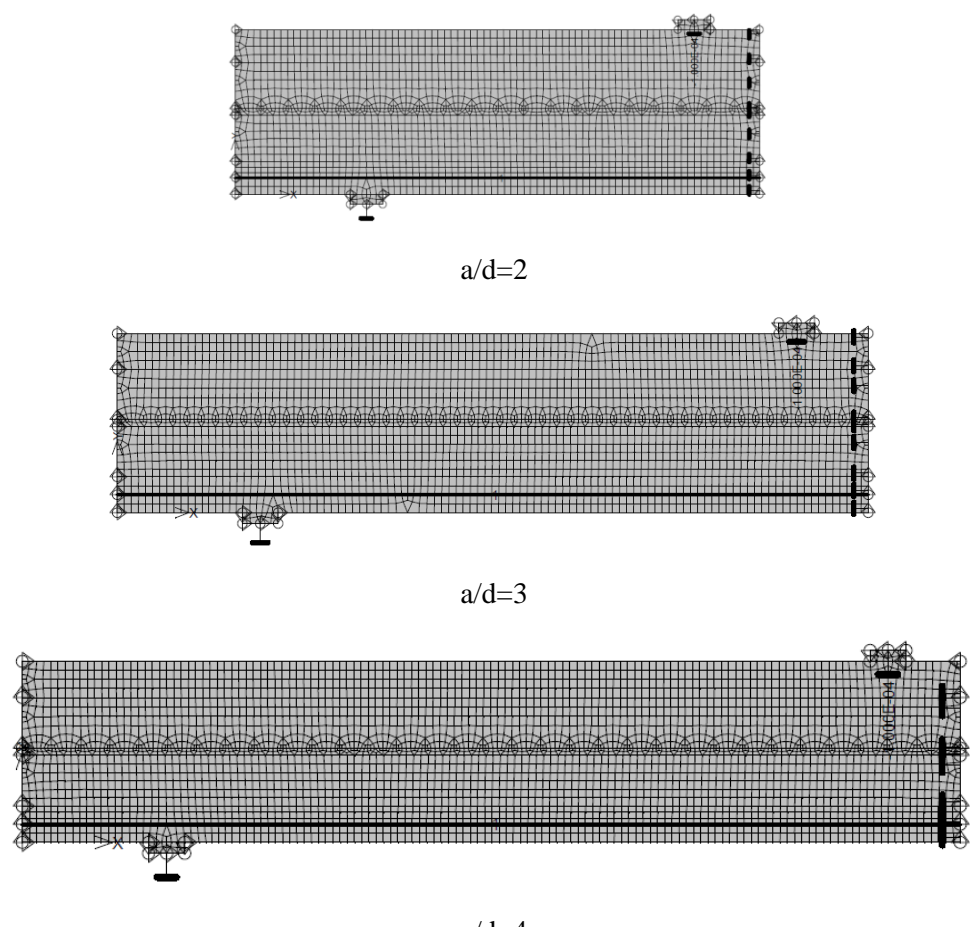
Beam no.	Number of ASR layers	Ec,red (MPa)	Reinforcement ratio	Tensile strength ft (MPa)	Fracture energy Gf (MN/m)
3B0	/	/	2%	2.30	5.80E-05
3B1.4	1	10000	2%	0.80	1.90E-05
3B1.5	1	20000	2%	1.60	3.80E-05
3C0	/	/	1%	2.30	5.80E-05
3C1.4	1	10000	1%	0.80	1.90E-05
3C1.5	1	20000	1%	1.60	3.80E-05
3D0	/	/	0.3%	2.30	5.80E-05
3D1.3.6	1	6000	0.3%	0.48	1.14E-05
3D1.4	1	10000	0.3%	0.80	1.90E-05
3D1.5	1	20000	0.3%	1.60	3.80E-05

## 5.3.1.3 a/d=4

Table 40 a/d=4 beam properties

Beam no.	Number of ASR layers	Ec,red (MPa)	Reinforcement ratio	Tensile strength ft (MPa)	Fracture energy Gf (MN/m)
4B0	/	/	2%	2.30	5.80E-05
4B1.4	1	10000	2%	0.80	1.90E-05
4B1.5	1	20000	2%	1.60	3.80E-05
4C0	/	/	1%	2.30	5.80E-05
4C1.4	1	10000	1%	0.80	1.90E-05
4C1.5	1	20000	1%	1.60	3.80E-05
4D0	/	/	0.3%	2.30	5.80E-05
4D1.3.6	1	6000	0.3%	0.48	1.14E-05
4D1.4	1	10000	0.3%	0.80	1.90E-05
4D1.5	1	20000	0.3%	1.60	3.80E-05

Mesh sizes are listed in Table 41, mesh type is quadrilateral, an example of mesh, load and boundary conditions is shown in Figure 80:



a/d=4

Figure 80 Mesh, load and boundary conditions

Table 41 Mesh size

Material	Mesh size (mm)
Concrete	20
<b>Reduced concrete</b>	10
Steel plate	20

All the calculation results related to this part, including force-displacement response, crack pattern and principal strain pattern can be found in <u>Appendix 2</u>.

## 5.3.2 Moment & shear capacity of original models

Moment capacity  $F_{u,moment}$  and shear capacity  $F_{u,shear}$  of original models can be done by hand calculation (see Appendix 3). The lower value of  $F_{u,moment}$  and  $F_{u,shear}$  is denoted as  $F_{u,theory}$ , which means ultimate shear force according to theory. The theory results correspond well with ATENA results

 $F_{u,basic}$  except several cases. When low a/d and high reinforcement ratio work at the same time, theory results overestimate its capacity too much.

Table 42 Theory results of ultimate load and failure mode of sound beams

Beam number	Fu,shear (kN)	Fu,moment (kN)	Fu,theory (kN)	Fu,basic (kN)	Fu,basic/ Fu,theory	Failure mode
2B0	585	946	585	349	0.60	shear
2C0	464	473	464	293	0.63	shear
2D0	311	142	142	151	1.06	bending
3B0	309	631	309	291	0.94	shear
3C0	245	315	245	242	0.99	shear
3D0	164	95	95	105	1.11	bending
4B0	285	473	285	286	1.01	shear
4C0	226	237	226	204	0.90	shear
4D0	151	71	71	80	1.13	bending

With all the calculation above, failure mode of each beam can be predicted according to bending and shear capacity. When the shear force at the reinforcement yielding level is smaller than shear capacity, bending failure will occur. And it holds the other way around as long as the reinforcement ratio satisfies the requirements to avoid brittle failure.

Also, there is another possibility. When ASR layers exist, the weak ASR layers might fail if shear stress in this layer is higher than layer strength.

## 5.3.3 Moment & shear capacity of models with ASR layers

With a set of models with different ASR influence, the ultimate load for these models and the possible reduction can be seen below in Table 43, Table 44 and Table 45. As explained in the introduction part, basic model for Beam 2B1.4 is Beam 2B0, and so on in a similar manner.

Table 43 Ultimate load and failure mode of beam series 1.3.6

Beam number	Fu,asr (kN)	Fu,asr/Fu,basic	Failure mode
2D1.3.6	151	1.00	ASR-affected bending
3D1.3.6	103	0.98	ASR-affected bending
4D1.3.6	78	0.98	ASR-affected bending

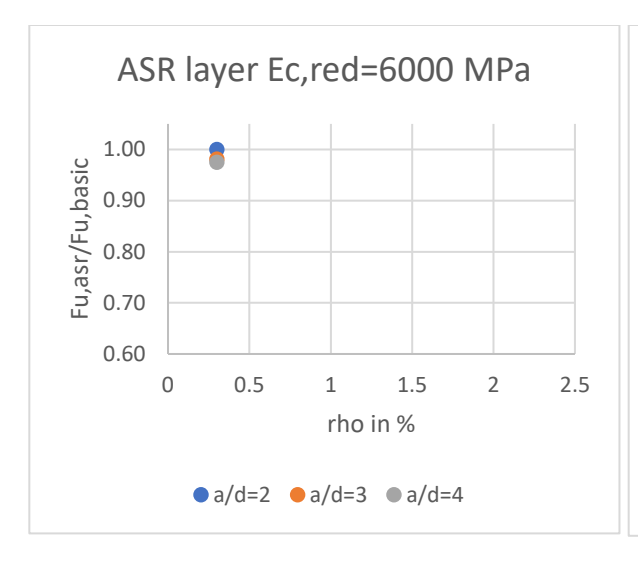
Table 44 Ultimate load and failure mode of beam series 1.4

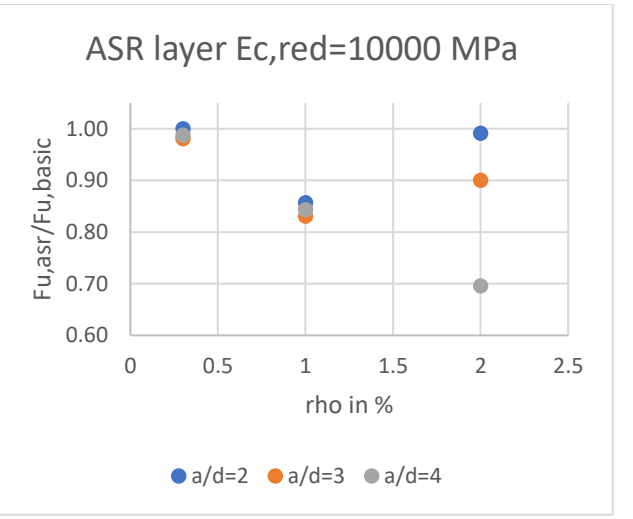
Beam number	Fu,asr (kN)	Fu,asr/Fu,basic	Failure mode
2B1.4	346	0.99	ASR-affected shear
2C1.4	251	0.86	ASR-affected shear
2D1.4	151	1.00	bending
3B1.4	262	0.90	ASR layer
3C1.4	201	0.83	ASR layer

3D1.4	103	0.98	bending
4B1.4	199	0.70	ASR layer
4C1.4	172	0.84	ASR layer
4D1.4	79	0.99	bending

Table 45 Ultimate load and failure mode of beam series 1.5

Beam number	Fu,asr (kN)	Fu,asr/Fu,basic	Failure mode
2B1.5	349	1.00	shear
2C1.5	289	0.99	shear
2D1.5	153	1.01	bending
3B1.5	285	0.98	ASR-affected shear
3C1.5	238	0.98	shear
3D1.5	103	0.98	bending
4B1.5	276	0.97	ASR-affected shear
4C1.5	193	0.95	ASR-affected shear
4D1.5	79	0.99	bending





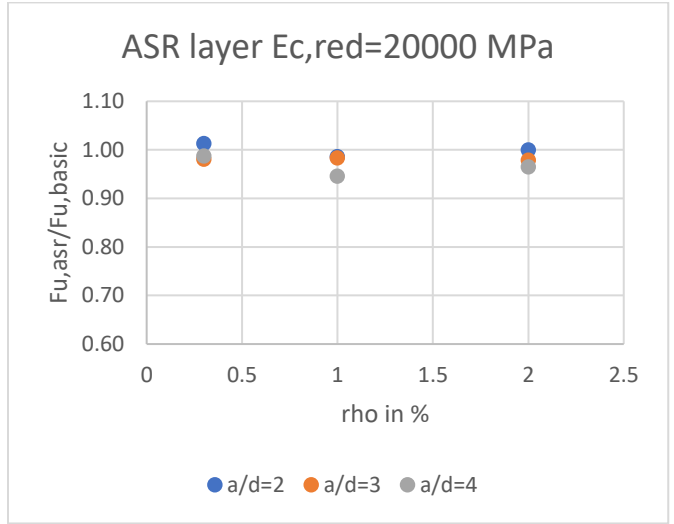


Figure 81 Ultimate load comparison with different a/d and reinforcement ratios

For original beams with shear failure mode, ASR layer failure occurs more with a weaker Young's modulus (Ec,red=10000 MPa). Though it does not necessarily result in a significant reduction in ultimate load. Even the largest reduction is approximately 1/3 of the original value. With a stronger ASR layer, shear failure becomes the main failure mode. ASR layer failure occurs when a/d and reinforcement ratio are relatively large. Ultimate load is rarely affected by ASR layer in this series of beams.

For original beams with bending failure mode, ASR layers might have an effect on the crack pattern when ASR layers are weak. Some cracks occur there. With a stronger ASR layer, the effect becomes smaller. Overall, the ultimate load is rarely affected by ASR layers.

#### 5.3.4 Failure mode

The failure mechanisms can be classified into several types, in beams with a comparatively higher reinforcement ratio,

- 1) ASR layer failure when ASR layers are relatively weak.
- 2) ASR-affected shear failure. It is also called ASR slip failure in literature (Abe, Kikuta, Masuda, & Tomozawa, 1989). Diagonal shear cracks will follow the direction of ASR cracks partly when they come across each other. This occurs as a transition from ASR layer failure to shear failure, when properties of ASR layers are in a medium level.
- 3) Shear failure. This occurs when properties of ASR layers are close to sound concrete.

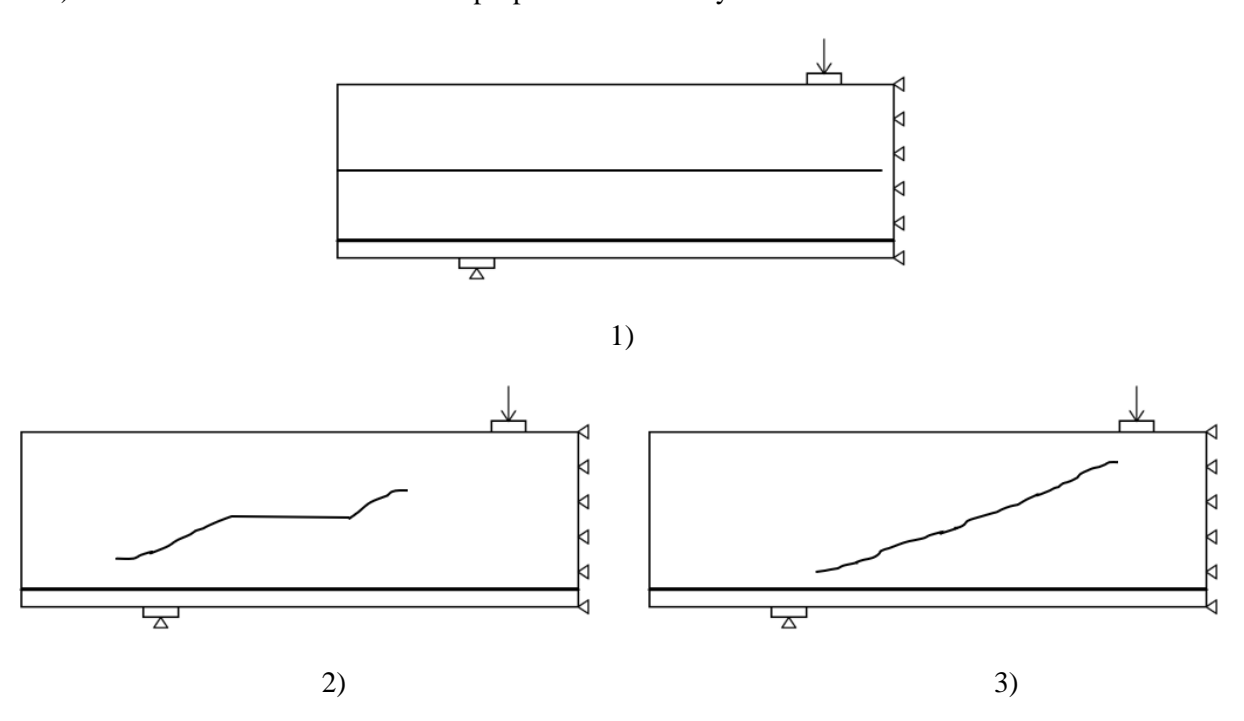


Figure 82 Failure mode of reinforced beams: 1) ASR layer failure (top), 2) ASR-affected shear failure (bottom left) and 3) shear failure (bottom right)

In beams with a low reinforcement ratio (required minimum reinforcement ratio in this study),

- 1) ASR-affected bending failure. When ASR layers are weak, the cracks in ASR layers appear almost at the same time with bending cracks.
- 2) Bending failure. Generally, the influence of ASR layers on bending failure is limited.

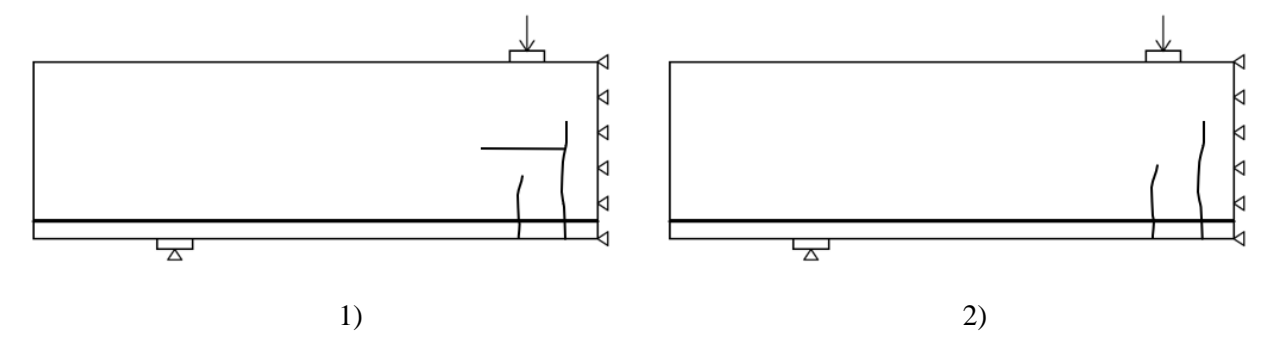


Figure 83 Failure mode of reinforced beams: 1) ASR-affected bending failure (left) and 2) Bending failure (right)

## 5.4 ATENA analysis of models with prestressing

#### 5.4.1 Introduction

A positive effect is brought to structures by ASR expansion, named chemical prestress. Tensile stresses are induced in reinforcement, with compressive stresses in the surrounding concrete. Shear resistance could be increased by this effect. In this case, shear failure might switch to bending failure due to the chemical prestress effect.

Taking beams with 2% reinforcement ratio as a reference, an analysis simulating the effect using physical prestress could be done.

The yielding strain of reinforcement can be calculated as

$$\varepsilon_{v} = \sigma_{v} / E_{s} = 435 / 200000 = 0.22\%$$

Without experimental data in this analysis, we assume the steel strain due to chemical prestress is 0.3 of the yielding strain, which is 0.066%. The initial steel stress due to chemical stress can be calculated as

$$\sigma_s = \varepsilon_s \cdot E_s = 0.066\% \cdot 2 \cdot 10^5 = 132 \text{MPa}$$

Prestress force applied at reinforcement is

$$F_p = \sigma_s \cdot A_s = 132 \cdot 2\% \cdot 500 \cdot 500 = 660kN$$

Other calculation results in prestressing analysis, including force-displacement response, crack pattern and principal strain pattern can be found in Appendix 4.

## 5.4.2 Force-displacement curve and failure mode

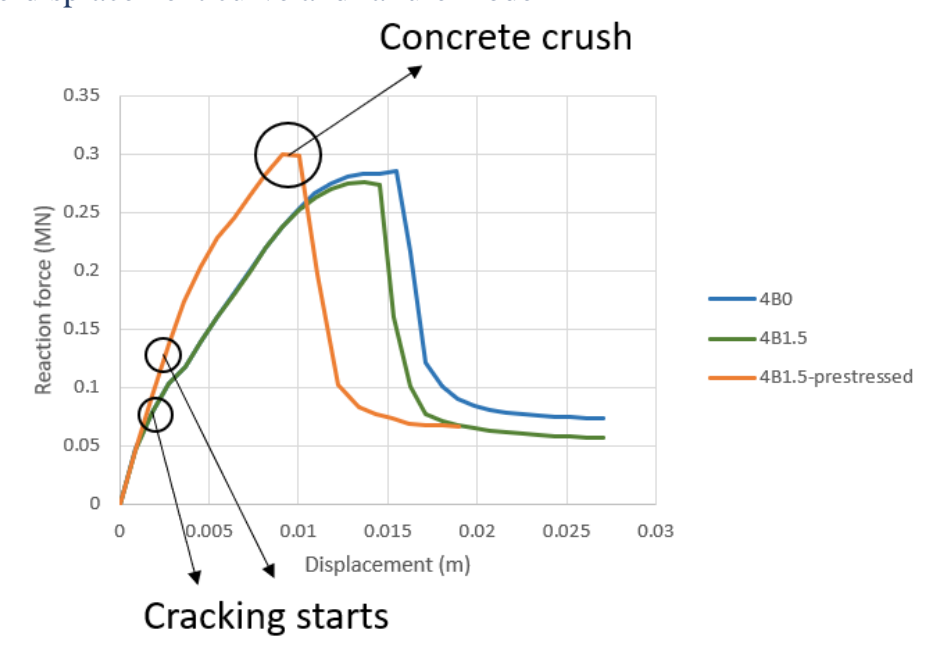
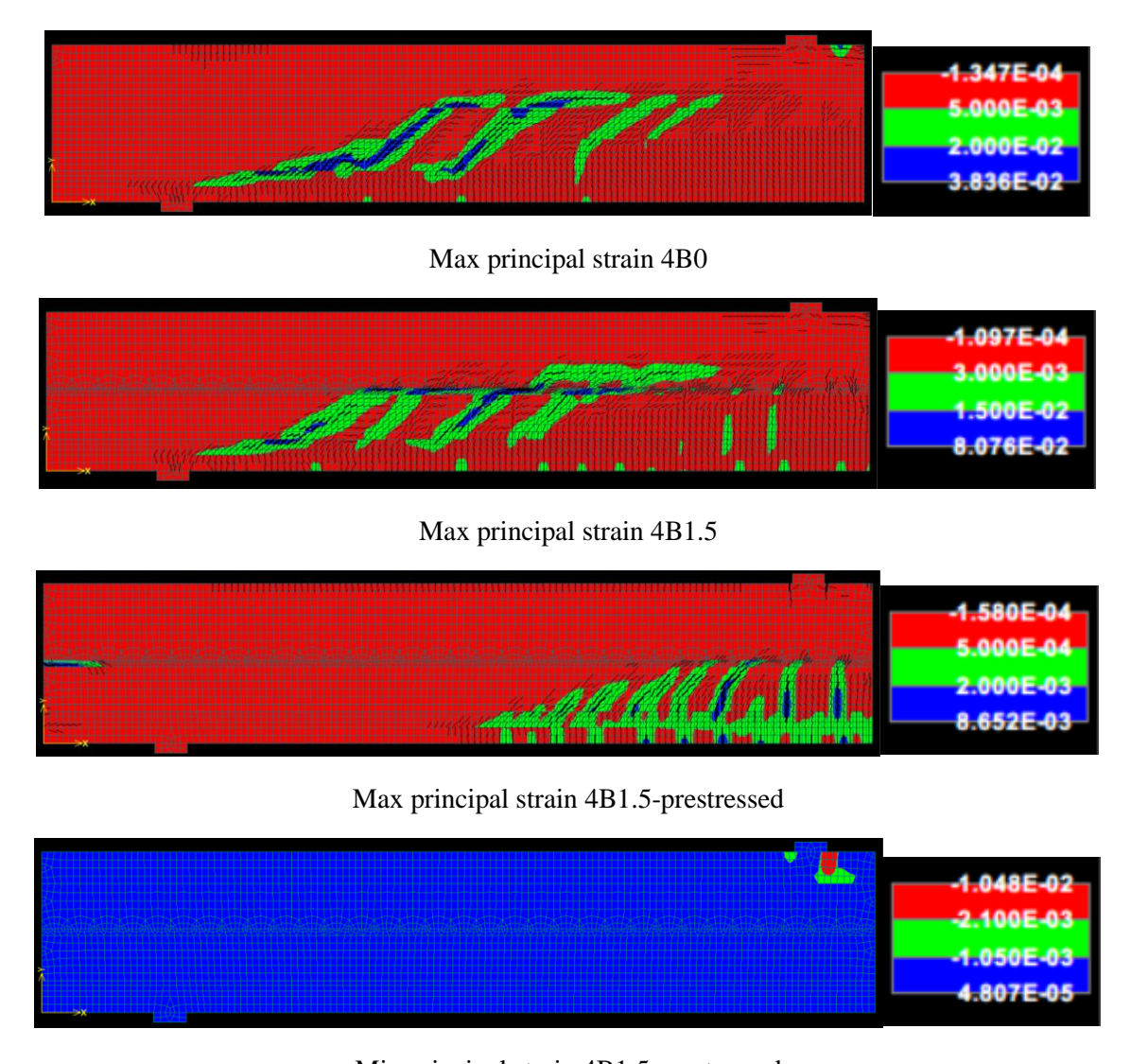


Figure 84 Force-displacement curve for sound beam 4B0, ASR-affected beam 4B1.5 and ASR-affected beam with prestressing 4B1.5-prestressed



Min principal strain 4B1.5-prestressed

Figure 85 Principal strain pattern for beams 4B0, 4B1.5 and 4B1.5-prestressed

With the prestressed steel, the beam stiffness after crack has increased. An increase in the ultimate load is also observed comparing to the beam without prestressing. The ultimate load of prestressed beam goes to the level of slightly higher than the sound beam. The property reduction due to ASR cracks are compensated by prestressing.

The beams without prestressing fail in shear or ASR-affected shear, while the presence of prestressing changes the failure mechanism from shear to bending. No steel yielding occurs, the loss of structural capacity is due to concrete crush. A part of concrete crush (red in min principal strain 4B1.5-prestressed in Figure 85) is observed near the loading point.

#### 5.4.3 Discussion

Prestressing gives the possibility of changing the failure mechanism from shear to bending. It is caused by the earlier concrete crush in this case. Chemical prestress effect might be presented by directly adding this physical prestress.

## 5.5 ATENA analysis of models with prestressing and bond

#### 5.5.1 Introduction

As stated in previous chapter, bond degradation is expected to occur as a result of ASR. And the numerical analysis including bond model does provide a better fitting with experimental results. The development and implementation of appropriate bond models for ASR-affected concrete would be of value for structural elements that are susceptible to bond slip.

In this analysis, poor bond model according to Model Code 1990 is used. The prestress level is taken the same as models with only prestress. The steel strain due to chemical prestress is assumed to be 0.3 of the yielding strain, which is 0.066%. The initial steel stress due to chemical stress can be calculated as

$$\sigma_s = \varepsilon_s \cdot E_s = 0.066\% \cdot 2 \cdot 10^5 = 132 \text{MPa}$$

Prestress force applied at reinforcement is

$$F_p = \sigma_s \cdot A_s = 132 \cdot 2\% \cdot 500 \cdot 500 = 660kN$$

Also, beam 4B0 is taken as a reference here. Other calculation results in the analysis with prestressing and bond model, including force-displacement response, crack pattern and principal strain pattern can be found in Appendix 5.

#### 5.5.2 Force-displacement curve and failure mode

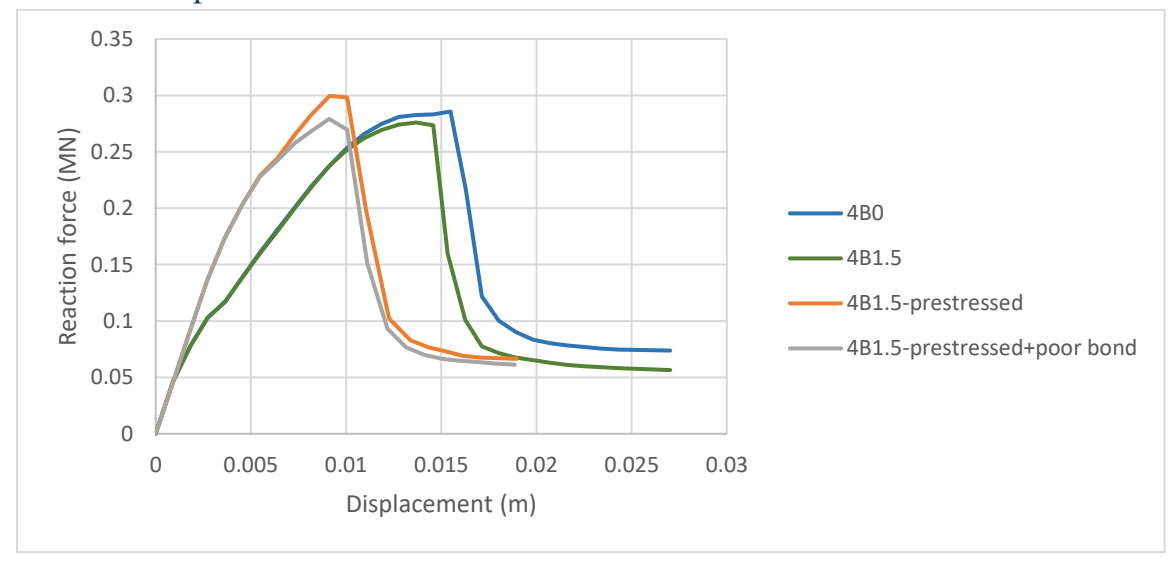
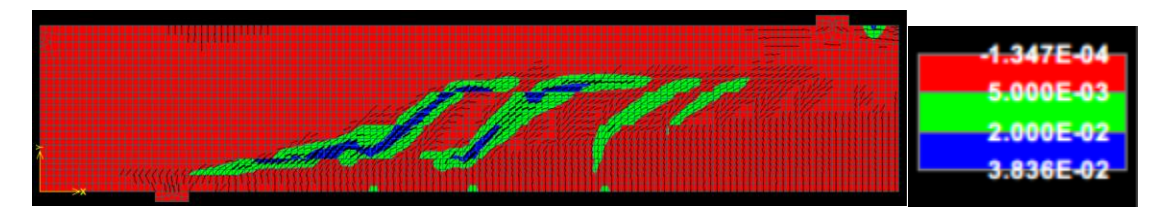
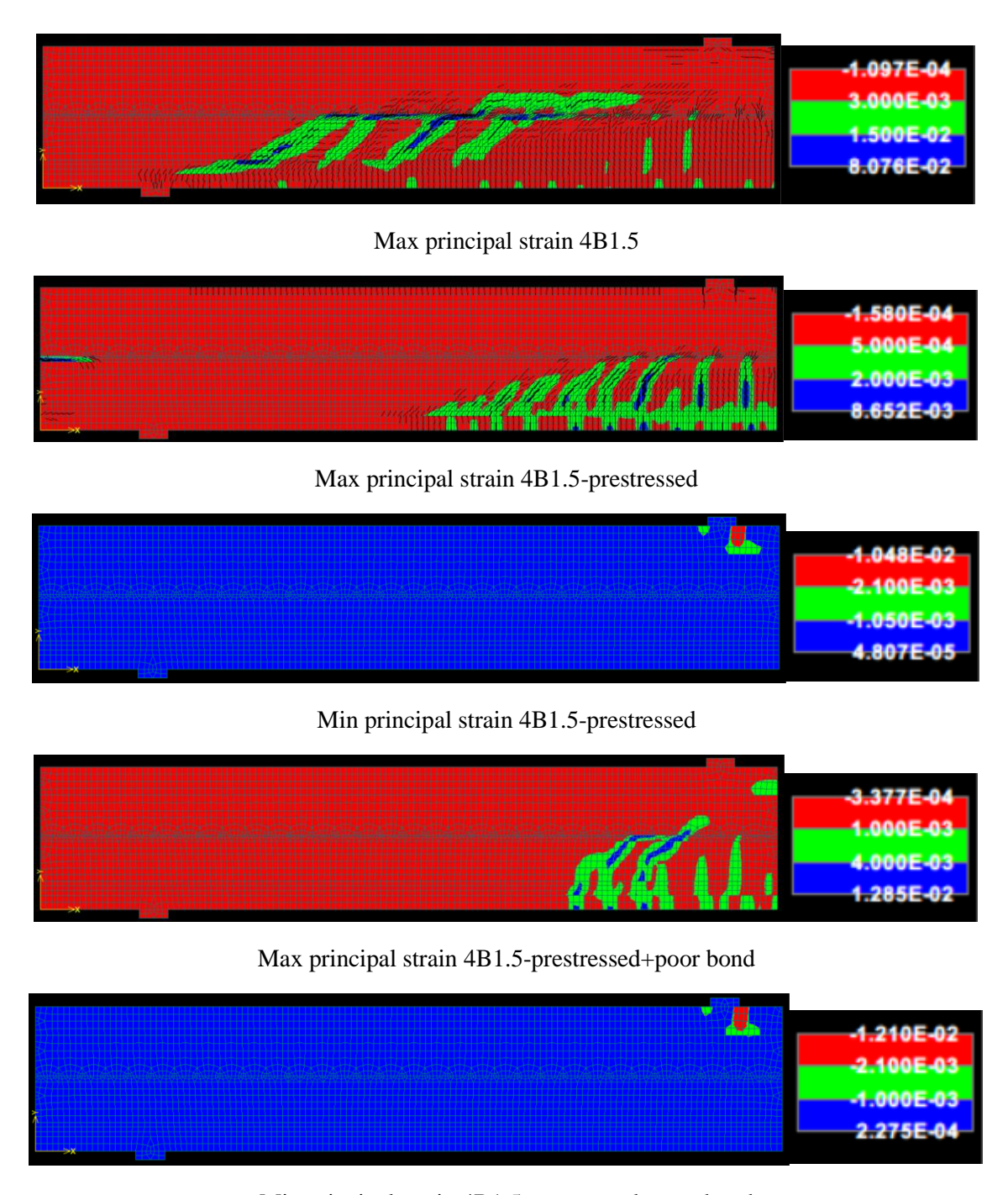


Figure 86 Force-displacement curve for sound beam 4B0, ASR-affected beam 4B1.5, ASR-affected beam with prestressing 4B1.5-prestressed, ASR-affected beam with prestressing and poor bond 4B1.5-prestressed+poor bond



Max principal strain 4B0



Min principal strain 4B1.5-prestressed+poor bond

Figure 87 Principal strain pattern for beams 4B0, 4B1.5, 4B1.5-prestressed and 4B1.5-prestressed+poor bond

The main difference between prestressed model and prestressed model including poor bond is the ultimate load. In beam 4B1.5-prestressed+poor bond, the detrimental effect of bond model and property reduction overcomes the beneficial effect due to chemical prestressing. Its ultimate load is reduced to less than that of the unaffected beam. Unlike prestressing, the beam stiffness after cracking is not affected by bond model.

Taking the bond model into account, similar with the prestressed beam, this beam also fails in bending. No steel yielding occurs, and the loss of structural capacity is due to concrete crush. The concrete crush part observed near the loading point is shown in red in min principal strain 4B1.5-prestressed+poor bond in Figure 87.

#### 5.5.3 Discussion

As shown in Appendix 5, for unaffected beams failing in bending, the poor bond model underestimates the ultimate load too much and causes brittle failure, which cannot reflect the experimental results. For unaffected beams failing in shear, the poor bond model reduces its ultimate load comparing to perfect bond model. Due to both the beneficial effect of chemical prestress and detrimental effect of bond model, there is no certain trend of increase or decrease in the resulting ultimate load.

#### 5.6 Conclusions

The main goal of this chapter is to investigate more about the parameters which affect the beam behavior. With all the supporting analysis above, these conclusions can be summarized as follows,

- 1) For models with the same a/d and reinforcement ratio, various ASR layer properties in a practical range do not give a significant impact to the ultimate load level. In bending failure beams, almost no change in load capacity, this is in line with (Fan & Hanson, 1998). In beams fail in shear, the ultimate load for ASR-affected beams ranges from about 75% to nearly 100% of the unaffected one, this is in line with (den Uijl J., 2000). While increase in load capacity (Ahmed, Burley, & Rigden, 1998) is only observed when prestressing is included in the model. Introducing bond model will decrease its load capacity.
- 2) As for failure mode, without prestressing, only failure mode change from shear to ASR layer slipping failure is observed. This is in line with (Abe, Kikuta, Masuda, & Tomozawa, 1989), see Figure 78. While a switch from shear to bending failure (Ahmed, Burley, & Rigden, 1998) and (Inoue, Fujii, Kobayashi, & Nakano, 1989) happens when taking prestressing into account.
- 3) The diagonal shear cracks or vertical bending cracks tend to partly follow ASR cracks when they propagate to the level of ASR layers. Weaker ASR layers will induce denser cracks and a longer crack range in horizontal direction, thus ASR layer failure is more likely to occur. This effect on crack pattern is also observed from (Abe, Kikuta, Masuda, & Tomozawa, 1989).
- 4) Similar trend shows in models with 1 or 2 ASR layers, no failure mode change is seen when only number of ASR layers changes. The differences between their peak forces are small.
- 5) ASR layers give a larger influence when shear failure tends to occur in the beam. Bending failure is seldom affected by ASR layers. From (Ahmed, Burley, & Rigden, 1998), (den Uijl J., 2000), (Fan & Hanson, 1998), (Kobayashi, Inoue, Yamasaki, & Nakano, 1988) and (Inoue, Fujii, Kobayashi, & Nakano, 1989), load capacity for beams in shear failure varied a lot, both increase and decrease were observed, and in some cases the failure mode changed to bending. However, for beams failed in bending, the influence on load capacity was ignorable, and no switch from bending to shear failure was found.

## 6 Summary

In this thesis, the ASR-layer model is proposed and analyzed with ATENA comparing to analytical and experimental results. In horizontal direction, the expansion is restrained by reinforcement. Due to this restrained effect, the greatest expansion occurs at the least confinement direction, and the cracks become oriented in the same direction as confining stresses. Introducing horizontal ASR layers, the property reduction caused by ASR is assumed to concentrate in these layers, while the other part of the structure remains unaffected sound property. As for induced stress caused by restraint, an initial steel strain is added to reinforcement as a simulation of this chemical prestress effect.

- 1) The reinforcement would make an unignorable difference in the ASR affected structures. With the presence of longitudinal reinforcement, the ASR expansion is restrained in horizontal direction, resulting in non-uniform expansion in the structure. This would also affect ASR cracks, they are oriented more parallel to the existing reinforcement. In the first part, the ASR-layered model is proposed to simulate the restrained effect due to reinforcement. In order to model the ASR cracks, the horizontal ASR layers with reduced properties are introduced to the sound structure. The chemical prestress effect exists in ASR-affected structures due to reinforcement restraint, this effect will result in the restrained expansion and induced stresses. Prestress is introduced to this model to analyze this chemical prestress effect. When the beneficial effect of prestressing overcomes the influence of property reduction, an increase of load capacity in affected beam is observed. Both models without and with prestress are analyzed. Also, the neglection of ASR influence on reinforcement bond should be noticed. The bond strength is found to be lower in ASR affected structures (Ahmed, Burley, & Rigden, 1999), and the decrease of bond strength is likely due to the formation of ASR gel. Therefore, an analysis on bond model is performed here.
- 2) In the second part, a series of basic beams in four-point bending test are numerically analyzed to investigate the influence of different parameters. The shear span to effective depth ratio (a/d ratio), the reinforcement ratio, the number of ASR layers and the reduction rate of ASR layer properties are investigated in this part. Starting from un-prestressed model, later prestressed model as well as the model with both prestress and bond, research on the influence of prestress and bond model is done. It is observed by a lot of experiments as stated in literature review, many cases showed almost no reduction, a small reduction or even an increase in ultimate load. The beneficial effect of hydration of the cement, the presence of tensile reinforcement inducing prestress, the ASR gel acting as a strong filler, could compensate for some detrimental effect of cracks due to ASR (Ahmed, Burley, & Rigden, 1998). For the failure mechanism, in many cases it did not change, in some cases a transition from shear to bending failure occurred, but no opposite trend was observed.
- 3) To apply this model in analyzing an ASR affected structure, the input parameters are number of layers, ASR layer properties, prestressing level and bond-slip model. The cracking pattern of ASR affected structure could give a clue to choose the number of layers, it could be done by counting the number of possible long cracks formed on the surface. Without knowing the accurate property of ASR cracks, it is a safe way to use the lower bound curve from (ISE, 1992), the suggestion property values are given once the expansion is known. The result could give a lower bound estimation of load capacity. With measured steel strain or steel stress, the

prestressing model could be established. The poor bond model from Model Code is suggested to get a good prediction on the failure mechanism.

## 7 Conclusions and recommendations

#### 7.1 Conclusions

The aims of this research are to propose a new method to analyze ASR-affected structures, compare the numerical results from ATENA with available experimental results, and perform a basic analysis to investigate the influence of different parameters on structural behavior of ASR-affected structures. The main conclusions are summarized as follows:

- 1) In numerical analysis, the influence of property reduction on load capacity is larger when no prestress is considered. While with prestressing, the load capacity could be increased comparing to non-prestressed models. The chemical prestress and hogging effect play a role in increasing the beam stiffness.
- 2) Without prestressing, no change of failure mechanism from shear to bending is observed, which means the influence of chemical prestressing should not be neglected.
- 3) An increasing level of prestress changes the failure mode from shear to bending. It is caused by an earlier yielding of reinforcement and earlier concrete crush. However, this prestressed model could not obtain the correct failure mechanism sometimes.
- 4) When analyzing shear failure structures, including the bond-slip effect in prestressed model, the poor bond model according to Model Code fits the experimental results well. But bond strength of ASR affected structures remains unknown up to now, not many researches have been done before
- 5) ASR gives a larger influence when shear failure tends to occur in the beam. While bending failure is seldom affected by ASR.
- 6) In case of sound beam failing in shear, the ultimate load for ASR-affected beams ranges from about 75% to nearly 100% of the unaffected one, it mainly depends on the residual properties of ASR layers.
- 7) No obvious influence could be linked to a/d ratio and reinforcement ratio when the structures suffer from ASR.
- 8) The difference caused by 1 or 2 ASR layers is relatively small. It will not affect the failure mechanism.
- 9) The ultimate load reduces with an increasing reduction level of ASR layer properties. However, in experiments it is hard to separate this detrimental effect and some beneficial effect such as chemical prestress.
- 10) However, there are some limitations of this model. The expansion caused by ASR is not directly modelled, so the hogging effect would be underestimated when unequal reinforcement in top and bottom exists. Information on ASR layer property is quite limited, it would be difficult to measure the cracking part of ASR affected structures alone. In addition, the chemical prestress and possible cracking depend on the amount of ASR expansion as well as the reinforcement arrangement and amount, but they are not considered to correlate with each other in this model.

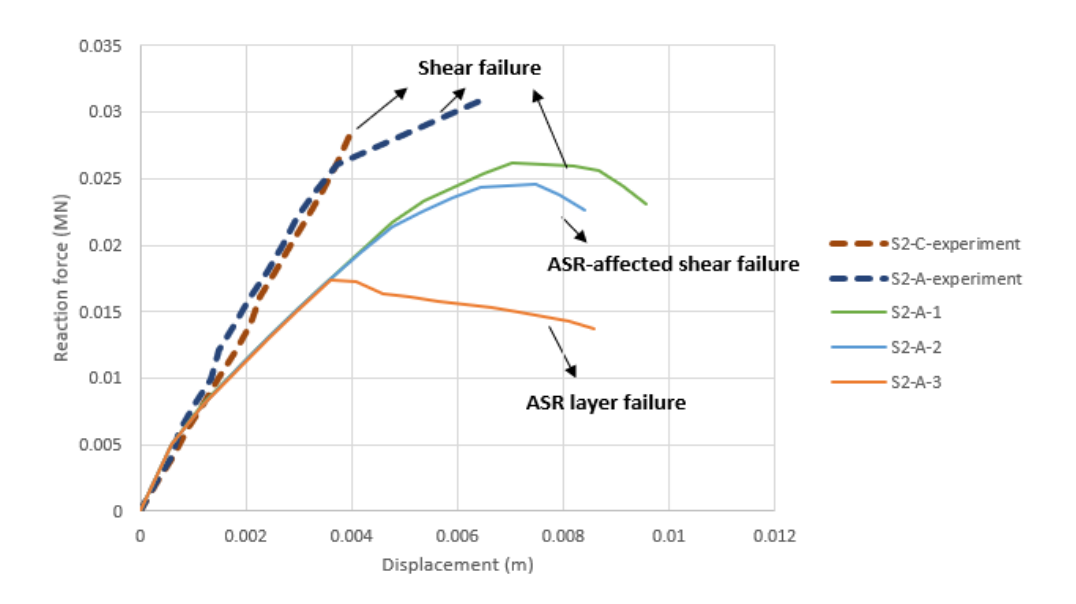


Figure 88 Influence of ASR layer material properties (-1, -2, -3 represent the amount of property reduction in ASR layers, -3 shows the largest reduction)

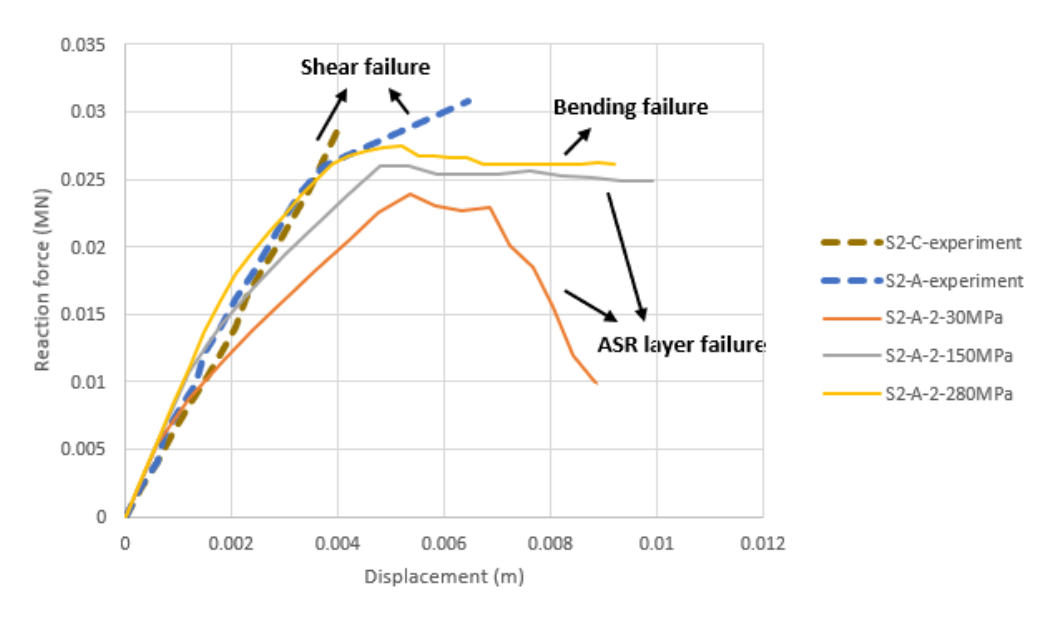


Figure 89 Influence of prestressing level (30MPa, 150MPa and 280MPa represent the initial tensile stress induced in reinforcement)

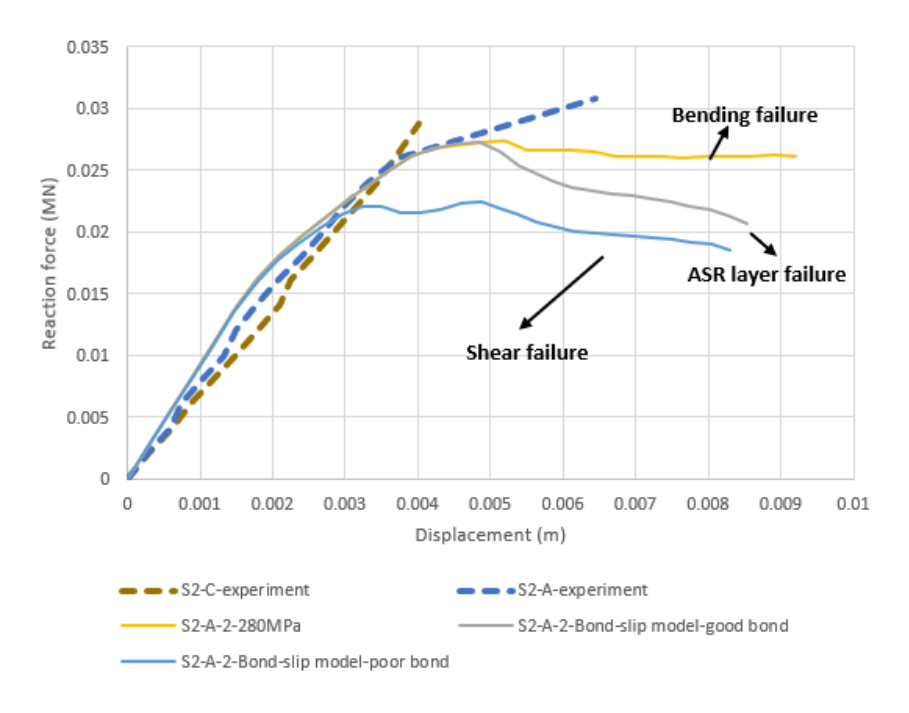


Figure 90 Influence of reinforcement bond

## 7.2 Recommendations

There are some more points worth further research.

- 1) More experiments could be done to get the relationships between ASR cracking property reduction and chemical prestress. It would be useful to achieve the numerical relations, after which, the input of the model could be more accurate.
- 2) Chemical prestressed model could be modified. The expansion due to ASR is not included in this model, this is one of the differences between chemical prestress and physical prestress. The formation of expansive ASR gel provides a larger upward deflection in real structure than FE model prediction.
- 3) Bond slip might occur due to ASR gel. In this thesis, perfect bond, good bond and poor bond (bond-slip model calculated according to Model Code) are modelled. Prestressing in combination with a poor bond could predict the failure mode well, but the input values for bond model in ASR affected structures need more research.
- 4) As a basic step, only structures without stirrups are modelled in this thesis. However, the failure mechanism changing from shear to bending in available tests all occurred in beams with stirrups. This work could be furthered with this ASR layered model with prestressing and bond-slip, which is proved to be capable of modelling the structures without stirrups.

## **Appendix**

## Appendix 1 Calculation on ATENA models a/d=2

## Appendix 1.1 Force-displacement response

No reinforcement, 1 layer:

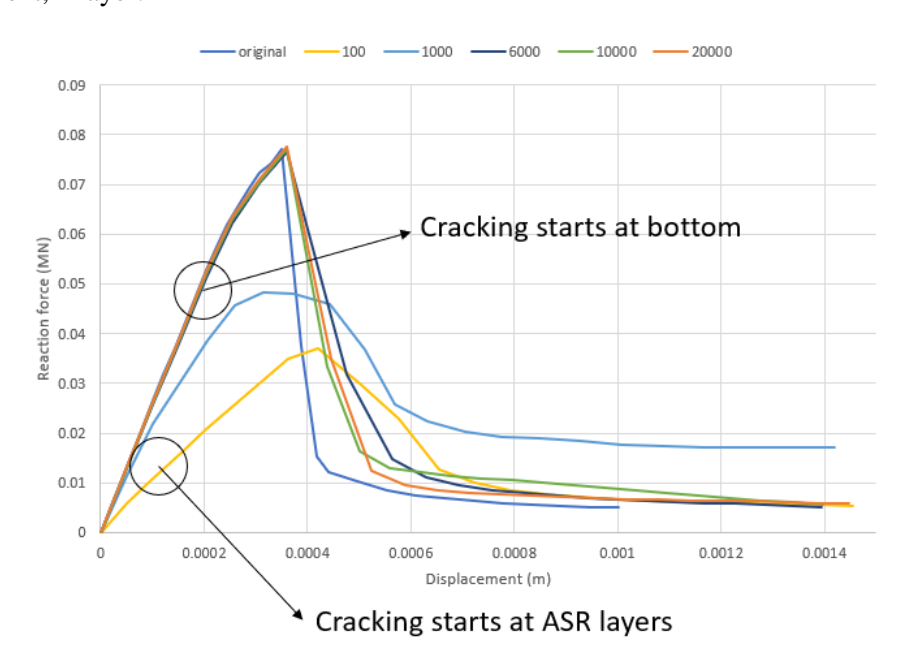


Figure 91 Force-displacement curves for beams with no reinforcement, 1 ASR layer

#### No reinforcement, 2 layers:

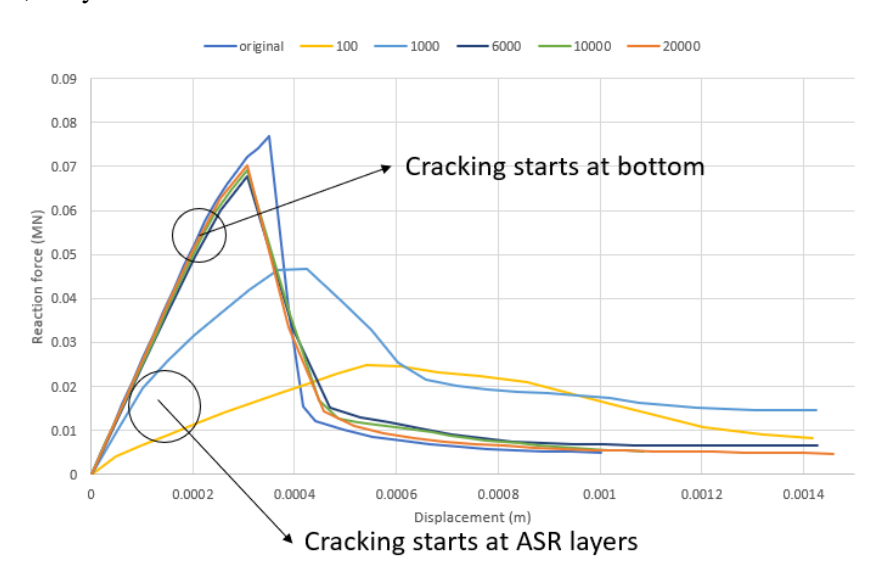


Figure 92 Force-displacement curves for beams with no reinforcement, 2 ASR layers

When no reinforcement exists, for models with either 1 ASR layer or 2 ASR layers, the first parts of the curves are all linear when Ec,red>6000 MPa. In this part the beams take load without cracks. Before the curves show a peak, a less steep nonlinear part is observed due to the occurrence of cracks. While for

models with Ec,red<1000 MPa, these beams work with cracks at an early stage. The weak layers between upper and lower parts are a reason for the decreased structural capacity.

These peaks almost overlap with each other especially when Ec,red>6000 MPa. For the 1-layer model of Ec,red=100 MPa, its reaction force value at first peak is about half of the original model. And the slope of the curve is smaller than others, which results in a less steep curve. For the 2-layer model of Ec,red=100 MPa, its peak reaction force is even lower. For the model of Ec,red=1000 MPa, the reaction force peak value is about 1/3 less than that of the original model, while its slope is in between the Ec,red=100 MPa and others.

### 2% reinforcement, 1 layer:

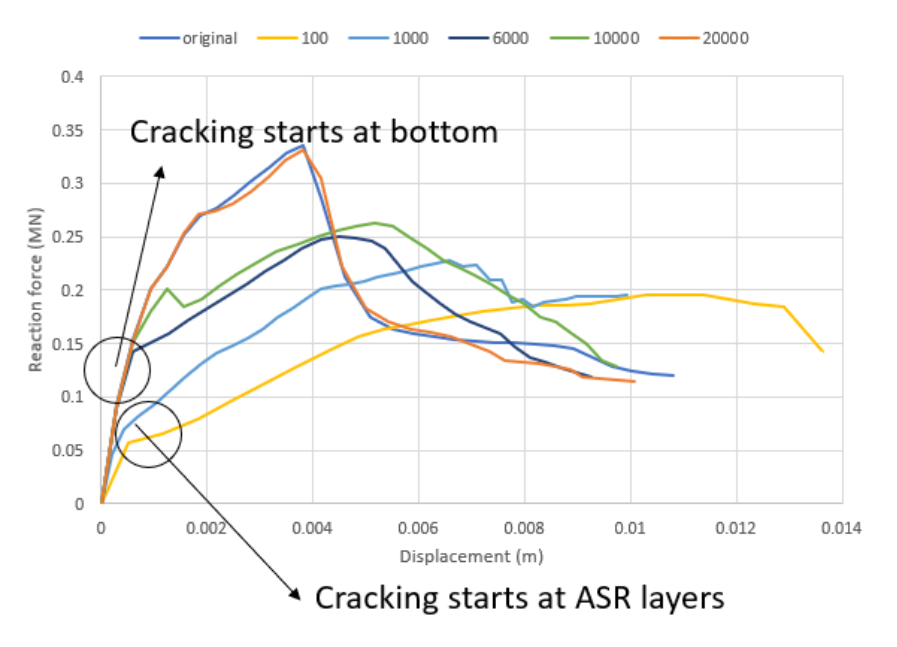


Figure 93 Force-displacement curves for beams with 2% reinforcement, 1 ASR layer

2% reinforcement, 2 layers:

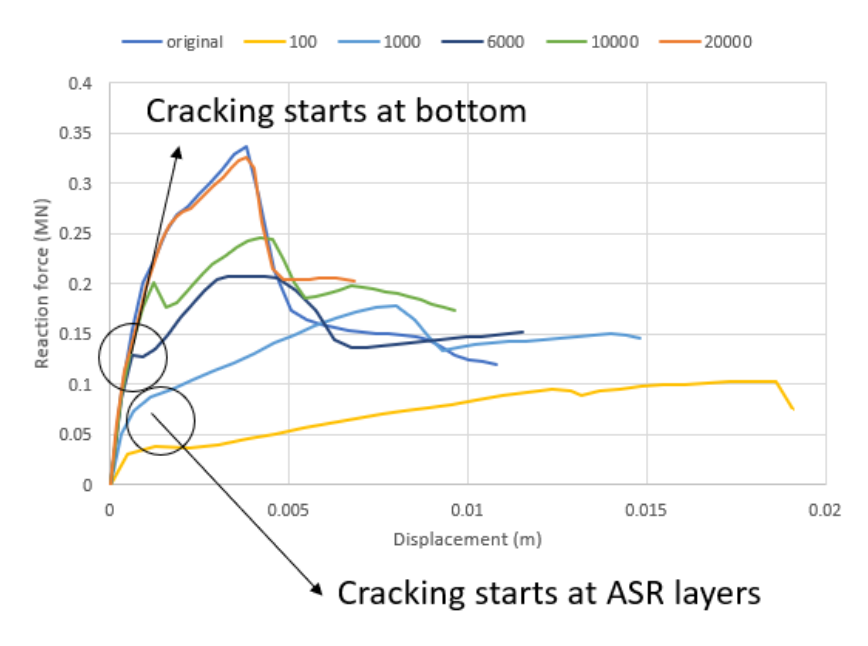


Figure 94 Force-displacement curves for beams with 2% reinforcement, 2 ASR layers

For beams with 2% reinforcement ratio, similar trend as models with no reinforcement also applies. A more ductile beam behavior shows here due to the presence of reinforcement. For 2-layer model with Ec,red=6000 MPa, the peak load reduction is a bit larger than 1-layer model with the same Ec,red, which are both 2/3 the value of basic model.

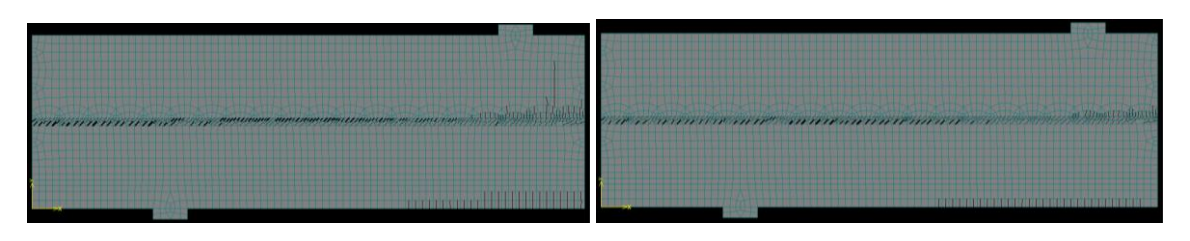
To sum up, models with 1 ASR layer and 2 ASR layers show similar trend in force-displacement diagrams. However, the models with 1 ASR layer mostly have a slightly higher peak reaction force than models with 2 ASR layers, though the difference is not too much. From the analysis above, for beams with 1 or 2 ASR layers, when Ec,red>6000 MPa, the influence of number of ASR layers on structural capacity is limited compared with other parameters. An interesting result from other researches is that with the increasing expansion of ASR, the minimum Young's modulus of affected concrete is around 20% of sound value, which is 6000 MPa in this analysis.

# Appendix 1.2 Crack pattern

Original with no reinforcement:



1 layer:

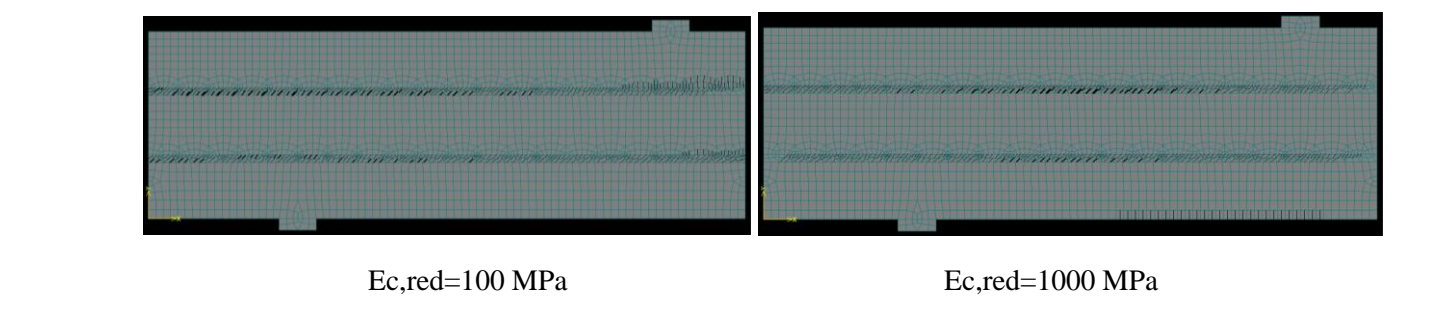


Ec,red=100 MPa Ec,red=1000 MPa



Ec,red=6000 MPa Ec,red=10000 MPa Ec,red=20000 MPa

#### 2 layers:



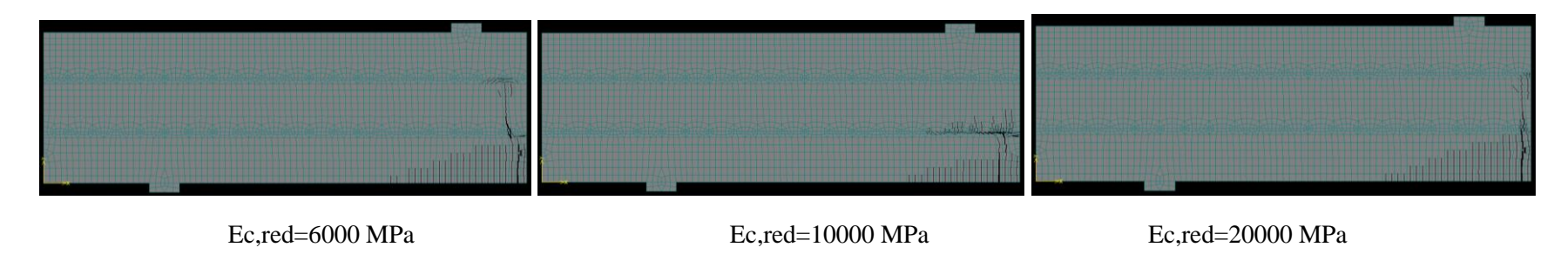


Figure 95 Crack patterns for beams with no reinforcement

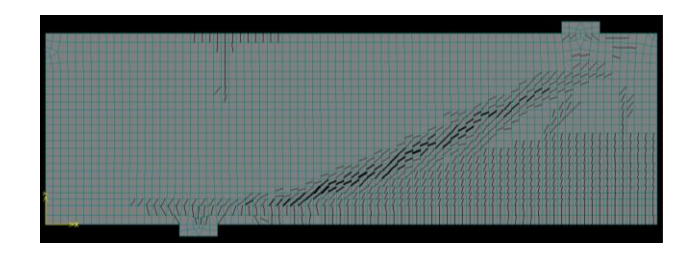
The crack patterns for each beam at ultimate load are shown in Figure 95.

The beams with ASR layers are influenced by these layers and show some different behavior, two types of behavior can be defined.

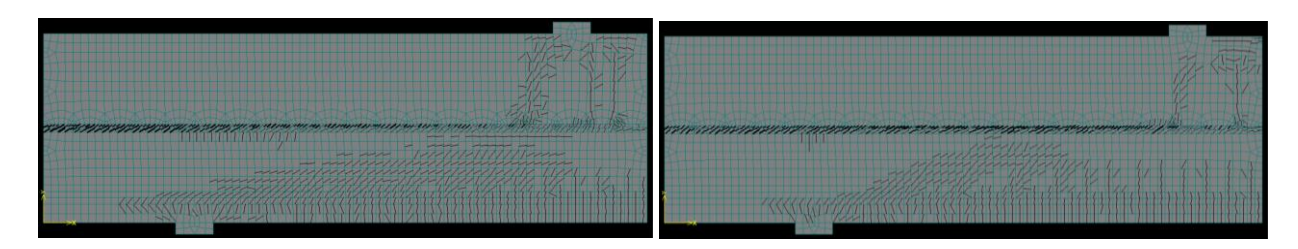
Different from the beam without ASR, major cracks tend to occur at the location of ASR layers in Beam 2A1.2 and 2A1.3. And these beams are more like two separate beams stacking together due to the very low material properties (Young's modulus 100 MPa and 1000 MPa) in ASR layer. Similar results also reflect in Beam 2A2.2 and 2A2.3 with 2 ASR layers.

For beams with higher material properties (Young's modulus>6000 MPa) in ASR layers, brittle failure occurs as the original model. However, the bending cracks tend to partly follow the horizontal ASR cracks as well as develop upwards when they intersect with ASR layers.

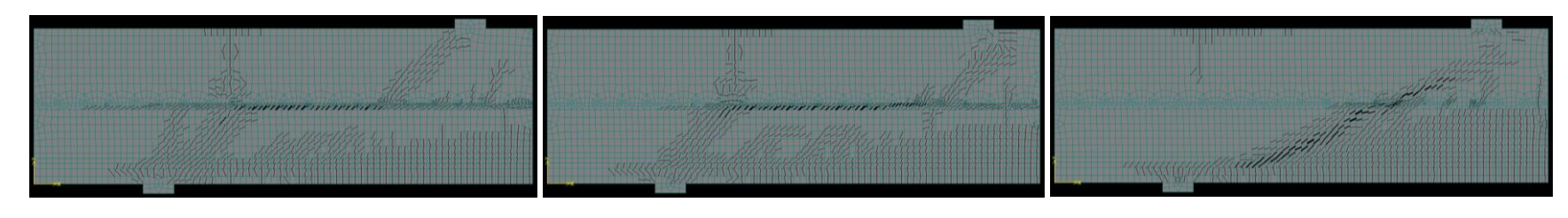
## Original with 2% reinforcement:



## 1 layer:

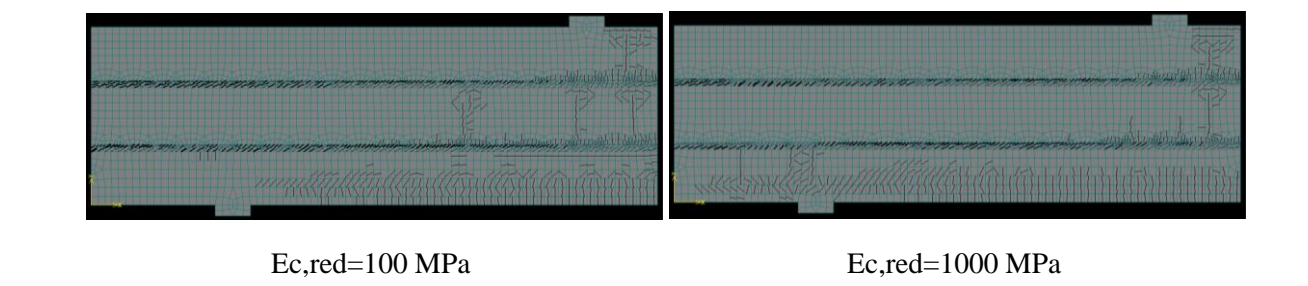


Ec,red=100 MPa Ec,red=1000 MPa



Ec,red=6000 MPa Ec,red=10000 MPa Ec,red=20000 MPa

## 2 layers:



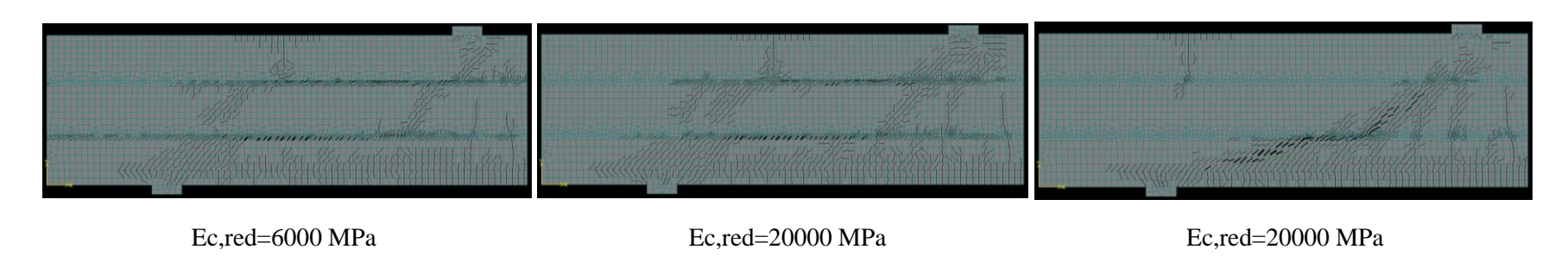


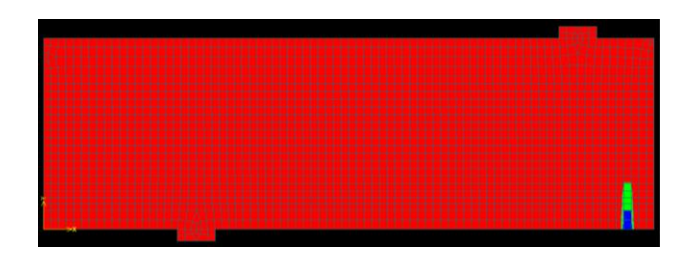
Figure 96 Crack patterns for beams with 2% reinforcement

The original model shows typical shear cracks, which originate from the bottom flexural cracks.

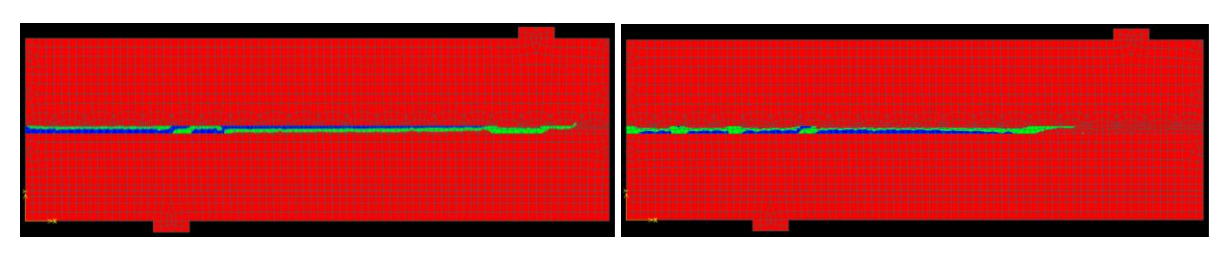
The beams with weak ASR layers, which means their property reduction is more than 1/3, have cracks in the ASR layers, shear cracks are not obviously observed.

For beams with ASR layers property reduction less than 1/3, obvious shear cracks can be observed. These cracks tend to partly follow ASR cracks when they propagate to the level of ASR layers.

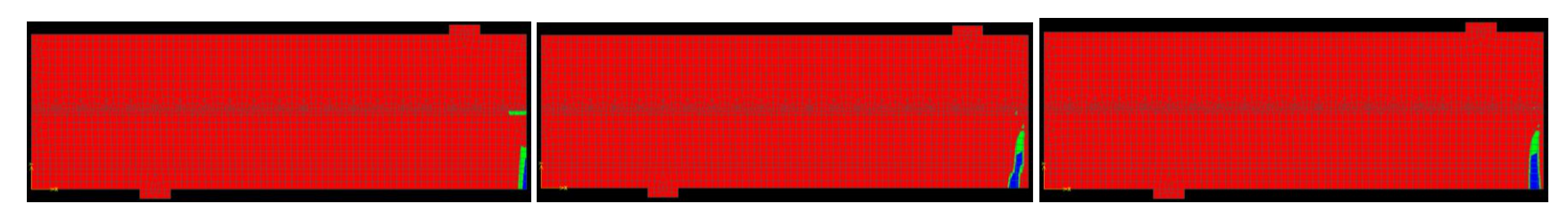
# Appendix 1.3 Principal strain Original:



1 layer:







Ec,red=6000 MPa Ec,red=10000 MPa Ec,red=20000 MPa

### 2 layers:

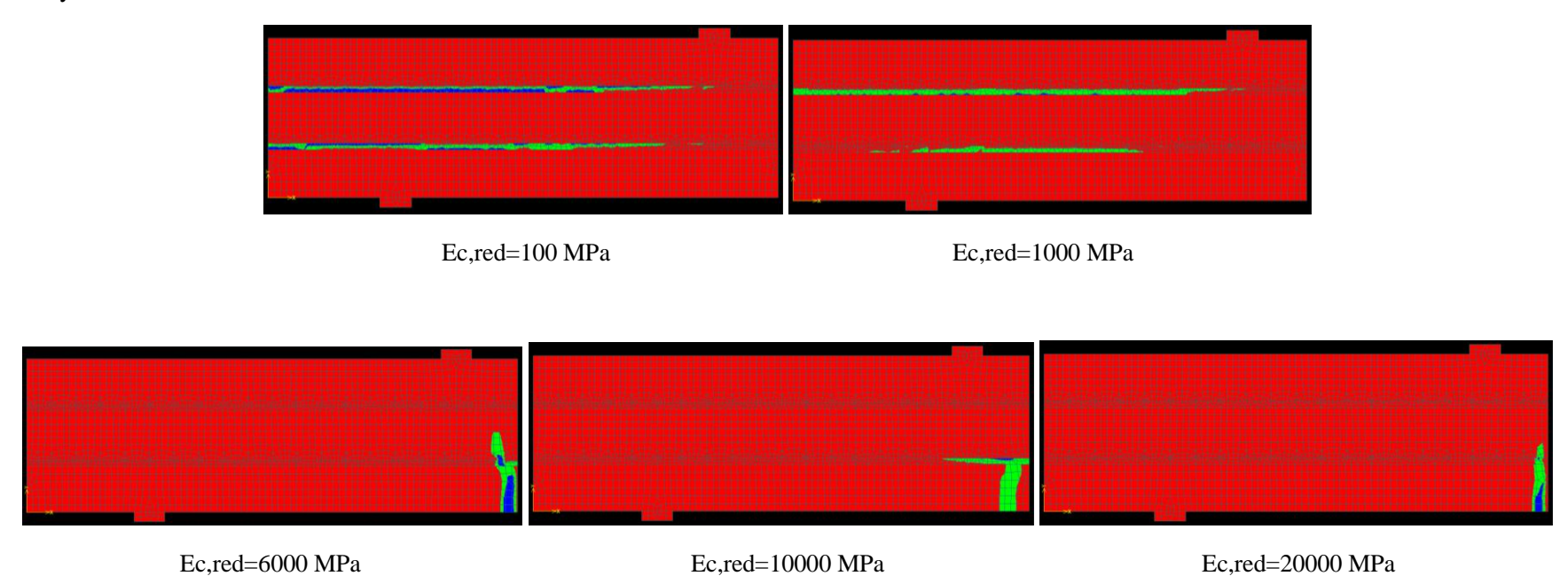
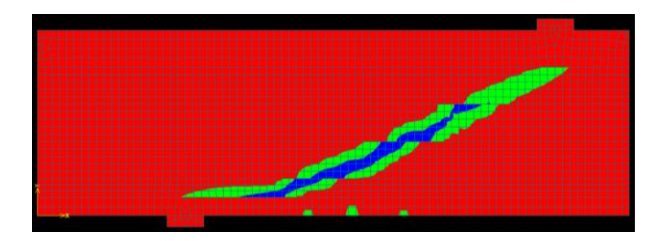


Figure 97 Principal strain patterns for beams with no reinforcement

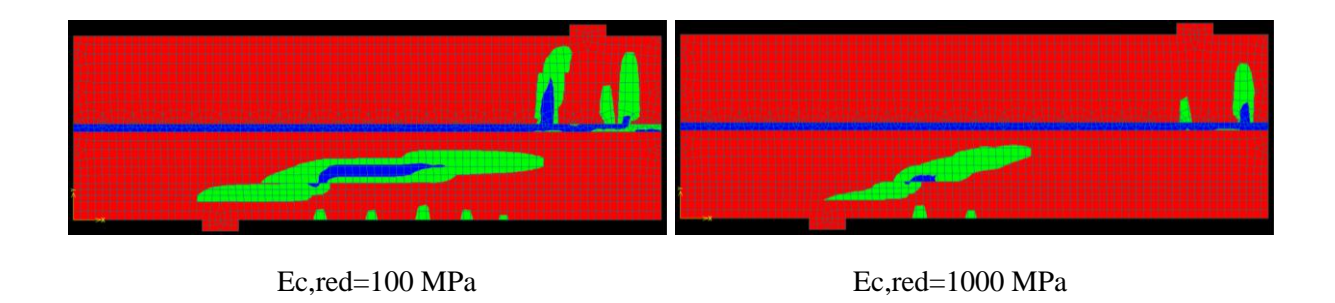
Figure 97 illustrates principal strains when ultimate load is applied. The failure mechanisms can be classified into 2 types,

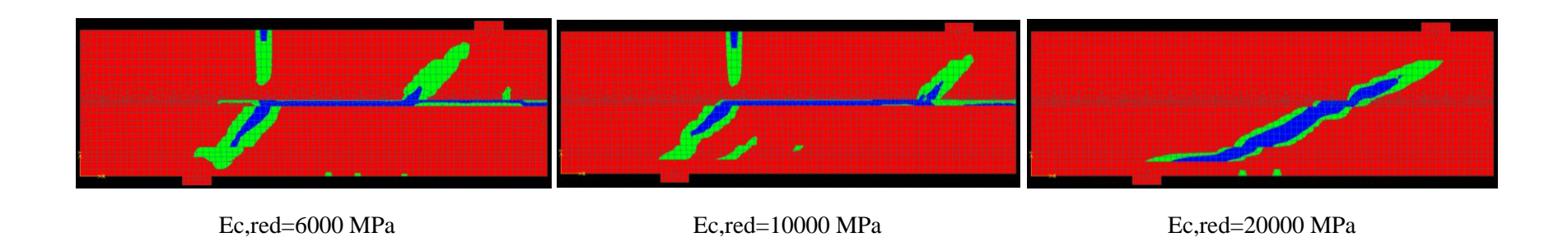
- 1) Brittle failure at the bottom near the middle, this situation occurs when property reduction of ASR part is not too much.
- 2) Failure of ASR layers when these layers are weak.

# Original:

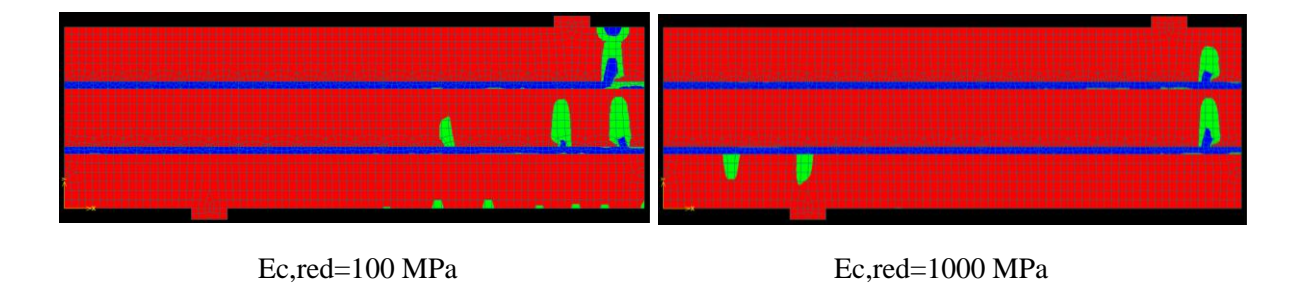


# 1 layer:





#### 2 layers:



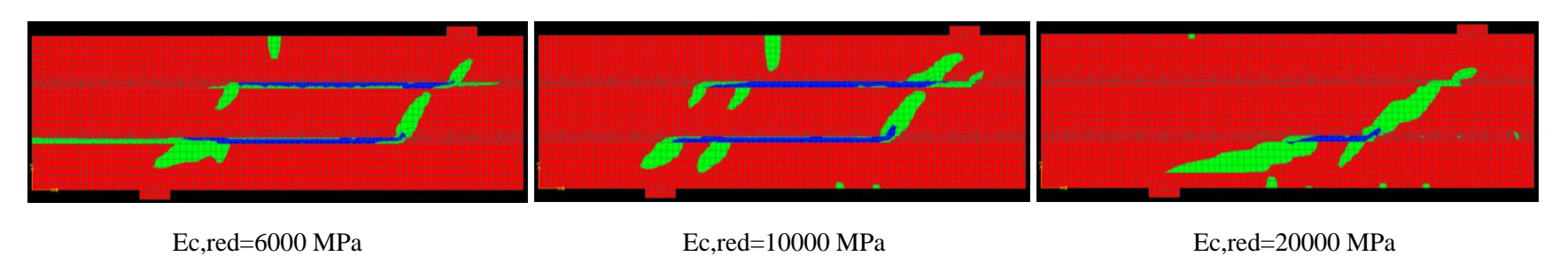


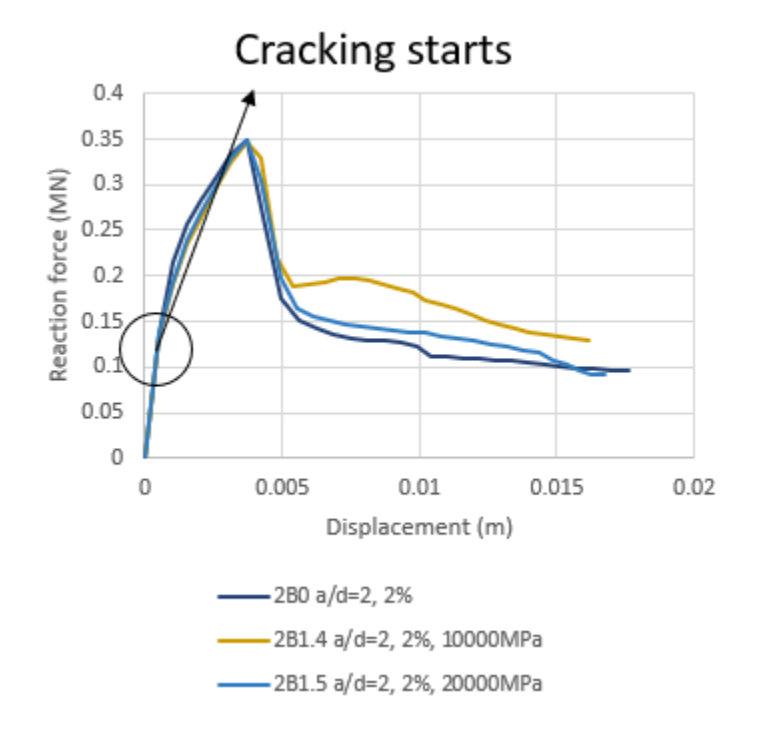
Figure 98 Principal strain patterns for beams with 2% reinforcement

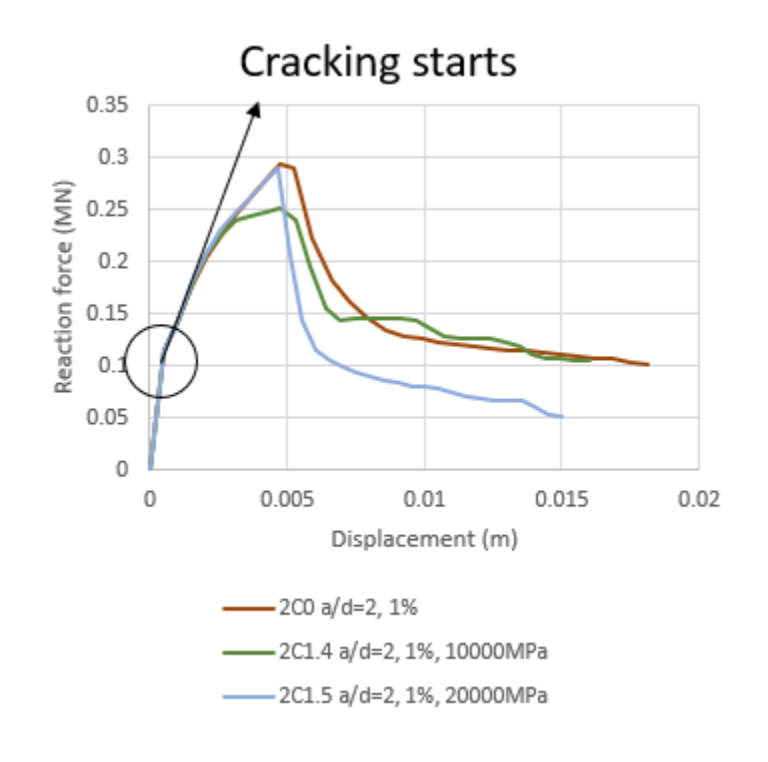
Figure 98 shows principal strains of models with 2% reinforcement ratio when ultimate load is applied. All failures occur in the part between the point-load and the its nearest support. The failure mechanisms can be classified into 3 types,

- 1) ASR layer failure when ASR layers are relatively weak.
- 2) ASR-affected shear failure, also defined as ASR slip failure in literature (Abe, Kikuta, Masuda, & Tomozawa, 1989). Diagonal shear cracks will follow the direction of ASR cracks partly when they come across each other. This occurs as a transition from ASR layer failure to shear failure, when properties of ASR layers are in a medium level.
- 3) Shear failure when reduction in ASR layers is not too much.

Appendix 2 Calculation on ATENA models with various a/d ratios

Appendix 2.1 Force-displacement response a/d=2:





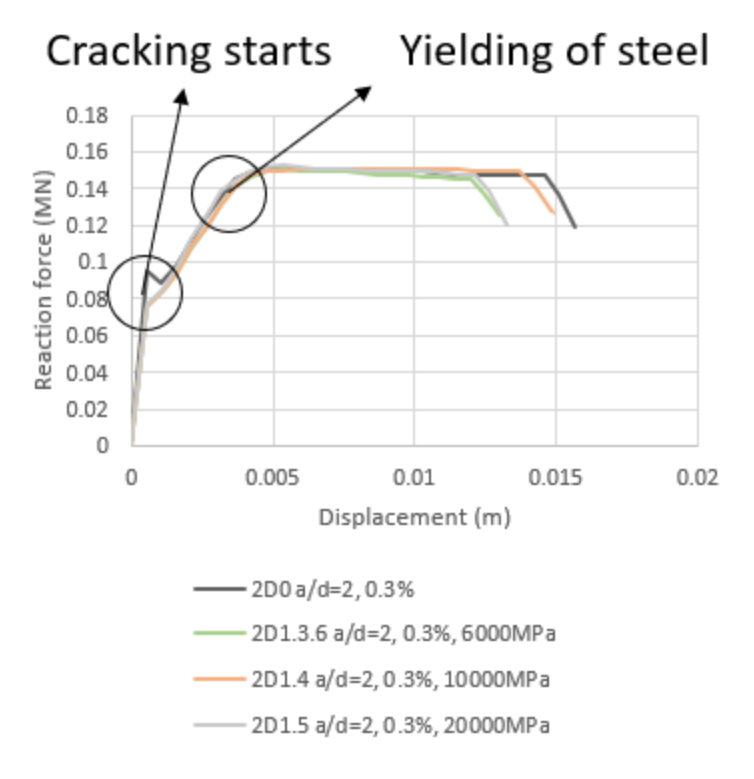
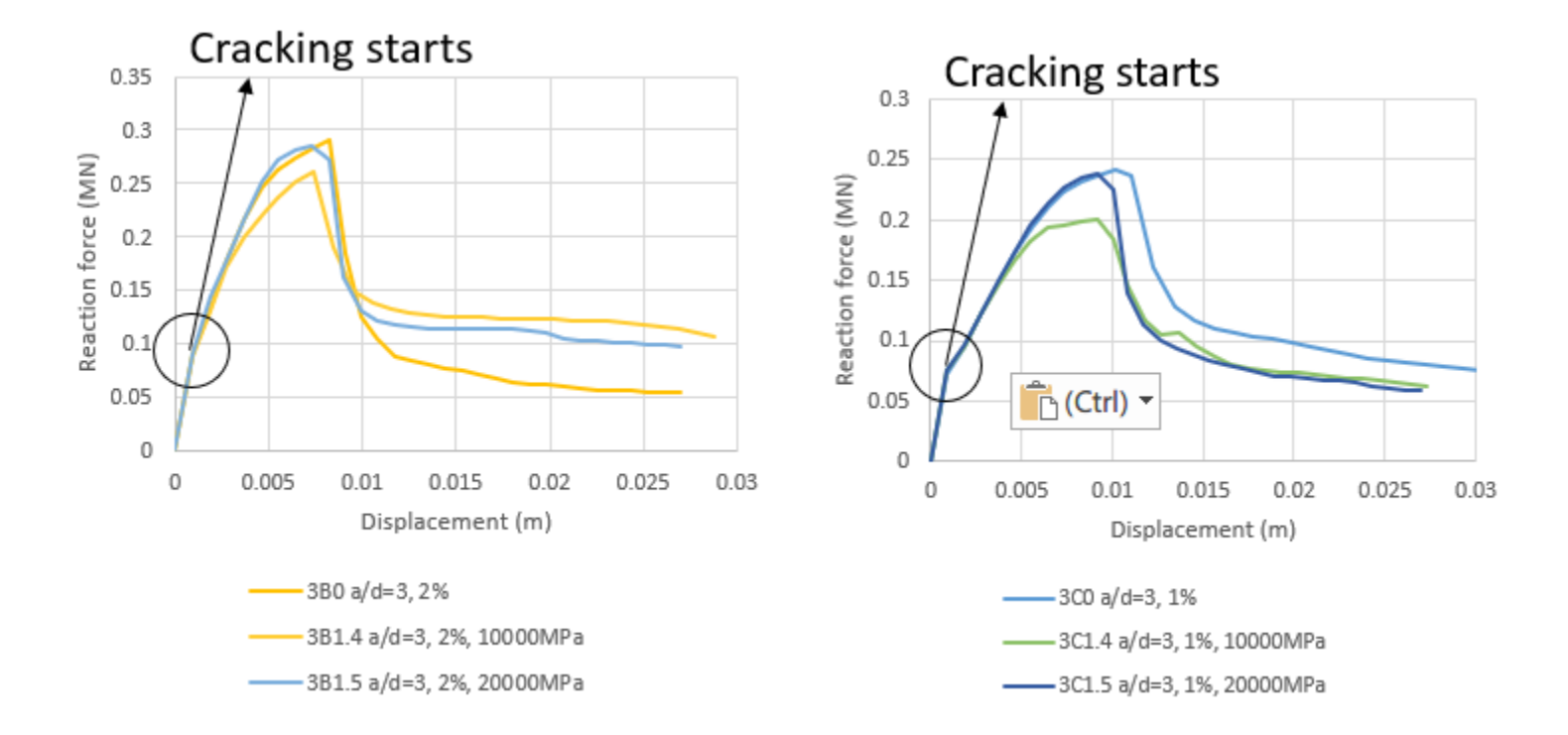


Figure 99 Force-displacement diagrams for a/d=2 beams

### a/d=3:



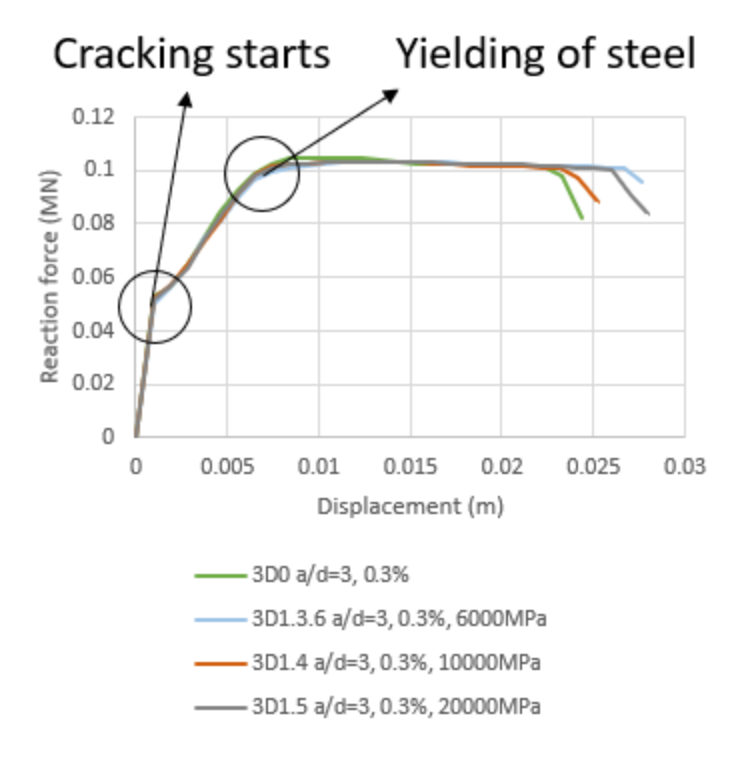
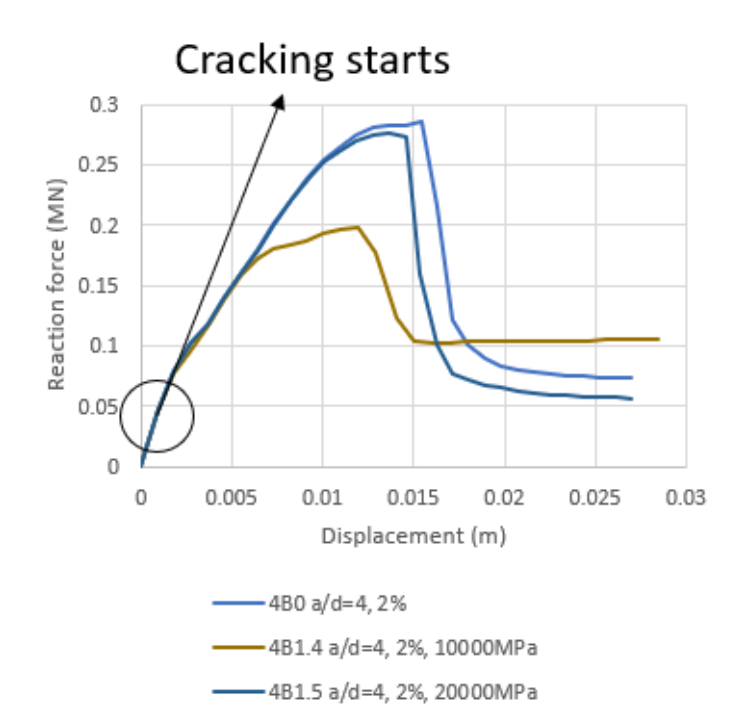
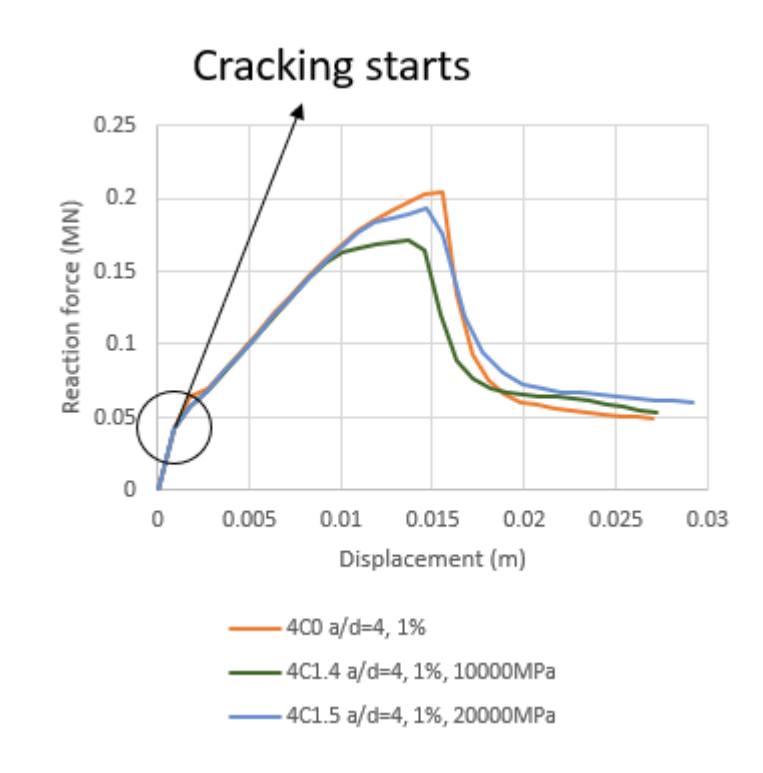


Figure 100 Force-displacement diagrams for a/d=3 beams

### a/d=4:





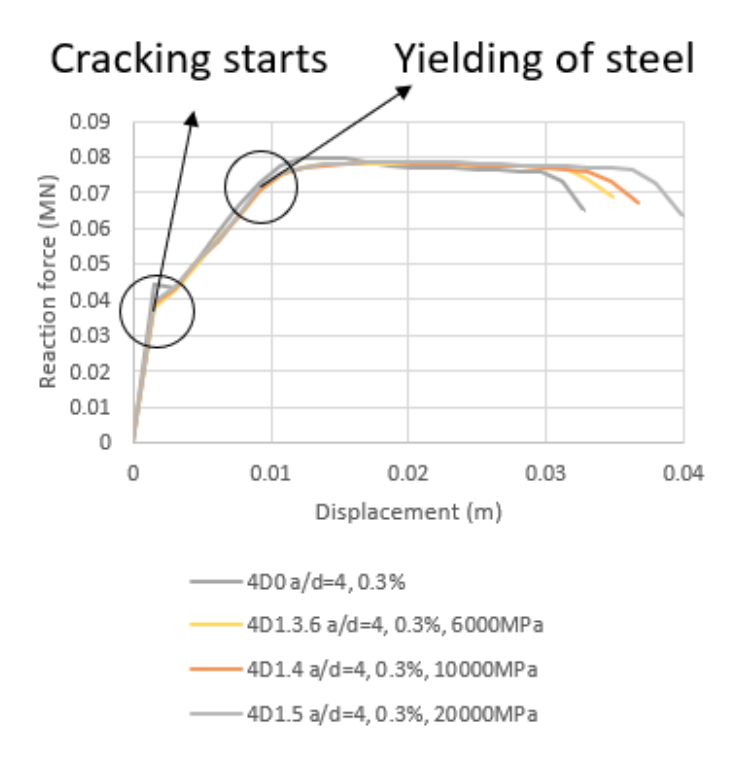


Figure 101 Force-displacement diagrams for a/d=4 beams

For models with the same a/d and reinforcement ratio, no matter what failure mode occurs, within a certain range of material properties in ASR layers (Young's modulus between 6000 MPa and 30000 MPa, the practical value measured in laboratory), there will be no significant impact to the ultimate load level. The largest reduction in the models above occurs in 4B1.4, whose peak force is 1/3 lower than the original beam.

In practical, the possible ASR might not result in a huge decrease in ultimate load until ASR material property reduction is quite severe.

# Appendix 2.2 Crack pattern a/d=2:

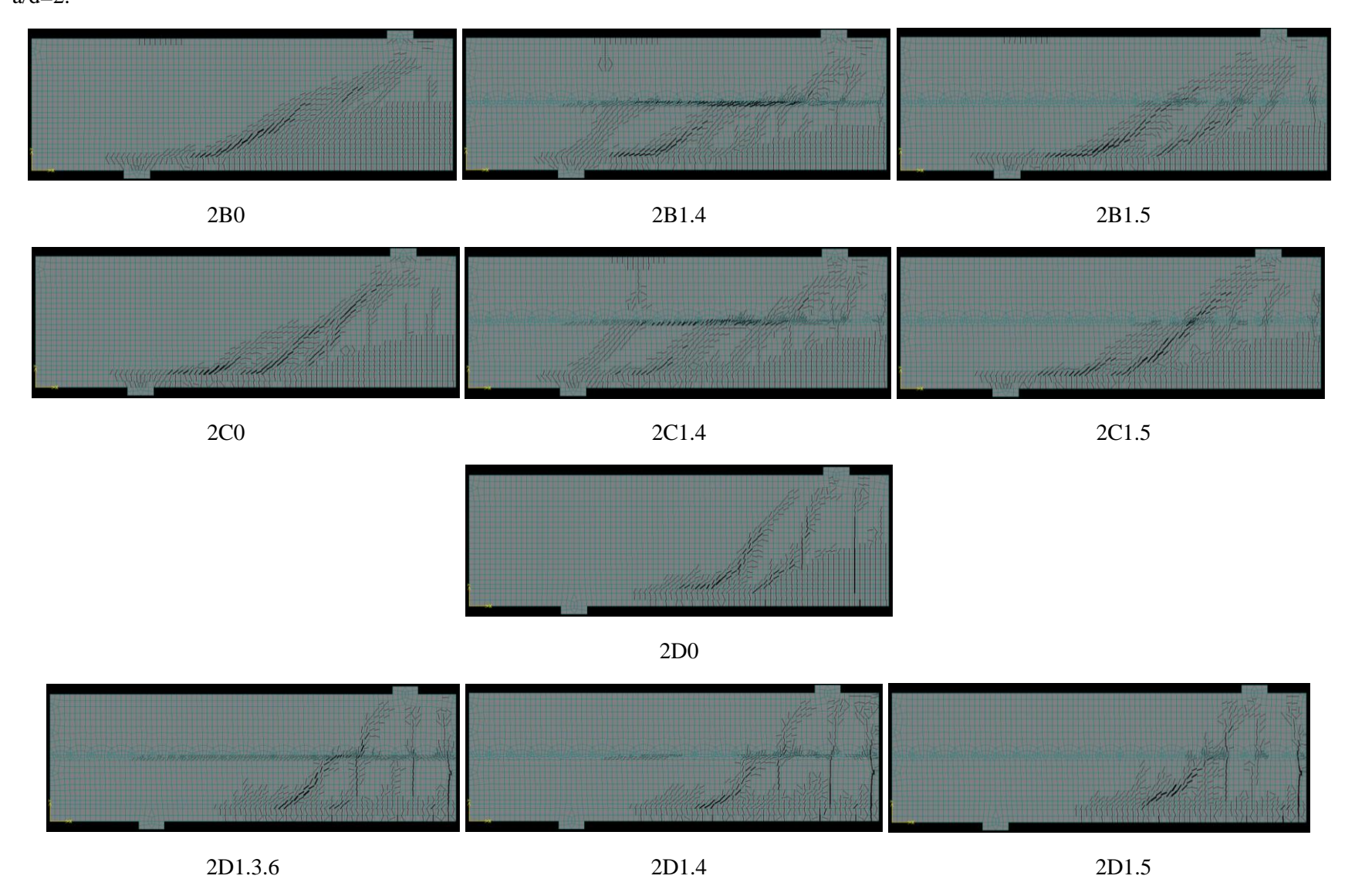


Figure 102 Crack patterns for a/d=2 beams

### a/d=3:

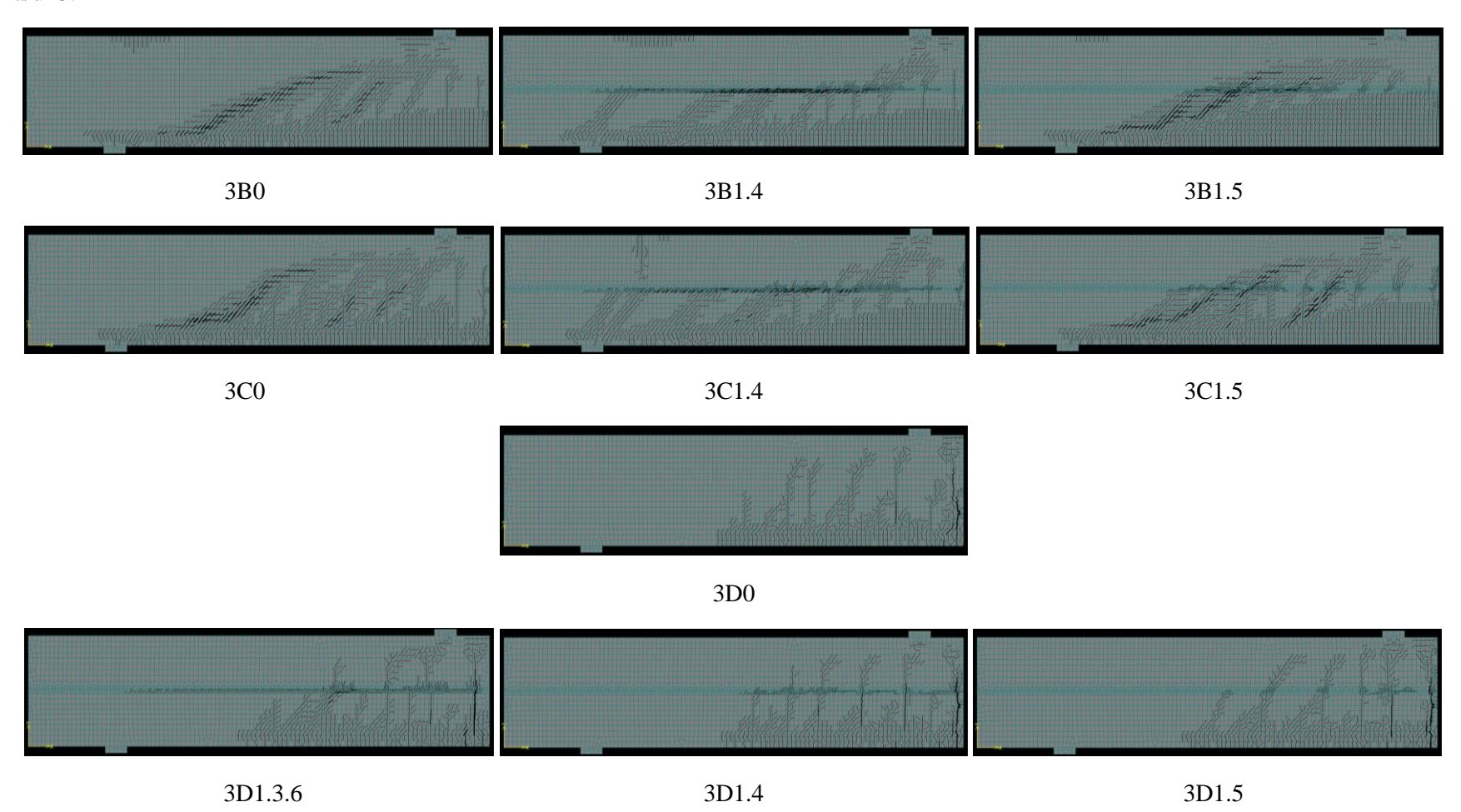


Figure 103 Crack patterns for a/d=3 beams

### a/d=4:

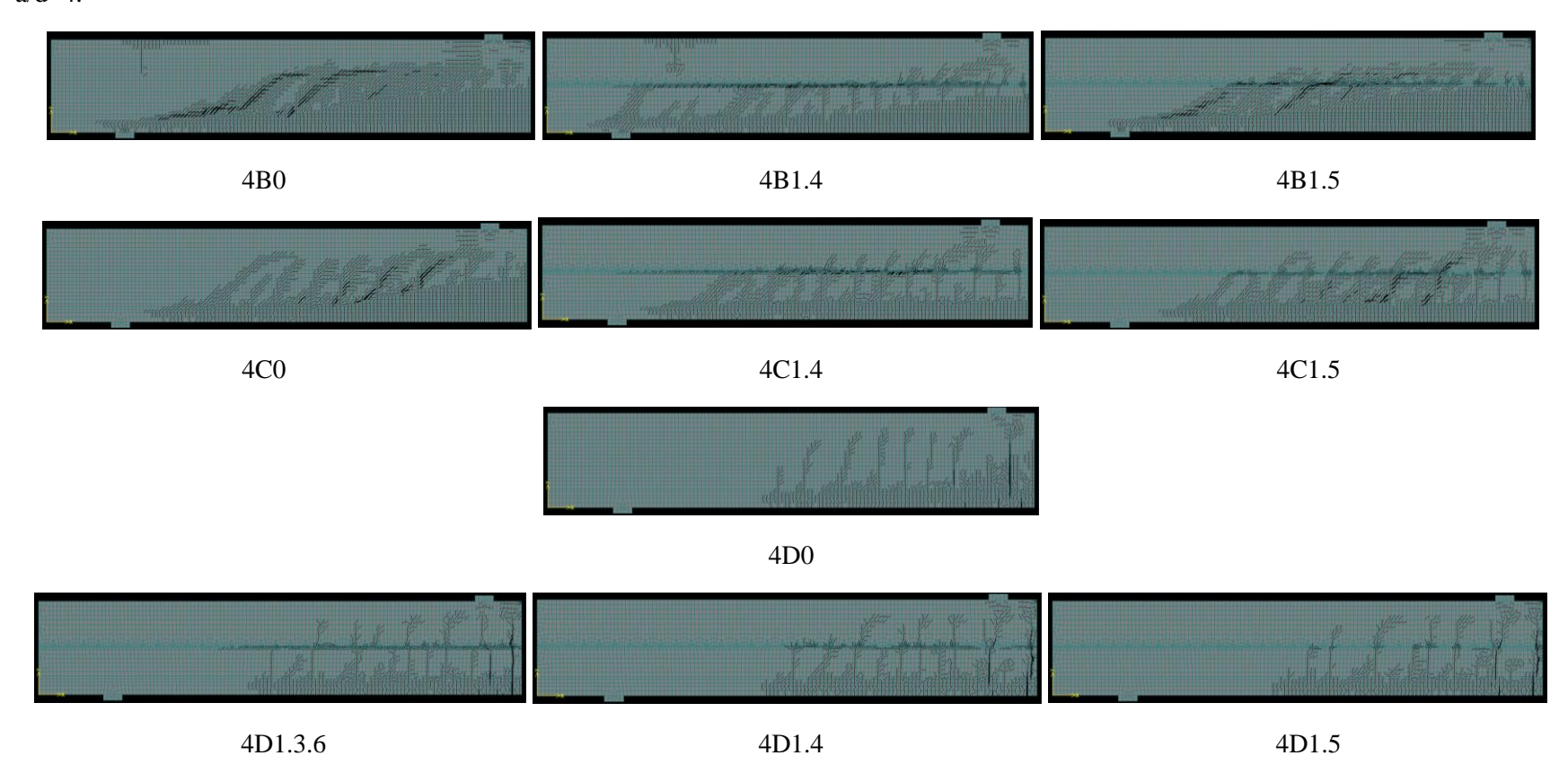


Figure 104 Crack patterns for a/d=4 beams

Similar trend also applies in the models with various a/d ratios above, in addition to the shear cracks when a/d=2. In this discussion, Young's modulus of ASR layers ranges from 10000 MPa to 30000 MPa. For 0.3% reinforcement ratio models, Young's modulus of ASR layers ranges from 6000 MPa to 30000 MPa.

The diagonal shear cracks or vertical bending cracks tend to partly follow ASR cracks when they propagate to the level of ASR layers. The property of ASR layers has an influence as well as a/d ratio and reinforcement ratio. Weaker ASR layers will induce denser cracks and a longer crack range in horizontal direction. A larger reinforcement ratio will generate similar results.

# Appendix 2.3 Principal strain a/d=2:

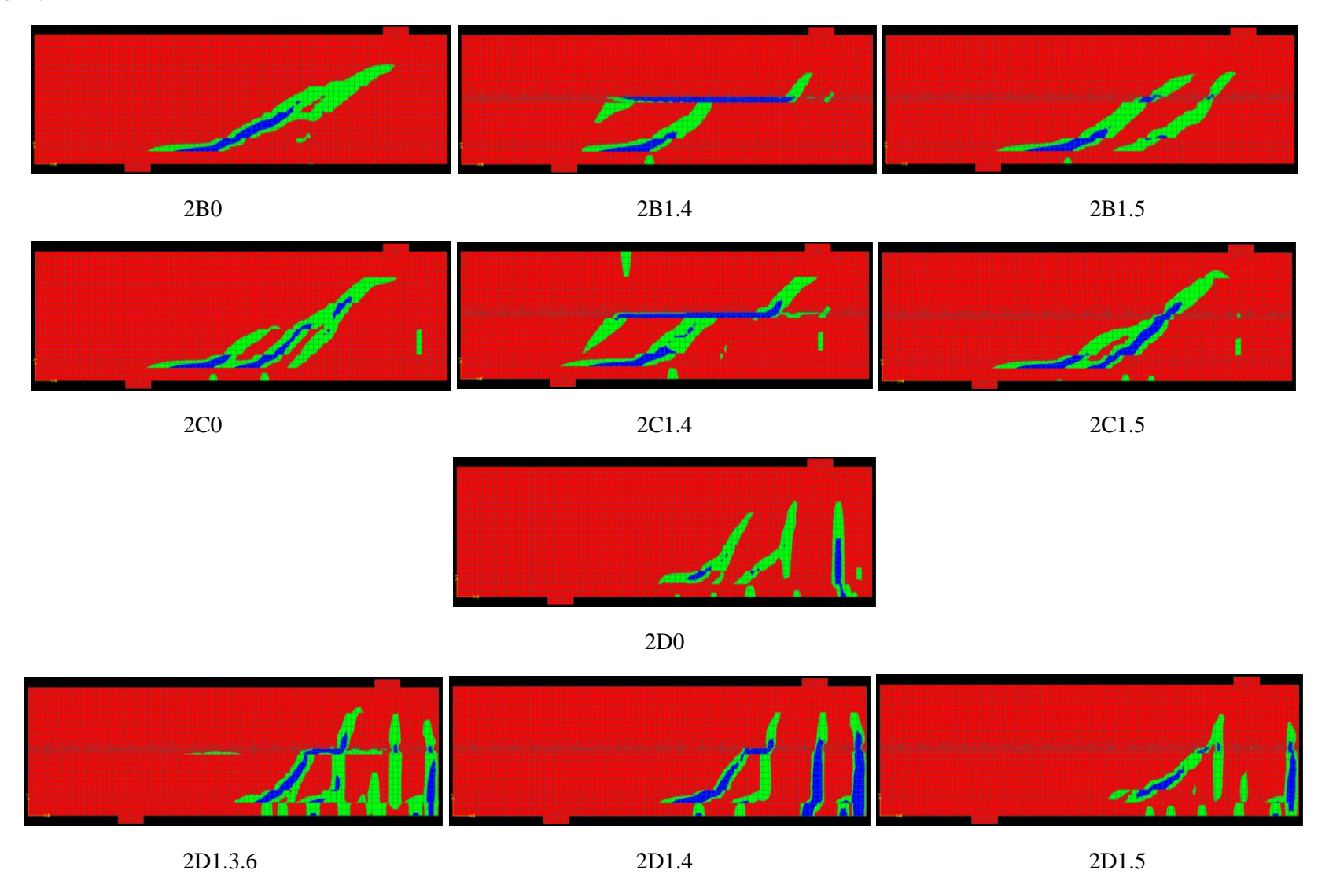


Figure 105 Principal strains for a/d=2 beams

### a/d=3:

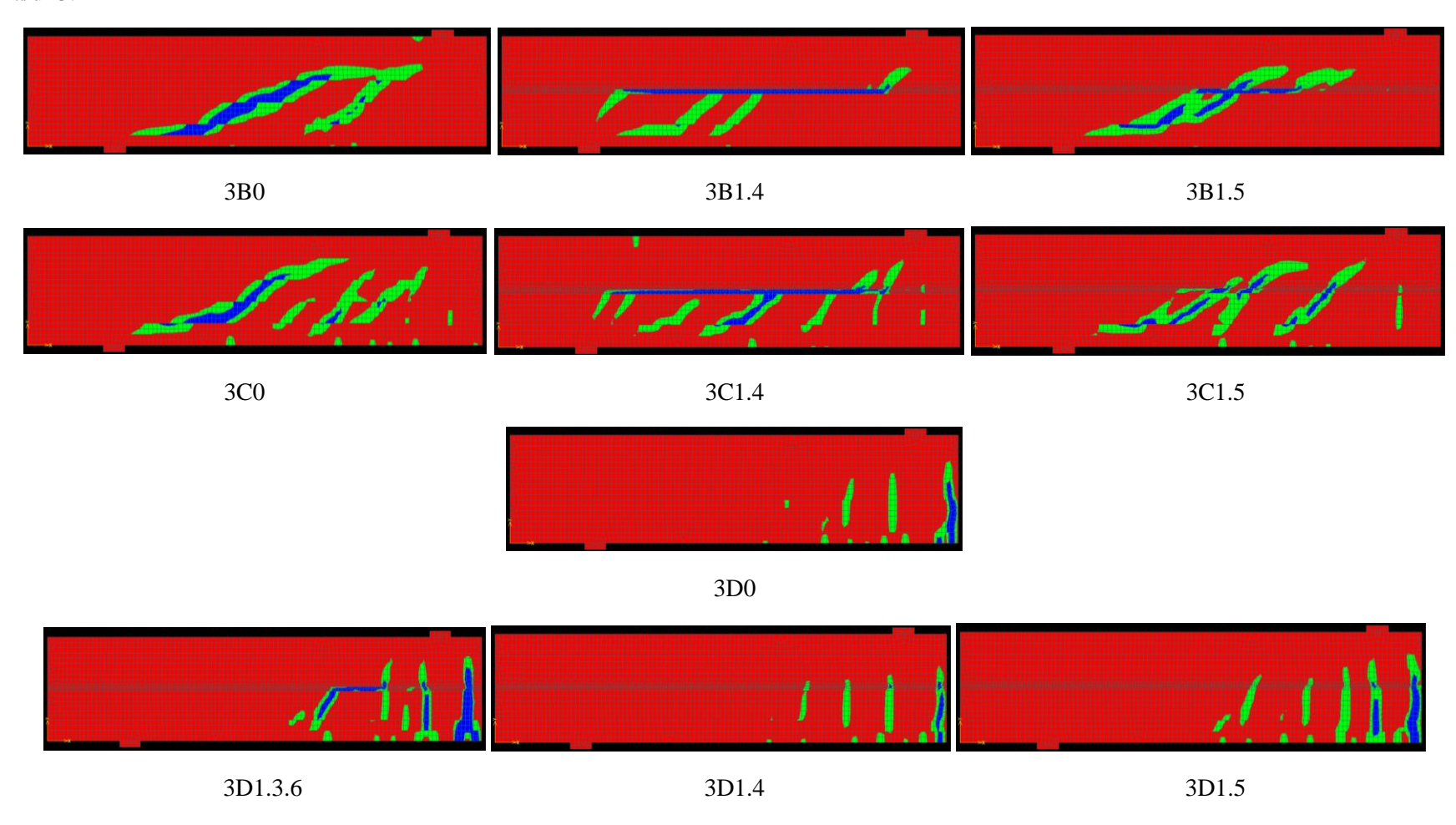


Figure 106 Principal strains for a/d=3 beams

### a/d=4:

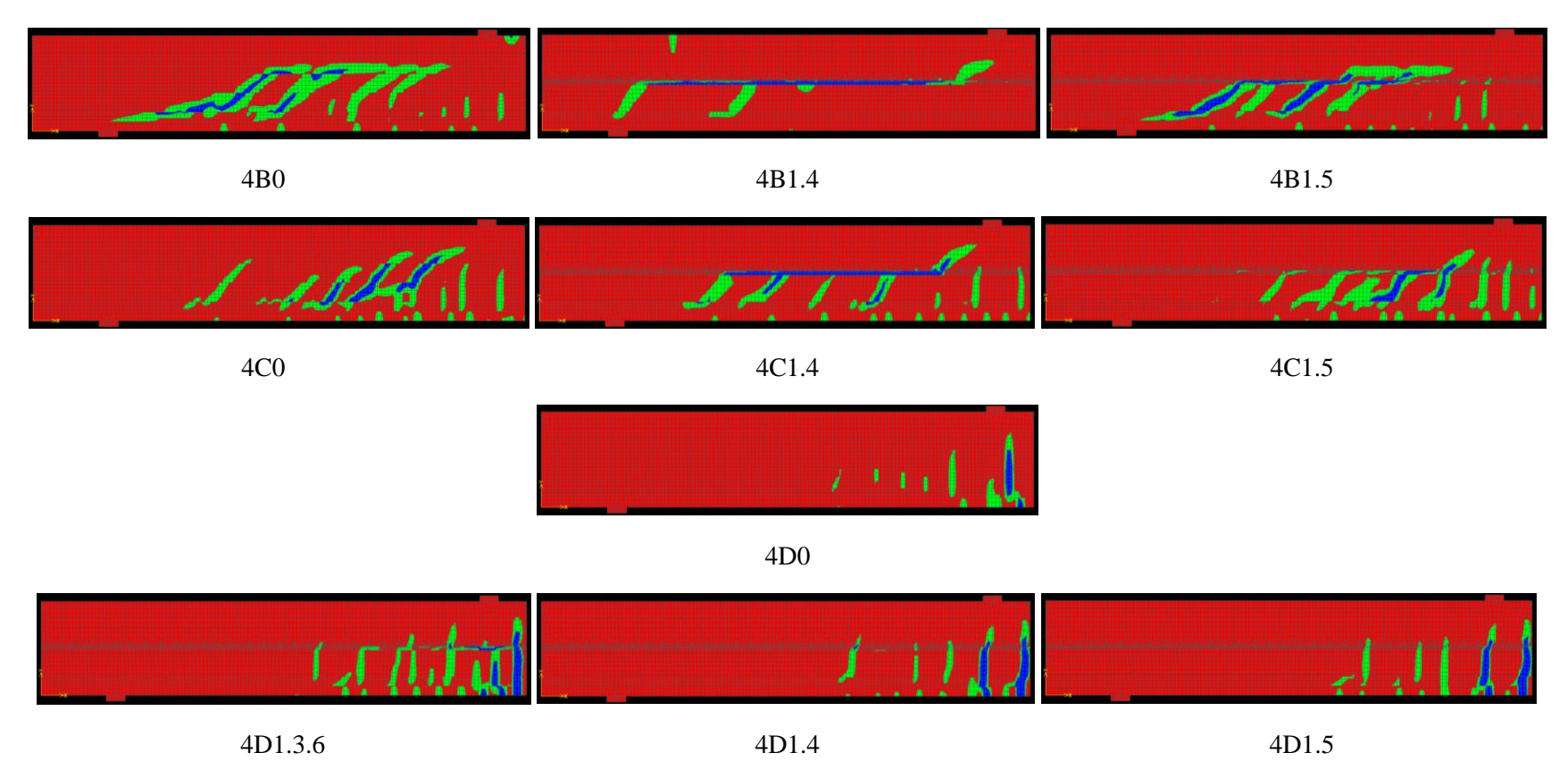


Figure 107 Principal strains for a/d=4 beams

Figure 107 shows principal strain plots from ATENA for beams with ASR layers at the stage where the ultimate load is applied. Different failure mechanisms may occur even in beams with the same a/d ratio. The failure mechanisms can be classified into several types,

- 1) ASR layer failure when ASR layers are relatively weak.
- 2) ASR-affected shear failure. It is also called ASR slip failure in literature (Abe, Kikuta, Masuda, & Tomozawa, 1989). Diagonal shear cracks will follow the direction of ASR cracks partly when they come across each other. This occurs as a transition from ASR layer failure to shear failure, when properties of ASR layers are in a medium level.
- 3) Shear failure. This occurs when properties of ASR layers are close to sound concrete.
- 4) ASR-affected bending failure. When ASR layers are weak, the cracks in ASR layers appear almost at the same time with bending cracks.
- 5) Bending failure. Generally, the influence of ASR layers on bending failure is limited.

### Appendix 3 Calculation of bending & shear capacity of original models

Moment capacity of beams not influenced by ASR can be calculated according to Eurocode. The yield strength of reinforcement is 435 MPa. Assuming the lever arm is 0.87 times distance from top of beam to the center of reinforcement, also making use of the distance between loading point and the nearest support, it is possible to calculate at which shear force the reinforcement will yield.

$$M = F_s z = \frac{f_{yk}}{\gamma_s} A_s z = \frac{f_{yk}}{\gamma_s} A_s \cdot 0.87d$$

$$F_{u,mom} = M / a = \frac{f_{yk}}{\gamma_s} \rho b d \frac{0.87}{a / d} = \frac{0.87 f_{yk} \rho b d^2}{\gamma_s a}$$

Table 46 Bending capacity calculation

Beam number	a (mm)	d (mm)	b (mm)	<b>z</b> (mm)	rho in %	As (mm2)	M (kNm)	Fu,moment (kN)
2B0	1000	500	500	435	2	5000	946	946
2C0	1000	500	500	435	1	2500	473	473
2D0	1000	500	500	435	0.3	750	142	142
3B0	1500	500	500	435	2	5000	946	631
3C0	1500	500	500	435	1	2500	473	315
3D0	1500	500	500	435	0.3	750	142	95
4B0	2000	500	500	435	2	5000	946	473
4C0	2000	500	500	435	1	2500	473	237
4D0	2000	500	500	435	0.3	750	142	71

From the results of original model, it is possible to get ultimate shear force of the beam not affected by ASR. According to Rafla, the following formulas can be used to determine shear strength without ASR. Several sets of models with various a/d ratio and reinforcement ratio are discussed here.

$$F_{u,theory} = \alpha_u d^{-0.25} \sqrt{f_{cc}} \sqrt[3]{\omega_0} b d$$
With  $\alpha_u = 0.90 - 0.03 \frac{a}{d}$  for  $\frac{a}{d} \ge 3.5$ 

$$\alpha_u = 0.795 + 0.293(3.5 - \frac{a}{d})^{2.5}$$
 for  $2.0 \le \frac{a}{d} \le 3.5$ 

Table 47 Shear capacity calculation

Beam	fcc	a	d	b	a/d	alpha u	rho in %	Fu,shear (kN)
number	(MPa)	(mm)	(mm)	(mm)				
2B0	30	1000	500	500	2	1.60	2	585
2C0	30	1000	500	500	2	1.60	1	464
2D0	30	1000	500	500	2	1.60	0.3	311

3B0	30	1500	500	500	3	0.85	2	309
3C0	30	1500	500	500	3	0.85	1	245
3D0	30	1500	500	500	3	0.85	0.3	164
4B0	30	2000	500	500	4	0.78	2	285
4C0	30	2000	500	500	4	0.78	1	226
4D0	30	2000	500	500	4	0.78	0.3	151

The lower value of  $F_{u,moment}$  and  $F_{u,shear}$  is denoted as  $F_{u,theory}$ , which means ultimate shear force according to theory.

## Appendix 4 Calculation on ATENA models with prestressing

# Appendix 4.1 Force-displacement response a/d=2:

0

0.005

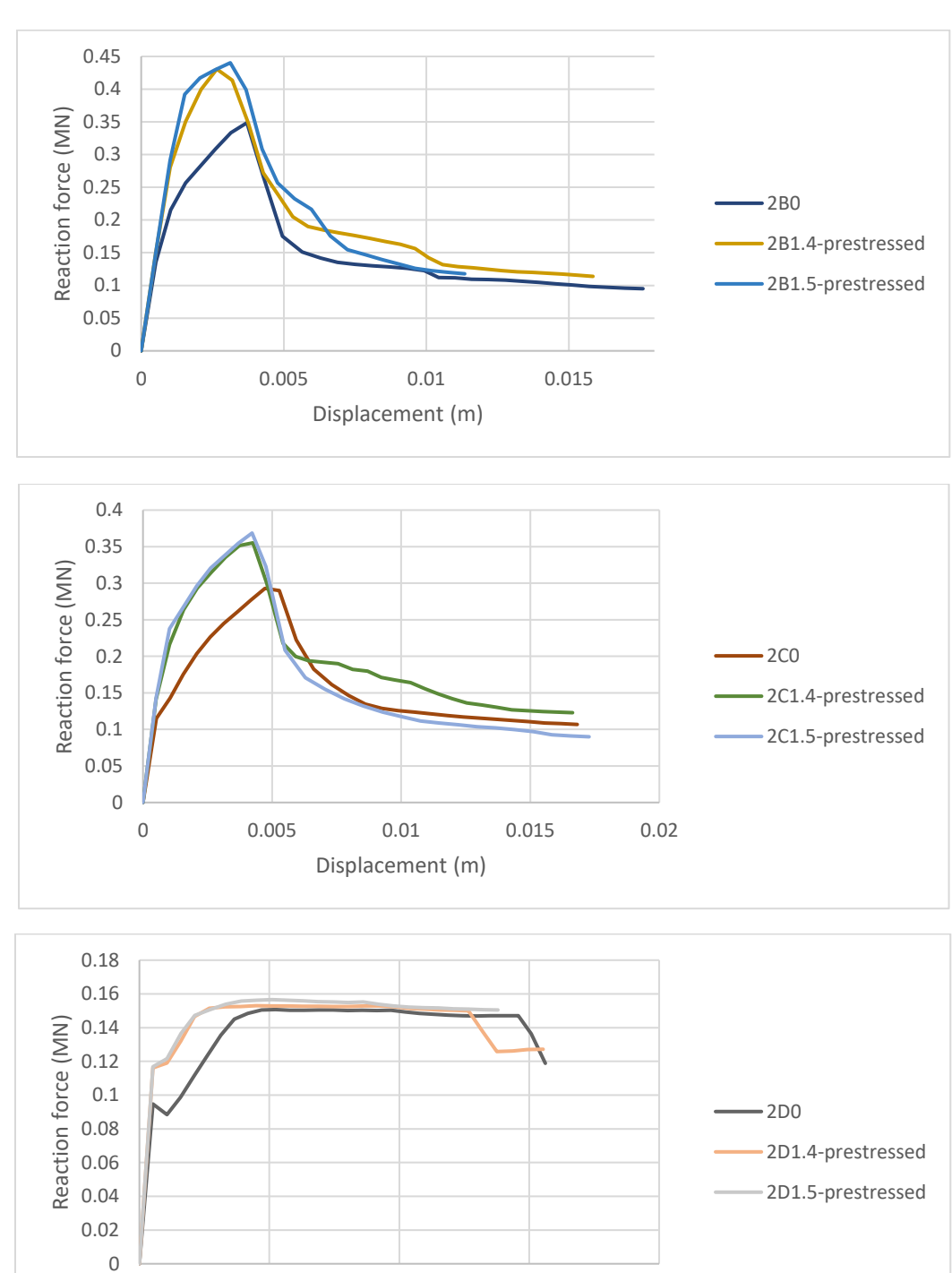


Figure 108 Force-displacement diagrams for prestressed a/d=2 beams

0.015

0.02

0.01

Displacement (m)

#### a/d=3:

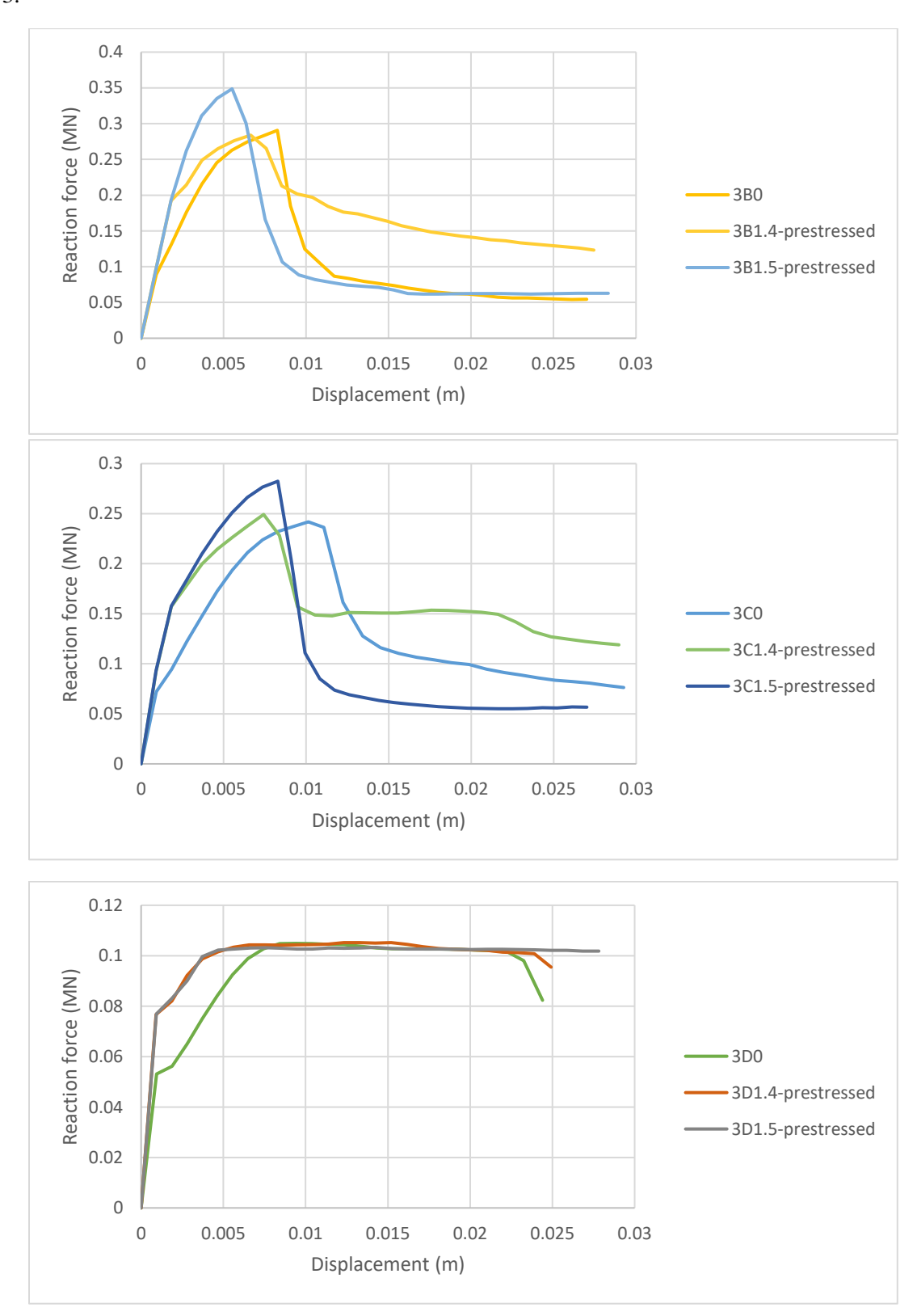


Figure 109 Force-displacement diagrams for prestressed a/d=3 beams

#### a/d=4:

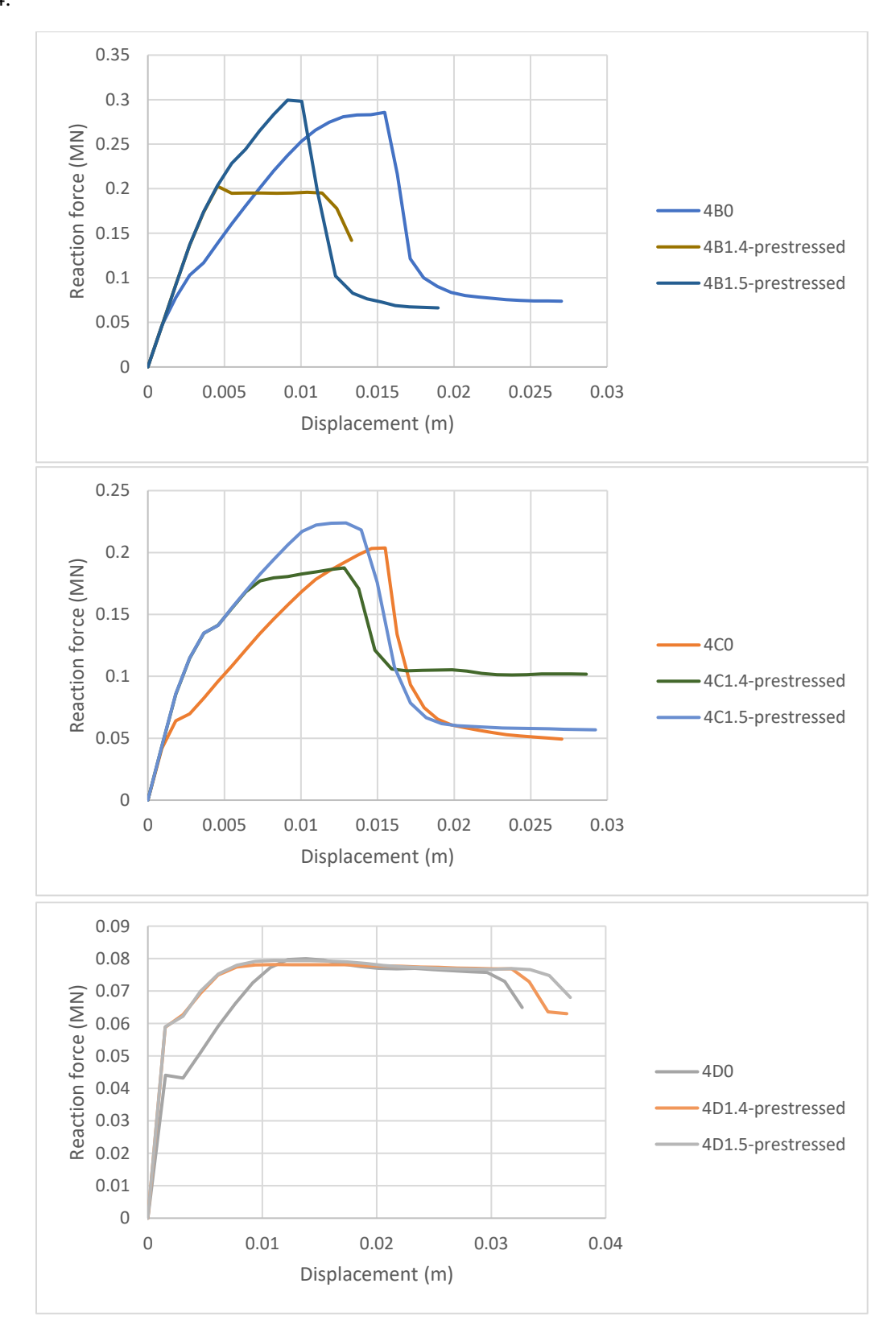


Figure 110 Force-displacement diagrams for prestressed a/d=4 beams

# Appendix 4.2 Crack pattern a/d=2

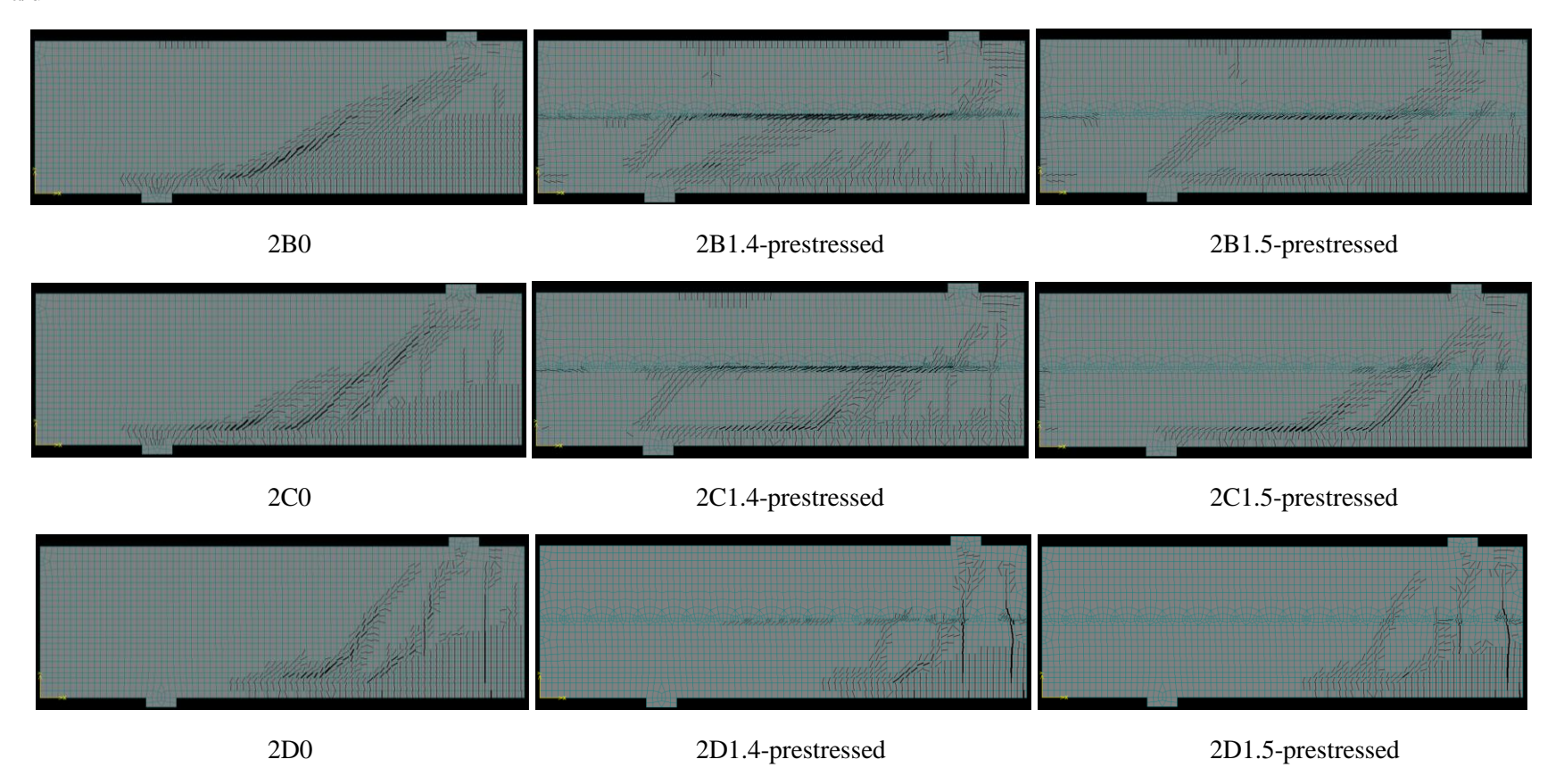


Figure 111 Crack pattern for a/d=2 beams

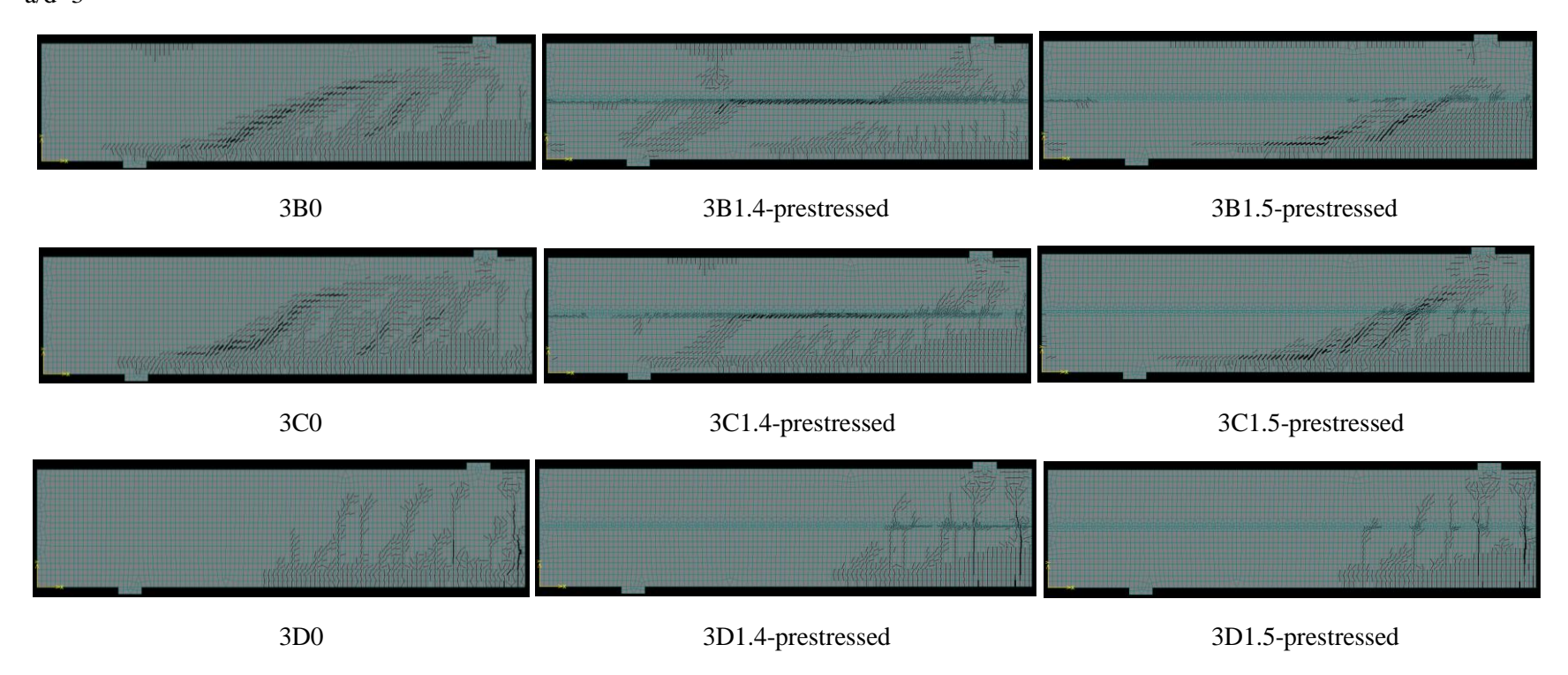


Figure 112 Crack pattern for a/d=3 beam

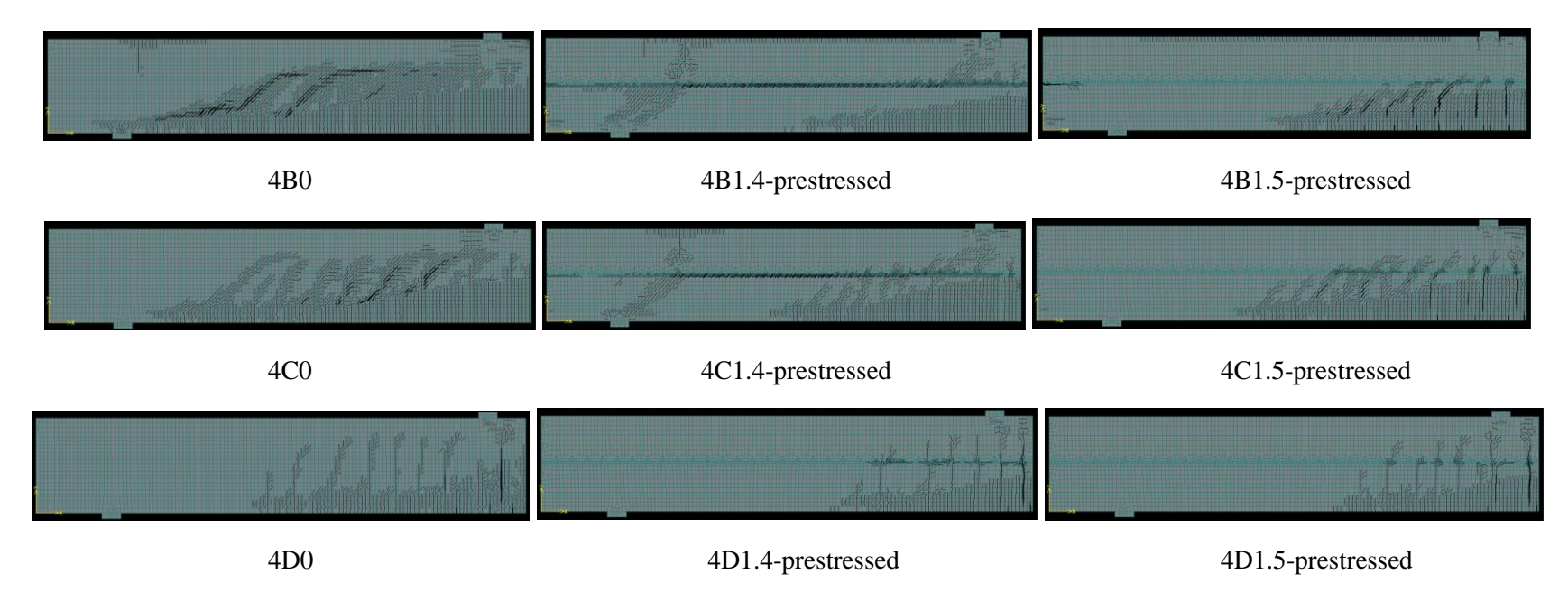


Figure 113 Crack pattern for a/d=4 beam

# Appendix 4.3 Principal strain a/d=2

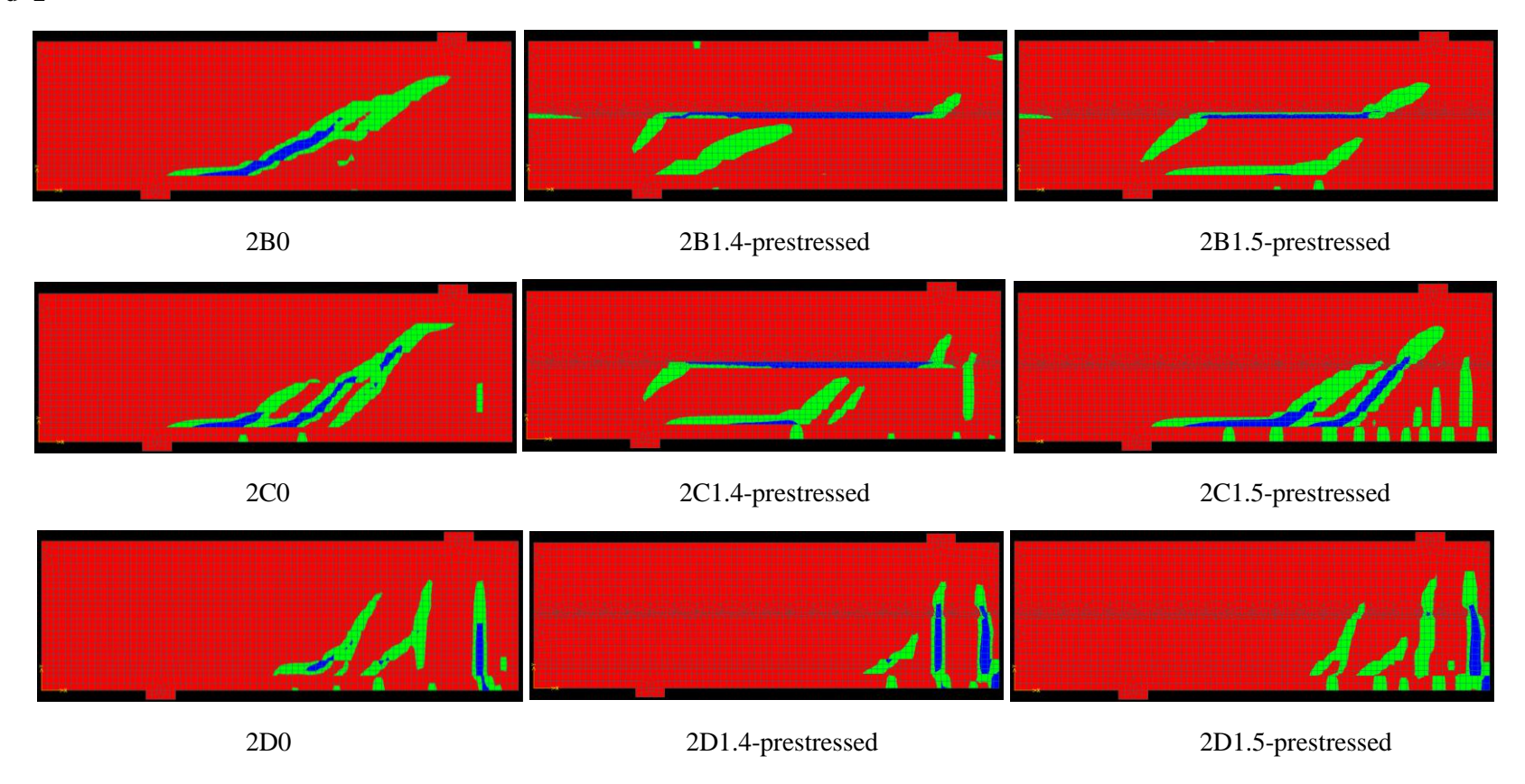


Figure 114 Principal strain for a/d=2 beams

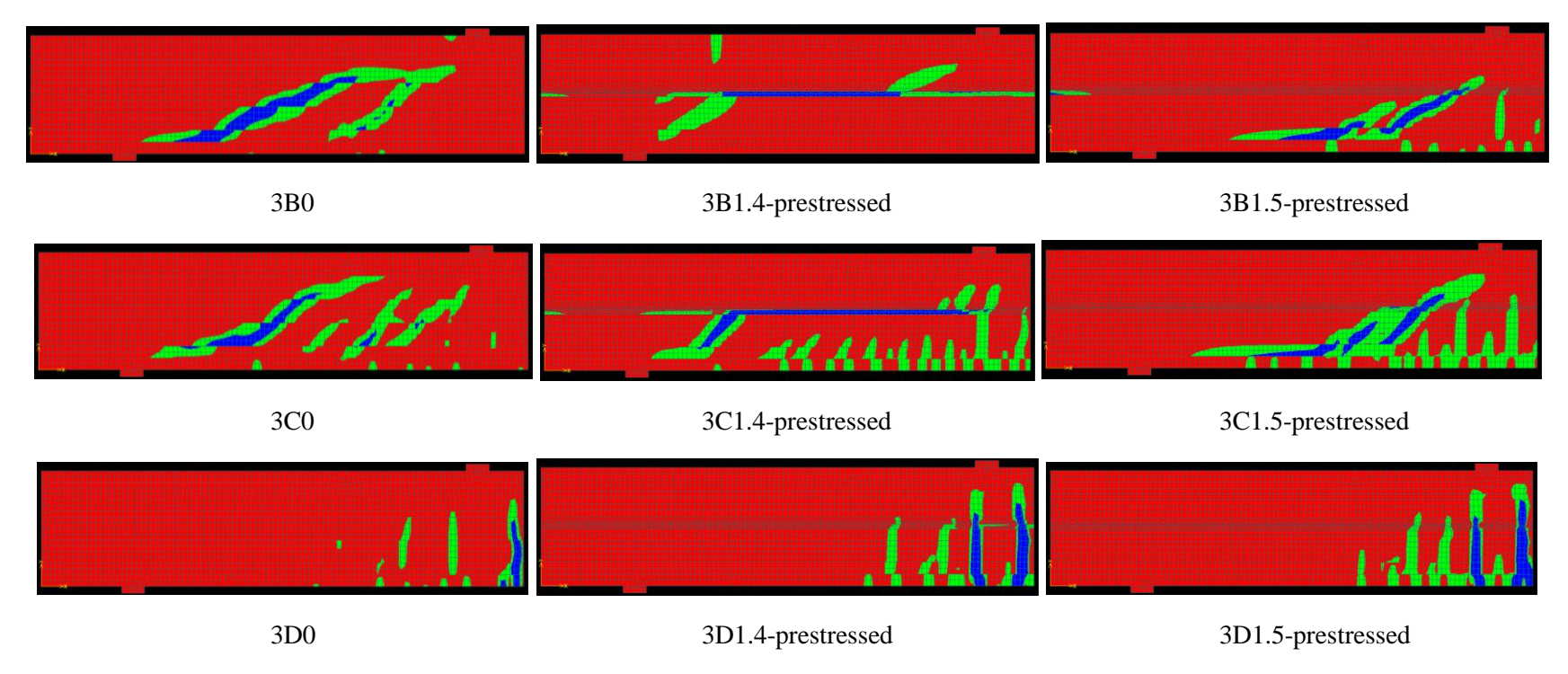


Figure 115 Principal strain for a/d=2 beams

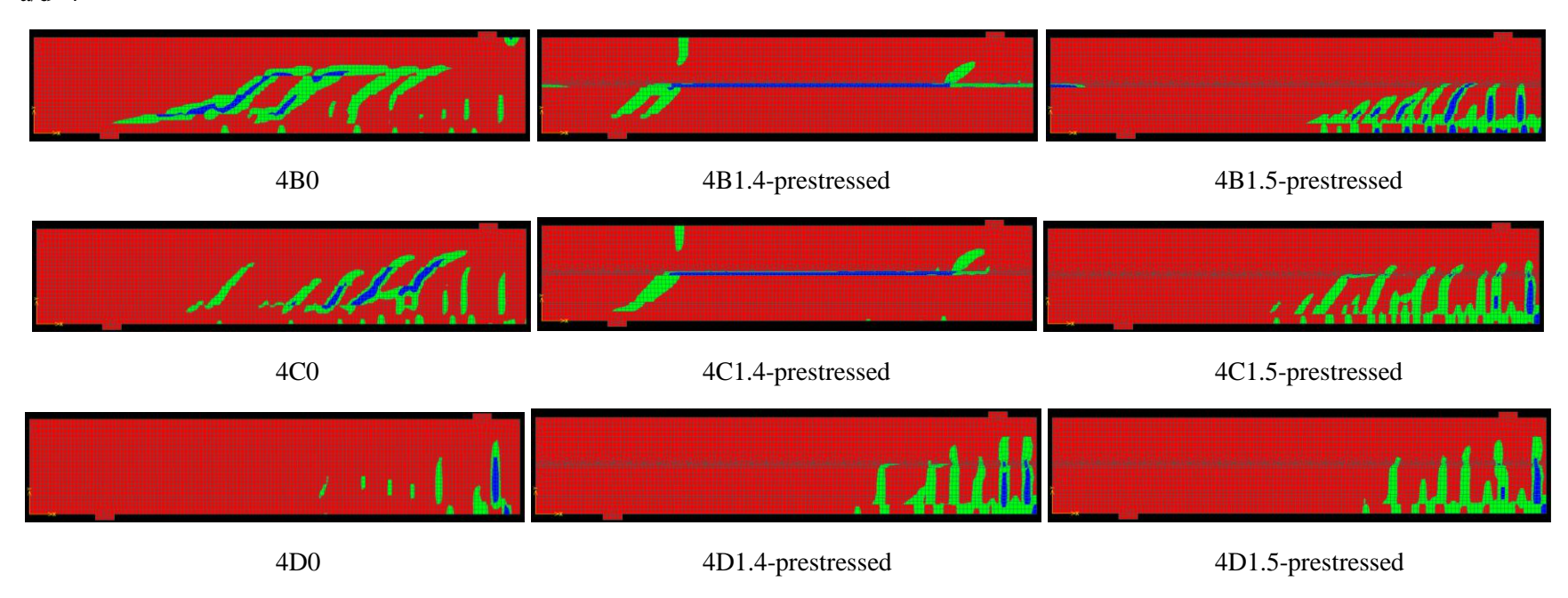


Figure 116 Principal strain for a/d=2 beams

Appendix 5 Calculation on ATENA models with prestressing and bond model Appendix 5.1 Force-displacement response a/d=2:

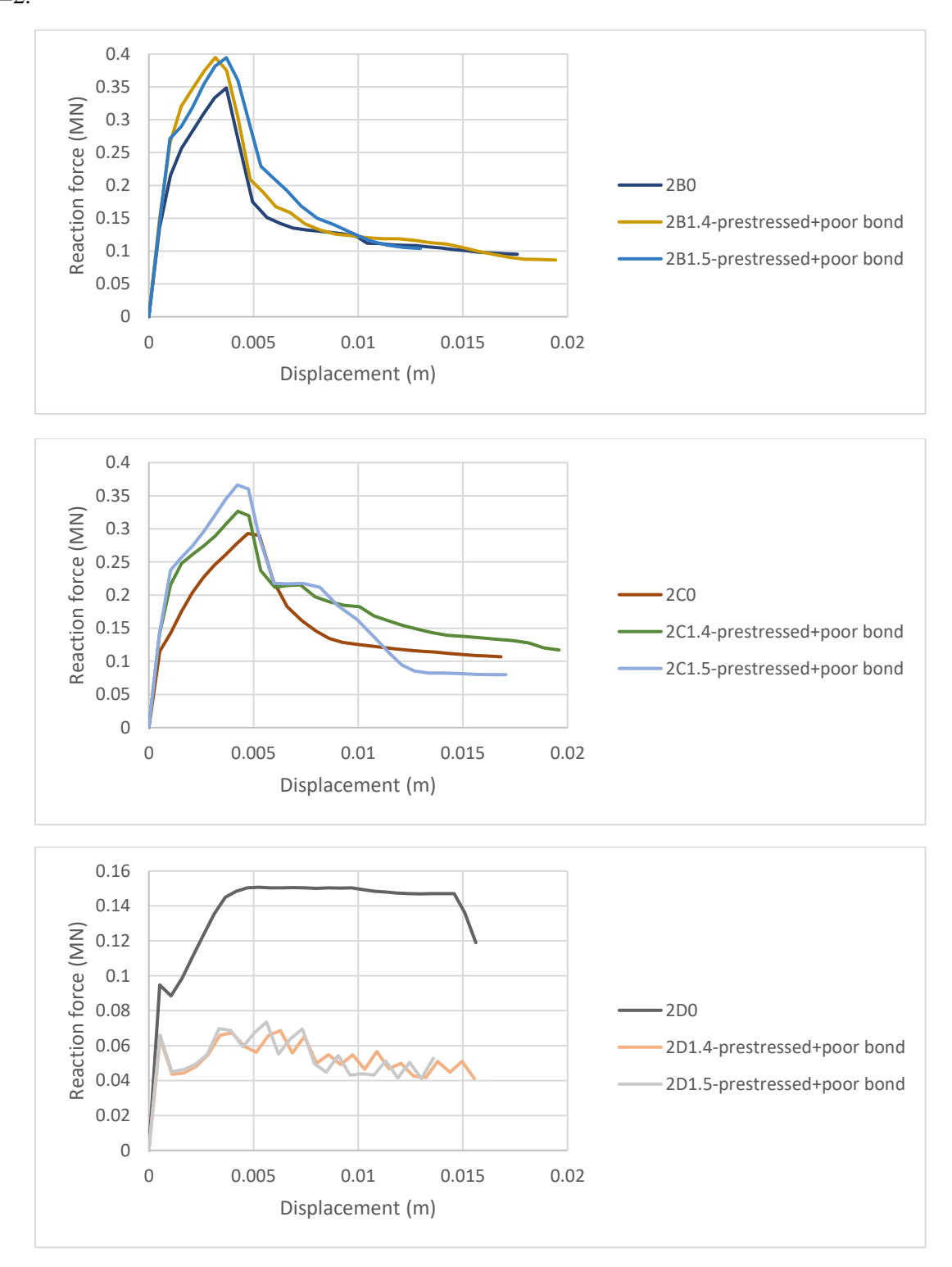


Figure 117 Force-displacement diagrams for a/d=2 beams

#### a/d=3:

0.02

0

0

0.01

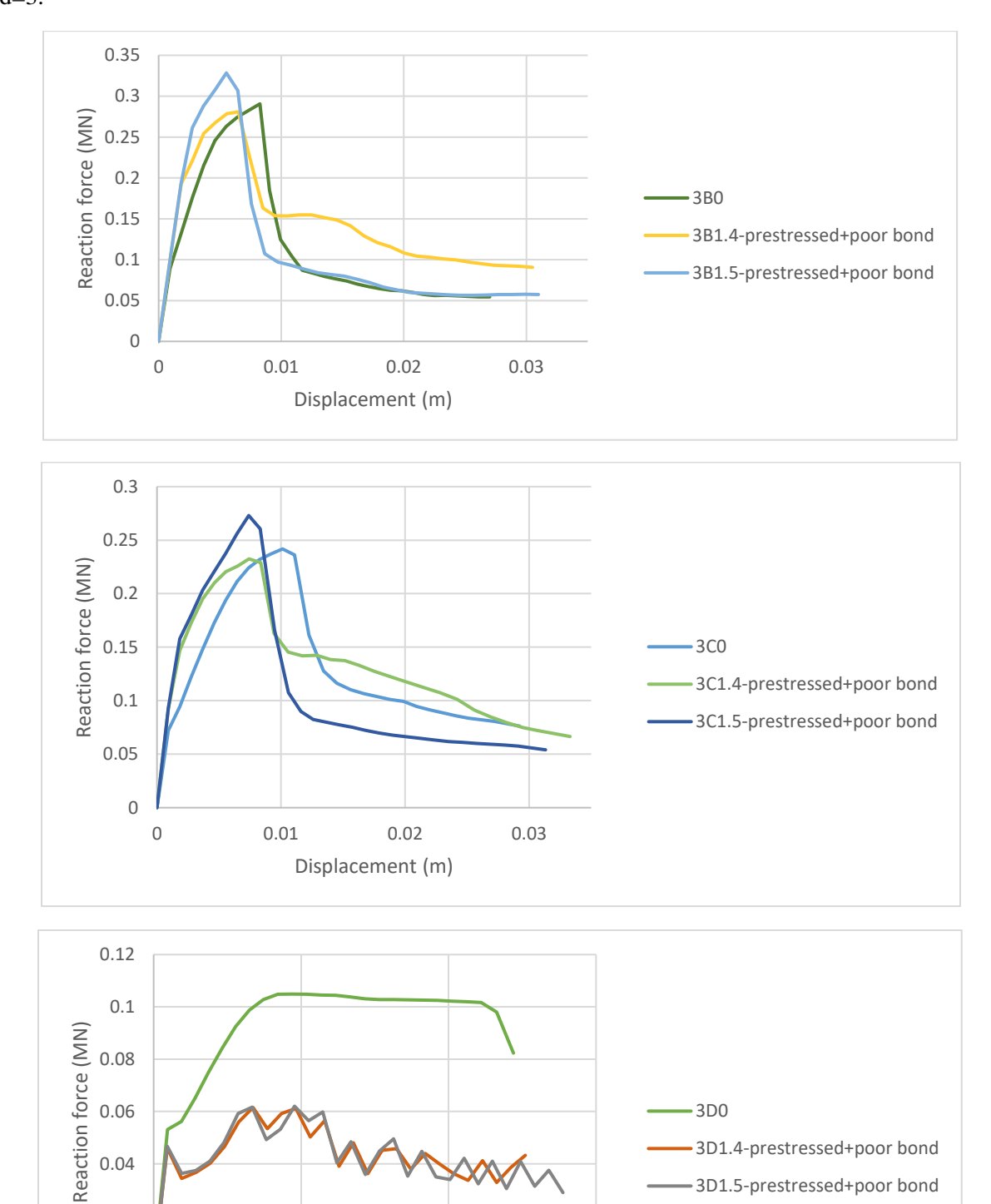


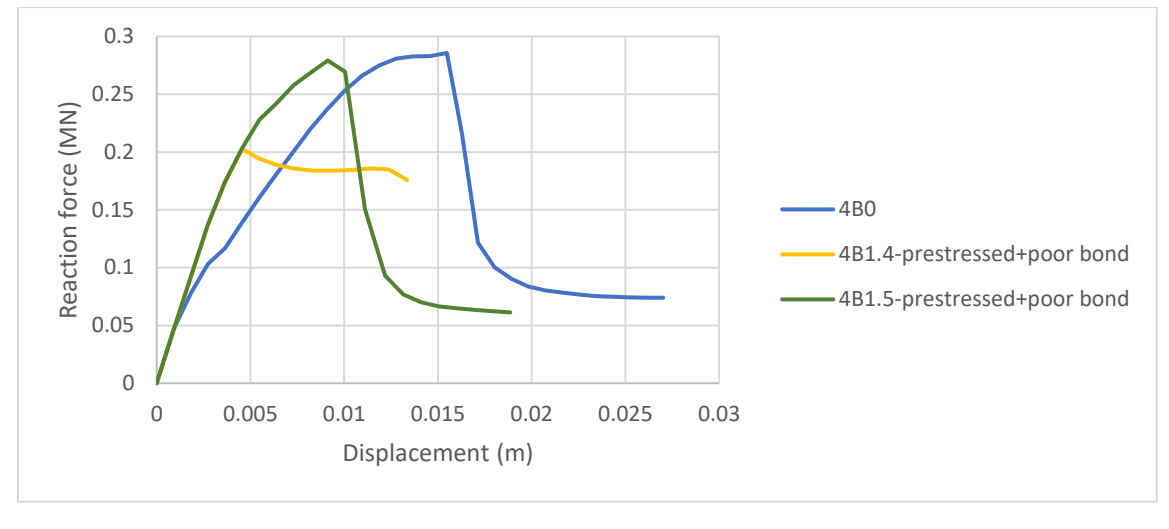
Figure 118 Force-displacement diagrams for a/d=3 beams

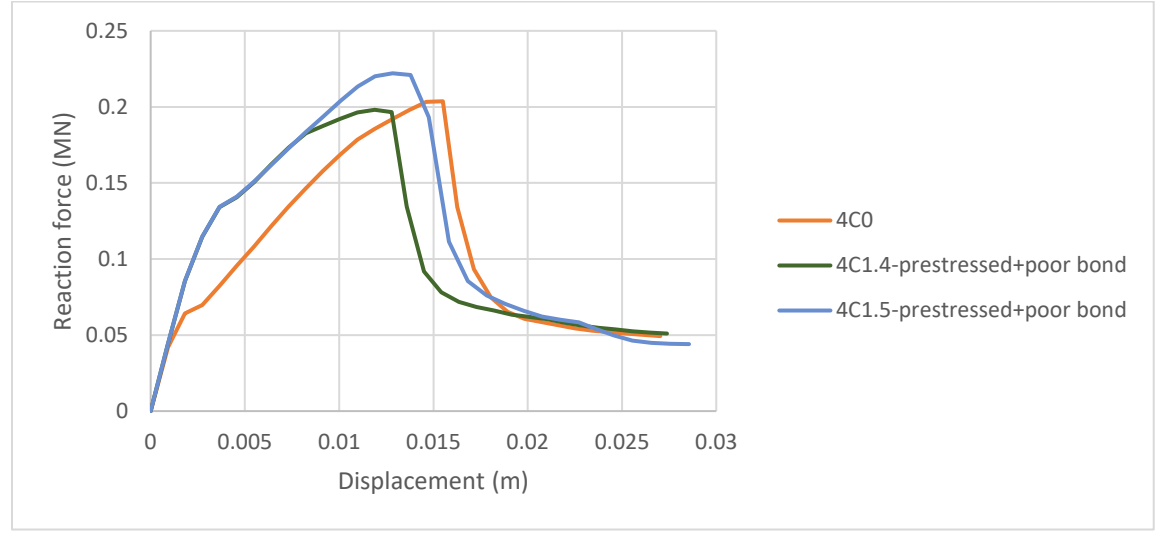
0.03

0.02

Displacement (m)

#### a/d=4:





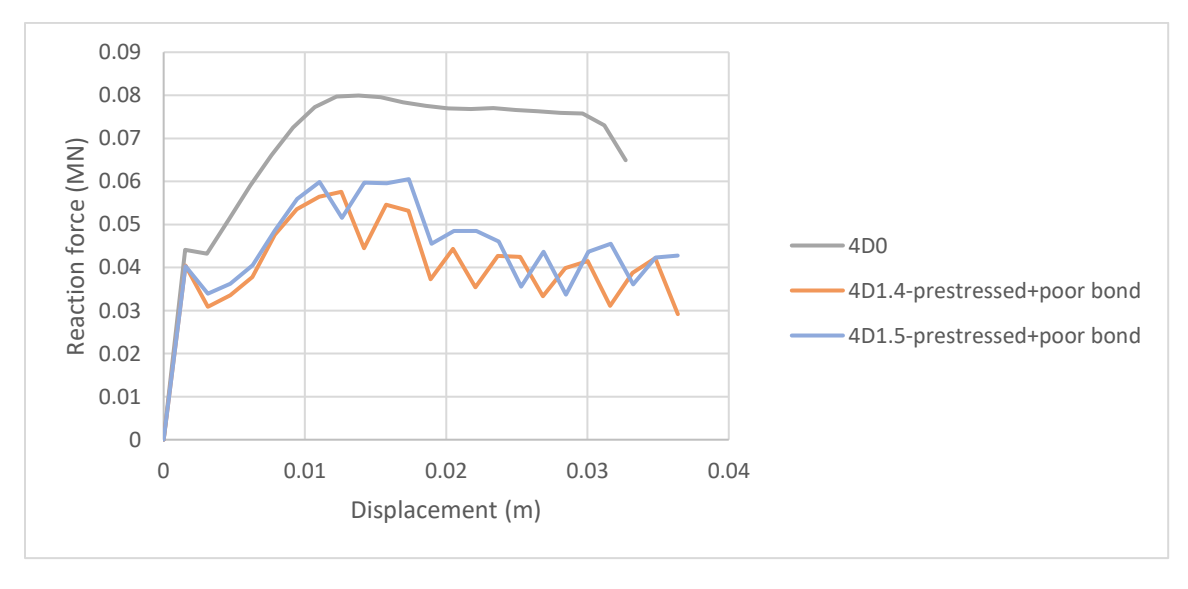


Figure 119 Force-displacement diagrams for a/d=4 beams

# Appendix 5.2 Crack pattern a/d=2:

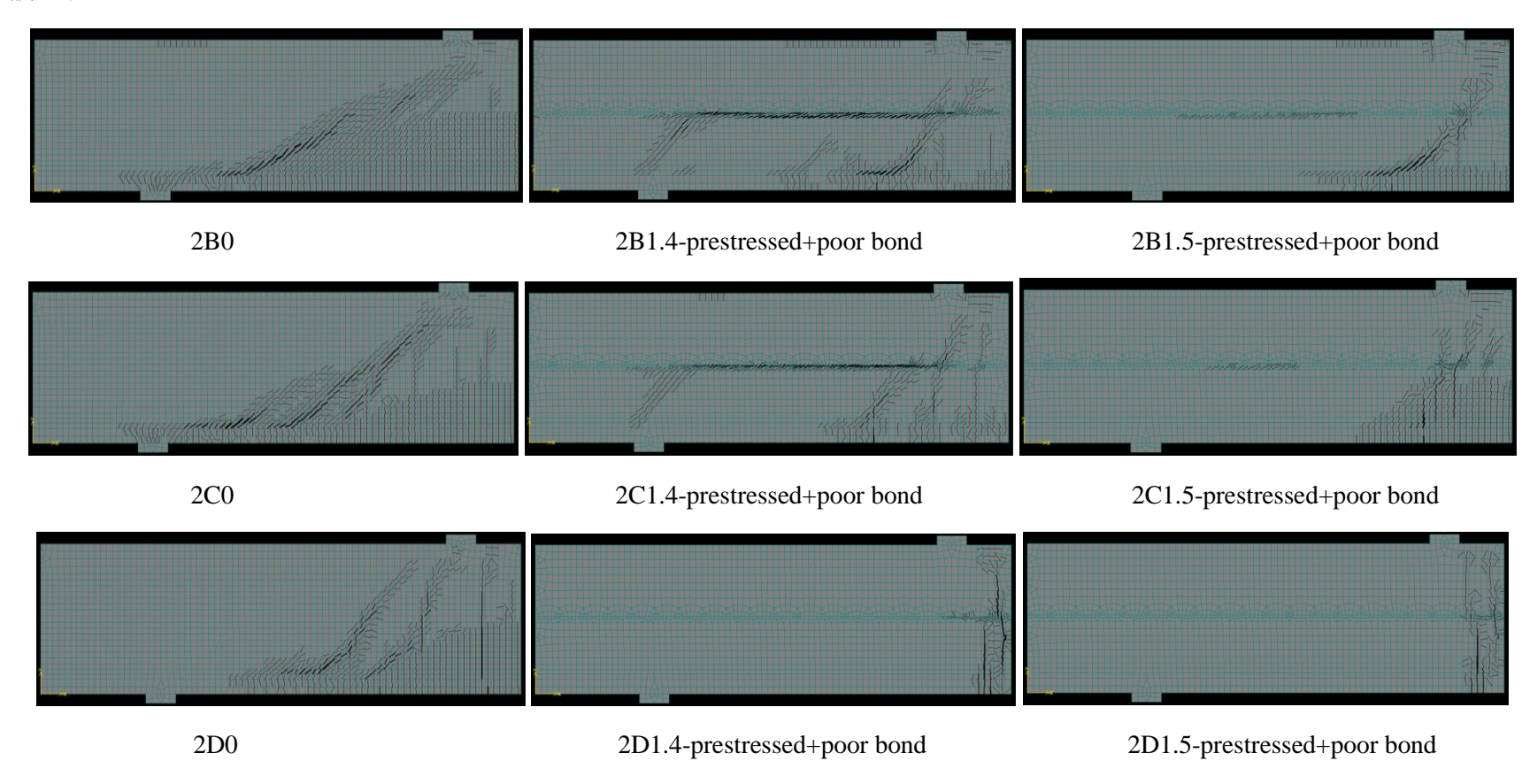


Figure 120 Crack patterns for a/d=2 beams

### a/d=3:

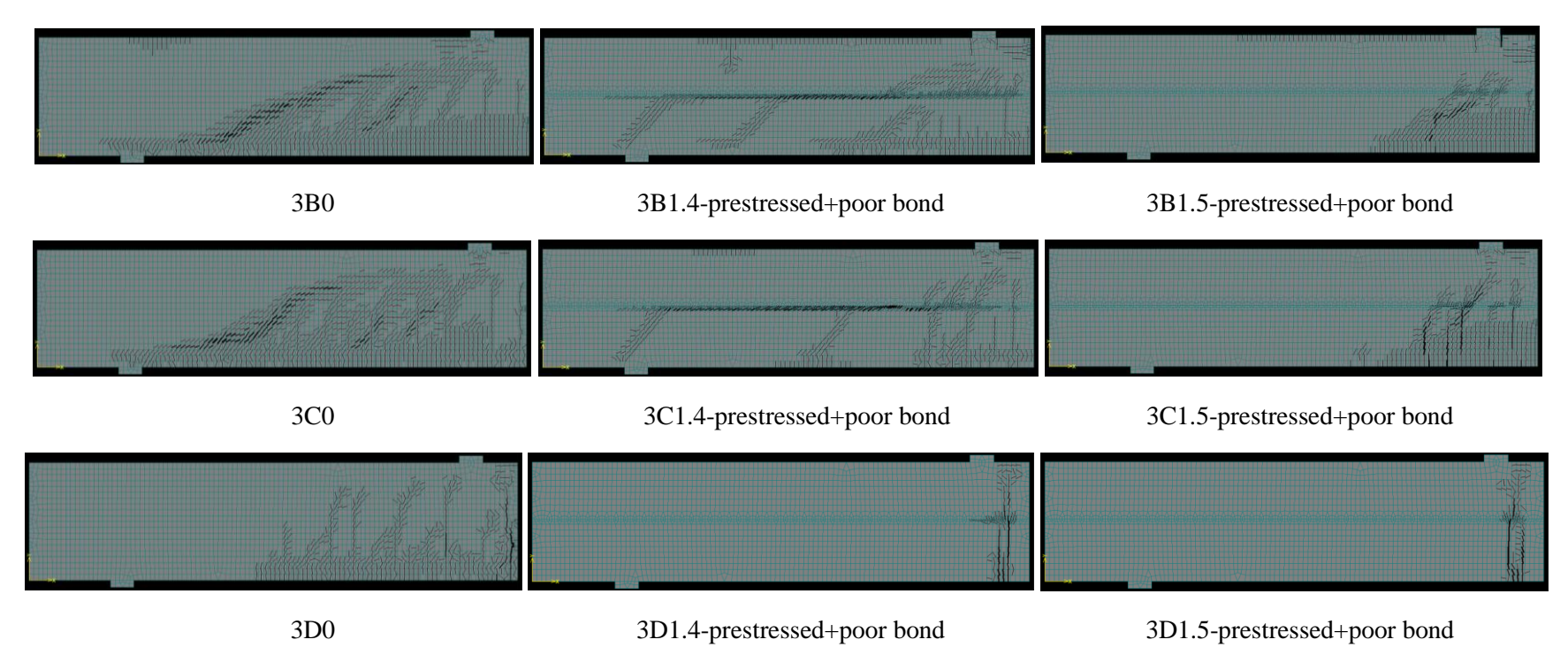


Figure 121 Crack patterns for a/d=3 beams

### a/d=4:

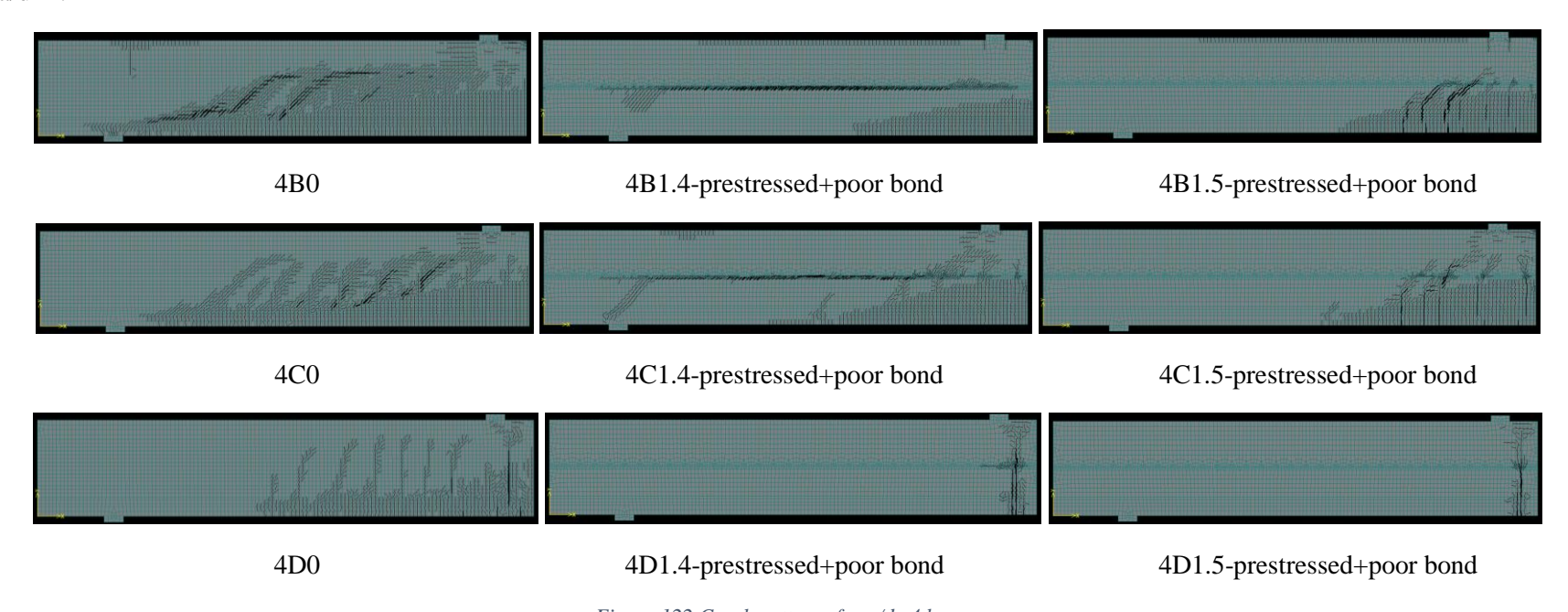


Figure 122 Crack patterns for a/d=4 beams

# Appendix 5.3 Principal strain a/d=2:

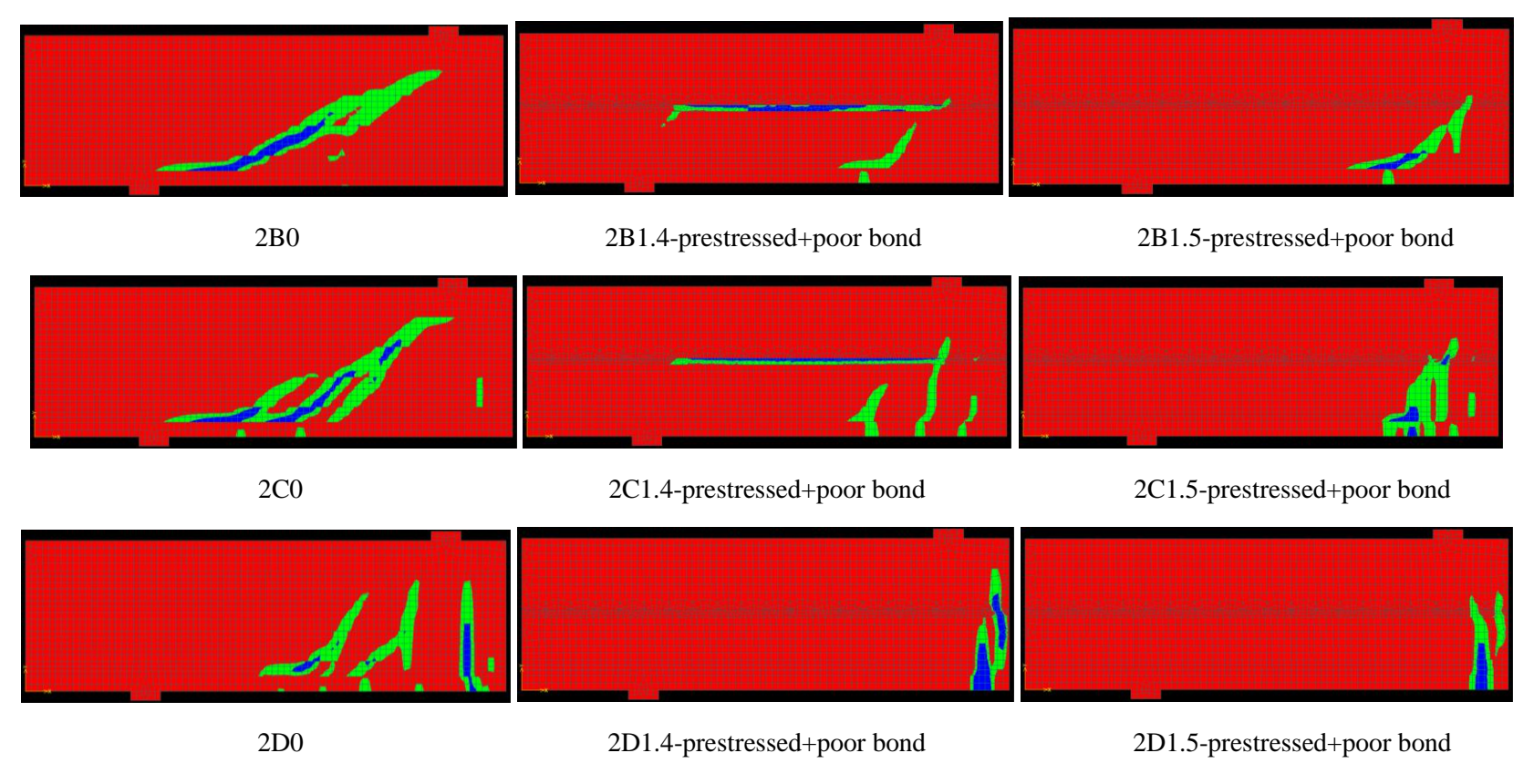


Figure 123 Principal strain for a/d=2 beams

### a/d=3:

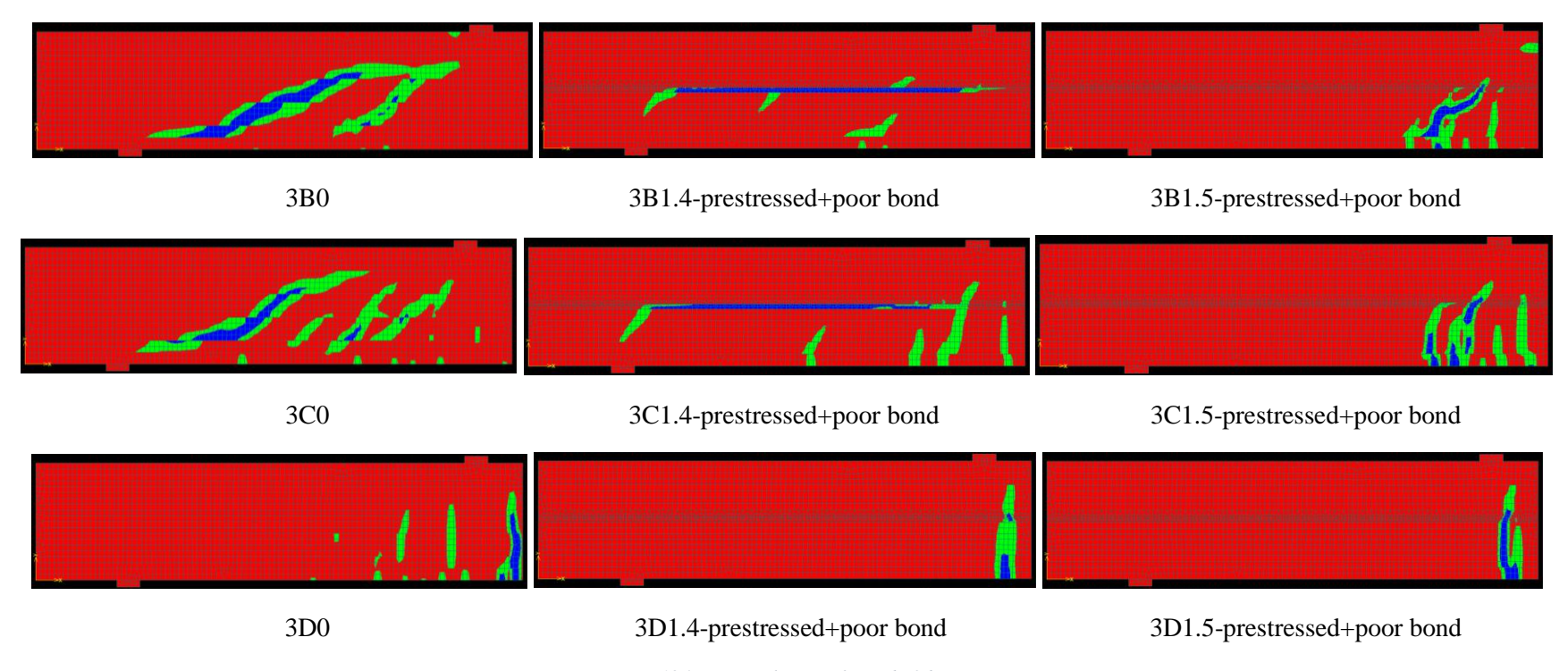


Figure 124 Principal strain for a/d=3 beams

#### a/d=4:

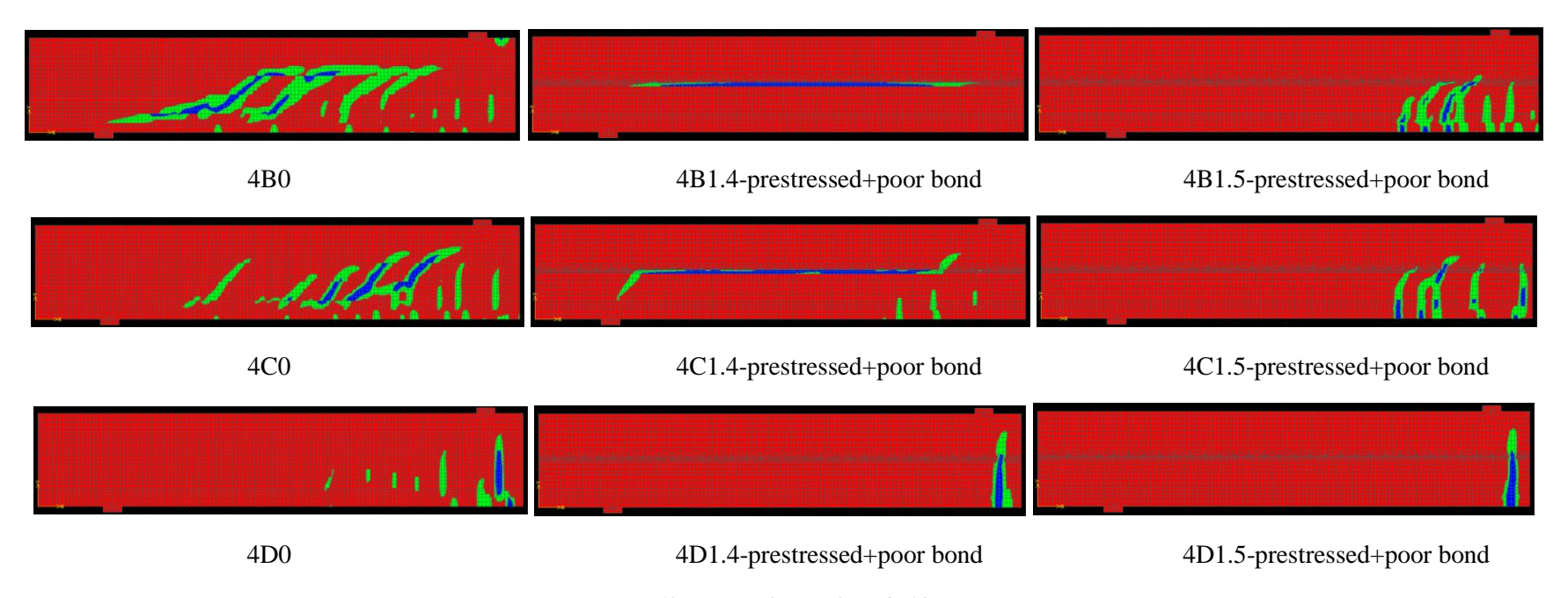
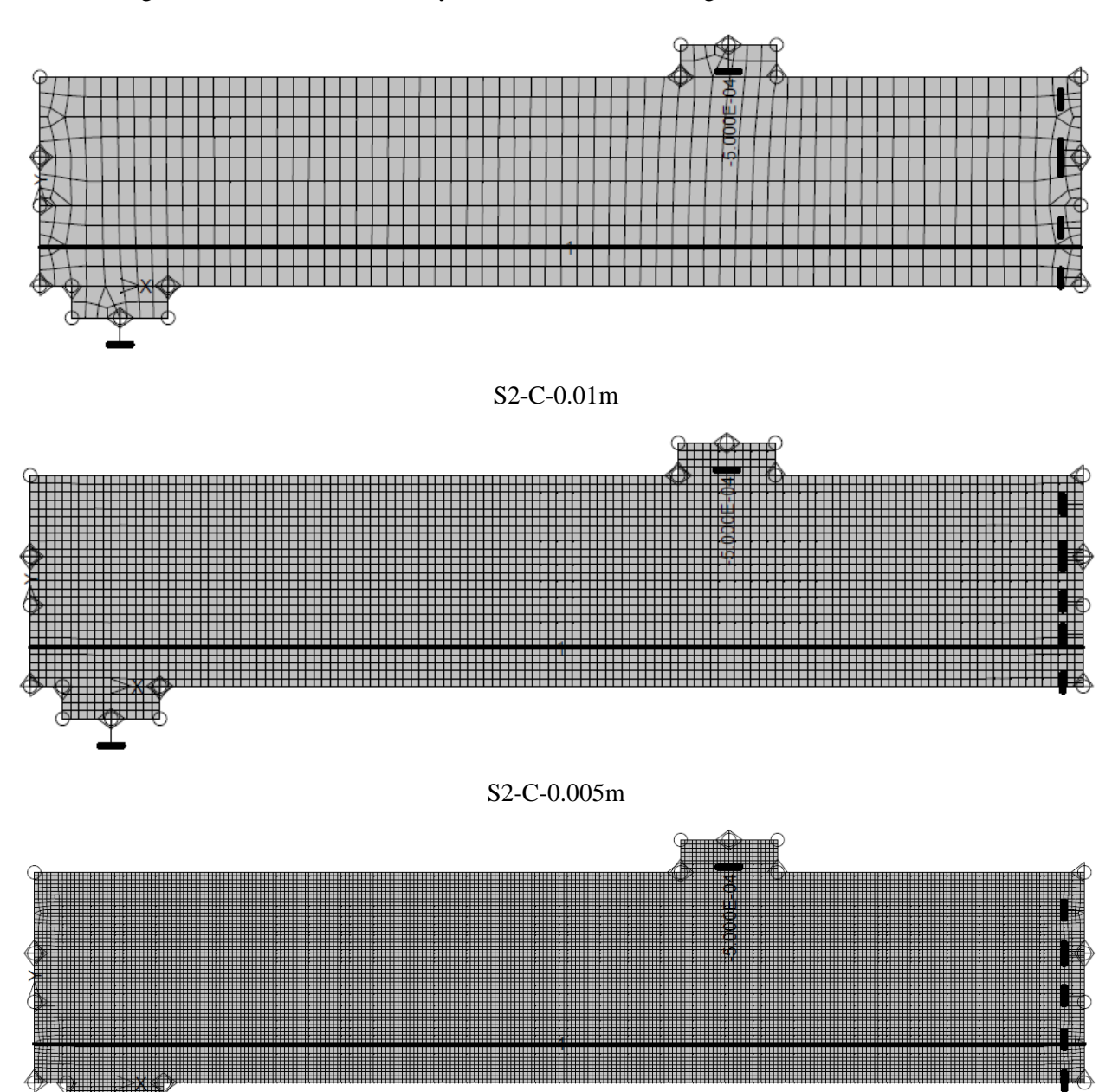


Figure 125 Principal strain for a/d=4 beams

### Appendix 6 Element size study for beam S2-C

Before investigating the ASR-affected models, to reduce deviation due to finite element models, a parameter study on element size is necessary. Three sets of element sizes are performed for beam S2-C, 0.01m, 0.005m and 0.0025m respectively. Mesh type is chosen as quadrilateral as it is commonly used in structural grids.

The mesh together with load and boundary condition is shown in Figure 126.



S2-C-0.0025m

Figure 126 Mesh, load and boundary condition

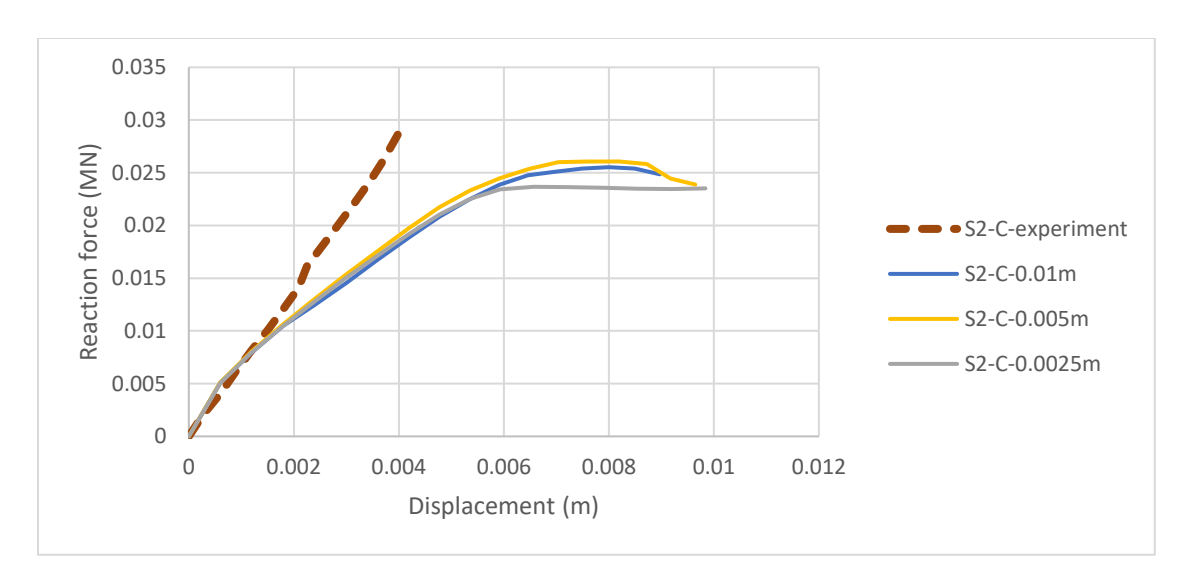


Figure 127 Force-displacement diagram S2-C with different element sizes

Comparing the force-displacement curves from FEM and the experiment, FEM results underestimate the stiffness after cracking. A possible reason might be beneficial effect of chemical prestressing is not taken consideration of.

However, the ultimate load for FEM results can be predicted quite well comparing with experiment. Numerical results are slightly less than experimental result. Mesh size 0.0025m takes much longer calculation time. Therefore, to reach a balance between analysis result and calculation time, mesh size 0.005m is chosen for ASR-affected beams.

### Appendix 7 Limit check of steel strain in S2-C

It is necessary to check the measured steel strain value in unaffected beam S2-C to make sure it is within the limit value. According to RILEM recommendation (TC Membership, 2003), the mean steel strain in the reinforcement allowed under the relevant combination of loads for the effects of tension stiffening, shrinkage, etc. could be calculated as:

$$\varepsilon_{cm} = \frac{\sigma_s}{E_s} \left[ 1 - \beta_1 \beta_2 \left( \frac{\sigma_{sr}}{\sigma_s} \right)^2 \right]$$

Where:

 $\sigma_s$  = the stress in the tensile reinforcement calculated on the basis of a cracked section

 $\sigma_{sr}$  = the stress in the tensile reinforcement calculated on the basis of a cracked section under loading conditions causing first cracking

 $\beta_1$  = coefficient which takes account of the bond properties of the bars

- = 1.0 for high bond bars
- = 0.5 for plain bars

 $\beta_2$  = a coefficient which takes account of the duration of the loading of repeated loading

- = 1.0 for single, short term loading
- = 0.5 for a sustained load or for many cycles of repeated loading

For members subjected only to intrinsic imposed deformations,  $\sigma_{s}$  may be taken as equal to  $\sigma_{sr}$  .

The calculation of  $\sigma_{sr}$  is shown as following:

$$\sigma_{sr} = \frac{f_{ctm}}{\rho} (1 + \alpha_e \rho)$$

In this case,  $f_{ctm} = 4.11 MPa$ ,  $\alpha_e = \frac{E_s}{E_c} = \frac{200000}{34000} = 5.9$ ,  $\rho = 2\%$ , the resulting  $\sigma_{sr}$  is 230 MPa.  $\sigma_s$  is

taken as equal to  $\sigma_{sr}$  due to the structure is subjected only to intrinsic imposed deformation.  $\beta_1$  is taken as 0.5 for plain bars,  $\beta_2$  is taken as 1.0 for single, short term loading. Therefore, the steel strain could be

calculated, 
$$\varepsilon_{cm} = \frac{\sigma_s}{E_s} \left[ 1 - \beta_1 \beta_2 \left( \frac{\sigma_{sr}}{\sigma_s} \right)^2 \right] = \frac{230}{200000} \left[ 1 - 0.5 \cdot 1 \cdot \left( \frac{230}{230} \right)^2 \right] = 5.75 \cdot 10^{-4}$$
, which is 575

micro strain.

The measured steel strain value in beam S2-C from test is 120 micro strain, obviously it does not exceed the limit value according to RILEM recommendation. This proves that during testing, beam S2-C is not affected by ASR.

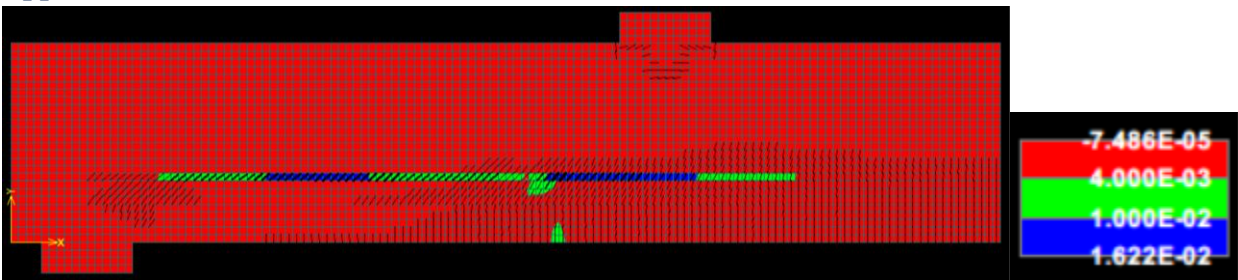
### Appendix 8 Discussion on fixed shear retention factor

### Appendix 8.1 Introduction

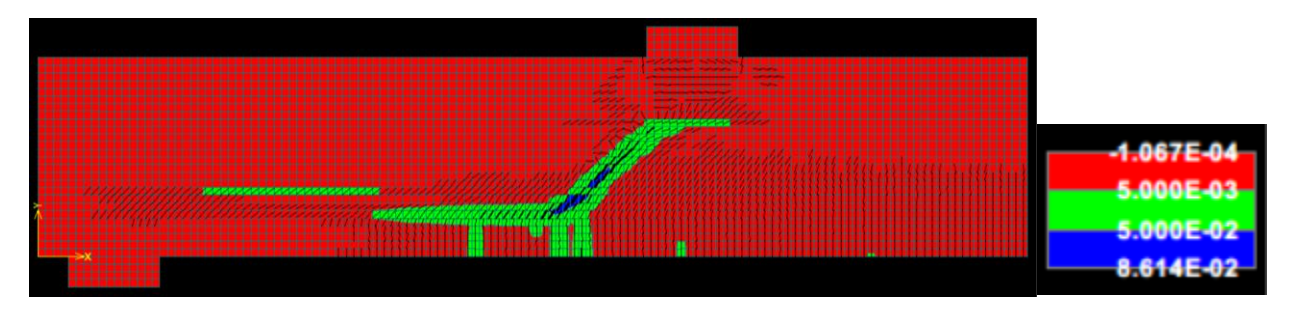
Variable shear retention factor is used in previous analysis, analysis on fixed shear retention factor will be presented in this part. According to parameter study, the shear retention factor will influence the failure mechanism. As fixed shear retention factor increases from 0 to 1, aggregate interlock effect increases, thus resulting in the failure mechanism transition from ASR layer to shear to bending failure.

From a practical perspective, only shear failure and bending failure occurred in many available experiments. It would be useful to know when the failure mechanism transition will happen in terms of fixed shear retention factor. Taking beam S2-A-2 with prestressing and poor bond as an example, several beams with different fixed shear retention factors are analyzed.

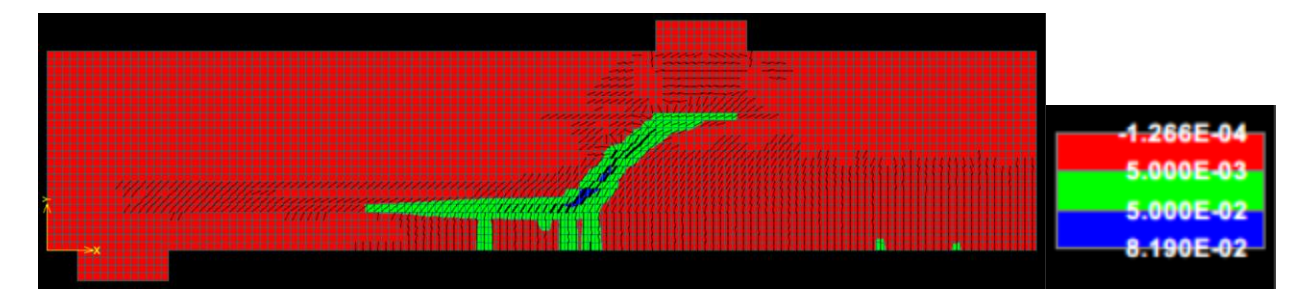
Appendix 8.2 Failure mechanism



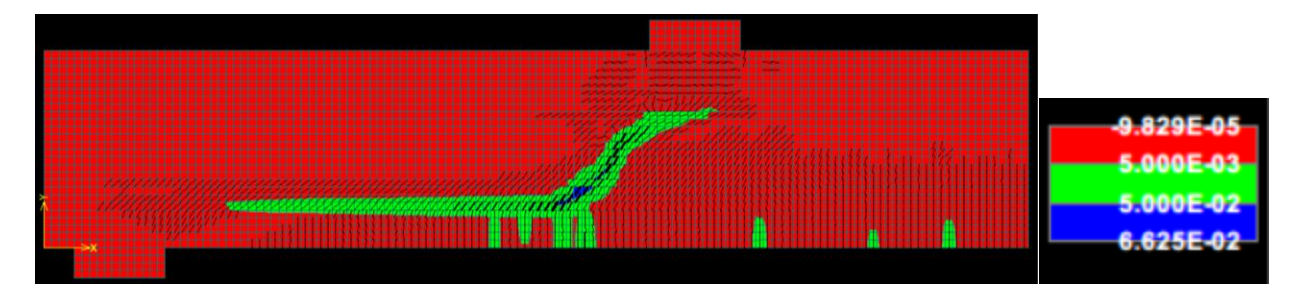
Fixed shear retention factor=0



Fixed shear retention factor=0.05



Fixed shear retention factor=0.1



Fixed shear retention factor=0.2

Figure 128 Principal strain pattern for models with fixed shear retention factors

With the fixed shear retention factor at a small range close to 0, failure mechanism changes from ASR layers to shear failure. The behavior of aggregate interlock could be a reason. As shear retention factor increases, comparing to the sound concrete, the ASR layer is not an obviously weaker part any more, therefore they can cooperate with each other. In this case, when shear retention factor reaches 0.1, the ASR layer failure could be prevented.

#### Appendix 8.3 Discussion

In this analysis, the influence of fixed shear retention factor is investigated. According to the principal strain pattern, the failure mechanism would be wrongly predicted if shear retention factor is set to be too small. The possible reason could be that the expansive ASR gel still has some ability to transfer stresses, which could be seen as aggregate interlock. To avoid the underestimation of aggregate interlock level, it is suggested to use a value no less than 0.1 when adopting a model with fixed shear retention factor.

### Bibliography

- Abe, M., Kikuta, S., Masuda, Y., & Tomozawa, F. (1989). Experimental Study on Mechanical Behavior of Reinforced Concrete Members Affected by Alkali-Silica Reaction. 8th International Conference on Alkali-Aggregate Reaction, (pp. 691-696).
- Adam, V., Reissen, K., & Hegger, J. (2017). Influence of Support Conditions on Shear in RC Members without Shear Reinforcement. *Fib Symposium*. Maastricht, the Netherlands.
- Ahmed, T., Burley, E., & Rigden, S. (1998). The Static and Fatigue Strength of Reinforced Concrete Beams Affected by Alkali-Silica Reaction. *ACI Materials Journal*, 356-268.
- Ahmed, T., Burley, E., & Rigden, S. (1999). Effect of Alkali-Silica Reaction on Tensile Bond Strength of Reinforcement in Concrete Tested under Static and Fatigue Loading. *ACI Materials Journal*, 419-428.
- Cervenka, V., Jendele, L., & Cervenka, J. (2016). *ATENA Program Documentation Part 1 Theory*. Prague, Czech: Cervenka Consulting s.r.o.
- Chana, P., & Korobokis, G. (1991). Structural Performance of Reinforced Concrete Affected by Alkali Silica Reaction: Phase 2. *Transport and Road Research Laboratory*.
- Chen, X. (2018). Finite Element Modelling of ASR Affected Reinforced Concrete Beams Based on Realistic Pre-damage. Rotterdam, the Netherlands: Master Thesis.
- Clayton, N., Currie, R., & Moss, R. (1990). The Effects of Alkali Silica Reaction on the Strength of Prestressed Concrete Beam. *The Structural Engineer*, 287-292.
- Cope, R. (1993). The Prediction of Stress Distributions in Reinforced Concrete Affected by Alkali Aggregate Reaction. *Transport Reserch Laboratory*.
- den Uijl, J. (2000). Residual Capacity after ASR Attack Cross-force Tests on Beams from the Viaducts Zaltbommel and Heemraadsingel (in Dutch). Delft.
- den Uijl, J. (2000). Structural Consequences of ASR: An Example on Shear Capacity. Delft, the Netherlands.
- Esposito, R. (2016). *The Deteriorating Impact of Alkali-Silica Reaction on Concrete*. Delft, the Netherlands: PhD Thesis.
- Fan, S., & Hanson, J. (1998). Effect of Alkali Silica Reaction Expansion and Cracking on Structural Behavior of Reinforced Concrete Beams. *ACI Structural Journal*, 498-505.
- Fan, S., & Hanson, J. (1998). Length Expansion and Cracking of Plain and Reinforced Concrete Prisms Due to Alkali-Silica Reaction. *ACI Materials Journal*, 480-485.
- Farage, M., Alves, J., & Fairbairn, E. (2004). Macroscopic Model of Concrete Subjected to Alkali-Aggregate Reaction. *Cement and Concrete Research*, 495-505.
- Ferche, A., Sheikh, S., & Vecchio, F. (2017). Toward Macro-Modeling of ASR-Affected Structures. *ACI Structural Journal*, 1121-1129.

- Inoue, S., Fujii, M., Kobayashi, K., & Nakano, K. (1989). Structural Behaviour of Reinforced Beams Affected by Alkali-Silica Reaction. 8th International Conference on Alkali-Aggregate Reaction in Concrete, (pp. 727-732).
- ISE. (1992). Structural effects of alkali-silica reaction Technical guidance on the appraisal of existing. London, UK: The Institution of Structural Engineers.
- Jones, A., & Clark, L. (1996). The Effects of Restraint on ASR Expansion of Reinforced Concrete. *Magazine of Concrete Research*, 1-13.
- Kani, G. (1966). Basic Facts Concerning Shear Failure. ACI Journal Proceedings, 675-692.
- Kobayashi, K., Fukushima, T., & Rokugo, K. (2013). Shear Strength of ASR-Deteriorated RC Members and Shear Reinforcing Effect of Repair by Adding Rebar. *VIII International Conference on Fracture Mechanics of Concrete and Concrete Structures*.
- Kobayashi, K., Inoue, S., Yamasaki, T., & Nakano, K.-i. (1988). Alkali Aggregate Reaction in Prestressed Concrete Beams. *The International Journal of Cement Composites and Lightweight Concrete*, 233-240.
- Ng, K. (1991). Effect of Alkali Silica Reatcion on the Punching Shear Capacity of Reinforced Concrete Slab. Birmingham, UK: Phd Thesis.
- Pryl, D., & Cervenka, J. (2017). *ATENA Program Documentation Part 11 Troubleshooting Manual*. Prague, Czech.
- Rafla, K. (1971). Empirical Equations for the Calculation of the Shear Resitsance of Reinforced Concrete Beams. *Strasse, Brucke, Tunnel*, 311-320.
- Rots, J., & Blaauwendraad, J. (1989). Crack Models for Concrete: Discrete or Smeared? Fixed, Multi-directional or Rotating? Delft.
- TC Membership. (2003). RILEM TC 162-TDF: "Test and design methods for steel fibre reinforced concrete" σ-ε-design method Final Recommendation. *Materials and Structures*, 560-567.